UNIVERSITY OF SOUTHAMPTON
FACULTY OF ENGINEERING, SCIENCE & MATHEMATICS
School of Ocean and Earth Sciences

The Chemistry of Iron in Hydrothermal Plumes

by

Sarah Anne Bennett

Thesis for the degree of Doctor of Philosophy

May 2008

UNIVERSITY OF SOUTHAMPTON

ABSTRACT

FACULTY OF ENGINEERING, SCIENCE & MATHEMATICS

SCHOOL OF OCEAN & EARTH SCIENCES

Doctor of Philosophy

THE CHEMISTRY OF FE IN HYDROTHERMAL PLUMES

By Sarah Anne Bennett

This thesis investigates the role of submarine hydrothermal vents in the global marine Fe budget. While debate continues over the sources of dissolved Fe to the global deep-ocean dissolved Fe budget, it had been presumed, until recently, that all the Fe emitted from hydrothermal vents precipitates and sinks to the seafloor close to the vent source. However, in the open ocean, dissolved Fe exists at concentrations greater than the predicted solubility because of the presence of organically complexed Fe. If similar complexes were formed in the hydrothermal systems then there would be the potential for dissolved Fe export via hydrothermal plumes to the deep-ocean.

To investigate the fate of hydrothemally sourced Fe, samples were collected from high-temperature hydrothermal vent-field plumes at 9°N on the East Pacific Rise and at 5°S on the Mid-Atlantic Ridge. The samples from the East Pacific Rise were analysed for Fe and dissolved and particulate organic carbon. Although hydrothermal systems are presumed to be inorganically dominated, elevated concentrations of dissolved organic carbon compared to background seawater were detected in near-field buoyant plumes and the concentration of organic carbon appeared to relate to the total Fe concentration, consistent with the presence of some organic-Fe interaction.

Non-buoyant plume samples from the Mid-Atlantic Ridge were analysed for total dissolvable and dissolved Fe and Mn as well as speciation studies on a subset of the dissolved Fe samples using Competitive Ligand Exchange – Cathodic Stripping Voltammetry. The dissolved Fe concentrations in the dispersing plume were higher than predicted from dissolved Fe(II) oxidation rates alone. Further investigation into the speciation of the dissolved Fe revealed the presence of stable Fe-ligand complexes, similar to those detected in the open ocean, but with higher concentrations. If these Fe-ligand complexes were representative of all hydrothermal systems, submarine venting could potentially provide between 11 to 22% of the global deep-ocean dissolved Fe budget.

Buoyant plume samples from the same vent site were analysed for total dissolvable and dissolved Fe and Mn as well as particulate Fe, Mn, P, V, Cu, Zn and the rare earth elements. Fe isotopes were also analysed in the particulate fraction, as a potential tool for tracing the biogeochemical cycle of Fe in the ocean. The forms of particulate Fe were elucidated using the particulate trace element data, enabling the isotope fractionation caused by Fe sulfide precipitation to be determined. A diagnostic isotope signature for a potential stabilised dissolved Fe fraction was predicted to be isotopically heavier than the original vent fluid, potentially enabling Fe inputs from hydrothermal vents to be traced throughout the ocean.

Graduate School of the

National Oceanography Centre, Southampton

This PhD dissertation by

Sarah Anne Bennett

has been produced under the supervision of the following persons

Supervisors:	Prof. Christopher German
	Prof. Peter Statham
Chair of Advisory Panel:	Prof. Eric Achterberg

Table of Contents

List of Figures

List of Tables

DECLARATION OF AUTHORSHIP

I, Sarah Anne Bennett, declare that the thesis entitled 'The Chemistry of Iron in Hydrothermal Plumes' and the work presented in it are my own. I confirm that:

- this work was done wholly or mainly while in candidature for a research degree at this University;
- where any part of this thesis has previously been submitted for a degree or any other qualification at this University or any other institution, this has been clearly stated;
- where I have consulted the published work of others, this is always clearly attributed;
- where I have quoted from the work of others, the source is always given. With the exception of such quotations, this thesis is entirely my own work;
- I have acknowledged all main sources of help;
- where the thesis is based on work done by myself jointly with others, I have made clear exactly what was done by others and what I have contributed myself;
- Parts of this work have been published as:

Bennett, S. A., Achterberg, E. P., Connelly, D. P., Statham, P. J., Fones, G. R., German, C. R., 2008, The distribution and stabilisation of dissolved Fe in deep-sea hydrothermal plumes, Earth and Planetary Science Letters, 270: 157-167.

German, C. R., Bennett, S. A., Connelly, D. P., Evans, A. J., Murton, B. J., Parson, L. M., Prien, R. D., Ramirez-Llodra, E. Z., Jakuba, M., Shank, T. M., Yoerger, D. R., Walker, S. L., Baker, E. T., Nakamura, K. Hydrothermal activity on the Southern Mid-Atlantic: Tectonically and volcanically controlled venting at 4-5°S, Earth and Planetary Science Letters, In Press.

Signed: ……..

Date:…….

Acknowledgements

My utmost and greatest thanks go to my two supervisors, Chris German and Peter Statham, without whom this project would not have been possible. Chris has provided me with some marvellous opportunities, from diving in DSV *Alvin* to networking with all the 'big wigs', or should I say his 'drinking buddies', at AGU. He has imparted his knowledge on hydrothermal systems as well as teaching me some important lessons in scientific writing. At NOCS, Peter has done a marvellous job at keeping my PhD on track as well as a great support for the intricacies of analytical work.

Next, I would like to thank Eric Achterberg, whose role as a panel chair soon crossed over in my first year to an advisor for the electrochemical work. This piece of work was initiated after a conversation between Chris and Gary Fones at a Gordon Conference (Thanks guys!) and without Eric's support, this successful piece of work may never have been completed. Olivier Rouxel also provided me the opportunity to carry out some analytical work at Woods Hole Oceanographic Institution. Thank you for your help and letting me absorb some of your intelligence!

Doug Connelly has provided fantastic support during my PhD, both at sea and in the clean laboratory, teaching me the required techniques for trace metal analysis, thank you. Turki Al Said must also be mentioned here, for helping me keep my sanity in the electrochemistry lab, after hours spent making measurements, resulting in only a few data points! Thanks also to Darryl Green (aka Dazza) and his Spice girls (Belinda, Carla, Magda and Caroline) for provided me with an enlightening introductory experience on my first research cruise and the support since.

At this point, I would love to mention everyone who has helped me at sea but I fear I may forget someone… Without the crew, scientist and technical support team, work at sea would not be possible. I would like to make a special mention to Jim Ledwell for letting me piggyback on AT05-04, as well as Ryan, Cindy and Leah for making me feel so welcome. Thanks also to Nadine Le Bris for the sensor data from this cruise and to Dieter Garbe-Schönberg and Katja Schmidt for the vent fluid samples and associated major element data from 5°S MAR. This thesis has been illustrated with some fantastic maps and I must thank Alan Evans, Ryan Jackson and Rebecca Bell for obliging to make them for me!

My friends have been a great support to me during my PhD, even the ones who couldn't quite understand why I wanted to be a student for another three years, especially when they realised I had to work just as hard as them, in 'real' jobs! Thank you to Gail, Del, Teresa, Em, Lucy O, Lucy T and the climbers, Jo, Phil, Doug and Tammy. Thank you to my office mates, Aggie, Steve, Chris, Michelle and the late comers – Caroline and John – you provided me with some real entertainment! I do believe you were the first ones to drag me to the Platform – thank you to the regulars who made this pub the perfect place to unwind on a Friday night.

I think this leaves me with only a couple more people to thank, first to Paul, who not only has supported me as my partner but also as a constant 'oceanographic mentor'. His knowledge and experiences in oceanography far outweigh my own yet my endless questions never seem to tire him.

And finally to my family; my parents have provided me with emotional and financial support throughout my life, and I certainly wouldn't be where I am today without them – Thank you.

List of Abbreviations

ABE – Autonomous Benthic Explorer
ASCT – Axial summit collapse trough
ATP – Adenosine 5-triphosphate
BP – Buoyant plume
$CHCl_3$ – Chloroform
CIR – Central Indian Ridge
CLE-CSV - Competitive Ligand Exchange - Cathodic Stripping Voltammetry
CTD – Conductivity, temperature and density
dFe – Dissolved iron
DOC – Dissolved organic carbon
DOM – Dissolved organic matter
DSV – Deep submersible vehicle
EPR – East Pacific Rise
Fe – Iron
GFAAS – Graphite Furnace Atomic Absorption Spectroscopy
HMDE – Hanging mercury drop electrode
HNLC – High Nutrient – Low Chlorophyll
HNO_3 – Nitric acid
ICP-OES – Inductively Coupled Plasma – Optical Emission Spectrometry
ICP-MS – Inductively Coupled Plasma – Mass Spectrometry
KIPS – Kiel pumping system
L-ADCP – Lowered acoustic doppler current profiler
LDPE – Low density polyethylene
LMSW – Low metal seawater
MAPR – Miniature autonomous plume recorders
MAR – Mid-Atlantic Ridge
Mn – Manganese
NOCS – National Oceanography Centre, Southampton
OTE bottles – Ocean Test Equipment bottles
pFe – Particulate Fe
POC – Particulate organic carbon
REE – Rare earth element
ROV – Remotely operated vehicle
RSD – Relative standard deviation

SAPS – Stand alone pumps

SBDW – Sub-boiled distilled water

S.d. – Standard deviation

TdFe – Total dissolvable iron

TdMn – Total dissolvable manganese

TOBI – Towed Ocean Bottom Instrument

WHOI – Woods Hole Oceanographic Institution

[L] – Ligand concentration

[L_T] – Total ligand concentration

Chapter 1. Introduction

The aim of this thesis is to examine the influence of hydrothermal activity on the biogeochemistry of the ocean. Specifically, this study will investigate the fate of dissolved Fe emitted from high-temperature deep-sea hydrothermal vents and its biogeochemical cycle in the oceans.

1.1 Fe biogeochemistry in the oceans

Iron is the fourth most abundant element in the Earth's crust and the second most abundant metal. Iron in the crust (5.6%) is a stable element and forms thermodynamically stable compounds with oxides and carbonates. In comparison, the concentrations of dissolved Fe in the modern open ocean are very low – typically <1 nM (de Baar and de Jong, 2001). The reasons for these distributions relate to iron's chemical properties and behaviour.

Most of the Fe in the Earth's mantle, oceanic and continental crust is in mafic minerals where Fe is present in its more reduced +2 oxidation state. Once in the more oxidising ocean, Fe is thermodynamically stable as Fe(III), hence the lifetime of Fe(II) in the oceans depends on its oxidation half-life (Millero et al., 1987). In oxic marine conditions with neutral pH, Fe(II) is readily oxidised to Fe(III). The Fe(III) ion then forms complexes with a preference for oxygen-donor ligands forming sparingly soluble oxyhydroxides which precipitate and sink to the seafloor. Consequently, the concentration of Fe(II) in the oceans would be predicted to be negligible based purely on thermodynamic considerations.

Understanding the cycling of Fe in the oceans is important because Fe is thought to be a limiting micro-nutrient for primary production. Historically, primary production has been regarded as limited by the availability of light and macro-nutrients (nitrate, phosphate and silicate) and it was not until 1990 that it was hypothesised that Fe acts as a limiting nutrient in High Nutrient – Low Chlorophyll (HNLC) regions (Martin et al., 1994; Martin et al., 1990). These oceanic regions, for example the Southern Ocean and the North Pacific, have an abundance of macro-nutrients and light in the summer but are still deficient in phytoplankton. Primary production has been hypothesised to be limited

by the availability of Fe, even though dissolved Fe concentrations throughout the oceans are extremely low (<1 nM) and this hypothesis has since been validated by a number of controlled experiments (Boyd et al., 2000; Coale et al., 2004; Gordon et al., 1998; Lam and Bishop, 2008; Tsuda et al., 2007; Wong et al., 2006).

Recent work has demonstrated that in addition to the most stable complexes of Fe(III) that precipitate and sink to the seafloor as Fe oxides, organic Fe(III) complexes in the open ocean increase the solubility of Fe(III) in salt solutions, resulting in Fe availability to plankton (Liu and Millero, 1999; Liu and Millero, 2002). Fe exists at concentrations greater than the predicted solubility in both the surface and deep open-ocean (Millero, 1998) and >99% of dissolved Fe has been demonstrated to be complexed by stable organic ligands (Gledhill and Van den Berg, 1994; Rue and Bruland, 1997; Van den Berg, 2006). In the deep open-ocean an average concentration of 0.7 nM dissolved Fe exists (ranging from 0.4 to 1 nM)(Bergquist and Boyle, 2006) in association with Fe-binding ligands that are present in concentrations ranging from 0.7 to 1.4 nM. The organic ligands are presumed to be released by microorganisms but little is known about their chemical composition (Van den Berg, 1995). Organic Fe complexation will reduce the reactivity of the Fe species, preventing both precipitation of Fe and scavenging (adsorption/absorption) of Fe into/onto particulate phases.

In addition to dissolved organic Fe(III) complexes, low dissolved Fe(II) concentrations have previously been measured in; a) the surface ocean, where photo reduction causes a steady state presence of Fe(II) to be maintained in sunlit oxic waters (King et al., 1993); b) in anoxic basins where the lack of oxygen prevents Fe oxidation (Spencer and Brewer, 1971); and c) in chemically reduced high-temperature hydrothermal vent fluids, emitted from the seafloor. Particulate Fe(III) has also been found to be important in the oceans in a broader geochemical sense as a scavenging agent. In its oxide form, the Fe can adsorb trace elements and act as a net sink in their geochemical cycle (Bruland and Lohan, 2003).

There are a complex variety of Fe species present in oxic oceans and determination of the different Fe species is difficult. The current analytical procedure for the analysis of the Fe spectrum involves size fractionation, and is carried out with ~0.2 or ~0.4 µm membrane filters (Martin and Gordon, 1988). Within the 0.4 µm filtered fraction are the

'dissolved' species, which includes colloidal and soluble Fe species, separating out the particulate phase. Further filtration of the filtrate using a 0.025 or 0.05 μm filter can be used to separate the soluble fraction, leaving behind the Fe colloids on the filter (Nishioka et al., 2001). It is important to realise that the method is operationally defined as Fe is present in a spectrum of sizes ranging from simple ions to conventional particulate phases, and that these particulate phases are expected to be in a dynamic equilibrium. For example, nanoparticulate Fe species have recently been determined to be present in the 'dissolved' fraction.

It was not until very recently that analytical techniques and our knowledge of the oceans had progressed to a suitable level to enable accurate measurements of Fe in the ocean to be made. Prior to the 1990s, Fe contamination was a major source of error during the collection of samples, processing, storage and analysis (Landing and Bruland, 1987). Since the 1990's Fe measurement methods have improved (including the ability to measure stable isotope ratios for Fe) and contamination minimised. The biogeochemical cycle of Fe has now become of major interest to the scientific community, including the emerging GeoTraces program.

One of the goals of the GeoTraces study is to evaluate the sources, sinks and internal cycling of important oceanic species. For Fe, four main sources have been identified; riverine, atmospheric (aeolian), sedimentary and hydrothermal (Figure 1.1).

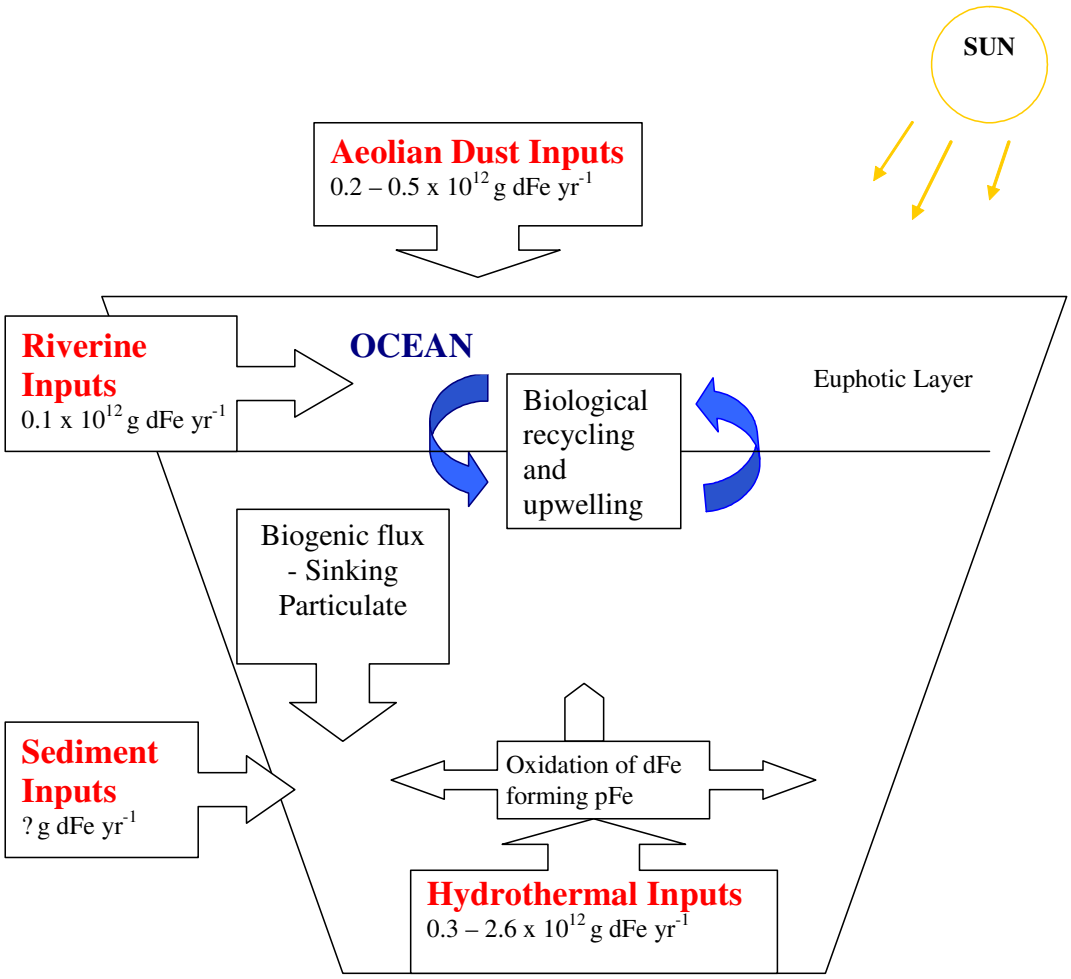

Figure 1.1 – Schematic of the dissolved Fe (dFe) inputs into the ocean. Data sources for aeolian and riverine inputs from Ussher at al. (2004); see text for hydrothermal input data sources.

Atmospheric inputs are considered the principal source of soluble Fe to the open ocean. The Fe source (arid and semi-arid regions of the world) is often thousands of miles away from the final destination and the Fe is associated with the deposition of aluminosilicate minerals from soil material, i.e. dust (<10 µm size particles);(Jickells and Spokes, 2001). This can occur through either wet or dry deposition and both are dependent on the aerosol size and Fe solubility once the Fe enters the surface ocean (Baker and Jickells, 2006; Buck et al., 2006). Particularly important areas are the large North African deserts, particularly the Sahara, which impacts the tropical North Atlantic, and Asian deserts, such as the Gobi in Northern China, which impacts the temperate North Pacific. Because

of the locations of these deserts and prevailing wind directions, dust input only affects specific regions of the global upper ocean (Jickells et al., 2005).

The overall annual dust flux to the oceans has been estimated to be on the order of magnitude of 500 x 10^{12} g yr^{-1} (Jickells, 1999). However, the proportion of dissolved Fe released from this particulate Fe flux is not well determined and there are large uncertainties over the magnitude of *dissolved* Fe input from dust to the ocean. The flux is predicted to fall in the range 0.2 to 0.5 x 10^{12} g dissolved Fe per year (i.e. 0.04 – 0.1% of the particulate Fe flux).

Rivers, unlike seawater, can carry dissolved Fe concentrations as high as 40 μg L^{-1} with a flux of 1.54 x 10^{12} g y^{-1} transported to the ocean margins (Duce and Tindale, 1991; Martin and Windom, 1991). However, even though dissolved organic matter (DOM) has the ability to keep trace metals in solution in rivers at high pH, that DOM (and hence also the associated Fe) is removed from solution very efficiently in estuaries, as a result of rapid flocculation that occurs upon mixing of fresh water with seawater. This same complexation can lead to significant dissolved Fe removal (Boyle et al., 1977; Moore et al., 1979; Sholkovitz and Copland, 1981), such that only ~10% of the dissolved riverine Fe remains in solution to be exported from estuaries and enter the ocean basins (Martin and Windom, 1991). The resultant net dissolved Fe flux from rivers is ~0.1 x 10^{12} g per year.

The role of sediments as an input of dissolved Fe to the ocean has received much less attention than the previous two inputs already discussed. However, sediment inputs are certainly a potential source of Fe that merits further attention (Landing and Bruland, 1987). As particulate matter, enriched in trace metals, reaches the seafloor it is subject to diagenesis. As sediments compact, pore water fluids are produced and advected to the surface. The chemistry of this fluid depends on the redox conditions of the sediments and below ~8 to 15 cm, the sediments become anoxic (Libes, 1992). In anoxic ocean basins, diagenesis will lead to the dissolution of all Fe and Mn oxides, which will then be released into the overlying water column where they will remain stable. However, this situation is unusual as most ocean basins are oxic. Here, any reduced Fe(II) in the pore water fluid will advect upwards to shallower oxic levels within the sediments, where the Fe(II) will be oxidised and precipitated before even being released to the overlying water

column. However, in coastal and high productivity regions, where there is a high deposition of organic matter to the sediments, the anoxic/oxic interface is at the same level as the seafloor. This means that dissolved Fe(II) can flow directly up into the water column (Elrod et al., 2004; Severmann et al., 2006). Therefore if Fe(III) is stabilised by the organic rich sediments (Froelich et al., 1979), the solubility of the Fe(III) species will be increased, preventing precipitation in the oxic basin. The flux of dissolved Fe from sediment inputs has not been quantified.

The focus of this study, however, will be the potential of hydrothermal inputs as a source of dissolved Fe to the ocean. The concentration of dissolved Fe(II) in high-temperature hydrothermal end-member fluids is on the order of 1 mM or higher (i.e. approximately ~1 million-fold higher than ambient deep-ocean concentrations) and what is particularly notable is that all this Fe is injected into the ocean in dissolved form.

The gross flux of hydrothermal fluid to the oceans has been an important question for understanding the chemical impact of hydrothermal systems on the ocean and simple thermal calculations of hydrothermal power outputs have provided the magnitude of hydrothermal circulation (Elderfield and Schultz, 1996; Mottl, 2003). These estimates have been achieved using various geochemical methods such as ^{3}He/heat, Mg, Sr isotopes, Li isotopes and Ge/Si ratios, but not without issues associated with each of the methods. These estimated heat fluxes have been converted to water fluxes by estimating how much of the heat flux is made up of high-temperature flow compared to low temperature diffuse flow. This introduces large uncertainties because the partitioning of heat between these two flow regimes remains largely unresolved.

More recently thallium has been used to constrain axial high-temperature and off-axis low-temperature hydrothermal water fluxes as more than 99% of the Tl-budget of high-temperature vent fluids originates from the leaching of oceanic crust (Nielsen et al., 2006). High-temperature vent fluid flux has been estimated to make up 20% of the thermal energy available on-axis and the high-temperature water flux has been constrained to lie in the range 0.17 - 2.93 x 10^{13} kg yr^{-1} with a best estimate of 0.72 x 10^{13} kg yr^{-1}. Assuming a vent fluid dissolved Fe concentration range of 0.75 – 6.5 mM, the corresponding gross hydrothermal Fe(II) flux would be ~0.3 to 2.6 x 10^{12} g dissolved Fe per year. This, therefore, could potentially be the largest supplier of

dissolved Fe to the deep-ocean, but until now it has been presumed that all this Fe precipitates close to the vent source with no dissolved Fe entering the global biogeochemical budget. Consequently, a detailed consideration of the hydrothermal input of Fe to the global ocean and its fate, is both timely and important to understanding the Fe cycle in the ocean.

1.2 Hydrothermal activity

Evidence for the presence of hydrothermal venting on the seafloor first occurred in the 1960's in the Red Sea (Degens and Ross, 1969), with the detection of metal rich sediments and hot salty water (40 – 60°C) within the depths of the ocean basins. Because the central depths of the Red Sea are the site of active tectonic rifting and separation between the African and Arabian plate, it was hypothesised that similar chemical and physical anomalies may be observed along other mid-ocean ridge (MOR) spreading centres. Further evidence came from ^{3}He anomalies detected in the Pacific Ocean, which could only be sourced from active degassing of the earth's interior (Clarke et al., 1970).

As the concepts of plate tectonics and seafloor spreading became widely accepted by the scientific community during the 1960's and 1970's, questions arose over the balance between the radioactive build up of heat in the mantle and its release into the ocean. The spreading of tectonic plates at mid-ocean ridges, provided the most likely location for heat loss, but heat flow probes measuring thermal conduction could not balance the heat budget. This led to the suggestion that convective processes, with seawater percolating into the crust, heating up and then discharging at the seafloor could carry the 'missing' heat flux from the Earth's interior to the ocean.

In 1977, along the Galapagos Spreading Centre in the Eastern Equatorial Pacific, warm hydrothermal fluids (up to 17°C, diffuse flow) composed of chemically altered seawater were observed during a submersible dive in the DSV *Alvin* (Corliss et al., 1979). These warm hydrothermal fluids were collected and analysed for their chemical composition. Then by assuming that the source of these fluids must have had an end-member Mg concentration of zero, Edmonds et al. (1979) predicted that there must be fluids with temperatures as high as 350°C. Within months, he was proved right, with the discovery

of the first high-temperature 'black smoker' vents at 21°N along the East Pacific Rise (EPR)(Ballard and Grassle, 1979; Spiess et al., 1980). These vents were emitting hot (up to 380°C) chemically rich, high-temperature fluids up into the water column.

Since their discovery, new sites of hydrothermal activity have been detected throughout the ocean basins (Figure 1.2), even along the slowest spreading ridges, such as the Southwest Indian Ridge (German et al., 1998) and the Gakkel Ridge (Edmonds et al., 2003). Hydrothermal circulation occurs predominantly along mid-ocean ridges, but also at back-arc spreading centres formed behind ocean-ocean subduction zones and at areas of hot-spot intraplate volcanism (e.g. Hawaii). However, the bulk of hydrothermal flux is likely to occur on the fastest spreading ridges, where ^{3}He anomalies have been detected to be greatest along with an increased magmatic heat flux (Baker et al., 1996; Baker and German, 2004).

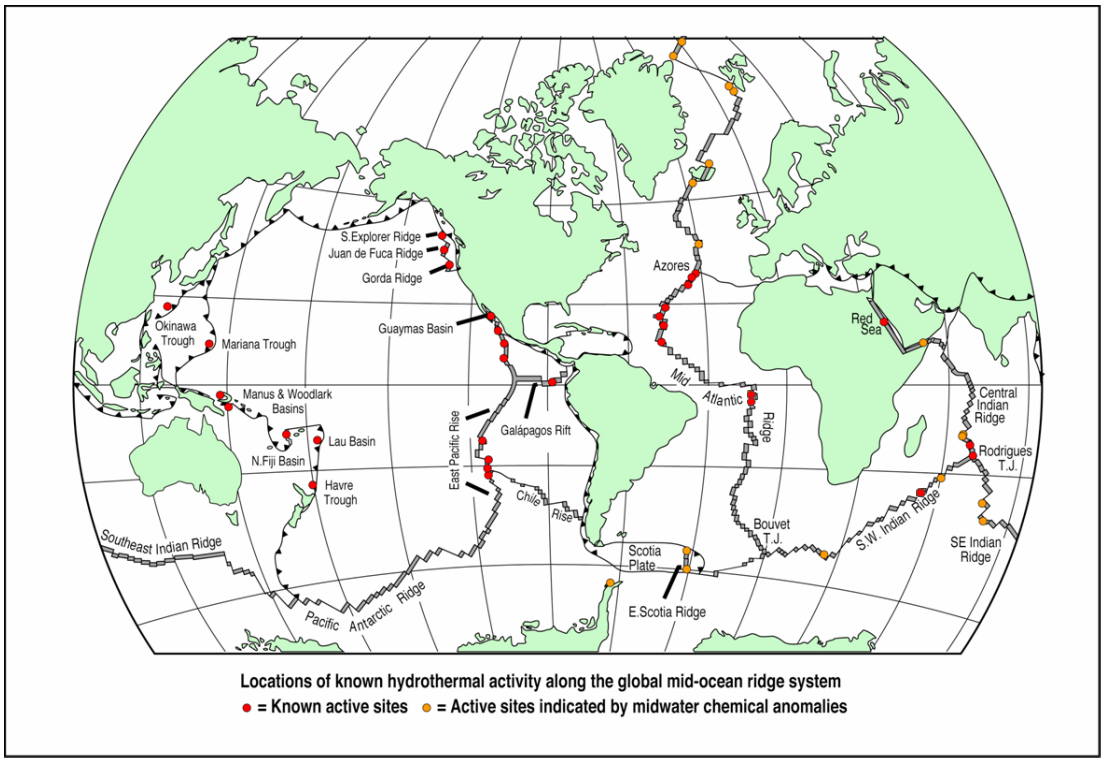

Figure 1.2 - Modified Hydrothermal system distribution map from German and Von Damm (2004) – The discovery of new sites at 5°S MAR and along the SW Indian Ridge have been added to this diagram.

1.2.1 Hydrothermal circulation

During hydrothermal circulation, seawater percolates into young ocean crust where it is heated and then undergoes chemical modification through reactions with the surrounding rock, both depleting and enriching the water with chemical elements. As the fluids heat up to temperatures greater than 400°C, they become buoyant and rise rapidly back to the seafloor where they are emitted into the water column with temperatures of the end-member fluids ranging from 350 to 400°C (Figure 1.3). The two main processes taking place in this 'hydrothermal flow cell' are phase separation and water-rock interactions.

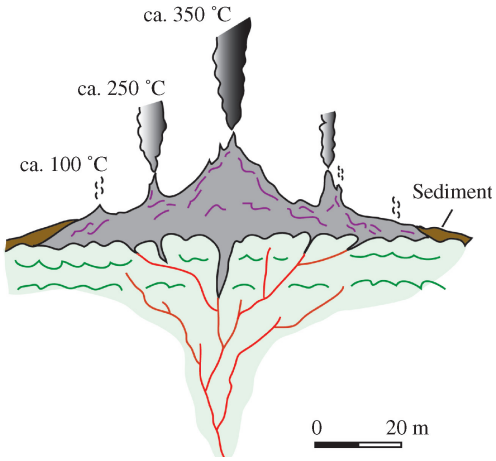

Figure 1.3 - Schematic illustration of hydrothermal circulation (German and Von Damm, 2004)

Water-rock reactions occur throughout the hydrothermal flow cell. Anhydrite formation results in loss of SO_4^{2-} from the fluids and Mg-OH silicate formation results in the loss of Mg. During Mg-OH silicate formation, H^+ is released resulting in the fluids becoming more acidic. Sulfate is also reduced to H_2S, as observed by high concentrations in the end-member fluids and the seawater becomes highly reducing - as indicated by the presence of H_2S, H_2 and CH_4. End-member vent fluids are also typically enriched in a range of metals, including iron and manganese, which are the two most abundant cations (Edmond et al., 1979), and chloride becomes the only major anion, making the cations form chloro-complexes (German and Von Damm, 2004). The chlorinity of end-member hydrothermal fluids has been observed to vary between 6 and 200% of seawater concentration.

The concentration of chloride is believed to be controlled by phase separation. Phase separation is the transformation of a homogeneous solution into two or more phases. The exact nature of the process depends on the pressure and temperature of the system. No hydrothermal fluid has been detected to have a chlorinity exactly the same as seawater, therefore all hydrothermal fluids are believed to have experienced phase separation at some stage during their circulation through the oceanic crust.

As the fluid is phase separated, it separates out into a phase with chlorinity higher than seawater and a phase with chlorinity less than seawater. At temperatures and pressures below the critical point of seawater (407°C and 298 bar) the low chlorinity phase occurs as a vapour (sub-critical phase separation), whereas above the critical point of seawater, a small amount of high chlorinity liquid condenses from the seawater-like fluid (Super-critical phase separation). Halite also forms in some systems removing chlorinity from the fluid (Figure 1.4). Phase separation occurs when a fluid reaches sufficiently high temperature for any given depth (pressure) of hydrothermal circulation to intercept the phase boundary. To date, most fluids that have been studied have undergone phase separation below the critical point of seawater. However, in 2006 a new vent site, Turtle Pits, was discovered at 5°S along the Mid-Atlantic ridge (MAR) (German et al., 2008a). This site was found to emit fluids at 407°C, at 3000 m water depth, i.e. close to the critical point of seawater. This is the highest temperature ever measured for an end-member hydrothermal fluid and the presence of vapour bubbles observed in the venting fluids supported the interpretation that phase separation was occurring at this site, close to the critical point of seawater (Haase et al., 2007; Koschinsky et al., 2006b).

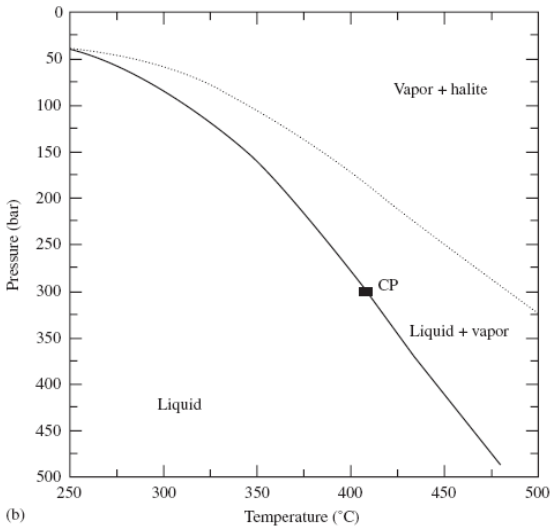

Figure 1.4 - Phase separation diagram from German and Von Damm (German and Von Damm, 2004) CP is the critical point of seawater.

In high-temperature fluids, most cations behave conservatively with chloride. Dissolved gases, by contrast, do not and are partitioned preferentially into the low chlorinity or vapour phase (German and Von Damm, 2004).

1.3 Hydrothermal plumes

As high-temperature hydrothermal fluids exit a vent, they are initially buoyant and rise between 150 and 400 m above the seafloor undergoing ~10^4-fold dilution with the surrounding water before neutral buoyancy is obtained (Lupton et al., 1985). The exact height reached by the buoyant plume is dependent both on the source fluid and the water column. The vent fluid has an initial buoyancy and is less dense than the surrounding seawater and therefore as the plume rises, it entrains denser fluid from the ambient water column. The stratification of the ambient water column then determines how far the plume will rise until it is at the same density as the surrounding seawater (German and Von Damm, 2004).

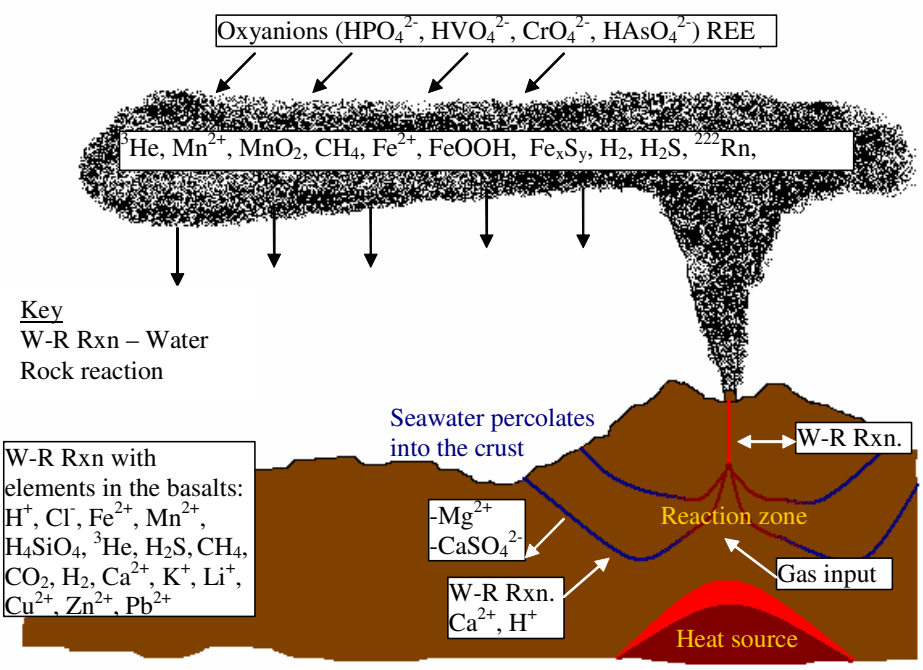

Figure 1.5 - Schematic of the chemical reactions occurring during hydrothermal cycling. Modified from http://www.pmel.noaa.gov/vents/chemistry/images/vents 2.gif

As hydrothermal fluids enter the open ocean and are diluted, they mix with oxygen rich alkaline seawater and rapidly cool from 350°C toward background deep-ocean temperatures (typically ~2°C). This quenching of a hot saturated fluid results in many of the dissolved species originally present in the vent fluids to precipitate out and deposit as sulfides, silicates, oxides and carbonates on the immediately adjacent seafloor (Figure 1.5) modifying the gross hydrothermal flux of the elements to the ocean.

Once the density of the buoyant plume matches that of the seawater, after approximately an hour after leaving the vent, the plume becomes neutrally buoyant forming non-buoyant plumes that then disperse laterally away from the vent site by deep-sea currents (Lupton et al., 1995). These plumes can be advected tens to hundreds of kilometres away from the vent source and plumes have been traced using ^3He over distances of up to 2000 km across the Pacific ocean (Jenkins et al., 1978; Jenkins et al., 1980; Lupton and Craig, 1981; Lupton et al., 2004).

When considering the impact of hydrothermal systems on the chemical composition of the oceans, black smoker chimneys are thought to be the predominant chemical source because many species only remain in solution at high temperature. Even so, entrainment of adjacent lower temperature 'diffuse flow' fluids (Mottl and McConachy, 1990) could still influence the chemical impact of these systems on the oceans. On-axis diffuse flow fluids entrain seawater in the subsurface environment and, therefore, their chemical compositions are lowered because of sub-surface precipitation (James and Elderfield, 1996a). Nevertheless the chemical composition of such fluids remains enriched when compared to background seawater. Diffuse flow is entrained along with background seawater into the high-temperature plumes and >50% of the heat within hydrothermal plumes has typically been determined to be sourced from diffuse flow (e.g. Lavelle and Wetzler, 1999; Veirs et al., 2006). Therefore even though diffuse flow fluids are not as chemically enriched as their high-temperature counterparts, entrainment of this flow into high-temperature plumes will still result in these chemicals, enriched in diffuse flow fluids, having the potential to affect ocean biogeochemistry.

1.3.1 Fe cycling in hydrothermal plumes

During the first few seconds of venting, Fe precipitates out to form polymetallic sulfides followed by Fe(II) oxidation and the formation of Fe oxyhydroxides. By contrast, Mn, which is also present in high concentrations as Mn(II), does not readily enter into any sulfide minerals and exhibits a much slower oxidation rate. Although Mn is thermodynamically unstable in its reduced (+2 oxidation state) form in the oxygenated deep-ocean, it only precipitates as oxides over time scales of days-weeks in dispersing non-buoyant hydrothermal plumes. This implies a kinetic control to oxidation and it has been widely reported that microbial activity catalyses Mn oxidation in hydrothermal plumes (Cowen et al., 1998; Cowen et al., 1986; Dick et al., 2006).

In the North Atlantic, where the mid-ocean ridge vents are bathed in oxygen rich North Atlantic Deep Water (NADW), Fe oxidation rates are fast. Rudnicki and Elderfield (1993) estimated that approximately half the dissolved Fe(II) initially present in the vent-fluids is removed as Fe sulfides in the first few seconds of venting followed by oxidation of the remaining Fe(II) in a matter of minutes. In other words, oxidation of all the Fe(II) will occur in less time than it takes for the plume to reach neutral buoyancy. Therefore all the Fe emitted from the hydrothermal vents had previously been assumed to be

quantitatively precipitated by the time of arrival at non-buoyant plume height (German et al., 1991; German et al., 1990).

Subsequently however, the following year, observations along the Juan de Fuca Ridge demonstrated the presence of dissolved Fe in non-buoyant plumes (Massoth et al., 1994) and the Fe oxidation half-life was predicted to be 32 hours (Chin et al., 1994). Certainly not all the Fe had precipitated by non-buoyant plume height. This was also seen along the EPR at 9°50'N during an in-situ filtration experiment of the particulate phase in the non-buoyant plume. Sherrell et al. (1999) observed much lower particulate Fe concentrations compared to a similar study that had been carried out in the non-buoyant plume at TAG (German et al., 1990), but also reported significant dissolved Fe concentrations: different oxidation rates appeared to be present at different vent locations.

Field and Sherrell (2000) explained these observations with the use of the theoretical oxidation rate calculation defined by Millero et al. (1987);(Equation 1.1). This equation demonstrates that Fe oxidation is dependent on oxygen concentrations and the pH in the seawater. The influence of the hydroxyl concentration is greater than the influence from the oxygen concentration because the rate of oxidation is second order with respect to OH^- and first order with respect to O_2.

$$-d[Fe(II)]/dt = K[OH^-]^2[O_2][Fe(II)] \quad (1.1)$$

Consequently, Field and Sherrell (2000) predicted that there should be a decrease in the oxidation rate of hydrothermally sourced dissolved Fe along the path of the thermohaline circulation, as both the pH and dissolved oxygen concentration decrease. At the beginning of the thermohaline cycle, North Atlantic Deep Water formation results in Mid-Atlantic Ridge vent sites being bathed in oxygen rich water. By contrast, the East Pacific Rise and Juan de Fuca Ridge vents emit fluids at the far end of the thermohaline conveyor where progressive in-situ oxidation of organic matter along this deep-ocean pathway, leads to more oxygen depleted (less oxidising) deep-ocean waters. Field and Sherrell (2000) calculated the Fe oxidation half-life for different vents sites along the

thermohaline circulation dependent on the local seawater composition at each site. The results are shown in Figure 1.6.

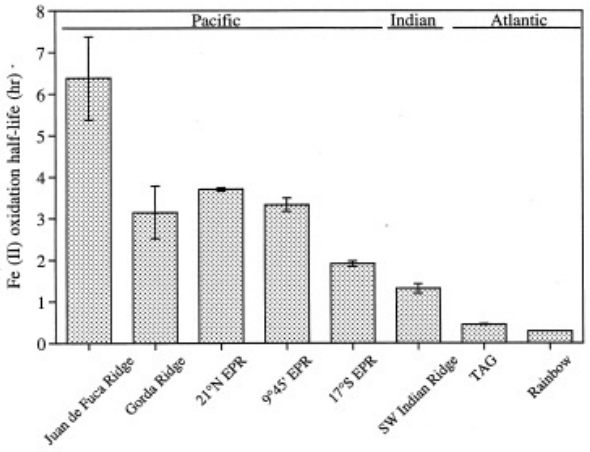

Figure 1.6 – Calculated theoretical Fe(II) oxidation half-lives at vent locations throughout the ocean basins (Field and Sherrell, 2000).

These results demonstrated that theoretically the oxidation half-lives along the thermohaline circulation should increase from ~30 minutes in the North Atlantic to ~6 hours in the Northeast Pacific. Subsequent work (Statham et al., 2005) has shown that the Fe-oxidation rates in hydrothermal plumes does, indeed, decrease progressively from the Atlantic to the Indian and Pacific Oceans. In the Indian Ocean, the experimentally determined Fe oxidation half-life was 2.5 hours but the rate of oxidation did not rigorously follow first order kinetics for either plume samples or for background water collected at plume height. This, together with the measured half-life being longer than that calculated by Field and Sherrell (2000), led to the suggestion that Fe oxidation and removal in hydrothermal plumes was not purely inorganic (Statham et al., 2005).

Previously, James and Elderfield (1996b) observed at TAG that 50% of the Fe in the non-buoyant plume was in the dissolved fraction (sample partitioned through a 0.4 µm membrane filter), even though all the Fe had already been oxidised. They explained this as due to the presence of colloidal Fe(III) species (James and Elderfield, 1996b). Apparent Fe-organic and Fe-sulfide interactions have also been speculated to be present in end-member hydrothermal fluids at the Logatchev vent-site (15°N, Mid-Atlantic Ridge)(Schmidt et al., 2007).

The oxidation rates calculated by Field and Sherrell (2000) are all less than 8 hours suggesting that within 48 hours all the Fe should have oxidised and precipitated. Therefore with a current speed of 2 cm s^{-1}, all the Fe should have precipitated within less than 5 km of the vent site and deposited to the seafloor within length scales of no more than a few tens of kilometres (Cave et al., 2002). Therefore parallel studies have examined the influence of hydrothermal particulate Fe species on trace elements and the transport of particulate material from the hydrothermal plumes to the seafloor.

1.3.2 Trace elements in hydrothermal plume particles

Early investigations of non-buoyant plumes and hydrothermal sediments demonstrated a close relationship between particulate Fe concentrations and numerous other elements. Current understanding suggests that there are three classes of behaviour with respect to Fe particles present within plumes: 1) Chalcophile co-precipitation, 2) Oxyanion co-precipitation and 3) Rare earth element (REE) scavenging (e.g. German and Von Damm, 2004).

Initially co-precipitation of chalcophile elements, including Cu, Zn and Pb, occurs during the formation and transport of polymetallic sulfides which preferential settle from the buoyant and non-buoyant plume (Edmonds and German, 2004; German et al., 1990). This results in a graphical relationship between chalcophile elements and Fe that demonstrates generally a positive correlation, but one that exhibits a negative departure from linearity as Fe sulfides are preferentially lost from the plume, relative to oxyhydroxides, at increasing distance from the vent site (Figure 1.7).

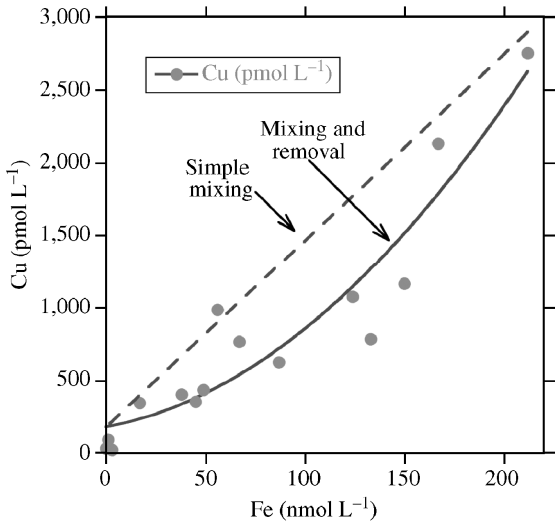

Figure 1.7 - Plot of particulate copper *vs.* particulate Fe filtered in-situ from the TAG hydrothermal mound, MAR, 26°N (German and Von Damm, 2004)

Co-precipitation is also observed for the oxyanions during the formation of Fe-oxyhydroxides. The elements appear to be incorporated into plume particles with fixed molar ratios of P, V, As, Cr and U relative to Fe (Edmonds and German, 2004; Feely et al., 1998; German et al., 1991; Trocine and Trefry, 1988). The elements are believed to be scavenged from the deep open-ocean as none of them are sufficiently enriched in end-member vent fluids. For these elements, therefore, hydrothermal plumes act as a geochemical sink. The ratio of these elements to Fe does not change on dilution or dispersal of the plume, resulting in a graphical positive correlation between the oxyanions and Fe, with no departure from linearity (Figure 1.8).

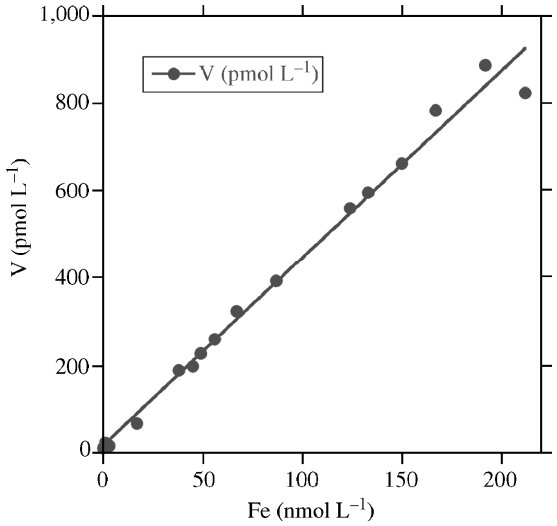

Figure 1.8 - Plot of particulate vanadium *vs.* particulate Fe filtered in-situ from the TAG hydrothermal mound, MAR, 26°N (German and Von Damm, 2004)

Finally particle reactive tracers, such as the REEs, are scavenged by Fe oxyhydroxides continuously throughout a dispersing hydrothermal plume. Other examples of particle reactive tracers are beryllium, yttrium, thorium and protactinium. They show a graphical positive correlation with Fe but this time with a positive departure from linearity, indicating increased X:Fe ratios with decreasing Fe concentrations, consistent with scavenging at increasing distance from the vent (Figure 1.9)(German et al., 2002; German et al., 1990). REEs, as one example, are scavenged from both vent fluids and ambient seawater, however the amount scavenged exceeds the dissolved flux of REEs entering from the vents. Therefore hydrothermal plumes also act as a sink for these elements. Also, close to the vents, sulfidic sediments have been observed to have REE distribution patterns similar to those of the vent fluid. This in not observed in the non-buoyant plumes because as the plumes disperse away from the source, these vent fluid distribution patterns become overprinted by REE scavenging from the surrounding seawater by Fe oxyhydroxides (German et al., 2002).

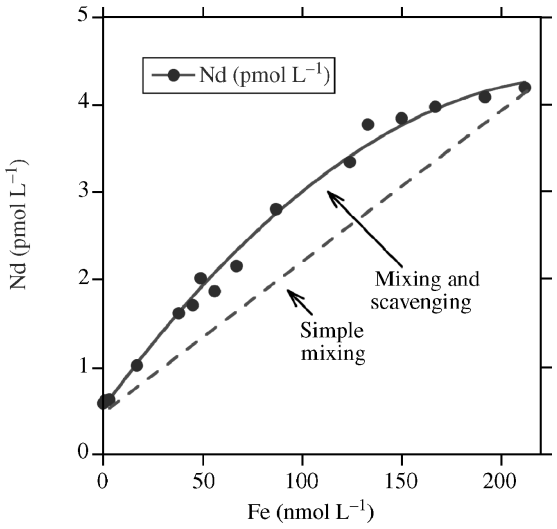

Figure 1.9 - Plot of particulate Nd *vs.* particulate Fe filtered in-situ from the TAG hydrothermal mound, MAR, 26°N (German and Von Damm, 2004)

Therefore all these trace elements which associate with particulate Fe within the hydrothermal plumes, will eventually be transported to the seafloor forming hydrothermal sediments along the ridge axis or adjacent ridge flanks (Cave et al., 2002).

1.3.3 Fe in hydrothermal sediments and deposits

Hydrothermal deposits were first documented during the Challenger Expedition from 1873 to 1876, but it was not until 1969 that these deposits were recognised to be a result of emanations coming from oceanic ridges (Bostrom et al., 1969). Hydrothermal sediments along the ridge flanks were recognised long before vents were discovered (e.g.Bender et al., 1971) and only subsequently interpreted to be the result of plume fall out and/or (for sediments close to the active vent) to be the result of mass wasting (Mills and Elderfield, 1995). As Fe particles precipitate, they settle to the seafloor to form metaliferous sediments, both close to the vent site and along the flow of the non-buoyant plume. In particular, sediments accumulating beyond the immediate vicinity of the vent fields can be important for tracing hydrothermal plume history (Lalou et al., 1990; Metz et al., 1988) More recently, Cave at al. (2002) have used the same approach within the MAR rift valley to demonstrate that vigorous high-temperature venting has been occurring at the Rainbow vent site dating throughout the past ~10 kyr.

Both Fe and Mn within hydrothermal sediments can be used as tracers of hydrothermal plumes thousands of kilometres from hydrothermal sources and it has even been suggested that hydrothermal Fe has a distinct Fe isotope signature recorded in ferromanganese crusts throughout the past 10 Ma (Chu et al., 2006). High-temperature (>300°C) vent-fluids define a narrow range in Fe isotopic composition that is shifted to low δ^{56}Fe values (by -0.2 to -0.5‰) compared to igneous rocks (Beard et al., 2003b; Severmann et al., 2004; Sharma et al., 2001). Chu et al. (2006) determined negative δ^{56}Fe values in ferromanganese crusts from the Pacific, which became more negative with increasing Fe, Mn, Cu, Zn and V concentrations reflecting pulses of hydrothermal activity. However, the most distal sample, from any ridge crest in the Central Pacific ocean would have required stabilisation of dissolved Fe to be transported that far, because rapid oxidation would have otherwise removed most of the Fe in close proximity to the vent.

1.3.4 Organic matter in hydrothermal systems

The flux of particulate organic carbon from hydrothermal plumes to the seafloor has been observed to be elevated in near field hydrothermal plumes, relative to the background deep-ocean (German et al., 2002). But within only 300 m from a vent, the organic flux to the seafloor at that site was found to be similar to the background flux. However, very recent work by Toner et al. (2007) has demonstrated that organic carbon present in sediment traps deployed below a hydrothermal plume at 9°50'N EPR, coats particulate Fe(II) and Fe(III). Of particular relevance to this study, the Fe(II) is found to be stable in the presence of oxygen on time scales that exceed the calculated Fe(II) oxidation half-life. This, therefore, supports the hypothesis that organically complexed Fe species may be stable within hydrothermal plumes.

A variety of organic compounds have been identified in the deep-sea hydrothermal environment, ranging from simple compounds like methane and ethane to more complex compounds such as long-chain hydrocarbons, fatty acids and polycyclic aromatic hydrocarbons (McCollom and Seewald, 2007). What, then is the source of the organic carbon in these plume systems?

It is unlikely that the end-member vent-fluids are a source of organic carbon, because complex organic molecules are only stable in high-temperature vent fluids under exceptional circumstances. For example in either sediment-hosted hydrothermal systems (e.g. Guaymas basin, Middle Valley, Juan de Fuca Ridge) (Cruse and Seewald, 2006; Pearson et al., 2005) or, in bare-rock environments, at ultramafic-hosted vents sites such as the Rainbow hydrothermal field, MAR (Holm and Charlou, 2001). However, in diffuse flow areas at a basalt hosted system, dissolved organic carbon concentrations have been observed that reach concentrations of 39 - 69 μM, up to approximately double background deep-ocean waters (Lang et al., 2006). Diffuse systems, typically, host the most abundant chemosynthetic communities associated with seafloor hydrothermal venting and biological activity at these sites will presumably increase the organic carbon present within these systems. Therefore, entrainment of diffuse fluids into high-temperature plumes could provide a source of dissolved organic carbon to these hydrothermal plumes, which will be important if there is to be any stabilisation of dissolved Fe within these systems.

Microbial activity occurring at plume-height is another potential source of organic carbon for Fe complexation. Karl et al. (1988) reported a high abundance of bacteria only 25 cm above a vent orifice. These organisms must have been entrained into the plume from the surrounding area because they would not survive in the high-temperatures within the vent orifice. Higher up in the water column, non-buoyant plumes have also been observed to have chemolithotrophic based carbon production (reviewed by Cowen and German, 2003). In-situ production via chemolithoautotrophic and chemoheterotrophic bacteria occurs through the oxidation of CH_4 and H_2. On the EPR, long chain alkanes were detected up to 3 km from the vent site and were determined to be microbially mediated (Simoneit et al., 1990). In the case of Mn, microbially mediated oxidation of dissolved Mn(II) has been long established (Cowen and Bruland, 1985; Cowen et al., 1986). More recently, it has been hypothesised that Fe(II) oxidation may form the basis of chemosynthetic ecosystems in the water column, overlying the MAR (Zbinden et al., 2004).

Clearly, therefore, the potential exists for dissolved organic complexes to form within hydrothermal plumes as well as through entrainment of organic-rich diffuse flow fluids and background seawater that might lead to the stabilisation of dissolved Fe.

1.4 Structure and outline

This thesis aims to examine the influence of hydrothermal activity on the biogeochemistry of Fe in the ocean. Specific questions to be addressed are:

1) What are the concentrations of dissolved organic carbon present within high-temperature hydrothermal plumes, whether entrained or produced in-situ, that may have the potential to stabilise dissolved Fe?

2) If elevated concentrations of dissolved organic carbon are present in hydrothermal plumes, do these species form stabilised dissolved Fe-ligand complexes that can be exported to the deep-ocean?

3) Is there a diagnostic δ^{56}Fe isotope signature for any hydrothermally source dissolved Fe exported to the deep-ocean?

These questions will be addressed in order in the thesis as outlined below:

- Chapter 2 describes the methods used for collecting and analysing all samples, along with general procedures used throughout the work for trace element sample collection and analysis.

- Chapter 3 introduces the geological settings of the hydrothermal sites from which samples were collected and analysed. Two sites have been visited in this study, at 9°50'N along the East Pacific Rise and at 5°S along the Mid-Atlantic Ridge.

- Chapter 4 discusses the distributions of DOC and POC determined for samples collected at 9°50'N EPR. DOC and POC concentrations in buoyant plume samples collected above various vent orifices by submersible are compared to corresponding Fe and Mn concentrations. DOC and POC concentrations in CTD rosette samples collected from one buoyant plume and two non-buoyant plume profiles are also described relative to particulate concentrations in the water column.

- Chapter 5 analyses the concentrations of dissolved and total dissolvable Fe within non-buoyant plumes at 5°S MAR relative to the plume's distance from the nearest vent site. Select samples are analysed for dissolved organic Fe speciation.

- Chapter 6 introduces a unique set of samples which bisect a buoyant plume at 5°S and uses in-situ sensor data and elemental analyses to determine the context for where these new samples were collected.

- Fe isotope analysis of these same samples is then described in Chapter 7 and compared to the isotope composition of vent fluids collected from the same site.

- Finally in Chapter 8, I draw conclusions from the study as a whole and identify key future directions that should be followed to extend this study.

Chapter 2. Methods

2.1 Trace metal analysis – cleaning procedures

Within the ocean metal concentrations are extremely low. Fe is the 4th most abundant element in the Earth's crust yet in the ocean Fe concentrations are typically very low, less than 1 nM (de Baar and de Jong, 2001). Therefore a number of precautions must be taken during the sampling and analysis of seawater samples to avoid contamination. Sampling equipment and containers must have no metal in contact with the sample and be acid cleaned to remove any trace metals. When dealing with the samples a clean laboratory coat and gloves should be worn and human contact should be kept to a minimum where possible.

For this PhD work, analytical work was carried out both at the National Oceanography Centre, Southampton (NOCS) and Woods Hole Oceanographic Institution (WHOI), USA, and cleaning procedures varied slightly between the two institutions because of different set-ups. The following protocols were used throughout the PhD programme to minimise contamination.

2.1.1 Cleaning procedure of sampling equipment and containers

- Niskin/OTE (Ocean Test Equipment) bottles

Bottles were rinsed with seawater during a 'shake-down' station - a test run of the CTD equipment in the open ocean. The bottles were returned to the ship full of seawater and were spiked with HCl (final concentration 10%), in order to dissolve any metals within the seawater or adsorbed onto the Niskin bottle/OTE bottle. These were left to soak until required for sample collection.

- LDPE (Low density polyethylene) and Teflon bottles, Teflon vials, Teflon separating funnels and general equipment (@NOCS)

1. Week soak in Decon, followed by MQ rinse (Ultra pure deionised water (>18.2 MΩ cm^{-1}) dispensed from a Millipore Milli-Q system)

2. Three day soak in 50% HCl, followed by MQ rinse

3. Three day soak in 50% HNO_3, followed by MQ rinse, sub-boiled distilled water (SBDW – preparation described below) rinse and dried in a laminar flow hood

- Teflon vials had an additional cleaning step:

4. 5 ml concentrated HNO_3 in each vial, refluxed on a hotplate, followed by a SBDW rinse

- LDPE bottles (@WHOI – more concentrated samples)

1. Rinse in MQ water

2. Three day soak in 50% HCl, followed by MQ rinse

- Teflon vials (@WHOI)

1. Rinse in MQ water

2. Soak overnight in simmering 50% HNO_3, followed by MQ rinse

3. 5 ml concentrated HNO_3 in each vial, followed by MQ rinse

- Membrane filters

Membrane filters were soaked overnight in 10% nitric acid and thoroughly rinsed with MQ before use.

2.2 Reagent preparation

2.2.1 Sub-boiled distilled water (SBDW)

Ultra pure water was prepared by a distillation set up in a laminar flow hood. The MQ water was heated up in a quartz flask using two infra-red lamps. The water evaporated and condensed onto to a cold quartz finger running through the flask. The clean water then dripped into an acid cleaned Teflon bottle.

2.2.2 Nitric acid (Q-HNO_3) and Hydrochloric acid (Q-HCl)

Both HNO_3 and HCl (Fisher Scientific) were further purified using the same distillation apparatus as used for SBDW preparation

2.2.3 Ammonia (I-NH_4-OH)

Ammonia was isothermally distilled for purification. The ammonia partitioned itself between the impure ammonia solution and SBDW, in a closed container.

2.2.4 Mixed complexant

For solvent extraction of dissolved Fe and Mn (Section 2.4), a complexant was required. This consisted of 2% w/v ammonium 1-pyrrolidine dithiocarbamate (APDC, Sigma Aldrich) and 2% w/v diethyldithiocarbamic acid, as the diethyl ammonium salt (DDDC, Sigma Aldrich) dissolved in SBDW and filtered through a GF/F Whatman filter (0.7 µm, 47 mm diameter). The solution was poured into a Teflon separating funnel along with 5 ml of HPLC grade chloroform ($CHCl_3$, Fisher Scientific). The separating funnel was rotated for 6 minutes and after separation of the reagents, the $CHCl_3$ was discarded. This was repeated three times and the final solution was stored refrigerated in a Teflon bottle for a maximum of four days.

2.2.5 Synthetic ligands – TAC, 1N2N and SA

For Fe speciation studies (Section 2.6) a synthetic competitive ligand was required with a stability constant with Fe much greater than any potential natural ligands present. A 10 mM stock solution of 2-(2thiazolylazo)-p-cresol (TAC, Sigma Aldrich) and 1-nitroso-2-napthol (1N2N, Fluka) were each prepared in HPLC grade methanol (MeOH). Salicyaldoxime (SA, Sigma Aldrich Germany GmbH) was prepared in 0.1 M Q-HCl to the same concentration.

2.2.6 EPPS buffer

Also for Fe speciation studies a buffer was required. A 1.0 M trace metal buffer, N-(2-hydroxyethyl)piperazine-N';-2-propanesulfonic acid (EPPS) was prepared in MQ water, brought up to pH 8 with I-NH_4OH and cleaned through a Chelex 100 resin column (Bio-Rad) to remove trace metal cations (Donat and Bruland, 1988).

2.3 Sample collection

2.3.1 Cruise 1 – AT05-04 – Buoyant and non-buoyant plume sampling in the Pacific (Active participation)

For organic carbon analysis, a suite of water column samples were collected by CTD rosette from both buoyant and non-buoyant plumes using 10-litre OTE bottles internally sprung with silicone tubing. These were mounted in a CTD rosette consisting of a SeaBird SBE 9/11+ system coupled with a 24-position rosette. Water samples were collected based on real-time feedback from the CTD and in particular, the in-situ turbidity sensor, interfaced into the SeaBird CTD. Samples were also collected from directly above the vent orifice using 1 L externally sprung Niskins operated by the deep sea submersible, DSV *Alvin*. The samples were collected based on observations of black smokey water as seen through the port holes of the submarine and increases in temperature (up to 15°C).

On recovery of the CTD rosette or DSV *Alvin* to the ship, water samples were collected directly from the OTE/Niskin bottle into Teflon bottles (with 3-fold rinsing). A sub-sample of water collected directly above the vent orifice was collected in acid cleaned LDPE bottles and acidified to pH 1.6 using HNO_3 (Fisher Scientific, OPTIMA grade). In the laboratory, under a plastic, clean area, the samples were filtered through pre-combusted (400°C, >4 hours) GF/F filters (0.7 μm, 25 mm diameter, Whatman) into 40 ml I-CHEM, certified low level total organic carbon (TOC) vials. These were acidified with 40 μl trace metal HCl (Fisher Scientific, stored in glass) to pH 2 and stored at 4°C until analysis back in a land based laboratory. The GF/F filters were retained frozen, folded in combusted foil and the volume of filtered seawater was recorded to enable quantitative analysis of the particulate material.

2.3.2 Cruise 2 – CD169 – Buoyant and non-buoyant plume sampling in the Southern Atlantic (Active participation)

A suite of water column samples were collected by CTD rosette from both buoyant and non-buoyant plumes using 10-litre externally sprung Niskin bottles mounted in a CTD rosette consisting of a SeaBird SBE 9/11+ system coupled with a 24-position rosette mounted in a stainless steel frame. Water samples were collected based on real-time

feedback from the CTD and in particular, the in-situ transmissometer, interfaced into the SeaBird CTD.

On recovery of the CTD rosette, water samples were collected directly from the Niskin bottle into acid cleaned LDPE 1 L bottles (with 3-fold rinsing) for the analysis of total dissolvable Fe and Mn (TdFe and TdMn). These samples were then acidified to ~pH 1.6 using 1 ml quartz distilled concentrated HNO_3 (Q-HNO_3) per L. In a clean laboratory on board the ship, a portion of the remaining water was filtered under pressure (N_2 gas) through a 0.4 µm membrane filter (Whatman polycarbonate, 47 mm) that had been acid cleaned. The filtrate was collected into 2x acid cleaned LDPE 125 ml bottles for the analysis of dissolved Fe and Mn (dFe and dMn) and these samples were later acidified to pH 1.6 using Q-HNO_3. A sub-sample (~500 ml) of filtered water was taken from selected bottles, collected in acid cleaned Teflon bottles and immediately frozen for speciation studies. The filters were retained frozen in small polystyrene containers and the volume of seawater filtered through each membrane was recorded to enable quantitative analysis of the particulate material.

2.3.3 Cruise 3 – M68/1 - Vent fluid collection in the Southern Atlantic (No participation)

The vent sites discovered during CD169 were revisited the following year by a German group on board the FS Meteor during cruise M68/1. End-member fluids were collected by the Germans using a pumped flow-through system (Kiel pumping system, KIPS) made entirely of inert materials (perfluoralkoxy (PFA), polytetrafluorethylene (PTFE), and high purity titanium), operated by the remotely operated vehicle (ROV), MARUM Quest. A titanium nozzle was inserted directly into the vent orifice and the sample was pumped through PFA tubing into PFA sampling flasks. Parallel to the nozzle was an on-line temperature probe monitoring the in-situ temperature. The tubes and bottles were rinsed with hydrothermal fluid for a couple of minutes before sampling.

All KIPS samples were sub-sampled in the ship's laboratory immediately after recovery of the ROV in a class 100 clean bench (Slee, Germany). After sub-sampling for dissolved gas analysis, an aliquot of the original fluid was transferred into an acid cleaned polyethylene (PE) bottle (50 ml) and acidified with sub-boiled HNO_3 until all the precipitate had been dissolved. For some fluid samples, the precipitates had to be

dissolved by pressure digestion with HCl, HNO_3, and HF, followed by re-homogenization of the fluid sample. The remaining hydrothermal fluid was filtered under pressure (Argon, 99.999%) through a pre-cleaned 0.2 µm Nuclepore PC membrane filter using polycarbonate filtration units (Sartorius, Germany). An aliquot of the filtrate was acidified to pH 1 using sub-boiled concentrated HNO_3 in an acid cleaned (PE) bottle (50 ml).

2.4 Quantification of Fe and Mn in water samples

2.4.1 Background to Atomic Absorption Spectroscopy

Atomic absorption spectroscopy has been one of the preferred techniques for trace metal analysis since the 1980s (Gordon et al., 1982; Landing and Bruland, 1987) and involves a net absorption of radiation. The analyte atoms are first vaporized in a graphite furnace and a radiation frequency is chosen depending on the element to be analysed. The atoms absorb ultraviolet or visible light and make transitions to higher electronic energy levels. The analyte concentration is determined from the amount of absorption (Atkins, 1999).

Due to the trace quantities of Fe present in our samples, a pre-concentration step was required prior to Graphite Furnace Atomic Absorption Spectroscopy (GFAAS) involving chelation of the metals in the seawater with ammonium 1-pyrrolidine dithiocarbamate (APDC) and diethyldithiocarbamic acid, as the diethyl ammonium salt (DDDC)(See Section 2.2.4) followed by solvent extraction with $CHCl_3$ and back extraction into Q-HNO_3 (Bruland et al., 1979; Statham, 1985). Detection limits were determined by the levels present in a SBDW blank (Landing and Bruland, 1987).

2.4.2 Procedure

In a Class 100 clean room, under a laminar flow hood, a ~100 ml sample of seawater was accurately weighed into a 250 ml Teflon separating funnel. The seawater was neutralized with I-NH_4OH to pH 7 – 8.5, tested by taking a 60 µl sub-sample and using a hand held pH meter. To this sample 3 ml of mixed reagent was added followed by 3 ml of HPLC grade $CHCl_3$. The sample was then mixed on a mechanical rotating table for 6 minutes and then left to allow the phases to separate. The denser chloroform layer was drawn off and retained in a labelled Teflon pot (25 ml). The addition of $CHCl_3$ and

mixing was repeated twice more with 2 ml aliquots, giving a total volume of 7 ml of $CHCl_3$ extract in the Teflon vial.

100 µl HNO_3 was added to each $CHCl_3$ extract and the Teflon vials were placed on a Teflon coated hotplate (80°C) in order to evaporate off the $CHCl_3$. This was followed by the addition of 50 µl of HNO_3 which was again evaporated. To the dry residue, 100 µl HNO_3 was added, followed by 400 µl SBDW. The sample was then poured into a small acid cleaned vial, followed by a further 500 µl of SBDW used to wash any residue into the vial. This gave a total sample volume of 1 ml.

The extract was analysed for Fe and Mn by GFAAS using a Perkin Elmer AAnalyst 800 Atomic Absorption Spectrometer fitted with an auto-sampler. Fe and Mn, standards were prepared in 0.1% Q-HNO_3 from a series of dilutions of a 1000 µg L^{-1} standard (Sigma Aldrich Germany GmbH). These standards were diluted and used to calibrate the instrument; results were obtained in µg L^{-1} units. Results were processed according to the dilution and the mass of water extracted and final values reported in nanomoles per L (nM). Each sample was measured in triplicate and samples with standard deviations over 10% were reanalysed.

2.4.3 Detection limits and comparison with a standard seawater

A standard low metal seawater (LMSW), that has been repeatedly analysed for the last four years for precision and accuracy of the GFAAS technique, and a blank solution, were analysed at the beginning of each new batch of complexant (Table 2.1). This LMSW is directly traceable to a certified reference material.

Table 2.1 - Repeated blank and LMSW analysis results (Four blanks and four LMSW were measured for each new batch of complexant)

	Blank			LMSW	
	TdFe	**dFe**	**TdMn / dMn**	**Fe**	**Mn**
Average (nM)	0.49 (n=8)	1.19 (n=4)	0.09 (n=12)	72.3 (n=12)	2.34 (n=12)
Standard deviation	0.12	0.4	0.06	5.6	0.37

The limit of detections for Fe and Mn were determined to be 0.36 nM for TdFe and 1.2 nM for dFe and 0.18 nM for Mn (n = 3). The blank was seen to increase during the sample processing because of a 'carry over' effect from previous samples and this was taken into account when blank correcting the samples. The relative standard deviation for Fe analysis was 7.7% and for Mn analysis was 15.8%, calculated from repeat analysis of the LMSW standard.

2.5 Quantification of trace elements and Fe isotopes in particulate samples and vent fluids

2.5.1 Background to Inductively Coupled Plasma – Mass Spectrometry (ICP-MS)

Mass spectrometry is a sensitive analytical technique used to measure the mass to charge ratio of ions in a sample. It can be used to quantify the elemental composition of the sample as well as determine the isotopic compositions.

During analysis the sample is vaporised and bombarded with electrons to ionise the elements. These charged ions are accelerated through a potential field, focused through metal slits and then deflected, dependent on their mass, by a magnetic field onto a detector. The amount of deflection can be used to calculate the mass to charge ratio of the ion and from this the isotopic and chemical composition of the sample can be determined. Many elements can be analysed at the same time, making this a very efficient technique.

Until recently, the analysis of stable isotopes was restricted to light elements (e.g. H, C, N, O and S). Heavier elements such as Fe experienced precision errors and samples needed large isotopic shifts in order to observe differences. However, the recent advent of Multi-Collector Inductively Coupled Plasma Mass Spectrometers (MC-ICP-MS) has solved many of the previous problems, now making Fe isotope analysis a routine laboratory procedure (Dauphas and Rouxel, 2006).

2.5.2 The challenges involved with Fe isotope analysis

In preparation for isotopic analysis, the Fe must be separated from any isobaric elements that could potentially interfere with the various Fe isotopes, 54, 56, 57 and 58 (e.g. ^{54}Cr, ^{58}Ni, $^{40}Ar^{14}N$, $^{40}Ar^{16}O$, $^{40}Ar^{16}O^{1}H$ and $^{40}Ca^{16}O^{1}H$) and from any seawater matrix that could affect the mass bias of the mass spectrometer. Mass bias is the deviation of the measured isotope ratio from the true value caused by the different sensitivity of the instrument to mass and resulting in an observed preferential transmission of heavier ions over lighter.

Fe was separated using anion exchange chromatography in a HCl medium. The procedure results in the retention of Fe on the column at high molarity whilst any matrix species are removed. After matrix removal the Fe is eluted with a low molarity HCl solution (Rouxel et al., 2003).

High mass resolution techniques have been used throughout this isotope study to eliminate spectral interferences caused by the use of Argon gas that is used to generate the plasma. This technique enables the separation of molecular interferences from the Fe isotopes. The typical precision is less than 0.1 ‰ for $^{56}Fe/^{54}Fe$ and $^{57}Fe/^{54}Fe$ (Rouxel et al., 2005).

Even with the elimination of the sample matrix, mass bias can vary with time and instrumental set-up and therefore comparison with a known standard must be carried out before and after every sample measurement. This is known as the standard-sample bracketing method. The reference material routinely used is IRMM-014, from the Institute for Reference Materials and Measurements of the European Commission (Taylor et al., 1992).

2.5.3 Fe isotope representation

Iron isotope measurements are calculated relative to the isotopic composition of a reference material. This gives a δ value quantified in permil (‰).

$$\delta^{i}_{j}\,Fe = [(^{i}Fe/^{j}Fe)_{sample} / (^{i}Fe/^{j}Fe)_{standard} - 1] \times 10^{3} \qquad (2.1)$$

Table 2.2 shows the four stable isotopes of Fe and their natural abundance. Therefore 12 different δ values can be calculated from these four isotopes (Dauphas and Rouxel, 2006).

Table 2.2 – Isotope composition of natural iron

^{54}Fe	^{56}Fe	^{57}Fe	^{58}Fe
5.8%	91.8%	2.1%	0.3%

2.5.4 Background to Inductively Coupled Plasma – Optical Emission Spectrometry (ICP-OES)

ICP-OES is again a sensitive technique used to measure elemental concentrations. The instrument uses an argon plasma to dissociate the sample into its constituent atoms or ions and excites them to a level where they emit light of a characteristic wavelength. Light from the plasma and the atomic emissions are then detected axially and radially through a polychromator which separates the light into its component wavelengths. Again many elements can be analysed at the same time, making this an efficient technique.

2.5.5 Procedure – Extraction of particulate material from the filters

Elemental analysis was carried out both at WHOI and at NOCS. The most concentrated samples collected from a buoyant plume were analysed at WHOI for major, trace, rare earth elements (REEs) and Fe isotopes. Samples from the non-buoyant plume were analysed at NOCS for major elements only.

Both elemental analysis and isotopic analysis required the same initial filter digestion in order to extract the elements. In a clean room under a laminar flow hood, 47 mm filters

were heated to reflux in 10 ml of concentrated HNO_3 (WHOI – Fisher Scientific OPTIMA grade, NOCS – Q-HNO_3) in closed 30 ml acid cleaned Teflon vials for 72 hours. This procedure allows for the digestion of the sulfide and oxide phases, leaving behind the majority of the filter material and therefore minimising organic interference (German et al., 1991). Blank filters and empty vials were treated in the same way to give reagent blanks and procedural blanks. At WHOI, a background filter that had filtered 1 L of background seawater was used for the procedural blank, in the absence of an unused acid clean filter.

2.5.6 Preparation of extracted particulate material for major element analysis at NOCS

At NOCS, a 9 ml fraction of the extract was sampled, avoiding any disintegrated filter, using a clean pipette tip and transferred to an acid cleaned 15 ml Teflon vial. The solution was evaporated to dryness on a hot plate and re-dissolved in 1 ml Q-HNO_3 and 9 ml SBDW. This solution was directly analysed (due to expected low concentrations) with Inductively Coupled Plasma – Optical Emission Spectrometry (ICP-OES) by Darryl Green on a Perkin Elmer Optima 4300DV at NOCS. Stock 1000 µg L^{-1} standards (Specpure, Spex) of each element of interest were diluted with four varying concentrations in preparation for instrument calibration.

A marine mud standard, MAG-1, from the U.S. Geological Society was treated in the same way as the samples and used as a reference material. Table 2.3 shows the accuracy obtained during the analysis. In sample 1, too much sample was extracted relative to the standards used to calibrate the instrument, and in sample 2, even though less sample was extracted, the sample concentration was still greater than the standards, but better accuracy was obtained. All the elements could be accurately measured except for Al, which would have required an HF digestion, in order to completely destroy the aluminosilicate mineral structures in the marine mud. A residue remained after digestion of the mud, whereas no residue except for the filters remained during the filter digestion. It has already been shown that this digestion method enables extraction of both sulfide and oxide material (German et al., 1991).

Table 2.3 - Results from analysis of a certified reference material (MAG)

	MAG	Sample 1		Sample 2	
	Certified (mM)	Actual (mM)	%	Actual (mM)	%
Fe	852.1	703.9	83	795.8	93
Mn	13.8	13.2	96	13.4	97
Al	3211.1	792.8	25	264.3	8
Mg	744.1	744.6	100	748.5	101
Ca	238.8	250.5	105	238.4	100
Cu	0.5	0.5	104	0.5	101
Zn	2.0	2.2	111	2.1	107
Na	1226.2	1255.5	102	1227.0	100

The limit of detection of the technique is shown in Table 2.4, determined by repeat analysis of an acid blank (n=3). The filter blank, used for blank correcting the samples is also shown. The Zn, Fe and Al blank values were the most significant relative to their concentrations in the particulate material. However, the particulate samples were 100 times more concentrated during analysis.

Table 2.4 - Detection limits determined from blank acid analysis (n=10) and elemental concentrations from a blank filter (dl = detection limit).

	Acid blank dl (n=3)	Blank filter
Fe (nM)	16.54	1.42
Mn (nM)	0.90	0.01
Al (nM)	14.22	0.37
Mg (µM)	0.01	0.01
Ca (µM)	0.02	0.004
Cu (nM)	2.07	0.05
Zn (nM)	24.04	0.77
Na (µM)	0.10	0.05

2.5.7 ICP-OES for near-field plume samples

Analysis of Fe and Mn in the near-field plume samples collected directly above the vent orifice during AT05-04 were also carried out at NOCS using ICP-OES. A 4% dilution of each sample was carried out in 0.4 M Q-HNO_3 and directly measured using ICP-OES on a Perkin Elmer Optima 4300DV by Darryl Green at NOCS. Stock 1000 µg L^{-1} standards (Specpure, Spex) of Fe and Mn were diluted with four varying concentrations in preparation for instrument calibration within a standard 4% seawater matrix along with a blank solution containing just the 4% seawater matrix. A 4% IAPSO standard seawater was also run, even though it contained very low Fe and Mn concentrations, to check for contamination. The limit of detection of the technique is shown in Table 2.5, determined by repeat analysis of the seawater matrix blank. The detection limit values are relatively high, but relative to the samples (µM concentrations) these values are low.

Table 2.5 - Detection limits determined from blank seawater matrix analysis (n=10)

	Acid blank dl (n=3)
Fe (nM)	6.5
Mn (nM)	1.3

2.5.8 Preparation of extracted particulate material for major and trace element analysis at WHOI

At WHOI, a 1:100 dilution of the mother/initial solution with 2% HNO_3 was directly analysed with ICP-MS on a ThermoFinnigan Element2 at WHOI using medium resolution and a spray chamber for sample injection. Indium (final concentration 5 ppb) was added to each sample as an internal standard to correct for changes of instrument sensitivity. The detection limits are discussed in Section 2.5.10.

2.5.9 Preparation of particulate material for REE analysis and particulate material and vent fluids for isotope analysis at WHOI

The Teflon vials containing the initial solution of leached filters were placed on hot plate and the solution was evaporated to dryness. The solid residue was redissolved in 10 ml 1% HNO_3 in a closed vial with gentle warming. The samples were then centrifuged and separated from the filter remaining after the evaporation step. A known quantity of the solution was returned to the original Teflon vial and evaporated to dryness.

Preparation of the vent fluids for isotope analysis involved evaporating to dryness a known quantity of vent fluid. Depending on its concentration, between 3 to 5 ml of hydrothermal fluid was evaporated in an acid cleaned Teflon vial and then treated along with the other particulate samples using the following method.

The analytical procedure required for isotope analysis follows Rouxel et al. (2003) and Rouxel et al. (2007). The sample residue, after the digestion step, was dissolved in 4 ml of 6 M distilled HCl in a closed Teflon vial on a hot plate. After the sample had been left to cool, one drop (~ 10 µl) of H_2O_2 was added to prevent the possible reduction of Fe

during purification and to ensure complete oxidation of any residual ferrous Fe. The samples were then left for 24 hours to allow for complete degassing of the solution.

A precise volume of this solution, calculated from the initial elemental analysis carried out at WHOI, was then purified using anion exchange chromatography in an HCl medium. A 5 ml column was loaded with 1.5 ml Bio-Rad AG1-X8 anion resin 200 – 400 mesh (chloride form) which was acid cleaned with 10 ml 2 M HNO_3, 10 ml MQ water and 10 ml 2% Q-HCl and finally conditioned with 5 ml 6 M Q-HCl. Under these conditions, Fe was adsorbed onto the anionic resin and the sample matrix and REEs were further eluted using 17 ml of 6 M Q-HCl. For the extracted particulate samples, this fraction was collected in Teflon vials and evaporated to dryness. The remaining residue was dissolved in 2 ml of 2% HNO_3 and analysed for 14 REEs and Y by ICP-MS on a ThermoFinnigan Element WHOI, using an aridus desolvation chamber and low resolution. Again, Indium (5 ppb) was added to the samples as an internal standard to correct for mass bias.

Fe was then eluted from the column with 16 ml 0.24 M HCl, collected in Teflon vials and evaporated to dryness. The residue was re-dissolved in 2-3 ml of 2% HNO_3 and then further diluted to form a 1 ppm or 3 ppm Fe solution ready for isotope analysis.

Analyses of $^{56}Fe/^{54}Fe$ and $^{57}Fe/^{54}Fe$ were carried out on a ThermoFinnigan Neptune MC-ICP-MS by Olivier Rouxel at WHOI. Mass resolution power of about 8000 (medium resolution mode) was used to resolve isobaric interferences, such as ArO on ^{56}Fe, ArOH on ^{57}Fe, and ArN on ^{54}Fe. The samples were introduced into the plasma using a double spray quartz spray chamber system (cyclonic and double pass) and a microconcentric PFA nebulizer operating at a flow rate of about 200 µl min^{-1}.

Instrumental mass bias was corrected for using Ni isotopes as an internal standard and involves simultaneous measurement of a Ni standard solution (Malinovsky et al., 2003). Also a standard bracketing approach, which normalises the Fe isotope ratio to the average measured composition of a standard (IRMM-14) was carried out before and after each sample. The two methods combined, permits the verification of any instrumental artefacts generated by residual matrix elements.

^{54}Fe, ^{56}Fe, ^{57}Fe, ^{60}Ni and ^{62}Ni isotopes were counted on Faraday cups using the medium mass resolution mode. Baseline corrections were made before acquisition of each data block by completely deflecting the ion beam. Although separated, ^{52}Cr interferences were always checked before each sample analysis, using peak jumping mode of the Neptune. Purified particulate samples with low Fe concentrations were also analyzed using a desolvation nebulizer (Cetac Apex) and X-cones (Thermo-Finnigan) to improve the sensitivity of the Neptune (Schoenberg and von Blanckenburg, 2005).

The internal precision of the data have 95% confidence levels based on isotopic deviation of the bracketing standards analysed during the session. The isotopic composition of the IRMM standard processed through the entire extraction procedure was 0.09‰ and was observed to be indistinguishable from pure solutions (Table 2.6). Any isotopic influence from the filter was too low to be an issue because of the low Fe concentrations (Table 2.4)

Table 2.6 - Results from analysis of a certified reference material (IRMM-014). The isotope composition of a pure IRMM-014 was measured and compared to three samples of IRMM-014 that had been processed through the sample extraction procedures (s.d. = standard deviation).

	$\delta^{56}Fe$	1 s.d.	$\delta^{57}Fe$	1 s.d.
IRMM-014	0.09	0.1 (2σ)	0.11	0.14 (2σ)
Ref 1	0.07	0.09	0.16	0.14
Ref 2	0.12	0.09	0.19	0.12
Ref 3	0.08	0.07	0.13	0.10

2.5.10 Detection limits of ICP-MS and comparison with standard rock samples

Stock 1000 µg L^{-1} standards (Specpure, Spex) of each element of interest were diluted in preparation for instrument calibration. The limits of detection of the technique are shown in Table 2.7 and Table 2.8, determined by repeat analysis of an acid blank. Again these blanks look big compared to the values on the filters, however the samples measured were 6 times more concentrated than their actual value ([Fe] = 6 x (20 to 300 nM). The blank filter, used for blank correcting the samples is also shown. The large blank values of Mg, S and Ca are due to the seawater matrix, because 1 L of background seawater had

been filtered through this filter. The other elements appear to be low relative to the concentrations in the samples (6 L of sample filtered). The blank values from the ICP-OES experiment were therefore used to correct for Mg, S and Ca present in the filter and the Cr values were treated with caution.

Table 2.7 - Detection limits determined from blank acid analysis (n=10) and elemental concentrations from a filter blank for major and trace elements (RSD = relative standard deviation).

	Acid blank			Filter blank
	(nM)	%RSD	dl (n=3) (nM)	(nmoles)
Mg	38.4	25	28.4	909
Al	42.5	57	73.0	0.48
P	43.8	27	3.5	0
S	280.9	6	51.3	299
Ca	553	13	208.2	186
Ti	1.6	64	3.1	0.0081
V	0.16	48	0.2	0.0532
Cr	0.12	36	0.12	0.97
Mn	0.44	18	0.24	0.16
Fe	8.7	44	11.6	4.5
Co	0.03	47	0.03	0.002
Ni	4.0	17	2.0	0.007
Cu	2.95	5	0.5	0.25
Zn	10.28	11	3.5	0
Mo	0.05	103	0.2	0.009

For the REEs, a processing blank was taken through all the purification processes, adding the eluent to an untreated separating column, to confirm that no contamination was present due to the AG1-X8 anion resin. These blank values were low relative to the concentrations in the samples, as were the instrument blanks.

Table 2.8 - Detection limits determined from blank acid analysis (n=10) and elemental concentrations from a filter blank for REEs.

	Acid blank			Processing blank	Filter blank
	($x10^{-5}$) (pM)	%RSD	dl ($x10^{-5}$) (n=3)(pM)	($x10^{-3}$) (pM)	(pmoles)
Y	40.5	44	53.4	32.5	0.86
Ba	1430	55	2364	4859	171.5
La	30.0	73	65.4	20.9	0.45
Ce	35.4	65	69.0	40.7	1.07
Pr	9.6	124	35.7	4.0	0.12
Nd	33.4	42	42.0	17.2	0.44
Sm	10.1	40	12.0	3.7	0.09
Eu	12.0	35	16.6	1.5	0.02
Gd	18.9	20	11.4	5.5	0.08
Tb	2.9	24	2.1	1.0	0.01
Dy	6.0	41	7.5	9.6	0.08
Ho	1.1	57	1.8	2.9	0.02
Er	3.4	63	6.6	10.9	0.05
Tm	1.0	70	2.1	2.0	0.01
Yb	6.4	36	6.9	13.9	0.04
Lu	2.3	55	3.9	2.5	0.01

The filter blank for REE was similar to the least concentrated sample and 20 times less than the most concentrated sample. Remembering that this filter had had seawater filtered through it, it was difficult to determine whether this was due to the filter or the seawater residue (filters were not rinsed with MQ at sea). However, the REE concentrations on the filters would have been six times greater again because 6 L of hydrothermal plume water had been filtered through them, making this blank less of an issue, certainly for the most concentrated samples. The REE data correction will be discussed further in Chapter 6.

A number of rock standards were prepared from a variety of sources including the U.S. Geological Survey and Centre de Recherches Petrographiques et Geochimiques. The

standards were digested using 3 ml HNO_3 and 2 ml HF in 30 ml acid cleaned Teflon vials. After evaporation on a hot plate at 60°C, the standards were digested using 6 ml of aqua regia (50:50 HNO_3:HCl) and heated on a hot plate with the lids on overnight. The lids were then removed and the acid left to evaporate. In preparation for the ICP-MS, the dry solid was dissolved in 10% HNO_3 and left on a hot plate to encourage dissolution. The standards were diluted in 1% HNO_3 to give a 1 ppm solution and 100 μl of this solution was diluted in 1% HNO_3 along with the addition of a indium spike (final concentration 5 ppm).

The standard values were taken from the Geostandards Special Issue (Govindaraju, 1994) and were used to confirm the accuracy of the elemental analysis. Table 2.9 and Table 2.10 shows the measured values and percent accuracy.

Most of the major/trace elements could be accurately measured, except for S, which had a range of accuracy for the four standards, higher and lower than its certified value. One of the standards when measuring for Cu, was four times its actual value, suggesting contamination.

For REE, the only element which appeared to show discrepancy was Gd, with two standards 40% greater than their actual value. However the other two standards showed complete recovery.

Table 2.9 - Results from analysis of a certified reference materials for major and trace elements

		CRPG BR	GIT-IWG BE-N	GIT-IWG WS-E	USGS BHVO-1
Mg (mM)	Certified	3294	3085	1395	1866
	Measured	3351	3516	1427	1771
	%	**102**	**114**	**102**	**95**
Al (mM)	Certified	2001	2037	2704	2686
	Measured	1913	2069	2776	2643
	%	**96**	**102**	**103**	**98**
P (mM)	Certified	146.6	155.5	41.3	38.7
	Measured	148.9	149.2	38.7	32.8
	%	**102**	**96**	**94**	**84**
S (mM)	Certified	14.1	9.6	16.5	3.1
	Measured	10.2	9.3	19.1	1.7
	%	**74**	**101**	**118**	**70**
Ca (mM)	Certified	2459	2534	1583	1977
	Measured	2684	2765	1695	2009
	%	**109**	**109**	**107**	**102**
Ti (mM)	Certified	325.5	329.3	298.6	345.1
	Measured	361.2	367.4	320.1	348.8
	%	**111**	**112**	**107**	**101**
V (mM)	Certified	4.6	4.4	6.5	6.2
	Measured	5.2	5.2	7.2	6.5
	%	**112**	**117**	**111**	**105**
Cr (mM)	Certified	7.1	6.8	1.8	5.5
	Measured	7.7	7.8	2.0	5.8
	%	**107**	**115**	**111**	**106**
Mn (mM)	Certified	28.2	26.3		23.9
	Measured	27.0	27.1	23.3	22.6
	%	**96**	**103**		**95**
Fe (mM)	Certified	1614	1609	1649	1546
	Measured	1600	1613	1638	1514
	%	**99**	**100**	**99**	**98**
Co (mM)	Certified	0.9	1.0	0.8	0.7
	Measured	1.1	1.1	0.8	0.8
	%	**112**	**108**	**107**	**105**
Ni (mM)	Certified	4.3	4.5	0.9	2.0
	Measured	4.9	4.9	0.9	2.1
	%	**113**	**111**	**98**	**103**
Cu (mM)	Certified	1.1	1.1	1.1	2.1
	Measured	1.2	1.2	3.3	2.2
	%	**106**	**108**	**313**	**104**
Zn (mM)	Certified	2.5	1.8	1.7	1.7
	Measured	2.8	2.1	1.9	1.4
	%	**112**	**114**	**105**	**78**
Mo (mM)	Certified	0.02	0.03	0.04	0.01
	Measured	0.02	0.03	0.03	0.01
	%	**102**	**102**	**94**	**91**

Table 2.10 - Results from analysis of a certified reference materials for REEs

		CRPG BR	GIT-IWG BE-N	GIT-IWG WS-E	USGS BHVO-1
Y(nM)	Certified	326.5	349.5	295.2	460.7
	Measured	361.3	364.8	302.6	486.9
	%	**111**	**104**	**103**	**106**
La (nM)	Certified	592.9	193.1	111.6	265.1
	Measured	622.7	190.5	111.7	290.2
	%	**105**	**99**	**100**	**109**
Ce (nM)	Certified	1086.6	420.8	276.8	544.3
	Measured	1109.5	414.4	268.3	561.4
	%	**102**	**98**	**97**	**103**
Pr (nM)	Certified	123.3	54.8	39.9	62.9
	Measured	126.5	53.2	37.6	69.1
	%	**103**	**97**	**94**	**110**
Nd (nM)	Certified	460.3	226.9	170.9	252.3
	Measured	483.4	222.7	172.0	283.0
	%	**105**	**98**	**101**	**112**
Sm (nM)	Certified	80.3	58.1	40.6	50.8
	Measured	84.2	56.0	40.2	55.5
	%	**105**	**96**	**99**	**109**
Eu (nM)	Certified	24.6	14.5	13.6	10.3
	Measured	26.7	14.3	13.4	10.9
	%	**108**	**99**	**99**	**106**
Gd (nM)	Certified	64.1	45.3	39.8	46.0
	Measured	91.2	48.4	39.5	63.8
	%	**142**	**107**	**99**	**139**
Tb (nM)	Certified	8.3	6.8	6.0	7.2
	Measured	9.3	6.5	5.8	7.3
	%	**112**	**96**	**98**	**102**
Dy (nM)	Certified	42.2	37.3	32.6	37.9
	Measured	43.2	37.1	33.3	41.7
	%	**102**	**100**	**102**	**110**
Ho (nM)	Certified	6.9	7.1	5.9	7.6
	Measured	7.0	6.8	6.0	8.0
	%	**101**	**96**	**100**	**106**
Er (nM)	Certified	15.7	18.2	15.1	21.1
	Measured	16.6	17.6	15.2	22.2
	%	**106**	**97**	**101**	**105**
Tm (nM)	Certified	2.1	2.4	2.0	3.2
	Measured	2.0	2.3	2.0	3.2
	%	**98**	**99**	**100**	**100**
Yb (nM)	Certified	10.6	14.4	11.5	19.3
	Measured	11.5	14.1	11.8	19.9
	%	**108**	**98**	**103**	**103**
Lu (nM)	Certified	1.4	2.0	1.6	2.9
	Measured	1.5	2.0	1.6	3.0
	%	**105**	**95**	**99**	**102**

2.5.11 Fe data - quality control for particulate Fe (pFe), dissolved Fe (dFe) and total dissolvable Fe (TdFe)

The sum of the particulate Fe (pFe) and dFe can be compared to the TdFe measured in the fluid samples (Appendix 2). These two values should be equivalent and will highlight any contamination/recovery issues. It became apparent that in some of the samples dFe concentrations were greater than TdFe concentrations suggesting contamination during filtration. In comparison, pFe concentrations appeared low with very few anomalous values. Contamination could have been caused by 'carry over' from previous sample during filtration. The contamination appeared to increase over the period of the cruise supporting that this was the case, becoming more apparent in the later CTD casts, where Fe concentrations were higher due to proximity to the vent source. However another problem became apparent in the buoyant plume samples; here the TdFe concentrations were around the same as the dFe concentration, but the pFe concentrations were much greater. This suggested that on initial sampling for TdFe on deck, the particulate Fe had settled to the bottom the CTD bottle. The CTD bottle was then transferred to the clean van and on removal, the pFe had redistributed in the bottle and was therefore separated during filtration. The TFe and dFe data was selected using the following parameters:

1) If pFe > 10 nM, i.e. for CTD 16 and two samples from CTD 11, calculate a new TFe concentration = pFe + dFe (to account for particle settling)

2) For the rest of the samples; if the relative percent different between TdFe and (pFe + dFe) is greater than 10%, calculate a new dFe concentration = TdFe - pFe

It became obvious in CTD 16 that particle settling was an issue because the calculated TFe concentration was much greater than the measured TdFe concentration. Here the pFe concentrations were up to 5 times greater than the measured TdFe concentration. By analysing the rest of the samples, the only other place this appeared to be an issue was for two samples from CTD 11. These two samples had pFe concentrations 5 times greater than the rest of the samples and again showed a large discrepancy between the TdFe concentration and the TFe concentration. All these samples had a pFe concentration greater than 10 nM, hence rule 1.

2.6 Iron speciation studies

2.6.1 Competitive ligand exchange - cathodic stripping voltammetry (CLE-CSV)

Cathodic stripping voltammetry (CSV) is a very sensitive but time consuming technique for the analysis of trace metals in seawater (Achterberg and Braungardt, 1999). A ligand is added to the seawater sample forming an adsorptive complex with the trace metal which is then detected using a Hanging Mercury Drop Electrode (HMDE). The metal ligand complex is adsorbed onto the surface of the Hg drop at a controlled potential and a current is produced upon a voltammetric scan towards a more negative potential. This current is a result of the reduction of either a reducible group on the ligand or of the metal itself. The limit of detection is typically 10^{-9} – 10^{-11}M (Achterberg and Braungardt, 1999).

Different metals have different ligands which are suitable for CSV. The ligand needs to be able to form a complex with the element of interest and have electroactivity. It appears that π–electron interactions from the ligand are significant for the adsorption process. For Fe, the use of four different ligands has been reported: 1-nitroso-2-napthol (1N2N) (Nagai et al., 2004), 2-(2thiazolylazo)-p-cresol (TAC) (Croot and Johansson, 2000), salicyaldoxime (SA) (Rue and Bruland, 1997) and 2,3-dihydroxynaphthalene (DHN) (Obata and Van den Berg, 2001). The experiment can be controlled by the careful selection of the ligand and its concentration giving a 'detection window' for the experiment (Van den Berg et al., 1990), which can detect varying strengths of ligands.

CLE-CSV is sensitive enough to be used for trace metal speciation studies and can be used to determine the presence of organic ligands. For this, a sample is titrated with Fe, enabling the determination of the stability constant of any unbound or competitively released ligand. The overall total ligand, [L] (including both complexed and excess organic ligands, inorganic colloidal ligands and crystalline Fe hydrolysis products (Gledhill and Van den Berg, 1995)) can then be calculated from equilibrium principles (Croot and Johansson, 2000; Gledhill and Van den Berg, 1995; Rue and Bruland, 1995; Van den Berg, 1995; Wu and Luther III, 1995).

The titration is carried out by splitting the filtered (0.4 μm) seawater sample into typically 10 sub-samples and adding increasing amounts of the metal under investigation.

The ligand and a buffer are then added and the samples are left to equilibrate, typically overnight. During this stage the added metal complexes with both naturally present ligand and the added synthetic ligand. If there is an excess of strong natural ligand in the sample, the metal will complex with this until it is all consumed and then the remaining metal will start to complex with the added ligand. There will also be an exchange of the added synthetic ligand with any weaker naturally occurring ligands attached to the metals in the sample. The net effect is a curve in the initial part of the titration plot (current *vs.* Fe concentration). After a ~20 hr equilibration, the samples are analysed electrochemically and the metal concentration associated with the added ligand is determined via the current the complex produces during reduction. Linear and non-linear data transformations are used to determine the ligand concentrations and stability constants (Boye et al., 2003; Boye et al., 2001; Croot and Johansson, 2000; Rue and Bruland, 1995; Van den Berg, 1995; Wu and Luther III, 1995). The theory is described in more detail below.

2.6.2 Theory behind speciation studies

Within ambient seawater samples, the following relationship exists:

$$[Fe_T] = [Fe'] + [FeL] \quad (2.1)$$

where $[Fe_T]$ is the total concentration of Fe in the sample, [Fe'] is the labile Fe i.e. Fe^{3+} species not bound in strong complexes and [FeL] is the concentration of the organically bound iron. Fe(II) is not considered, because in the time period of sample collection and processing, all the reduced Fe will have been oxidised. The equilibrium between the natural ligands present in the seawater and the inorganic Fe is expressed by:

$$Fe' + L' \leftrightarrow FeL \quad (2.2)$$

Where L' is the free organic ligand within the system. The conditional stability constant for the formation of the complex FeL ($K'_{Fe'L}$) is defined as:

$$K'_{Fe'L} = [FeL] / ([Fe'] \times [L']) \quad (2.3)$$

Where $K'_{Fe'L}$ is the conditional stability constant with respect to Fe' (Croot and Johansson, 2000). The value of $K'_{Fe'L}$ is conditional on the seawater composition (Gledhill and Van den Berg, 1994). To convert $K'_{Fe'L}$ to K'_{FeL}, the conditional stability constant with respect to free Fe^{3+}, $\alpha_{Fe'}$, the side reaction coefficient for Fe', can be applied:

$$\alpha_{Fe'} = [Fe']/[Fe^{3+}] \quad (2.4)$$

$$\alpha_{Fe'} = K'_{FeL}/K'_{Fe'L} \quad (2.5)$$

$\alpha_{Fe'}$ is normally quoted as 10^{10} (Hudson et al., 1992)

On addition of the competing ligand, TAC, a new equilibrium is set up:

$$[Fe_T] = [Fe'] + [FeL] + [Fe(TAC)_2] \quad (2.6)$$

The TAC ligand competes with the 'labile' species in the sample; weakly bound organic species in the FeL fraction as well as inorganic Fe species (Gledhill and Van den Berg, 1994). During the titration, an $Fe(TAC)_2$ fraction is determined at different Fe concentrations enabling the determination of FeL. This involves knowing the total Fe in the sample i.e. that initially present plus that added during the titration, and subtracting the $Fe(TAC)_2$ concentration measured by CSV.

$$[FeL] = Fe_T - [Fe(TAC)_2] \quad (2.7)$$

CSV measures a current (I_p) relating to the concentration of $Fe(TAC)_2$ via the sensitivity, S:

$$I_p = S \times [Fe(TAC)_2] \quad (2.8)$$

S can be obtained from the gradient of the titration curve (I_p *vs.* added Fe) at high concentrations of total Fe where all the organic ligands are saturated and a straight line exists.

The $Fe(TAC)_2$ concentration relates to the side reaction coefficient for $Fe(TAC)_2$ ($\alpha_{Fe'(TAC)2}$):

$$\alpha_{Fe'(TAC)2} = [Fe(TAC)_2]/[Fe'] \text{ and} \quad (2.9)$$

$$[Fe(TAC)_2]/[Fe_T] = \alpha_{Fe'(TAC)2}/ (1+\alpha_0 + \alpha_{Fe'(TAC)2}) \quad (2.10)$$

Where α_0 is the side reaction coefficient for naturally occurring ligands, including inorganic ligands with respect to Fe'. This side coefficient α_0 relates to the concentration of Fe' by:

$$[Fe']/([Fe_T] - [Fe(TAC)_2]) = 1/(1+ \Sigma K_i L_i') \quad (2.11)$$

Where K_i is the conditional stability constant and L_i is the concentration of the ith natural ligand. $[Fe_T] - [Fe(TAC)_2]$ is the residual Fe, representing all the forms of Fe not complexed to TAC. Rearranging Equations 2.3, 2.6 and 2.11, yields the reciprocal Langmuir isotherm (Croot and Johansson, 2000):

$$[FeL]/[Fe'] = K[L_T]/(1+K[Fe']) \quad (2.12)$$

The non-linear Langmuir isotherm can then be used to determine the ligand concentration and stability constants, $K'_{Fe'L}$, and can be solved using the Gerringa method (Gerringa et al., 1995) (P Croot, Ligfit: A Labview program for non-linear fitting of voltammetric titration data. IfM-Geomar, Kiel, Germany (2006)), with an inorganic side reaction coefficient as $\log\alpha_{Fe'} = 10$ and for TAC, $\log\alpha_{Fe(TAC)2} = 12.4$.

As well as the non-linear fit model, other methods exist for solving L and K. A second method used throughout this work is the Langmuir transformation method (or van den Berg linearization) (Ruzic, 1982; Van den Berg, 1982) based on the combination of the following two relationships:

$$[L]_T = [L'] + [FeL] \quad (2.13)$$

$$K'_{FeL} = [FeL] / [Fe^{3+}] \times [L'] \quad (2.14)$$

Combining these two equations by substituting for L', the free ligand within the system, forms the following linear relationship:

$$[Fe^{3+}]/[FeL] = [Fe^{3+}]/[L]_T + 1/(K'_{FeL}[L]_T) \quad (2.15)$$

$[Fe^{3+}]$ is directly related to the $Fe(TAC)_2$ concentration by α' – the overall α coefficient for inorganic complexation and complexation by TAC i.e. $\alpha' =. \alpha_{Fe'} + \alpha_{Fe'(TAC)}$, therefore:

$$[Fe^{3+}] = [Fe(TAC)]/\alpha' \quad (2.16)$$

Substituting Equation 2.16 into 2.15 for Fe^{3+}, is convenient as a current proportional to the $Fe(TAC)_2$ concentration is measured during the experiment.

$$[Fe(TAC)]/[FeL] = [Fe(TAC)]/[L_T] + \alpha'/(K'_{FeL}[L_T]) \quad (2.17)$$

Final substitution and rearrangement results in Equation 2.18:

$$[Fe']/[FeL] = [Fe']/[L_T] + 1/(K'_{Fe'L}[L_T]) \quad (2.18)$$

The ratio of [Fe']/[FeL] is plotted against [Fe'] giving a straight line and the y intercept and slope of the line can be used to obtain $K'_{Fe'L}$ and L (Rue and Bruland, 1995):

$$\text{Slope} = 1/[L_T] \quad (2.19)$$

$$\text{y-intercept} = 1/(K'_{Fe'L}[L_T]) \quad (2.20)$$

2.6.3 Instrumentation

Electrochemical measurements were carried out using a Metrohm VA 663 Stand, with a Hanging Mercury Drop Electrode (HMDE), glassy carbon working electrode, Ag/AgCl

reference electrode and a µAutolab potentiostat (Ecochemie, NL). The equipment was computer controlled with an EcoChemie bv Autolab software version 4.9.4 (Windsor Scientific Ltd).

2.6.4 Method development

A series of experiments were conducted on a high Fe seawater sample in order the find the most appropriate ligand for the analysis of the hydrothermal samples and to optimise the experimental conditions for the analysis.

TAC was chosen due to a lack of background peak and a good clear signal. A large peak due to TAC complexes had previously been reported to be a problem, but due to the higher concentrations in our samples this was not an issue (Obata and Van den Berg, 2001). Method development was carried out to determine the optimum experimental conditions using a filtered (0.4 µm) unacidified hydrothermal seawater sample, which had not been frozen. An aliquot (10 ml) of this sample was pipetted into a Teflon cell, along with 50 µl of 1 M EPPS (final concentration 5 mM), 10 µl of 10 mM TAC (final concentration 10 µM) and 100 µl of 1 µM Fe standard (final concentration 10 nM). The voltammetric settings used were as follows (Table 2.11).

Table 2.11 - Voltammetric settings

Scan	Differential pulse
Nitrogen purge	180 s
Equilibrium time	10 s
Initial potential	-0.4 V
Final potential	-0.9 V
Step potential	2.55 mV
Modulation amplitude	49.95 mV
Stirrer speed	2000 revs min^{-1}
Hg drop size	0.52 mm

The deposition potential was varied from -0.3 and -0.4 V with an adsorption time of 600 s (Figure 2.1a).

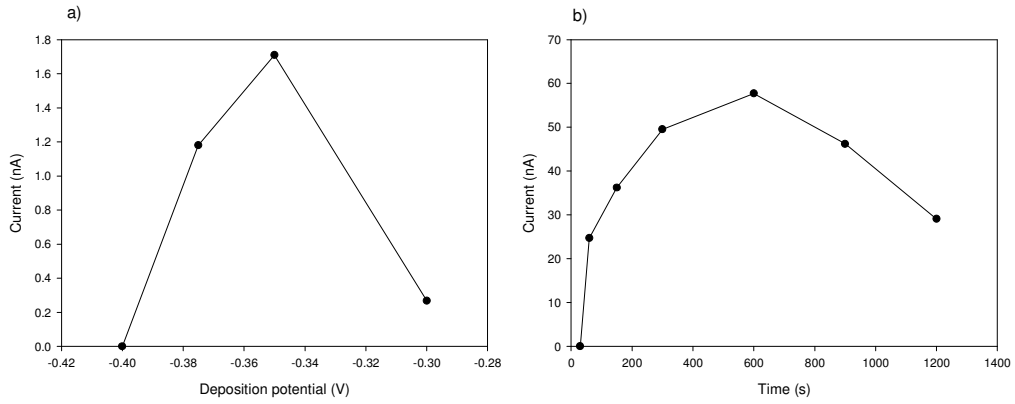

Figure 2.1 - a) CLE-CSV Fe reduction peak current as a function of deposition potential for differential pulse voltammetry b) CLE-CSV Fe reduction peak current as a function of adsorption time.

A potential of -0.35 V yielded the greatest response and then dropped steeply away either side. This potential of -0.35 V was used for all future work. Previously, Croot et al. (2000) had found a narrow window of deposition potentials between -0.3 and -0.5 V, where the Fe(TAC) species were seen to be adsorbed. They determined an optimal sensitivity at -0.38 V, slightly more negative than that determined in this study.

The adsorption time of the experiment was then varied and the current was seen to increase and then plateau (Figure 2.1b). The optimum time was found to be 600 s. After 600 s the peak current decreased which is likely to be due to the higher concentrations of Fe in the samples and therefore saturation of the Hg drop. This was different to the results from Croot et al. (2000), where they saw a linear response with an adsorption time varying from 250 s to 600 s. An adsorption time of 600 s was used for low Fe samples and the remaining method development experiments, reducing to 300 s for samples >5 nM.

The ligand concentration was varied from 5 to 40 µM and the optimum concentration was found to be 10 µM (Figure 2.2a). There was a steep increase from 5 to 10 µM and then the peak current plateaued and began to decrease. As the stirring speed was increased the peak current increased (Figure 2.2b). After 2000 revolutions min^{-1} the rate of increase in current began to decrease.

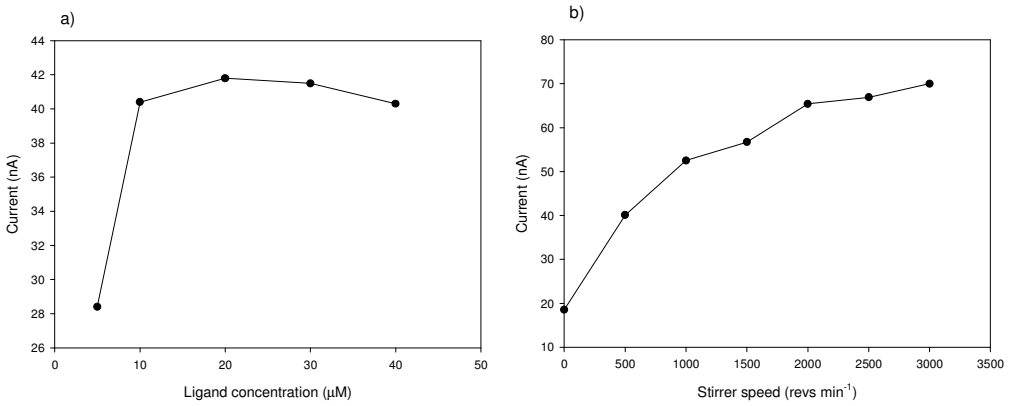

Figure 2.2 - a) CLE-CSV Fe reduction peak current as a function varying ligand concentration b) CLE-CSV Fe reduction peak current as a function of stirring speed

In order to determine the Fe concentration limits of the experiment, the linear response was checked for increasing Fe concentrations. The Fe peak was seen to increase linearly with Fe concentration until 50 nM (Figure 2.3). By decreasing the adsorption time, the upper concentration limit of the experiment can be increased.

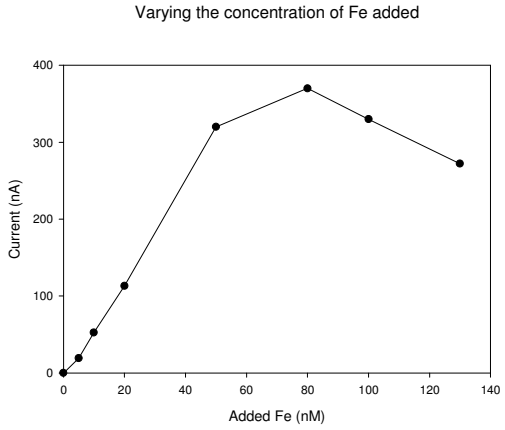

Figure 2.3 - CLE-CSV Fe reduction peak current as a function varying Fe addition to determine the concentration limits of the technique

A slight curve is seen from 0 – 5 nM inferring the presence of natural organic ligands in the sample, this could also be due to a lack of precision at lower Fe concentrations but later, in samples containing no ligand excess, a straight line was observed. The sample used in the method development had not been frozen and therefore bacteria within the seawater could have produced organic complexes. This experiment shows that the limit

of detectable Fe with an adsorption time of 600 s is 50 nM, which will be important to consider when looking at the high Fe samples from the vent plumes. Fe concentrations in the non-buoyant plumes at 5°S range from 10 nM to 54 nM with frozen dFe samples ranging from 2.3 nM to 33 nM (Appendix 2 and 3). These conditions are therefore suitable for the lower Fe concentration range of the samples (<25 nM) but for the samples with Fe concentrations greater than 25 nM, a decreased adsorption time will be required. Loss of linearity, if it occurs, will be obvious during the titration.

2.6.5 Titration Experiment.

Using the optimal experimental conditions determined above, a titration experiment was carried out. Previous studies had utilised either one hour or overnight equilibrium times between the addition of all the reagents and the start of the analysis. For our work, overnight equilibrium was chosen due to the higher Fe concentrations present in our samples and the recent debate in the literature about the kinetics of the system (Discussed in Chapter 5)(Town and van Leeuwen, 2005a).

2.6.6 Procedure for hydrothermal samples

A filtered sample (0.4 µm filtered), was defrosted overnight and gently mixed. In a laminar flow hood, sub-samples of 10 ml were pipetted into a series of pre-cleaned Teflon pots (25 ml) and each sample was treated in the following way with a 15 minute time lag between the sub-samples. To the sample, 100 µL of 1 M EPPS was added followed by Fe with concentrations ranging from 0 to 20 nM. The Fe was allowed to equilibrate for one hour at laboratory temperature and at the end of this period 10 µL of 10 mM TAC was added. The samples were left to equilibrate overnight.

The first sample was then transferred to a Teflon cell and placed in the Metrohm stand. The sample was de-aerated for three minutes with nitrogen gas and subsequently the $Fe(TAC)_2$ complexes were adsorbed onto a fresh Hg drop. The potential was scanned using differential pulse voltammetry with the conditions outlined above (Section 2.6.4) along with a deposition potential of -0.35 V and adsorption time of 600 s or 300 s. The stripping current from the adsorbed $Fe(TAC)_2$ was recorded at an electrode potential of -0.41 V. The Teflon cell was rinsed between the analysis of each sub-sample with MQ water and the sub-samples were run in order of increasing Fe additions. Contamination

was kept to a minimum by regular acid cleaning and was found to be negligible throughout the experiments. This was confirmed with the analysis of MQ water, as an $Fe(TAC)_2$ peak could not be determined prior to Fe addition.

2.7 Dissolved organic and particulate organic carbon analysis

The measurements of dissolved organic carbon (DOC) and particulate organic carbon (POC) in the ocean have become routine measurements because of their link to primary productivity. A number of different analytical techniques have been applied for the determination of DOC however, the High-Temperature Combustion (HTC) technique used here is the most widely used. This is because of its good oxidation efficiency of DOC to CO_2 and its high sensitivity and precision measurements of CO_2 using infra-red absorption (Pan et al., 2005).

Particulate organic carbon is measured using a high temperature combustion technique. For aqueous samples, a known amount of seawater must be filtered and then the dry mass of the filter is combusted. This requires the filters to have been combusted at 400°C for more than 4 hours prior to sample filtration to remove any POC on the filter. The methods used for both analyses are described below.

2.7.1 Particulate Organic Carbon (POC)

The GF/F filters were unfolded, removed from the foil and placed in small polystyrene containers. The filters were then treated with sulfurous acid under vacuum for 24 hrs to removed the inorganic carbonates (Verardo et al., 1990). The filters were dried at 60°C for 24 hrs, quartered and packaged in pre-combusted aluminium foil (Hilton et al., 1986). The samples were then analysed on a Thermo Finnigan Flash EA1112 elemental analyser using Acetanilide as a calibration standard. Filter blanks were used for blank correcting the sample and are shown in Table 2.12. The limit of detection of POC was determined to be 1.65 μg (n = 3). Measurements were carried out by Robert Head at the Plymouth Marine Laboratories.

Table 2.12 - Detection limits determined from blank analysis of a filter (n=2)

	Blank
	POC
Average (µg)	5.49
Standard deviation	0.55

2.7.2 Dissolved Organic Carbon (DOC)

Determination of DOC was carried out on a Coupled High-Temperature Combustion Total Organic Carbon-Nitrogen Chemiluminescence Detection (HTC TOC-NCD) system. The measurements were performed using a Shimadzu TOC 5000A total carbon analyser coupled with a Sievers NCD 255 nitrogen chemiluminescence detector (Pan et al., 2005). A procedural blank of MQ water, filtered on board the ship, gave a detection limit of 1.89 µM (n = 3) and the accuracy of the technique was determined from the analysis of a certified reference material (Table 2.13). Analysis was carried out by Xi Pan at NOCS.

Table 2.13 - Detection limits determined from blank analysis of MQ water (n=3) and results from analysis of a certified reference material

	Procedural Blank	CRM (µM)	
	DOC	Certified	Measured
Average (µg)	4.6	44-46	44.2
Standard deviation	0.63		

2.8 Quality Control

For each of the methods described above, the detection limits and accuracy (when a certified reference material is available) have been described. During sample analysis, repeat analyses were carried out to ensure data precision. If the data varied by more than 10%, the samples were re-run. For the AAS and POC data, the replicates had less than a 10% relative standard deviation. ICP-MS relative standard deviation errors are shown in

the appendix as well as the errors for DOC and Fe isotopes. Samples for the electrochemistry work were run twice with good repeatability.

2.9 Summary

The methods described above were used to produce data for the following chapters:

Chapter 4 : DOC and POC analysis

ICP-OES

Chapter 5 : Speciation analysis of Fe using CLE-CSV

Seawater Fe and Mn analysis using atomic absorption spectroscopy

Particulate analysis of the major and trace elements using ICP-OES

Chapter 6 : Seawater Fe and Mn analysis using atomic absorption spectroscopy

Particulate analysis of the major and trace elements using ICP-MS

Particulate analysis of REE using ICP-MS

Chapter 7 : Isotope analysis using MC-ICP-MS

Chapter 3. Geological Setting

3.1 9°N East Pacific Rise

The hydrothermal samples discussed in Chapter 4 were collected from the well characterised basalt hosted vent system at 9°50'N along the fast spreading East Pacific Rise (EPR)(Figure 3.1). This site has been the subject of detailed multi-disciplinary studies for more than a decade making it one of the best characterised vents, worldwide. However, sampling for this study took place on board the *R.V. Atlantis* (AT05-04) at the beginning of 2007, just less than a year after the occurrence of a mid-ocean ridge eruption along this ridge section (Tolstoy et al., 2006). During 2006, a rapid response cruise and cruises already scheduled to visit this area, focused their attention on the effects that the volcanic eruption event might have had on the areas of high-temperature venting, diffuse flow and the biological communities that these sites continue to host (Cowen et al., 2007).

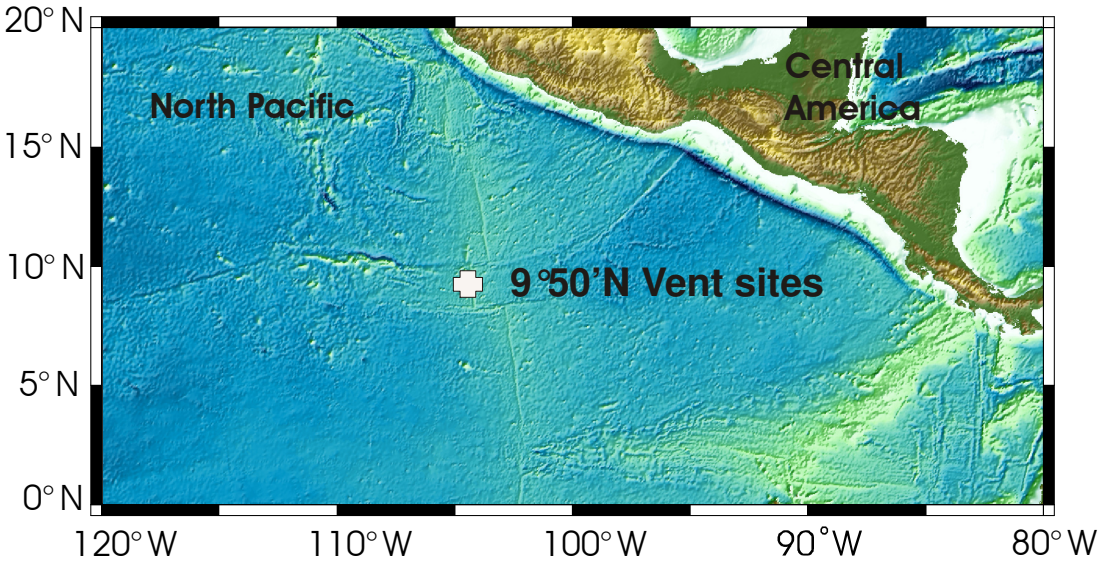

Figure 3.1 - Location map of the 9°50'N vent sites on the EPR

The EPR 9-10°N first became the focus of study in the early 1990s following the detection of an earlier volcanic eruption at this site (Haymon et al., 1991; Haymon et al., 1993). This area of fast spreading ridge (11 cm yr^{-1}) has been extensively studied since the early 1980's and therefore there is an extensive set of data describing the area's geology, biology and chemical diversity. It has been suggested that the location of the

hydrothermal vents at 9°50'N are being guided by two primary geological features; fractures associated with vertical to near-vertical dikes that fed the 1991 eruption and permeable zones created during the focussing of the eruptions and subsequent drainback of magma (Fornari et al., 2004).

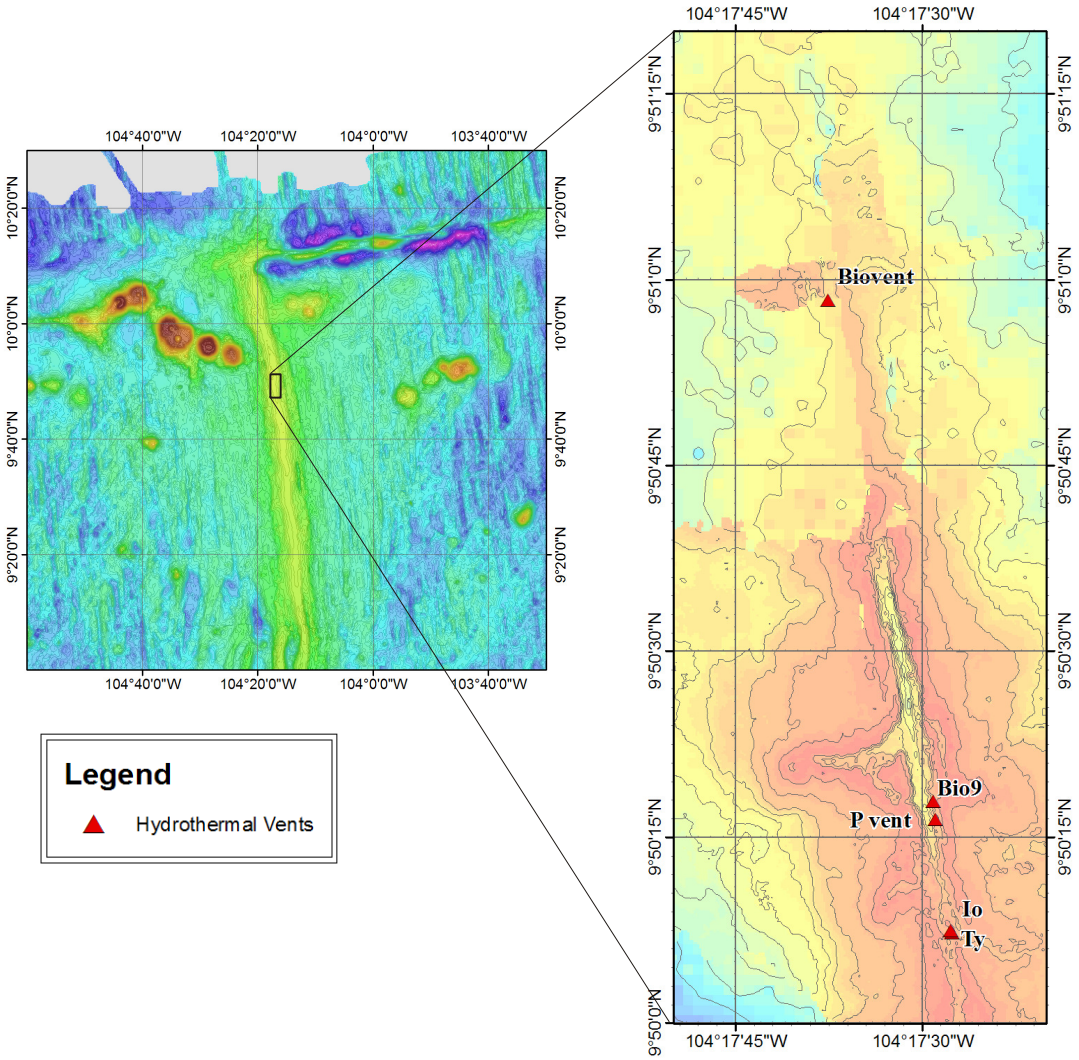

Figure 3.2 - Location map of high-temperature vent sites still present at 9°50'N on the EPR (Shallow to deep:red to yellow to blue)

At 9°50'N, an axial summit collapse trough (ASCT) is present at the ridge crest at 2500 m depth along a 4th order ridge segment, only 50 m wide and 20 m deep. Within this trough, four sites of high-temperature hydrothermal activity remained actively venting in Jan 2007: Biovent, Bio9, P vent and Ty/Io (Figure 3.2). There were also areas of diffuse flow, occupied by patches of Tevnia and Alvinella, but the majority of Riftia

and vent mussels present prior to the eruption were now extinct.

Biovent was comprised of two active black smoker chimneys encrusted with Alvinella and surrounded by pillow lava and white bacterial mats in the cracks. Diffuse flow was present in the vicinity of the high-temperature venting, hosting bacterial mats and limpets. Bio9 was comprised of a series of three black smoker chimneys (Bio9, Bio9' and Bio9"), encrusted with Alvinella. Again, diffuse flow was also present, hosting bacterial mats and Tevnia.

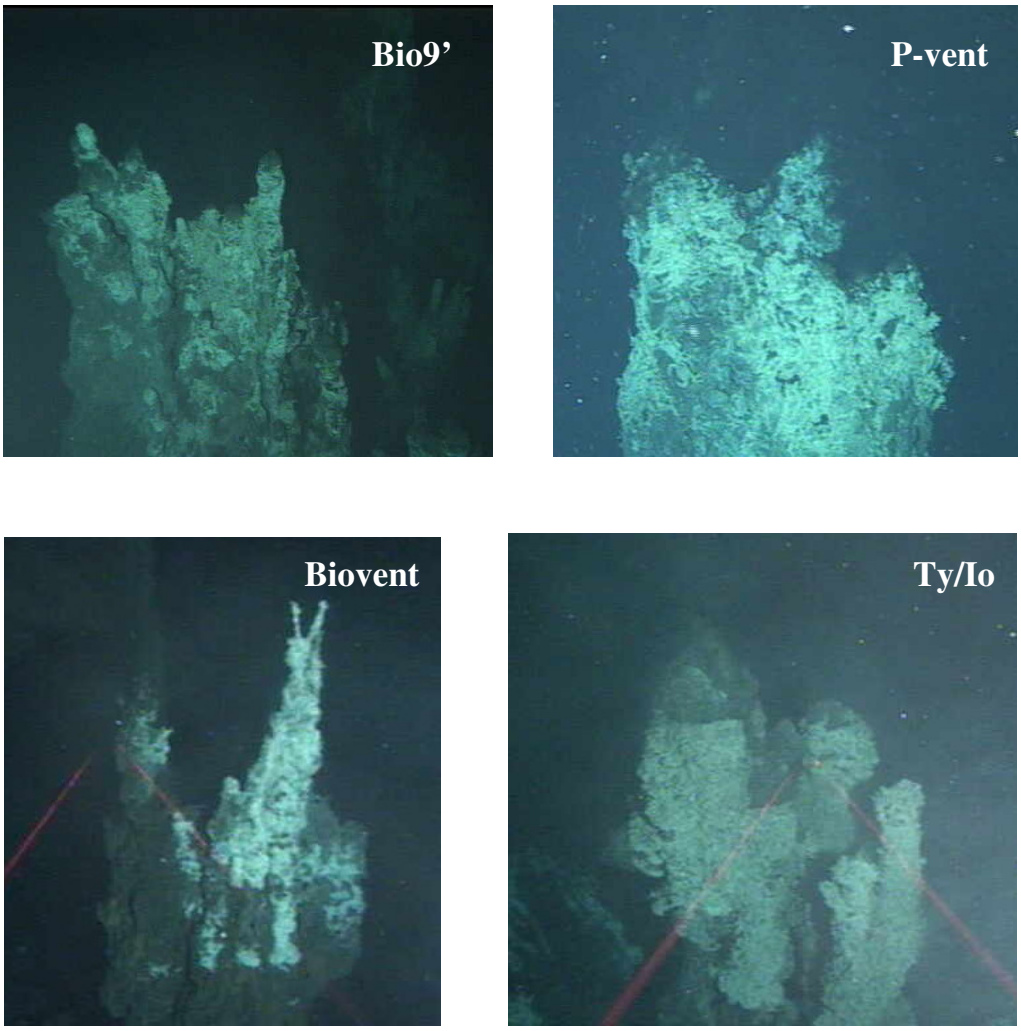

Figure 3.3 - Photos of the high-temperature chimneys sampled at 9°50'N EPR (AT05-04, photos taken from DSV *Alvin*)

The black smoker chimney at P vent, only 60 m south of Bio9, consisted of two spires, one of which was actively venting whereas the other seemed to have been disrupted by the recent volcanic activity. Alvinella were present on the sulfide walls at P-vent along with patches of Tevnia and one large, old Riftia. The chimney sampled near 9°50'07"N and labelled as Ty/Io could not be confirmed in Jan 2007 to be either Ty or Io, two independent black smoker chimneys that existed prior to the winter 2005/2006 eruption. Instead, the site sampled at this location was characterised by a suite of small (< a few meters high) black smokers with extensive Alvinella populations present. The diffuse flow at this site was extensive, hosting bacterial mats, limpets and patches of Tevnia (Figure 3.3).

3.2 4° - 5°S Mid-Atlantic Ridge

The samples discussed in Chapters 5, 6 and 7 were collected during two research cruises (RRS *Charles Darwin* CD169 and FS *Meteor* cruise M68/1) in 2005 and 2006. These cruises investigated the first sites of hydrothermal activity to be located anywhere on the Southern Mid-Atlantic Ridge (MAR) near 5°S (Figure 3.4).

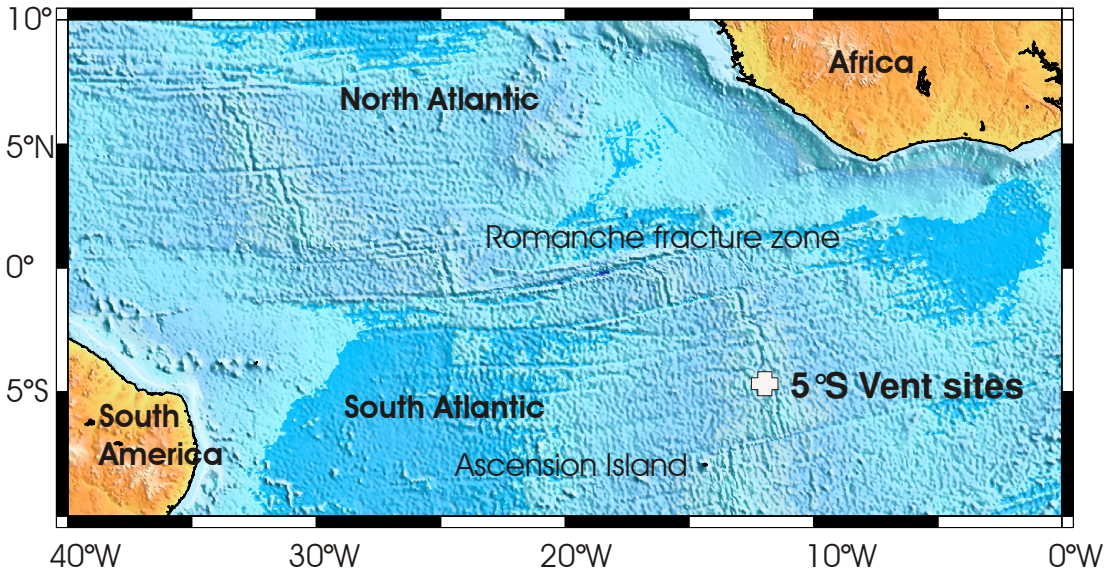

Figure 3.4 – Location of vent sites discovered on the R.R.S. *Charles Darwin* CD169

Initial location of the vents was carried out using a combination of NOC's Towed Ocean Bottom Instrument (TOBI), a 30 kHz deep-tow sidescan sonar vehicle, and the

Autonomous Benthic Explorer (ABE), Woods Hole Oceanographic Institution's deep-diving autonomous underwater vehicle (German et al., 2008a).

First, during CD169, a series of Miniature Autonomous Plume Recorders (MAPR's) were attached below and above TOBI, at 50 m intervals, to collect in-situ optical backscatter data from the water column over a range extending from 100 m below TOBI to 200 m above it as TOBI was towed along axis through the MAR rift valley at heights of 300 m - 500 m above the seafloor. MAPR instruments have sensors for temperature, pressure and optical backscatter and it is optical backscatter (a measure of the light reflected off any suspended particles in the water column) that is particularly useful in exploration for sites of high-temperature hydrothermal venting. High concentrations of suspended particles are typically absent from oceanic deep water far from land, but are present in abundance forming characteristic 'lenses' of particle rich water in hydrothermal plumes, rich in fine grained Fe-Mn oxyhydroxides ± sulfides. TOBI was towed along a 200 km section of the MAR between 2° and 6°S with significant anomalies observed at two locations near 4°S and near 5°S (German et al., 2008a; German et al., 2005).

At the more southerly of these sites, ABE was programmed to carry out a three dive survey at 4°48'S 12°22'W. Here, the median valley is at its shallowest (3000 m) forming a 10 km wide, hour-glass shaped plateau with spreading rates of ~3.2 cm yr^{-1} (DeMets et al., 1990). The lavas along this ridge segment are fresh and unsedimented suggesting recent and strong volcanic activity and high eruption rates (Haase et al., 2007). Seismic data suggested major eruptions in late June 2002 (German et al., 2008a).

The ABE dive protocol consisted of an initial dive ~300 m above the seafloor (at the height of the previously detected non-buoyant plumes). This was followed by a second dive, conducted at 50 m above the seafloor to conduct detailed mapping of the seafloor and, simultaneously to intercept the buoyant stems of any hydrothermal plumes present. Finally a series of dives, 5 m above the seafloor, determined the exact location of the vents and photographs were taken. Attached to ABE were CTD (conductivity, temperature and density) sensors, Eh sensors and a transmissometer (German et al., 2008c).

In this way, two new vent-sites were located in March 2005 (Red Lion and Turtle Pits) and a further, 3rd site in the 5°S segment, Comfortless Cove, was located during FS Meteor cruise M68/1 in May 2006. This site included two areas of diffuse flow; Golden Valley and Foggy Corner (Figure 3.5 and 3.6). The first ROV dives to the Red Lion and Turtle Pits sites were conducted aboard FS Meteor cruise M64/1 in 2005 but all the vent fluid samples reported here were collected by the remotely operated vehicle (ROV), MARUM Quest (Bremen) from Meteor M68/1.

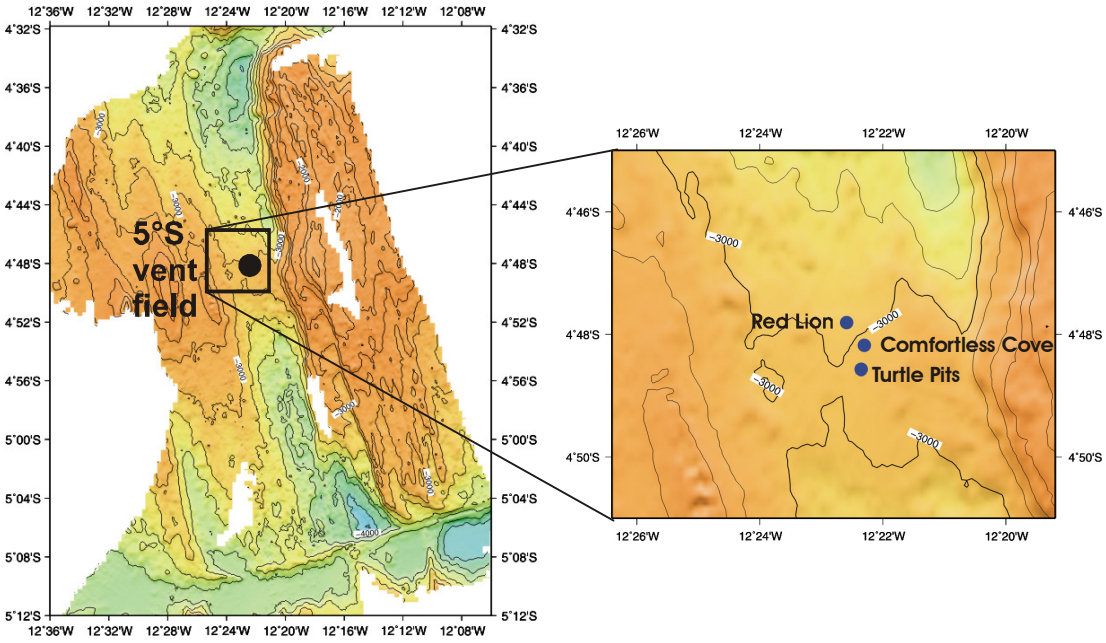

Figure 3.5 - Location map of vent sites in the 2 km section of ridge at 5°S MAR. The sites are superimposed onto a bathymetry map of the area (Shallow to deep:orange to blue)

Red Lion was made up of four active black smoker chimneys; Mephisto, Sugarhead, Tannenbaum and Shrimp Farm, each 4 – 6 m high and separated from each other by 10-15 m (Figure 3.6 and 3.7). There were also several inactive chimneys here. The freshly-erupted basaltic pillow lavas and lack of sediment suggested recent volcanic activity. Comfortless Cove had one active black smoker chimney, Sisters Peak, 13 m high and consisting of two spires, only one of which was actively venting. The eastern spire of this smoker was inactive whereas the western spire was venting acidic, phase separated fluids, at 400°C. The base of the chimney was colonised by mussels, crabs and shrimps.

There were two areas of diffuse flow in the vicinity of Sisters Peak: Golden Valley and Foggy Corner (Figure 3.6)(Haase et al., 2007).

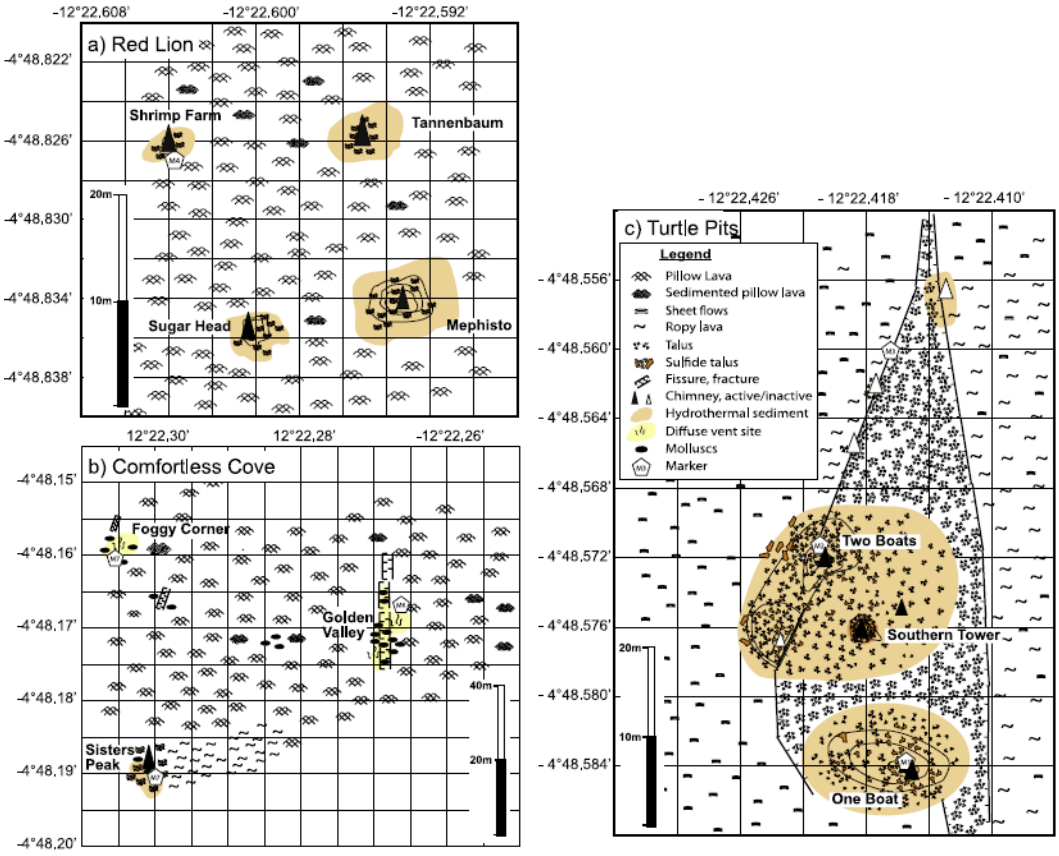

Figure 3.6 – Sketch maps of the three different vent locations (Haase et al., 2007)

The Turtle Pits field lies within a small depression, a similar setting to hydrothermal vent sites on the fast spreading EPR. A tall 9 m chimney, Southern Tower, was seen to have increased by 4 m when it was revisited in May 2006 and on two mounds of sulfide debris were numerous small active black smoker sites: One Boat and Two Boats. The fluids emitting from these mounds were phase separated, characterised by gas bubbles and hosting the hottest vent fluid temperatures ever recorded from the deep-ocean (Haase et al., 2007; Nature, 2006).

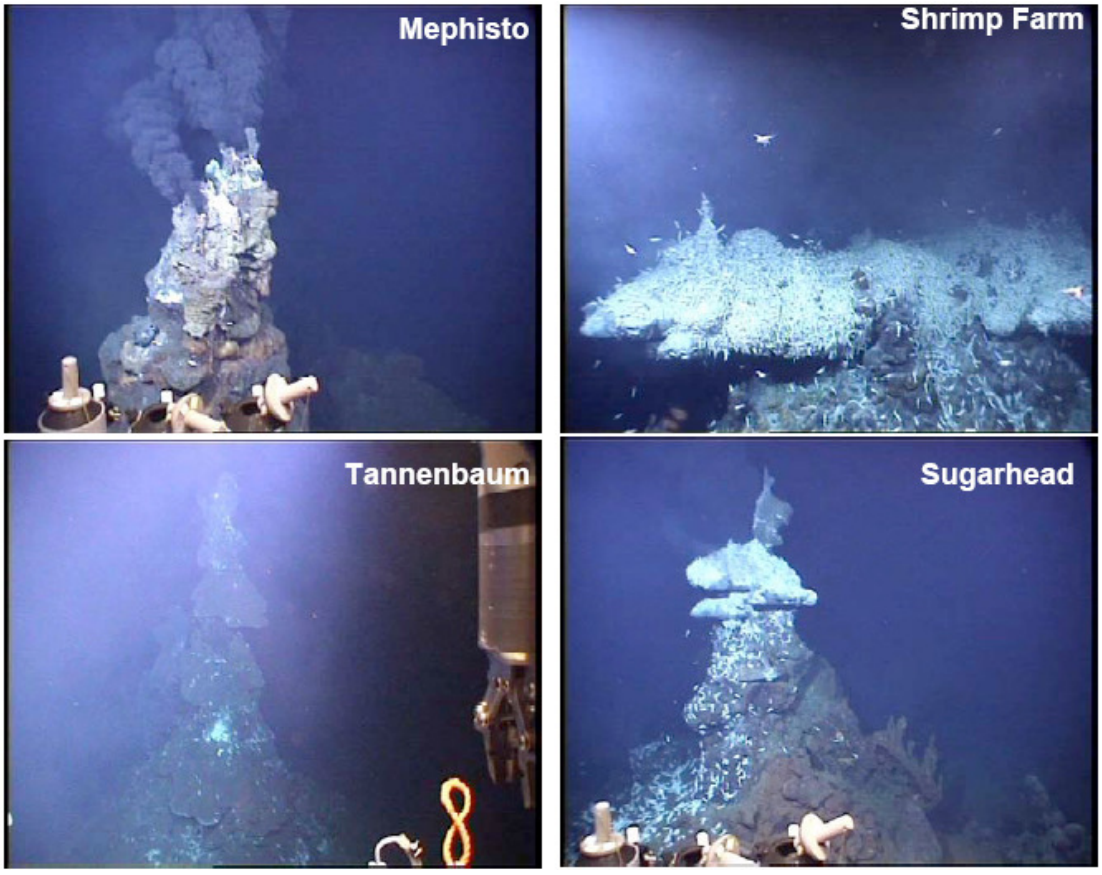

Figure 3.7 – Photos of the high-temperature chimneys at Red Lion vent field (Devey, 2006)

Chapter 4. Dissolved and particulate organic carbon in hydrothermal plumes

4.1 Introduction

Although it has long been recognised that Fe acts as an essential micronutrient for phytoplankton growth (Morel et al., 2004; Pollard et al., 2007), the debate over its sources and sinks persists (Ussher et al., 2004). One potential source of Fe to the surface ocean is through upwelling of dissolved Fe released from deep-sea hydrothermal vents (Boyle et al., 2005; Coale et al., 1991) – but this would require dissolved Fe to be stabilised in some form as it disperses away from a vent-site. This appears problematic because when vent-fluids first enter the base of the water column abundant polymetallic particulate phases are formed: predominantly Fe-rich sulfides and Fe oxyhydroxides (Feely et al., 1987b). In earlier work, it was often assumed that hydrothermal inputs of dissolved Fe to the deep-ocean should be negligible (German et al., 1991; Mottl and McConachy, 1990).

In the surface and deep-ocean, Fe exists at concentrations greater than the predicted solubility (Millero, 1998) and >99% of dissolved Fe (dFe, that fraction passing through a 0.4 µm filter (Cullen et al., 2006)) is complexed by stable organic ligands (Gledhill and Van den Berg, 1994; Rue and Bruland, 1997; Van den Berg, 2006). Organic Fe complexation acts to reduce the reactivity of the Fe species, preventing precipitation of Fe and scavenging into/onto particulate phases. Such complexes, if formed within buoyant hydrothermal plumes, would certainly have the potential to sustain enhanced dissolved Fe concentrations at least as far as non-buoyant plume height.

In order for organic Fe complexation to occur there must be a source of organic carbon to the plume. High-temperature hydrothermal systems have been considered to be inorganically dominated because of the breakdown of organic molecules at high temperatures. Consequently very few analyses of dissolved and particulate organic carbon (DOC and POC) have been conducted for hydrothermal plumes and it is unknown whether entrainment or production of organic material will occur within these systems. In general, however, organic compounds play a central role in marine biogeochemical cycles and the majority of them, originate from biogenic precursors. The POC fraction is

mainly composed of detritus as well as phytoplankton and bacteria while the DOC fraction is mainly composed of humic substances as well as excretions from animals, microorganisms and plants. The separation of DOC from the POC fraction is operationally defined as that which passes through a 0.7 µm GF/F filter. Therefore some biological species, such as bacteria and archaea, may exist in both fractions. However, bacteria and archaea will mainly exist in the POC fraction along with other biotically (and abiotically) produced organic compounds.

In this chapter, DOC and POC data from hydrothermal plume of the basalt-hosted EPR (9°50'N) are presented. These analyses demonstrate the potential for organic complexation of Fe to occur within the hydrothermal plumes.

4.2 Hydrothermal plume sampling

Near-field buoyant plume samples were collected from above four high-temperature vent sites; Bio9', P vent, Biovent and Ty/Io, using 1.5 L Niskin bottles placed in the basket attached to DSV *Alvin* (Figure 4.1). A total of eight samples were collected, with two samples from each site collected one after the other as DSV *Alvin* flew a few meters above the vent chimneys. Duplicate samples from each site were analysed for DOC, TdFe and TdMn, and one sample from each site was analysed for POC. As each sample was taken, temperature and H_2S concentrations were measured using an in-situ chemical probe, placed in the basket, adjacent to the Niskin bottles ((Sarradin et al., 2005), data from Nadine Le Bris, Ifremer, unpublished).

Additional samples were collected from buoyant and non-buoyant plumes at 9°50'N using a CTD rosette equipped with a turbidity sensor to detect the fine grained Fe-Mn and aid sample collection. These samples were analysed for DOC and POC, but not Fe and Mn. Initially, the rosette was deployed directly above the 9°50'N vent sites in order to collect buoyant plume samples, detected by the presence of both particle and temperature anomalies. This was followed by two more, at 0.5 and 2 km southwest of the vent sites, respectively, following the direction of the current and bisecting non-buoyant plumes, 100 to 200 m above the seafloor (Figure 4.1).

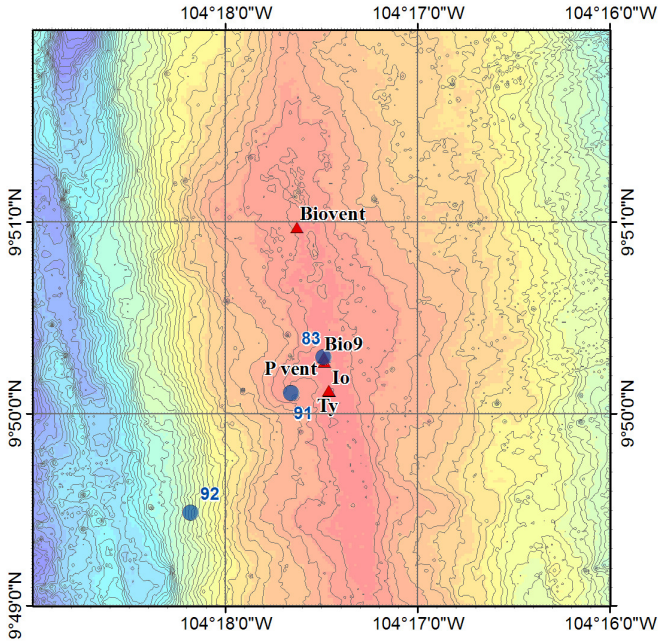

Figure 4.1 - Locations of CTD stations 83, 91, and 92 relative to the positions of the Ty/Io, Bio9', P vent and Biovent vent sites at 9°50'N EPR (Shallow to deep:red to blue)

4.3 Results

The time profiles of temperature and H_2S as DSV *Alvin* flew through high-temperature plumes are shown in Figure 4.2. Maximum temperatures in the plume ranged from 6.4 to 13°C compared to a background temperature of 2°C. Maximum H_2S concentrations ranged from 5 to 71 µM.

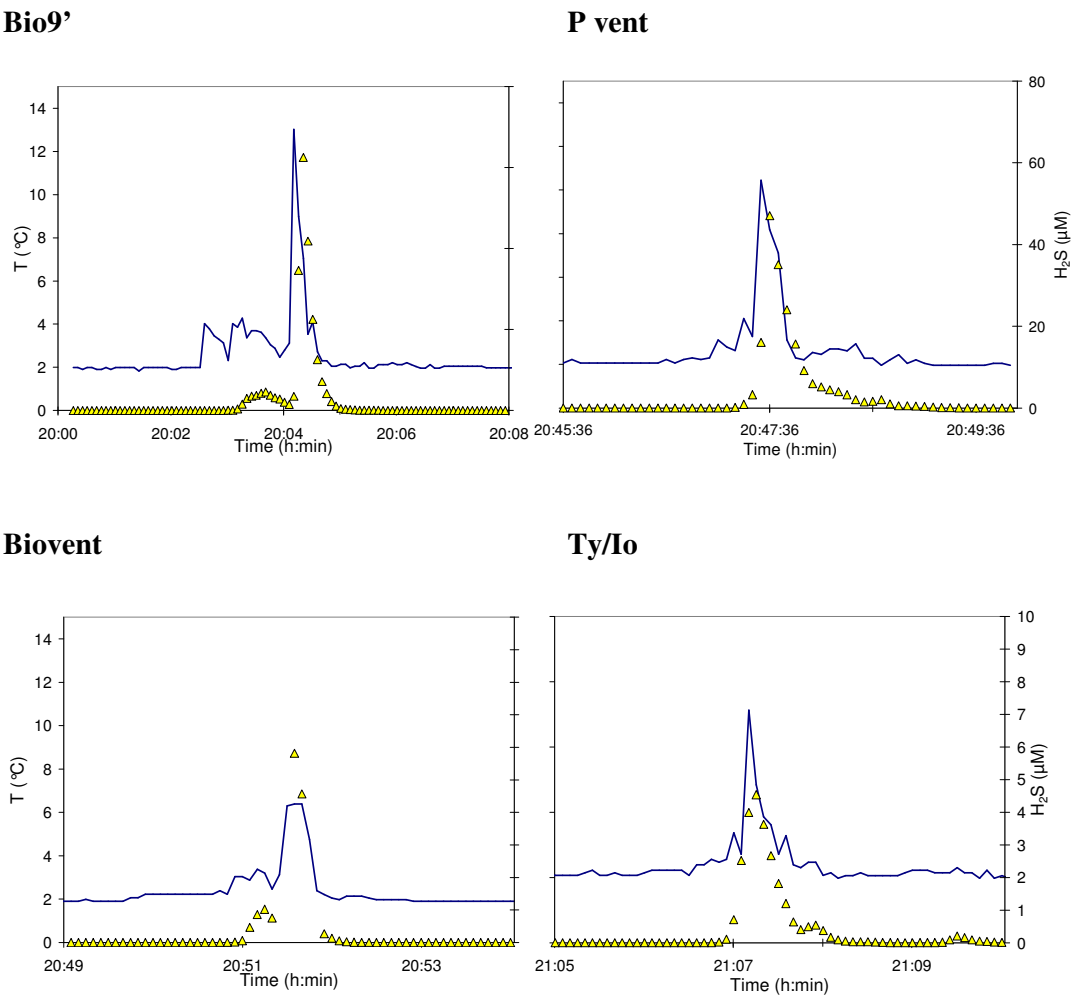

Figure 4.2 – Change in temperature and H_2S concentrations with time as DSV *Alvin* flew through the high-temperature plumes (Note scale differences for H_2S concentration). Yellow filled triangles are H_2S concentration (µM) and blue solid line is temperature.

The POC and DOC concentrations in the near-field vent samples and their respective TdFe and TdMn concentrations are shown in Table 4.1 along with maximum temperature and H_2S concentrations observed within the plumes. The POC concentrations ranged from 0.87 to 3.81 µM and the DOC concentrations ranged from 37.9 to 47.1 µM.

Table 4.1 – TdFe and TdMn, POC and DOC concentrations in the near-field plume samples collected at 9°50'N EPR along with maximum temperature and H_2S concentrations detected within the plume.

Vent site	[a]Temp (°C)	[a][H_2S] (µM)	[b][$Fe]_{Td}$ (µM)	[b][$Mn]_{Td}$ (µM)	[b][POC] (µM)	[b][DOC] (µM)
Biovent	6.4	6	3.50	2.00	0.87	40.0
			2.83	1.70		37.9
Bio9'	13	71	7.10	0.30	1.48	46.1
			6.18	0.27		43.9
P vent	10.5	54	4.74	0.53	3.74	41.5
			6.80	0.77		47.1
Ty/Io	7.3	5	1.75	0.60	3.81	44.0
			2.87	0.59		39.2

[a] Measured in-situ

[b] Measured in collected samples at NOCS

$[Fe]_{Td}$ and $[Mn]_{Td}$ represents the total dissolvable concentrations

The CTD depth profiles of POC, DOC and turbidity are shown in Figure 4.3. At CTD 81, strong particle anomalies, combined with temperature anomalies detected just above the seafloor and continuing up to 2460 m depth, demonstrated that a 40 m section through a buoyant plume had been sampled. Because the depth of the ASCT was only 20 m (Figure 4.1) the rising plume would not have been confined by topography having risen more than 20 m off the bottom. During the CTD cast, a Lowered-Acoustic Doppler Current Profiler (L-ADCP), attached to the CTD rosette, measured a current of 8.6 cm s^{-1} at 2400 m depth travelling in a southwesterly (199°) direction. This will have caused the plume to disperse away from the ridge axis during buoyant plume rise.

At CTD 91, particle anomalies were observed between 2350 and 2275 m (Density 1038.4 g L^{-1}), 150 to 210 m above the seafloor, demonstrating the presence of a non-buoyant plume at this site 500 m southwest of the 9°50'N vents. At this station, the L-ADCP measured a southwesterly (233°) current of 5.8 cm s^{-1} at non-buoyant plume height, confirming that the 9°50'N vents were the most probable source of this plume. Another 2 kilometres southwest of the vents, a much weaker non-buoyant plume was intercepted and sampled, occurring at the same density (1038.5 g L^{-1})(CTD 92) with

southwesterly (227°) currents of 5.7 cm s^{-1}. Once emplaced, non-buoyant hydrothermal plumes disperse along isopycnal (constant density) surfaces rather than at the same depth. Therefore if a lens of particle rich water is intercepted at two adjacent stations, it is a more robust argument to use density rather than depth to infer whether the two CTD casts are likely to have sampled the same non-buoyant plume. Therefore the plumes at CTD 91 and 92 must have sampled the same plume.

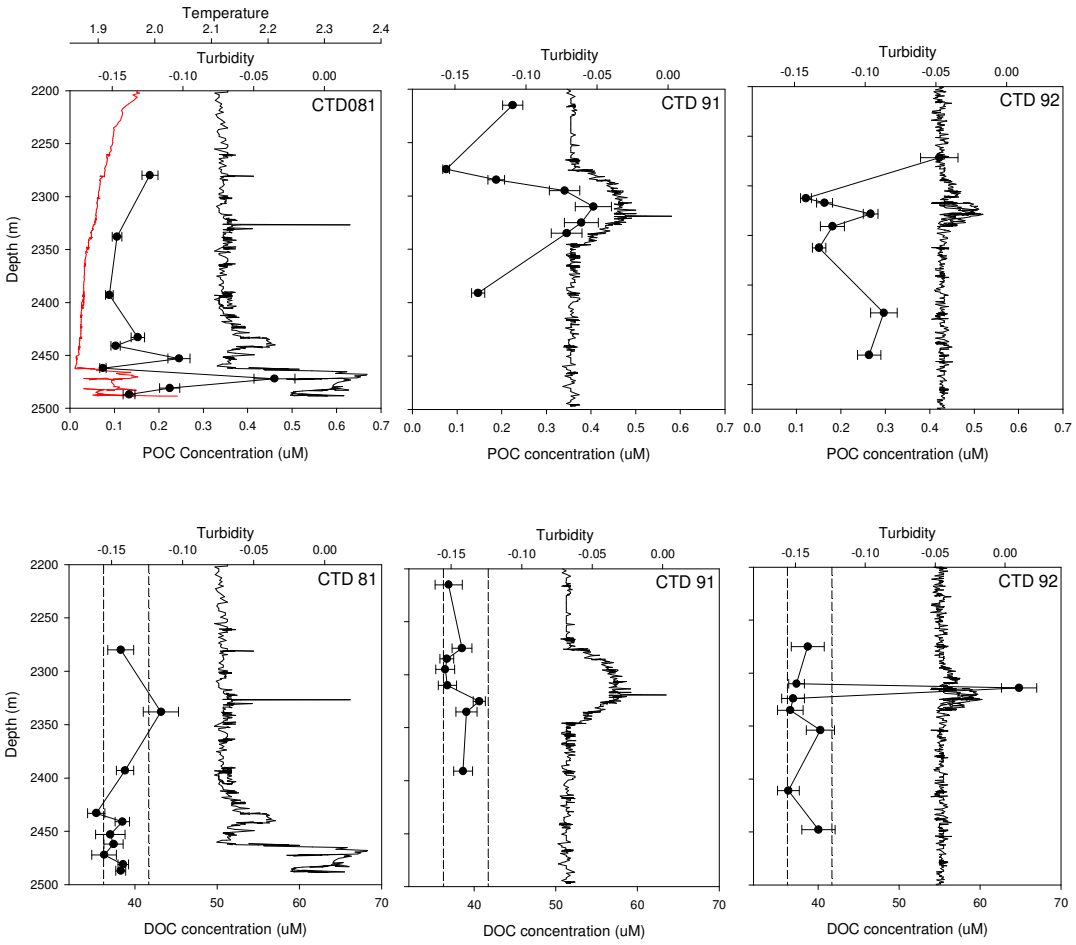

Figure 4.3 - Depth profiles of POC, DOC and turbidity for the CTD stations that intercepted buoyant and non-buoyant plumes at 9°50'N EPR. The solid red line indicates temperature, the solid black line indicates turbidity and the solid black circles indicate organic carbon. The dashed lines on the bottom three plots indicates the background DOC range.

DOC and POC concentrations were compared with samples collected during a background CTD cast 50 kilometres northwest of any hydrothermal activity (Appendix 1). The POC concentrations in the plume ranged from 0.07 to 0.48 µM

compared to an average of 0.39 µM measured in the background CTD cast. DOC concentrations ranged from 35.3 to 64.8 µM compared to an average of 38.7 µM again measured in the background CTD cast. Deep-ocean POC concentrations have previously been measured to range between 0.2 to 1.3 µM (Moran et al., 1999). Different sampling procedures can produce different estimates of the POC concentrations because of the low concentrations in the deep-ocean (Moran et al., 1999). In this study only 1 L of seawater was filtered through each filter, whereas in open ocean studies, POC is often measured using in-situ pumps which filter over 1000 L of seawater, allowing for a better estimate of the average POC concentration in the open ocean. Unfortunately such pumps were not available during this study and therefore it is difficult to compare the open ocean POC concentration measured in this study to previous open ocean studies (Millero, 2006).

4.4 Discussion

Before discussing the DOC data, the near field buoyant plume samples need to be put in context with respect to their dilution with the surrounding seawater. The in-situ sensor data collected whilst the Niskin bottles were being fired, is unlikely to represent exactly that present in the bottle, due to the time delay for the Niskin to be flushed with surrounding seawater. However, Fe and Mn measurements made on the samples collected in the Niskin bottles should enable an estimate of the plume dilution.

4.4.1 Dilution of the near-field plume samples

Our study was conducted in December 2006, approximately 12 months after the most recent eruptions at 9°50'N. Unfortunately, at this time, no post-eruption vent fluid data are available. However, between 1991 to 2002, the fluids at Bio9' and P vent showed unprecedented chemical changes (Von Damm, 2004; Von Damm et al., 1995). Intense sampling and analysis since a volcanic eruption in 1991, has allowed the evolution of a hydrothermal system to be studied. Chemical and temperature variations are suggested to have arisen in response to changes in the depth of seawater circulation to the heat source driving the system. The best estimate of the fluid compositions will be those documented after the 1991 eruption. During this period the Mn concentration in those end-member fluids for both P vent and Bio9' was ~ 100 - 200 µM (Von Damm, 2004).

If similar end-member Mn concentrations are assumed after the 2006 eruption to those present after the 1991 eruption, then the near-field samples can be predicted to have diluted with the surrounding seawater as shown in Table 4.2 (calculated using Equation 4.1 and an end-member Mn concentration of 200 µM throughout).

$$Dil = [Mn]_{Td}/[Mn]_{Em} \times 100 \quad (4.1)$$

Where $[Mn]_{Td}$ is the Mn concentration measured in the near field buoyant plume samples, $[Mn]_{Em}$ is the end-member Mn concentration (200 µM) and dil is the dilution.

The end-member Fe concentration can also be predicted using the Fe/Mn ratio in the near field buoyant plume samples and an end-member Mn concentration of 200 µM (Equation 4.2)

$$[Fe]_{Em} = [Fe]_{Td}/[Mn]_{Td} \times [Mn]_{Em} \quad (4.2)$$

Table 4.2 – Predicted dilution and end-member Fe concentration using an end-member Mn concentration of 200 µM. Also shown is the Fe/Mn ratio for the plume samples

Vent site	[a]% end-member fluid	[a][Fe] (µM) (end-mem)	$[Fe]_{Td}$ (µM)	$[Mn]_{Td}$ (µM)	Fe/Mn
Biovent	1%	351	3.50	2.00	1.8
	0.9%	333	2.83	1.70	1.7
Bio9’	0.2%	4769	7.10	0.30	23.8
	0.1%	4525	6.18	0.27	22.6
P vent	0.3%	1780	4.74	0.53	8.9
	0.4%	1763	6.80	0.77	8.8
Ty/Io	0.3%	580	1.75	0.60	2.9
	0.5%	968	2.87	0.59	4.8

[a]Calculated dilution and end-member Fe concentration from a predicted end-member Mn concentration of 200 µM.

The predicted end-member Fe concentrations are close in value to those measured by Von Damm (2004). The Fe/Mn ratios (Table 4.2) in the samples collected in this study vary between sites suggesting different chemical characteristics and different reaction zones beneath the seafloor (Von Damm, 1995), as has previously been observed by Von Damm (2004). Except for Ty/Io, duplicate samples have similar Fe/Mn ratios even though the samples were taken one after the other in different parts of the buoyant plume, demonstrating that the plumes were relatively homogeneous. As the end-member Fe/Mn ratio is not known and the ratios in the end-member fluids have varied considerably since the 1991 eruption, it is difficult to predict whether any Fe has been lost from the plume as Fe sulfides or indeed, whether any additional Fe has been entrained into the plume from the chimney or the seafloor. This may be an explanation for the different Fe/Mn ratios at Ty/Io. It has not been determined yet whether these samples were collected from the Ty or the Io buoyant plume, because of changes in the chimney structure since the eruption, hence the name Ty/Io.

The Fe/Mn ratio at Bio9' appears to be particularly high (23.8) but similarly high ratios were observed at P vent after the 1991 eruption (25.3)([Fe] = 4420 μM and [Mn] = 175 μM). Fe concentrations in vent fluids are controlled by both phase separation and water-rock reactions and are usually limited by the solubility of Fe sulfide minerals. However, when the hydrothermal fluids are close to the critical point of seawater, almost complete complexation of Fe with chloride can occur, maximising the transport of Fe (Von Damm et al., 2003). Therefore it might be predicted that the Bio9' fluids have been close to the critical point at the time of this study to explain such a high Fe/Mn ratio. The Fe/Mn ratios observed in the Ty/Io and Biovent fluids are more similar to the 3:1 ratio observed in many EPR metalliferous sediments, indicating that these fluids were less affected by the most recent eruption.

4.4.2 DOC and POC in the near-field plume samples

The DOC concentrations in the near-field plume samples ranged from 37.9 μM to 47.1 μM and are typically higher than background concentrations (38.7 μM). At Bio9' and P vent measured DOC concentrations were higher than at Biovent and Ty/Io, however, this DOC is unlikely to have been sourced directly from the end-member chimney. This is because complex organic molecules are only stable in high-temperature vent fluids under exceptional circumstances. For example in sediment-hosted

hydrothermal systems (e.g. Guaymas basin, Middle Valley, Juan de Fuca Ridge)(Cruse and Seewald, 2006; Pearson et al., 2005) or, in ultramafic-hosted vents sites such as the Rainbow hydrothermal field, MAR (Holm and Charlou, 2001). By contrast, DOC concentrations in end-member fluids at sites along the EPR are likely to be lower than background because of removal during circulation of the fluid through the oxidising crustal reservoir. For example, DOC concentrations in end-member fluids at the Main Endeavour field and at Axial Volcano on the Juan de Fuca ridge had average DOC concentrations of 15 and 17 μM, respectively, compared to 36 μM in the background seawater (Lang et al., 2006).

Additionally, for DOC in the near-field plume samples to have originated from the end-member fluids, the end-member concentrations would have had to have been extremely high in order to maintain increased DOC concentrations in the plume after dilution with the surrounding seawater. For example, if the fluids have experienced a 0.1 to 1% dilution with the surrounding seawater (Table 4.2), the end-member DOC concentrations would have had to have been between 1.2 to 12 mM (using a plume DOC concentration of 47.1 μM). Even in the highly productive upwelling regions such as the equatorial Pacific, DOC concentrations only reach 67 μM (Carlson and Ducklow, 1995). Therefore it is highly unlikely that the high-temperature vents were the source of DOC to the buoyant plume and therefore could not have been a direct result of the eruption. One particular organic carbon species that is enriched in the vent fluids is methane, which through Fischer Tropsch type reactions or chemolithoautotrophic and chemoheterotrophic bacteria, could result in the formation of hydrocarbons in the plume (Foustoukos and Seyfried, 2004). But again the concentrations of methane in end-member fluids are too low (10 – 2000 μM), particularly in basalt hosted systems, in order to produce the high DOC concentrations measured in the near-field plume samples (Charlou et al., 1998).

POC is also expected to be low in end-member fluids but in the near-field plume samples reported here (Table 4.1), POC concentrations are comparable to upper ocean POC concentrations (9 μM (Moran et al., 1999)). POC also shows a different trend to DOC with greatest concentrations observed at Ty/Io and P vent.

4.4.3 Sources of organic material

4.4.3 i) Entrainment

The most likely source of dissolved organic matter to the high-temperature samples is not from end-member vent fluids, but from diffuse flow entrained into the base of the turbulent buoyant plume. Diffuse systems typically host the most abundant chemosynthetic communities associated with seafloor hydrothermal venting and areas of high biomass were observed on the chimneys as well as in the areas surrounding the vents sampled. Within these environmental niches, dissolved organic carbon concentrations of 39 - 69 μM have been observed approximately double background deep-ocean values (Lang et al., 2006). Elevated POC concentrations (of up 18.3 μM) have also been observed in warm (20°C) waters at 21°N, EPR (Comita et al., 1984). In that study DOC concentrations were 53 - 71 μM, similar to the range reported by Lang et al. (2006). Lang et al. (2006) concluded that the high DOC concentrations present in the diffuse flow were a result of high microbial activity sustained by energy produced from the oxidation of sulfur species and H_2 (McCollom and Shock, 1997; Sarradin et al., 1999).

Entrainment of diffuse flow into buoyant hydrothermal plumes has been documented in both Atlantic and Pacific systems (Lavelle and Wetzler, 1999; Veirs et al., 2006). This results in buoyant plumes composed of 50 to 80% entrained diffuse flow. Lavelle and Wetzler (1999) used Al as a tracer of diffuse flow, as the Al signal in vent fluids is small (Lunel et al., 1990). They modelled a 50% dilution of the diffuse flow over a height rise of 35 m dependent on turbulent mixing with the surrounding seawater and the amount of diffuse flow in the area of interest. The buoyant plume in comparison experiences a 1000-fold dilution over the same rise distance above the seafloor.

In the model by Lavelle and Wetzler (1999), Al is used as a conservative tracer of diffuse flow. In comparison, organic carbon coming from the diffuse flow areas will be produced and consumed by bacteria in the water column and will therefore behave non-conservatively. Thus, the amount of DOC entrained will depend on other factors as well as dilution and may be either more or less concentrated than would be predicted from a simple dilution model.

4.4.3 ii) In-situ production

Another potential source of organic material to the high-temperature plume may be in-situ production from microbial activity. Elevated levels of bacteria in hydrothermal plumes were first observed by Winn and Karl (1986) in samples collected 20 and 50 m above a 10 m high chimney on the Endeavour Ridge. Microbial biomass was estimated by measuring particulate ATP, which can be used to estimate the living carbon fraction by multiplying ATP by 250 (Winn et al., 1986). In that study, 20 m above the chimney, the concentration of particulate living carbon was 1.2 µM and at 50 m it was 0.3 µM, similar to the POC concentrations measured in the near field plume samples collected from 9°50'N EPR. In a subsequent study, at Guaymas Basin, Karl (1988) determined that end-member black smoker fluids were devoid of any recognisable bacteria and contained negligible concentrations of ATP, but 25 cm above the vent orifice, plumes were enriched in bacteria and exhibited high ATP and POC concentrations. Guaymas basin is a very organic rich sediment hosted system and therefore organic compounds are expected to be stabilised. However, Karl (1998) suggested that microbial populations in the plumes must be entrained from ambient seawater, which must have come from areas of biological productivity surrounding the vent systems.

Biological activity in a plume will result in both the release, and consumption, of POC and DOC. In diffuse flow areas hosting biologically rich chemosynthetic communities, the rate of production is expected to be great, whereas in the buoyant plumes, the environment is potentially more toxic and therefore biological activity may be less diverse.

4.4.4 DOC and POC in the dispersing plume

The limit of detection of DOC in the buoyant and non-buoyant plume make it difficult to confidently associate a trend. The plume is at least 10 times more dilute than the near field buoyant plume samples and therefore the DOC concentrations lie within the background DOC range (vertical dashed lines, Figure 4.3). The only samples that appear to have a greater concentration of DOC, occur within the non-buoyant plume at a depth of around 2340 m at each of the CTD stations and reach a maximum concentration of 65 µM in the most distal plume (CTD 92). This is potentially due to production within the non-buoyant plume.

Mn oxidising bacteria have been detected previously in non-buoyant hydrothermal plumes and a correlation has been observed between pMn and bacterial capsules (Cowen and Li, 1991). Extracellular bacterial capsules are released by bacteria for the oxidation of Mn, catalysing the oxidation process. The typical size of an uncapsuled plume bacterium is 0.5 µm in diameter, forming part of a group of exopolymers, which are high molecular weight secretions dispersed within the DOC fraction (Decho, 1990). In the non-buoyant plume, elevated DOC concentrations are likely the result of these exopolymers.

The POC concentrations in the non-buoyant plumes are less than 0.5 µM but the variations are within the error of the analysis. The concentrations within the centre of the plume are greater than on the edges of the plume, but overall the POC concentrations are less than that measured in the background seawater. Above the plume the POC concentrations appear to be greater than normal background POC concentrations, whereas below the plume POC concentrations are closer to background. This is potentially due to the presence of zooplankton which live on the upper edges of dispersing non-buoyant plumes and feed off the organic plume material (Burd et al., 1992; Cowen et al., 2001).

In dispersing non-buoyant plumes sticky transparent exopolymer particles (TEP) have also been detected, which typically exist in the 2 – 100 µm size range (Prieto and Cowen, 2007; Shackelford and Cowen, 2006). These compounds are formed abiotically from dissolved material and are observed to increase with increasing distance from the vent site (Shackelford and Cowen, 2006). Other species in the particulate fraction will be viruses, which have adsorbed to particles and are sourced from the diffuse flow environment (Ortmann and Suttle, 2005). However because of their small size, these viruses could also be detected in the dissolved fraction

4.4.5 DOC relationship with Fe concentration

The most interesting result from this study is that DOC (in excess of background DOC concentrations), correlates positively with TdFe concentrations in samples from Biovent, Bio9', P vent and Ty/Io (Figure 4.4). Only one sample from Ty/Io lies off this trend, with an anomalously high DOC concentration relative to Fe. This samples also had a lower Fe/Mn ratio than the other Ty/Io sample (Table 4.2), because of a lower than

expected Fe concentration relative to Mn. This could be an analytical artefact resulting in pFe remaining in the Niskin bottle rather than being transferred to the sample bottle.

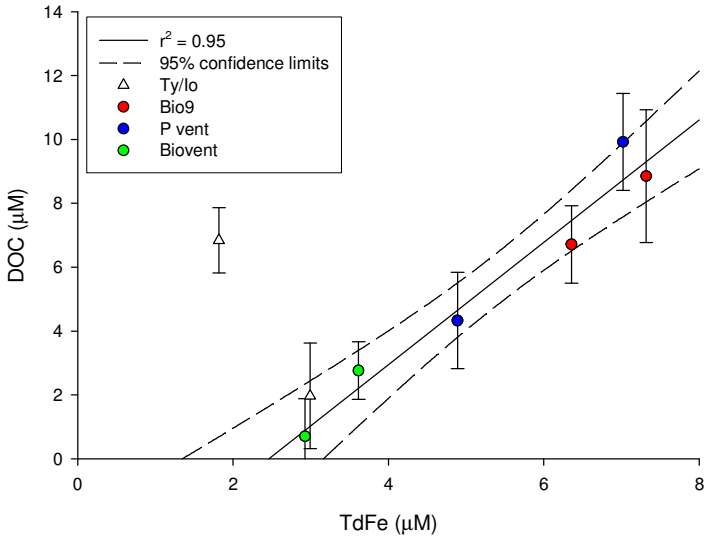

Figure 4.4 - Graph showing the linear relationship between DOC and TdFe with 95% confidence limits. Duplicate samples from each site are indicated and detailed in the key

The linear Fe/DOC relationship does not pass through the origin of the graph and by using 95% confidence limits, it can be demonstrated that between 1.7 to 3.5 µM of Fe does not correlate to DOC. This is likely to be particulate Fe within the total dissolvable Fe fraction, not associated with the DOC. The uncertainty in the DOC measurement is around 1 µM and the error for each analysis is shown in Figure 4.4. Even by taking the errors into account, distinct differences can be observed between the DOC concentrations in two samples from the same vent site. For example at P vent the DOC concentrations show no overlap and but these variations still appear to correlate with Fe concentration. Therefore the DOC concentration can not be just the result of variation between the different vent sites.

The relationship observed between TdFe and DOC is remarkable and difficult to explain. There is no equivalent relationship observed between TdFe and POC (Figure 4.5a), even though adsorption of Mn and Fe onto bacteria has been previous been detected in the POC fraction of the open ocean (Cowen and Silver, 1984). Nor is there an equivalent relationship observed between TdMn and DOC (Figure 4.5b).

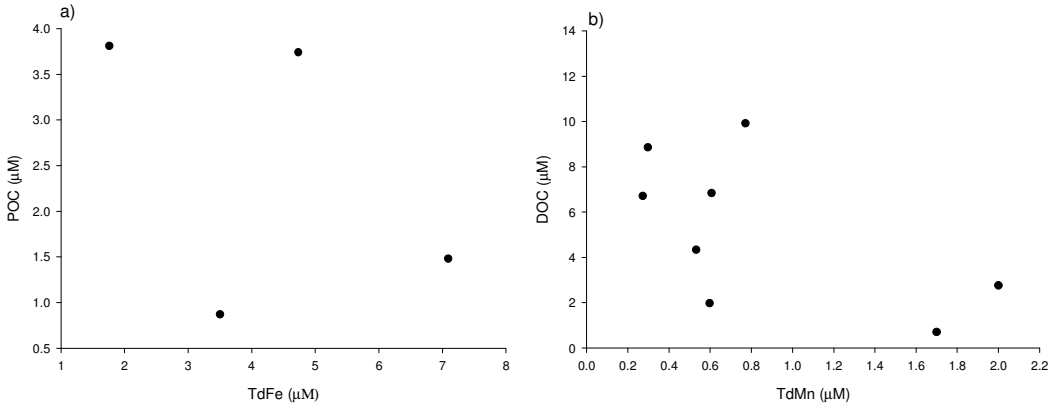

Figure 4.5 – a) Graph of POC relative to TdFe in the near-field plume samples b) Graph of DOC relative to TdMn in the near-field plume samples

It has previously been discussed, that DOC may be entrained into the buoyant plume from diffuse flow areas. But there is no easy explanation as to why DOC entrained into the plume should track the TdFe from vents across four different vent sites.

But what potentially could be happening is that Fe, stabilised by organic complexation, may be entrained from the diffuse flow areas as well as DOC. In 1991, diffuse flow around the Bio9 site was sampled and the chemistry of the fluids analysed. Fe and Mn concentrations had maximum concentrations of 151 µM and 29.8 µM respectively, compared to 2190 µM and 285 µM, in the end-member fluids (Von Damm, 2004; Von Damm and Lilley, 2004). These concentrations were in the same range as measured in diffuse flow at the TAG hydrothermal mound (James and Elderfield, 1996a), with maximum Fe concentrations around 800 µM.

But again, it is not easy in this case to claim that the source of TdFe in the buoyant plume at each of these high temperature vent sites is dominated by entrainment from diffuse flow areas.

DOC may also be produced in-situ in the buoyant plume, as extracellular compounds associating with the Fe. An equivalent process has been seen on land with the release of siderophores from the soil bacterium *Pseudomonas sp.*, in order to make the Fe more bioavailable (Hersman et al., 1996). Obviously this is a terrestrial process and in the

upper ocean siderophores have only been observed to be released under Fe stress (Reid et al., 1993), which is certainly not the case in these high-temperature plumes.

Recently, there have been a number of pieces of evidence that have suggested Fe oxidising bacteria to be significant around hydrothermal systems; 1) The presence of biogenic Fe oxide deposits in the hydrothermal sediments (Little et al., 2004) and 2) The isolation of Fe oxidising bacteria from low-temperature seafloor metal sulfide minerals in the vicinity of the vents on the Juan de Fuca Ridge (Edwards et al., 2003). Such species, if present in the high-temperature plumes, could be releasing extracellular compounds in order to quench abiotic oxidation. But again there is no direct evidence for such a process in the vents at 9°50' EPR.

Cowen and Li (1991) observed all pMn in the non-buoyant plume to be encapsulated by bacteria whereas Fe was observed to be both encapsulated as well as present as amorphous FeOOH particles in a non-buoyant plume. If these bacteria capsules associated with the Fe are a result of Fe oxidising bacteria, this would suggest that two competing oxidation processes must be occurring in the plume, both biotic and abiotic oxidation. Fe oxidising bacteria must compete with abiotic reaction kinetics in order to control oxidation processes occurring with ambient seawater. This would result in both encapsulated Fe and amorphous Fe oxyhydroxides in the non-buoyant plume, as observed. Mn oxidation is much slower, therefore microbial oxidation will be faster and will result in all the pMn being encapsulated. Increased concentrations of encapsulated Fe and Mn have been observed 50 km east of the East Pacific Rise at non-buoyant plume height (Cowen and Bruland, 1985). This suggests a potential stabilisation of colloidal and particulate Fe and Mn *from* hydrothermal systems.

However, even though we can not conclusively explain the relationship between TdFe and DOC, Toner et al. (2007), have demonstrated organic carbon interactions with Fe(II), at the 9°50' EPR vents too, suggesting a more hydrothermal-biological Fe-Carbon coupling at these sites than previously realised.

4.5 Summary

Elevated DOC and POC concentrations have been observed a few meters above high-temperature chimneys on the East Pacific Rise. Continued dilution of the plume resulted

in DOC and POC concentrations higher up in the buoyant plume becoming similar to background concentrations. The organic matter within the plumes may either be entrained or produced in-situ and a fraction of the POC is likely to be composed of bacteria.

Directly above the chimneys, the collected samples also had elevated Fe concentrations and in-situ chemical measurements detected elevated temperature and H_2S concentrations. The elevated Fe concentrations appeared to be directly related to the DOC concentration and it is suggested that this is a result of microbial activity either occurring in areas of diffuse flow and then entrained into the high-temperature plume or within the buoyant plume itself.

The detection of a relationship between Fe and DOC would be consistent with metal-organic interactions, which will be investigated further in the following chapter. This is the first time such a relationship has been observed between Fe and DOC, suggesting a much more important role of biological activity in the fate of Fe in high-temperature hydrothermal plumes, than has previously been recognised.

Chapter 5. Non-buoyant plumes – dissolved Fe distribution and stabilisation

[The majority of this chapter has already been published in Bennett et al., Earth and Planetary Science Letters, 2008, doi:10.1016/j.epsl.2008.01.048]

5.1 Introduction

An elevated concentration of dissolved organic carbon has been detected in high-temperature hydrothermal buoyant plumes from a basalt hosted system along the EPR. The DOC concentration, in excess of the background DOC, appears to be positively correlated to Fe, which suggests the potential of stabilised organic Fe complexes within high-temperature plumes. However, the presence of stabilised organic Fe species can only be speculated from the measurements and therefore within the following chapter, the stabilisation and speciation of Fe will be investigated further.

Analyses of total and dissolved Fe and Mn concentrations have been carried out in non-buoyant plumes at another basalt hosted vent system, this time between 4° - 5°S along the Mid-Atlantic Ridge. An in-depth study of stable Fe-ligand complexes has been carried on the dissolved Fe fraction, which will enable determination of any organically complexed dissolved Fe species within this system.

5.2 Hydrothermal plume sampling

During CD169 (Feb-Mar 2005, Chapter 3), non-buoyant plume samples were collected with a CTD rosette, which was deployed at various locations on the basis of evidence gathered from in-situ sensors attached to TOBI and ABE. During the first leg, the CTD rosette was deployed twice in a non-transform discontinuity between two adjacent ridge-segments near 4°00'S (Figure 5.1). The purpose of these stations was to intercept an optical plume detected in this area and collect samples for trace metal analysis to confirm whether or not this particle rich layer of water was hydrothermal in origin.

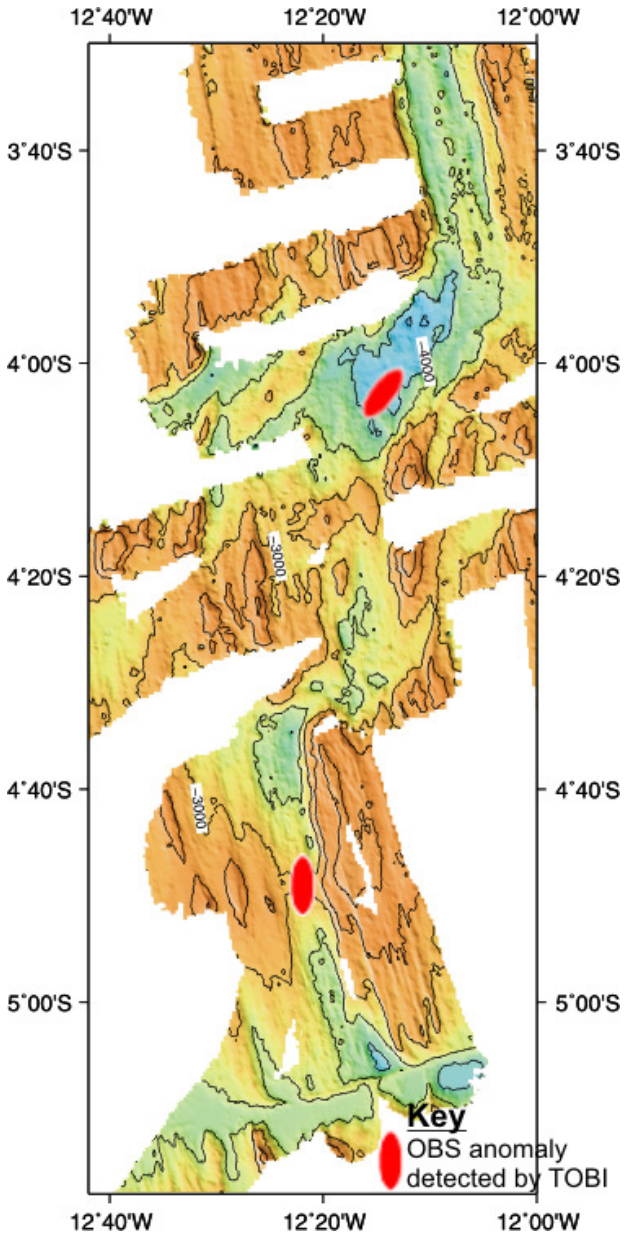

Figure 5.1 - Bathymetric map of two areas of the southern MAR where mid-water particle-rich lenses of water were detected by TOBI (Shallow to deep:orange to blue)

During the second leg, the second site (4°47'S, 12°22'W) with potential hydrothermal activity was chosen for a more in depth plume survey because of both proximity to port (hence increased sampling time) and the identification of extremely fresh lava-flows at this site. Figure 5.2 shows the location of the CTD stations, relative to the vent locations. CTD casts were initially targeted from TOBI/MAPR surveys, based on non-buoyant plume detections, but as further evidence was collected by ABE, CTD cast locations

were chosen with ever increasing precision. These plumes were likely to be sourced from the three high-temperature vent fields: Red Lion, Turtle Pits and Comfortless Cove (German et al., 2008a; Haase et al., 2007; Koschinsky et al., 2006b), all of which are located within 2 km of each other and close to the axial summit of a 2nd order segment of this slow-spreading ridge (Figure 5.2).

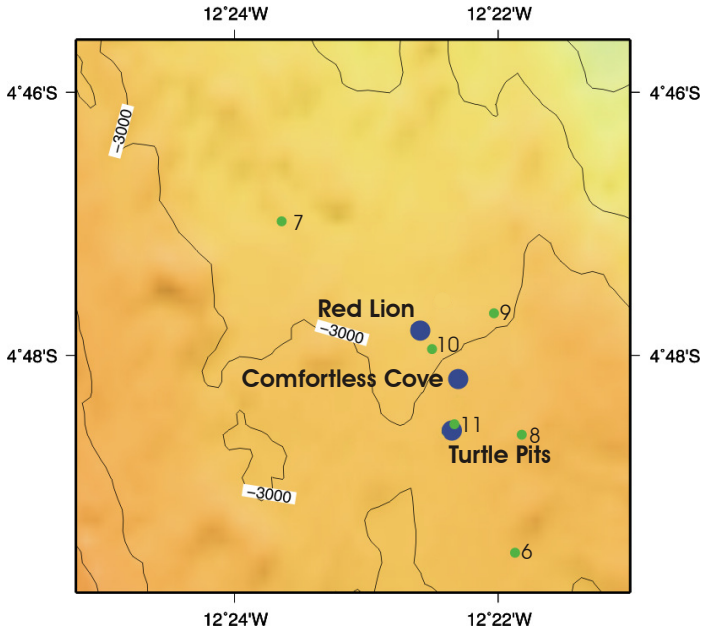

Figure 5.2 - Location map of the three high-temperature vent-sites recently located at 5°S MAR together with locations of CTD-stations occupied for this study

5.3 Results

5.3.1 CTD stations around the non-transform discontinuity at 4°S

The vertical profiles of TdFe, TdMn and light transmission at the two CTD stations located between two adjacent ridge-segments near 4°00'S are shown in Figure 5.3a and b. At CTD station 1, particles were observed between 3200 m and 3500 m by a decrease in the transmissometer signal and an increase in Fe and Mn (Figure 5.3a). The coincidence of both particle anomalies and elevated Fe concentrations at greater than 100 m above the seafloor are diagnostic of the presence of non-buoyant hydrothermal plumes in this area. Either side of this anomaly a transmissometer signal with only small deviations was observed. In comparison to the EPR non-buoyant plumes (Chapter 4), below the plume, the background seawater had a lower average transmissometer signal

than above the plume. This is due to the continual settling of particles from the plume to the seafloor increasing the suspended particle-load in deep waters below plume height when compared to the overlying deep-ocean water column.

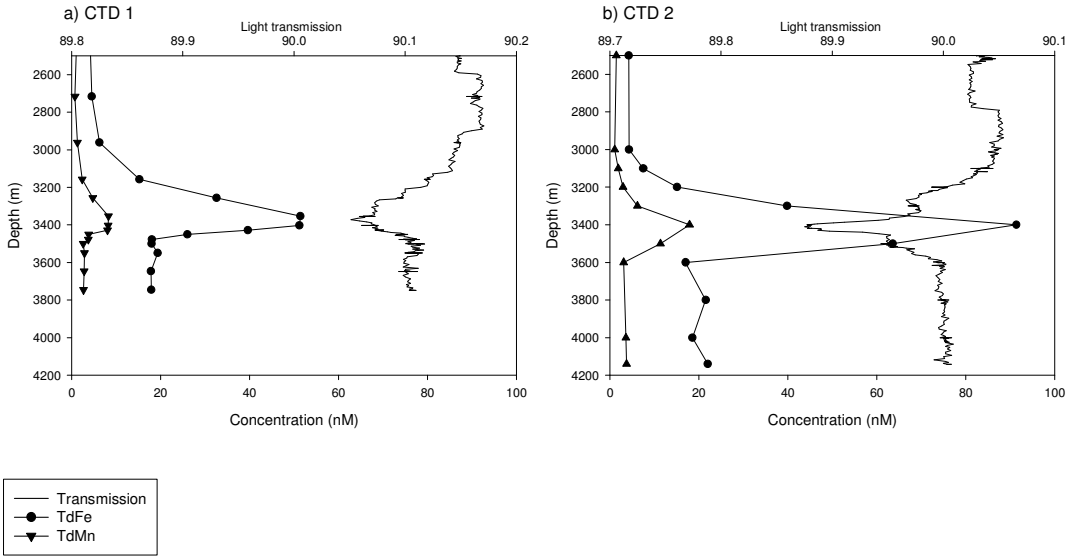

Figure 5.3 - a) and b) Depth profiles of total dissolvable Fe and Mn (TdFe and TdMn) and light transmission for stations that intercepted non-buoyant plumes at the non-transform discontinuity at 4°S.

A second CTD deployment was carried out 9.8 km north of CTD 1 with detection of even stronger Fe and Mn signals at exactly the same plume height (Figure 5.3b).

5.3.2 CTD stations around the fresh lava flows at 5°S

Vertical profiles of TdMn, TdFe, dFe and light transmission at the six CTD stations occupied near 5°S are shown in Figure 5.4 and Figure 5.5. Again Fe, Mn and particle anomalies at greater than 100 m above the seafloor support the presence of non-buoyant hydrothermal plumes in this area. The CTD stations were occupied at locations ranging between 0.2 and 2.5 km from the nearest known vent-sources (Table 5.1) and maximum concentrations fell in the range 13 - 30 nM for TdMn, 12-80 nM for TdFe and 9-64 nM for dFe. Particulate Mn remained below 0.3 nM, indicating that Mn was acting conservatively in this system (Appendix 2).

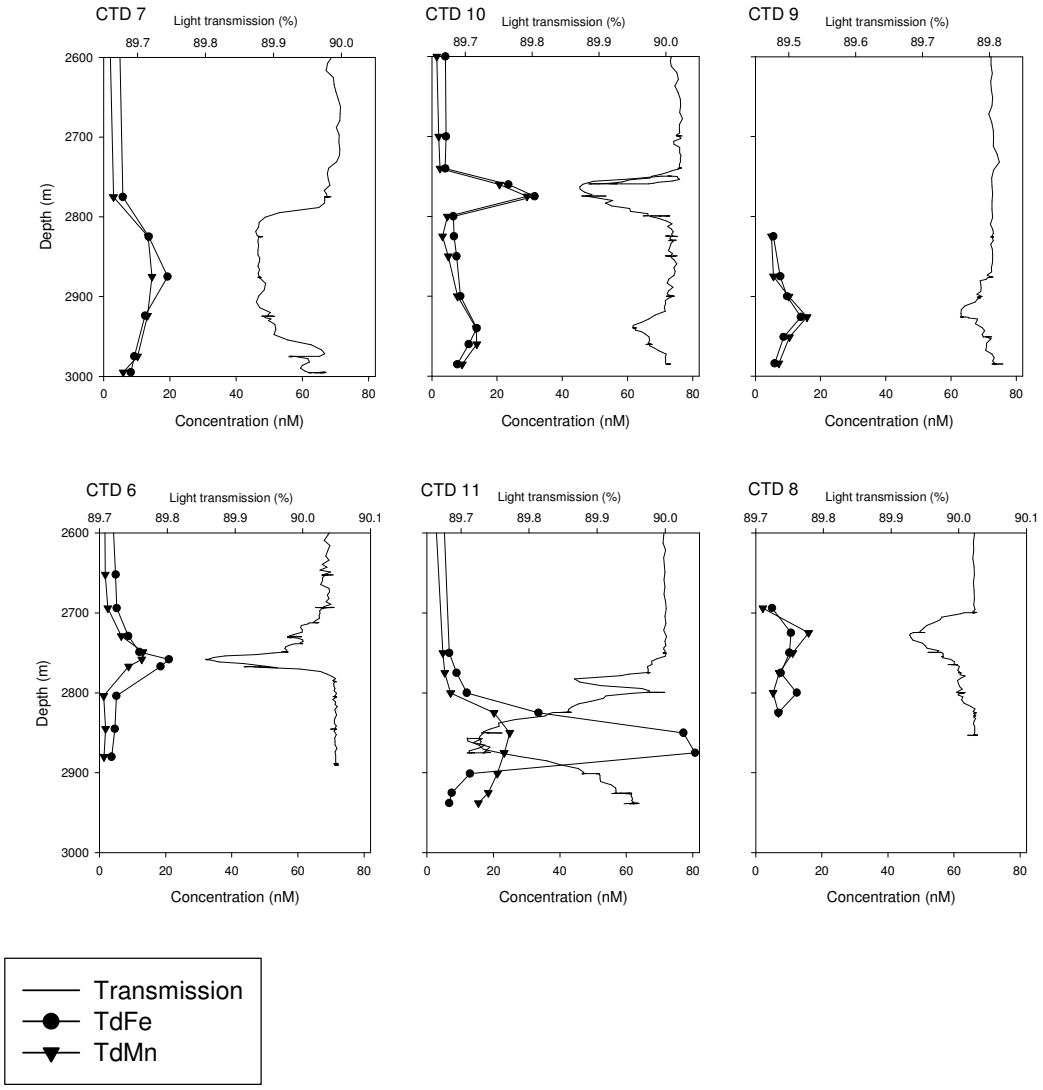

Figure 5.4 - Depth profiles of total dissolvable Fe and Mn (TdFe and TdMn) and light transmission for stations that intercepted non-buoyant plumes in the 5°S segment, MAR.

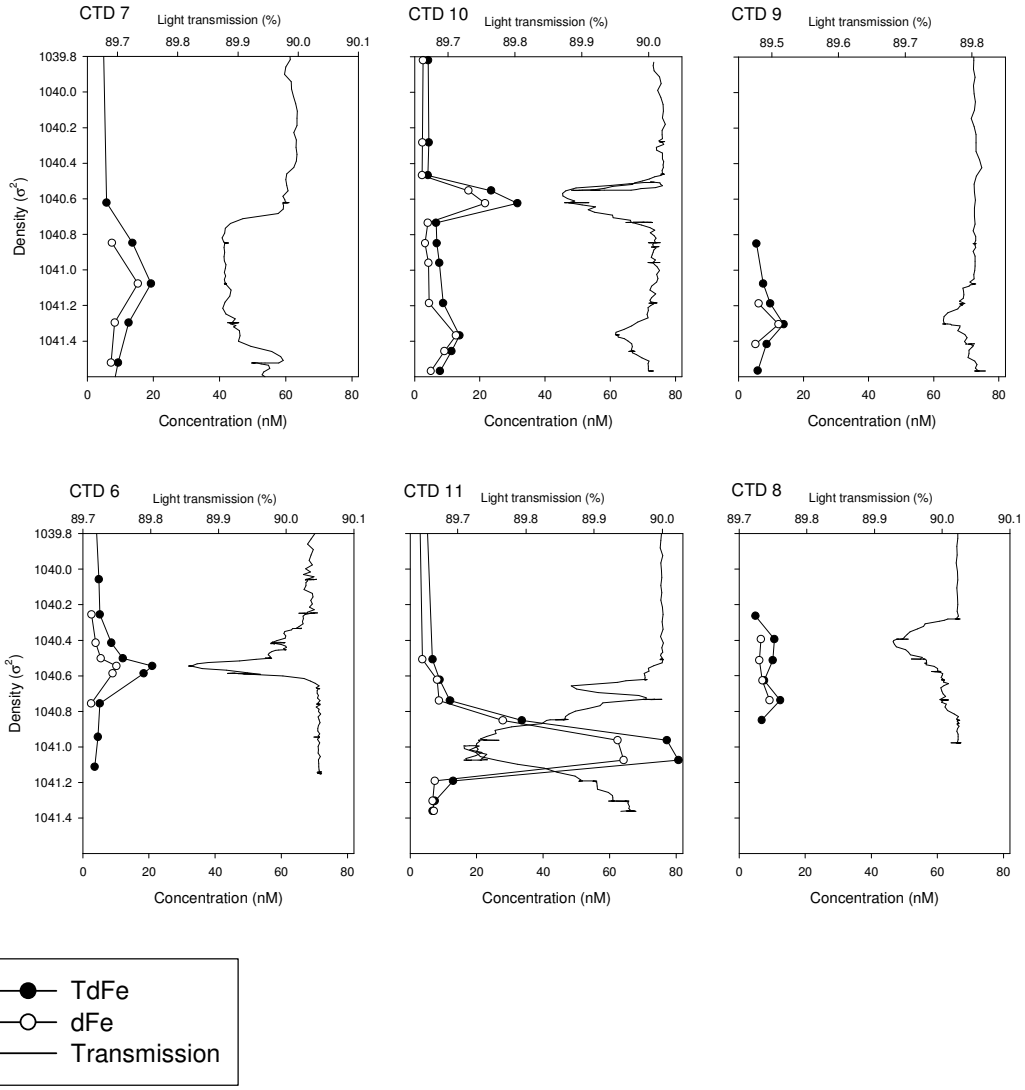

Figure 5.5 - Density profiles of total dissolvable Fe (TdFe), dissolved Fe (dFe) and light transmission for stations that intercepted non-buoyant plumes in the 5°S segment, MAR.

Table 5.1 - Distances of CTD-stations from nearest known vent-sites

CTD Station	Latitude	Longitude	Nearest vent source[a]	Range from nearest source (km)
6	4°49.50' S	12°21.87' W	TP	2.0
7	4°46.98' S	12°23.64' W	RL	2.5
8	4°48.60' S	12°21.82' W	TP	1.1
9	4°47.68' S	12°22.03' W	RL	1.0
10	4°47.95' S	12°22.50' W	RL	0.4
11	4°48.52' S	12°22.33' W	TP	0.2

[a]TP is the Turtle Pits vent site and RL is the Red Lion vent site

Samples from within the particle rich plume were selected for speciation studies but on analysis it became apparent that Fe concentrations in the centre of the plume were so large that any organic ligands present were saturated by Fe and could not be detected by CLE-CSV (e.g. Figure 5.6). However, a fraction of each sample was resistant to ligand competition and this, therefore, enabled determination of a stable Fe fraction. This fraction was interpreted to comprise of stable inorganic colloids and saturated organic complexes. The titration data were modelled using both a linear (Langmuir) and non-linear (Gerringa) approach (Chapter 2.6.2) with little difference observed between the two modelling techniques.

Table 5.2 - Speciation results from central plume samples with high Fe concentration

CTD	Depth (m)	$[Fe]_d$ (nM)	Stable Fe fraction (nM)		% stable Fe
			Langmuir	Gerringa	
7	2875	15.3	8.0	6.4	47
11	2825	27.9	13.6	13.4	48
16	2985	26.8	21.1	21.1	79
16	2981	20.7	13.7	13.0	65
16	2971	32.9	17.6	19.2	56

Samples from CTD16 were from the buoyant plume which will be described in Chapter 6. $[Fe]_d$ is the dissolved Fe concentration (0.4 µm filter).

Samples came from the farthest non-buoyant plume located at CTD 7, 2.5 km from the nearest vent site (Red Lion) and from the closest non-buoyant plume located at CTD 11, 0.2 km from the nearest vent site (Turtle Pits). Also three samples were analysed from the Red Lion buoyant plume, which will be described in Chapter 6. The dissolved Fe concentration in these samples ranged from 15.3 to 32.9 nM and between 47 and 79% of this Fe was determined to be stabilised.

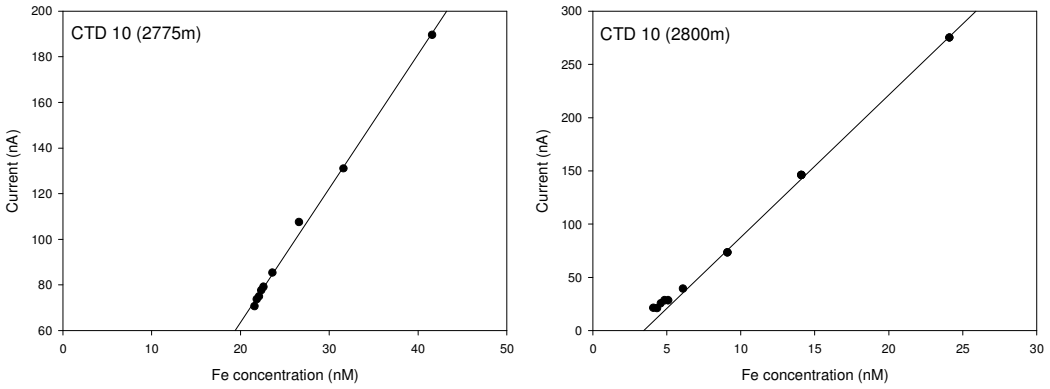

Figure 5.6 – Titration plots demonstrating ligand saturation (CTD 10 (2775 m)) and ligand detection (CTD 10 (2800 m)). Note the different scales on the axes.

Only at the shallower plume at CTD 10 – the closest station to the Red Lion vents – were any organic ligands detected (e.g. Figure 5.6). An example of the modelled data is shown in Figure 5.7 using the Langmuir transformation method. The gradient of the graph and the y intercept were used to calculate L and K, as described in Section 2.6.2.

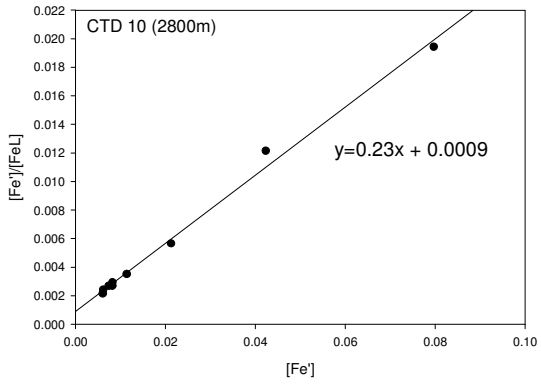

Figure 5.7 - Modelling the titration data using the Langmuir transformation method

At CTD 10, a full vertical profile of samples were collected through the plume for speciation studies. An enlarged section of this CTD cast, showing dFe and TdMn concentrations together with transmissometer data, is shown in Figure 5.8. Descending from above the top of the plume, dissolved Fe concentrations increased from 2.3 nM at 2739 m to 16.6 nM at 2759 m and 21.6 nM at 2775 m – the "core" of the non-buoyant plume. Below this depth, dissolved Fe concentrations decreased to 4.1 nM at 2800 m and 3.2 nM at 2825 m (Table 5.2). TdMn concentrations followed a similar pattern, with concentrations ranging from 2.5 to 29.2 nM (Figure 5.8).

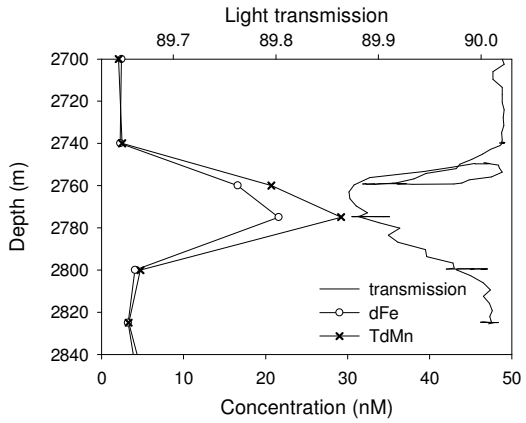

Figure 5.8 - Enlarged depth profile for dissolved Fe (dFe), total dissolvable Mn (TdMn) and light transmission for the shallower plume at CTD 10.

Again, ligands could not be detected in the two "plume-core" samples because the high dissolved Fe concentrations at these locations saturated any Fe binding ligands present. The stabilised fraction made up 32 and 37% of the dissolved Fe fraction. By contrast, ligands were detected on the upper and lower fringes of the plume. Below the core of the plume, the two deepest samples had total ligand concentrations of 4.2 nM at 2800 m and 3.4 nM at 2825 m along with corresponding conditional stability constants of $K'_{Fe'L}$, 11.5 and 11.0 (Table 5.3). Above the core of the plume, the shallowest sample, at 2739 m depth, had a ligand concentration of 2.5 nM with a corresponding conditional stability constant of $K'_{Fe'L}$ 11.1. All ligand concentrations and stability constants were calculated using the langmuir modelling method. The stability constant for the Fe ligand complex, $K'_{Fe'L}$, could only be determined for the low Fe samples when the ligand was not saturated.

Table 5.3 - Dissolved Fe speciation results

Depth (m)	$[Fe]_d$ (nM)	[L] (nM)	Estimated $K'_{Fe'L}$
2739	2.3	2.5	11.1
2759	16.6	n.d. (5.3)	n.d.
2775	21.6	n.d. (8.0)	n.d.
2800	4.1	4.2	11.5
2825	3.2	3.4	11.0

$[Fe]_d$ is the dissolved Fe concentration (0.4 µm filter). [L] is the total concentration of natural ligand within the sample and $K'_{Fe'L}$ is the stability constant of the complex. "n.d." indicates that an organic ligand could not be determined, but the stable Fe fraction is shown in brackets.

5.3.3 Speciation considerations

A series of recent publications have questioned exactly what is being detected by the CLE-CSV technique and a theoretical analysis of the kinetics has cast doubt on whether the calculation of the labile fraction and stability constants is correct (Town and van Leeuwen, 2005a; van Leeuwen and Town, 2005). The calculation of the stability constant requires equilibrium to have been attained between the natural system and any added Fe and ligand. The rate of formation of the $Fe(TAC)_2$ will be fast due to the excess concentration of added competitive ligand and its large conditional stability constant. Therefore the rate determining step will be the dissociation of the Fe ligand (FeL) complex and the concentration of the ligand should not matter. Calculations have shown that in a typical overnight equilibrium period, the 'detection window' is 3 – 8 orders of magnitude lower than the reported stability constants for natural FeL and the analysis will not have detected any such ligand. This is based on theoretical kinetics and in particular, the rate of water exchange in the inner coordination sphere of the metal ion. For Fe, this rate is slow and therefore it is calculated that it would take years for Fe to reach equilibrium.

One of the major flaws in this argument is the explanation for the curve observed in the titration plot for open-ocean water during ligand analysis with CLE-CSV. After UV irradiation and therefore destruction of the organic complexation the titration plot becomes a straight line plot (Hunter, 2005; Van den Berg, 2005). The rebuttal by Town argues that organic complexation may still be present, but one can not assume that the whole of the Fe ligand fraction is completely organically complexed (Town and van

Leeuwen, 2005b). This has been taken into consideration in this study and therefore the Fe ligand fraction has not been assumed to be completely organic.

Also, because the hydrothermal system is expected to be predominantly inorganic, it needs to be confirmed that no false positives occur due to the presence of inorganic colloids. Such complexes could potentially mimic the organic species by bonding and/or adsorbing the Fe added during the titration making it unavailable for complexation with the added synthetic ligand. Some laboratory experiments were carried out to investigate the effect of a completely inorganic system on the CLE-CSV method.

By using UV digested open-ocean seawater (Canary Basin, [dFe] = 0.26 nM) a purely inorganic system has been investigated (Van den Berg, 2005) which, when treated by adding an inorganic Fe(II) spike (Statham et al., 2005) and allowing its oxidation, mimics the inorganic aspects of a hydrothermal system. Repeated CLE-CSV analyses at increasing times after the first Fe addition have confirmed an absence of any organic ligands in the synthetic system, thereby providing us with strong evidence that a fraction of the ligands observed within our natural hydrothermal plume samples must indeed be organic in nature (Van den Berg, 2006)(Appendix 4).

5.4 Discussion

5.4.1 Hydrothermal plumes at the non-transform discontinuity

The two CTD stations occupied at 4°S at the non-transform discontinuity both exhibited high Fe and Mn concentrations (91 and 17.9 nM, respectively). These concentrations were comparable to those in the non-buoyant plumes above Rainbow and TAG in the North Atlantic. The setting of this non-buoyant plume is very similar to the Rainbow hydrothermal field, away from any neo-volcanic activity, however the vent site location at 5°S remains unknown (German et al., 2008a).

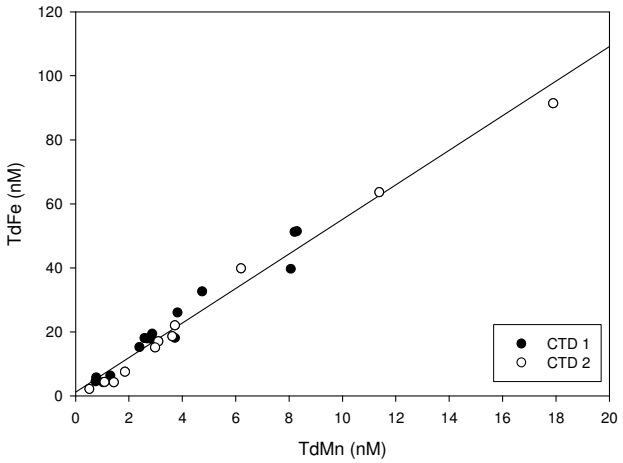

Figure 5.9 - Plot of TdFe *vs.* TdMn for both CTD 1 and CTD 2

The TdFe/TdMn ratio for the two CTD stations remained relatively constant throughout the plumes (Figure 5.9) and exhibited an Fe/Mn ratio equal to 5. Here, even though the distance between the two CTD stations is 9.8 km (Figure 5.10), the similarity in the Fe/Mn composition and plume height suggests that these two CTD stations are sampling the same plume. The concentrations of Fe and Mn are greater at CTD 2 than CTD 1 and therefore the plume cross section at CTD 2 must be closer to the actual vent site. This suggests that the vent site must be on the walls or right in the non-transform discontinuity.

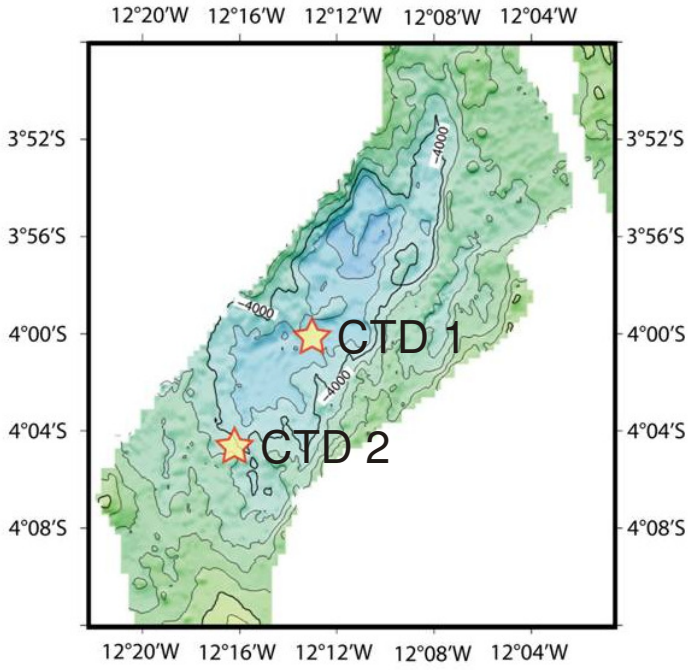

Figure 5.10 - CTD locations in the NTD at 4°S, MAR (German et al., 2008a)

5.4.2 Hydrothermal plumes at the 5°S ridge segment

The six CTD stations occupied at 5°S, extending from North to South across the axial summit at the centre of the 5°S ridge-segment (Figure 5.2), all exhibited evidence of non-buoyant hydrothermal plumes. Distances from the nearest vent-site to each station (Table 5.1) ranged from 0.2 km (CTD 11) to 2.5 km (CTD 7). Unsurprisingly, the strongest anomalies observed (Figure 5.4) were in the profiles for CTD stations 10 & 11, occupied at the very centre of the ridge-segment and immediately adjacent to, or directly above, known high-temperature vent-sites (Figure 5.2). However, the weakest hydrothermal plume signals were not observed at the most distal CTD stations (6, 7) occupied 2 km SE and 2.5 km NW away from the vent-sites (Figure 5.2 and Figure 5.4). Instead, it was at CTD stations 8 and 9, occupied just ~1 km from the vent-sites, but offset away from the axis toward the Eastern rift-valley wall, that the weakest plume-signals were observed. These distributions provide strong evidence that along-axis (NW-SE oriented) flow dominates dispersion of non-buoyant plume material within this ridge-segment, with much weaker advection across-axis toward the rift-valley walls.

These hydrothermal plumes exhibited much more varied Fe/Mn ratios than CTD 1 and 2, consistent with the presence of more than one vent source for these various plumes. The 5°S site has been studied in much more detail on two subsequent cruises since the sampling of the non-buoyant plumes, using remotely operated vehicles (ROV's) to investigate the location of vent sites on the seafloor. The locations of three separate vent sites, Turtle Pits, Comfortless Cove and Red Lion, have now been determined and each of these sites has the potential to be the source of each of the non-buoyant plumes sampled in this study. The Fe/Mn compositions of the end-member fluids at each vent site have been observed to vary (K. Schmidt, Jacobs University, Bremen)(Table 5.4). The lowest Fe/Mn ratio is observed at Red Lion (1.2), primarily because of low Fe concentrations at this site. In comparison, the Fe concentrations at Turtle Pits and Comfortless Cove are much higher and the corresponding Fe/Mn ratios are larger (8.2 and 5.3).

Table 5.4 - End-member vent fluid composition at 5°S

Vent site	[Fe] (nM)	[Mn] (nM)	Fe/Mn	(Fe-FeS)[a]/Mn
Red Lion	710	604	1.2	0.55
Turtle Pits	3980	487	8.2	4.1
Comfortless Cove	3640	690	5.3	2.7

[a] (Fe-FeS) is the Fe present in the plume after 50% of it has be lost as Fe sulfides to the seafloor

The Fe/Mn ratios within the plumes at 5°S are shown in Figure 5.11. None of the plumes appeared to demonstrate the same high Fe/Mn ratio observed in the end-member fluids at Turtle Pits and Comfortless Cove, even though the locality of the CTD stations, especially CTD 11, had a large potential of sampling these fluids. This suggests that Fe must have been fractionated from the plumes during plume dispersal. During the first few seconds of venting, it has been predicted that up to 50% of the Fe forms dense Fe sulfide precipitates which are then lost from the plume to the seafloor as the plume disperses away from its source (Rudnicki and Elderfield, 1993). Therefore the Fe/Mn ratio can be estimated for the non-buoyant plume after the loss of Fe sulfides (50%). The new Fe/Mn ratios are shown in Table 5.4 and with lines in Figure 5.11.

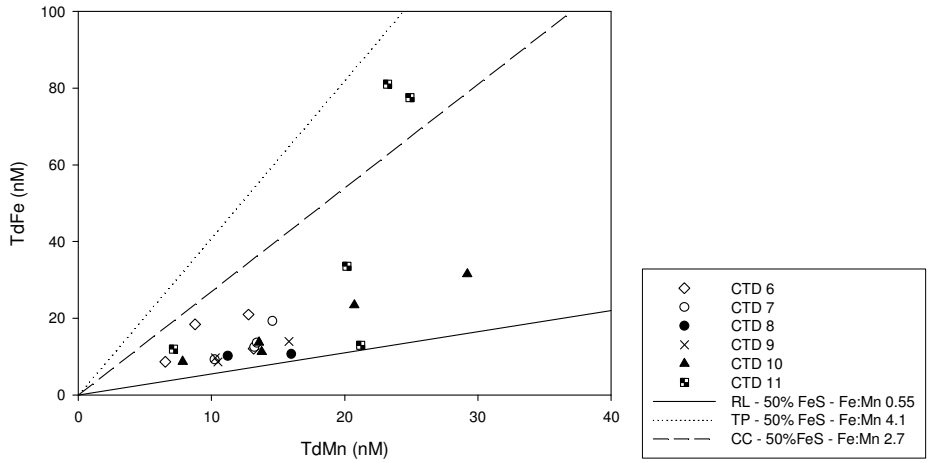

Figure 5.11 - Plot of TdFe *vs.* TdMn for CTD stations at 5°S. A line is present for each end-member vent fluid indicating the Fe/Mn ratio after fractionation of Fe sulfides (see text for explanation)

In the plumes, high Fe concentrations were only observed at CTD 11, which was located only 0.2 km away from the Turtle Pits vent site. Even so, the Fe/Mn ratio in the plume is still lower than the end-member fluid, even after accounting for 50% Fe loss as Fe sulfides and therefore further Fe must have been lost from the plume. However, the proximity of the CTD station to Turtle Pits and the high Fe concentrations confirms that Turtle Pits must be the source of this plume.

The percent of Fe lost from the plume can be calculated by using the end-member Fe/Mn ratio at Turtle Pits and calculating the amount of Fe that should have been present in the non-buoyant plume if the Fe had behaved conservatively relative to the amount of TdMn measured. The calculated TdFe concentration minus the measured Fe concentration gives the concentration of Fe lost from the plume, which can then be converted into a percentage. Therefore it can be calculated that 60% of the Fe must have been fractionated from the two central plume samples and 80% from the two outer plume samples. This is much more than is predicted by Rudnicki and Elderfield (1993) because of Fe sulfide loss and suggests that Fe oxyhydroxides are likely to lost in association with the Fe sulfides.

The rest of the plume samples have a much lower Fe/Mn ratio. It is more difficult to determine the source of these plumes because none of the plumes are in close proximity

to a vent site, like CTD 11. At this basalt hosted vent system, Fe sulfide loss will be expected during buoyant plume rise, therefore it is unlikely that a plume sourced from Red Lion will have the same Fe/Mn ratio as the end-member fluid. Therefore the plume at CTD 6, one sample from CTD 7 and the shallower plume at CTD 10 are likely to be sourced from either Turtle Pits or Comfortless Cove.

CTD 7 exhibits a broad, particle-rich maximum extending from ~2750-2950 m depth, at a distance of ~2.5 km down-plume from the nearest vent-site (Red Lion). This plume is therefore likely to be made up of the multiple plume-layers that formed close to the vent-sites which will have then coalesced through vertical mixing resulting in a single broad hydrothermal plume. Similar plume coalescence of multiple plume layers has been seen previously, at increasing distance down-plume from a vent site, e.g. over distances up to 12 km from the Rainbow vent site (German et al., 1996). In this study, the CTD 7 plume is potentially made up of vent fluid from each of the 5°S vent sites.

The plume samples from CTD 8, 9 and the deeper plume at CTD 10 have an Fe/Mn ratio less than one. For these plumes their source can not be determined and will depend on how much Fe has been fractionated during plume dispersal.

An important feature of these non-buoyant plumes is that the depths the plumes occur at are not consistent (Figure 5.4). Further, close to the segment centre, the profile at CTD 10 revealed evidence for two different hydrothermal plumes at ~2750 m and ~2950 m. Two processes might cause this. First, the height rise of a buoyant hydrothermal plume is a function of both the local water-column's density stratification and the buoyancy flux associated with any given vent-system (Lupton, 1995). Thus, two discrete vents situated in the same ridge-segment might easily give rise to plumes at two different emplacement heights – because they were located at different depths on the seafloor or because of different venting intensities, or both. Secondly, once emplaced, non-buoyant hydrothermal plumes do not disperse at a constant depth but along isopycnal (constant density) surfaces. Therefore, during flow over rough topography, or even during the course of a tidal cycle, the observed height of a single non-buoyant plume can routinely vary by 100 m or more (Rudnicki et al., 1994). In the latter case, while the depth of a plume might vary, the density at which the plume lies would not. Figure 5.12 shows the profiles for CTD stations 10 and 11 replotted against density rather than depth. What is

immediately apparent, is that the two plumes observed at station CTD 10 (midway between the Red Lion and Comfortless Cove vent-sites) lie on different isopycnal surfaces from that of the large plume from CTD 11 (occupied directly above the Turtle Pits vent-site). Thus, our near-vent plume data offer clear evidence for three discrete plumes, each sourced by a different hydrothermal vent. This is entirely consistent with the three high-temperature vent-sites, each made up of a number of vent chimneys, now known to exist on the underlying, axial-summit floor (Haase et al., 2007), as well as the potential for further undiscovered vents in this area.

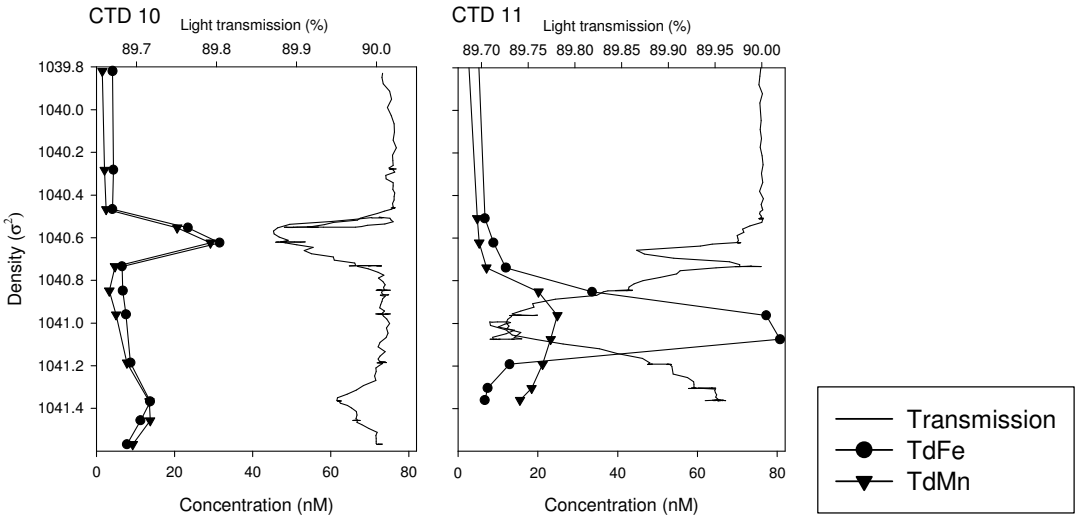

Figure 5.12 - Density profiles of Fe concentrations and light transmission for CTDs 10 and 11.

The non-buoyant plumes at 5°S are all plotted on a density scale in Figure 5.5. This demonstrates that the deeper plume at CTD 10 occurs at the same density as the plume at CTD 9 and the shallower plume occurs at the same density as CTD 8, suggesting that these pairs of plumes are from the same source.

5.4.3 Fe distribution

In order to determine how much dissolved Fe should remain in the plume as it disperses away from the vent site, the oxidation half-life is required for the 5°S vent sites. The rate of Fe oxidation varies between ocean basins because of varying oxygen and hydroxyl concentrations and can be calculated using the method of Field and Sherrell, 2000 (Table

5.5). Within this method, the Fe oxidation rate, K_1, is calculated from the first order rate equation (Equation 5.1) (Millero et al., 1987).

$$K_1 = K[OH^-]^2[O_2][Fe(II)] \quad (5.1)$$

The oxygen data were sourced from the WOCE hydrographic program at a station 700 km west of the vent sites (Line no AR15, 316N142_3, station 55). This oxygen data was also required to calculate the OH^- concentration at this site using:

$$pOH = pK_w - pH \quad (5.2)$$

pH and pK_w were calculated using the Lewis, E., and D. W. R. Wallace. 1998 program which was developed for CO_2 System Calculations (ORNL/CDIAC-105. Carbon Dioxide Information Analysis Center, Oak Ridge National Laboratory, U.S. Department of Energy, Oak Ridge, Tennessee). This program required silicate, phosphate, TCO_2 and TAlk data at the same location and depth as the plume samples collected in this study in order to calculate the correct pH and pK_w and this data was sourced using the same WOCE line as before. In-situ temperature data was sourced from the CTD deployment used to collect the samples.

Finally K is calculated using formulae in Millero et al, 1987:

$$\log K = 21.56 - 1545/T - 3.29I^{1/2} + 1.52I \quad (5.3)$$

Where $I = 19.9201 \times S / (10^3 - 1.00488 \times S)$, S is salinity and T is temperature in Kelvin (Millero et al., 1987). The results are shown in Table 5.5 and the half-life for Fe oxidation at 5°S is determined to be 27 minutes.

Table 5.5 - Calculation of Fe(II) oxidation rates at 5°S compared to TAG using the same method of Field and Sherrell, 2000

Depth	Temp (°C)	Salinity	O_2 (µmol kg^{-1})	pH_{sws}	pK_w	pOH	K_1	Fe (II) half life (hrs)
5°S (Red Lion)	**4°47.83' S**		**12°22.60' W**					
2700	2.5	34.91	242	7.964	14.082	6.118	0.0255	0.45
3000	2.4	34.90	247	7.957	14.076	6.119	0.0257	0.45
TAG	**26°08.20' N**		**44°49.5' W**					
2985	2.8	34.94	255	7.945	14.057	6.112	0.0279	0.41
3481	2.6	34.92	258	7.924	14.053	6.129	0.0258	0.45

(a) Oxygen data, temperature and salinity data sourced from WOCE hydrographic program, Line number A05, 29HE06_1, station 73.

The oxidation rate at 5°S is identical, within error, to the oxidation rate at the TAG hydrothermal mound in the North Atlantic. Further along the thermohaline circulation, oxygen concentrations decrease, resulting in a decrease in the oxidation rate. Therefore the Fe(II) half-life increases from 25 minutes in the North Atlantic to 1 hr and 18 minutes in the Southwest Indian Ocean to 6 hours and 23 minutes along the Juan de Fuca Ridge in the North Pacific (Field and Sherrell, 2000).

The small time difference observed between the half-life at TAG compared to 5°S can be explained by the oxygen and hydroxyl concentrations. The oxygen concentration at 5°S is only 12 µmol kg^{-1} lower than TAG whereas along the SW Indian ridge, the oxygen is up to 70 µmol kg^{-1} lower (Field and Sherrell, 2000). At the SW Indian Ridge the oxidation half-life is just over twice as long as the half-life at TAG. The hydroxyl concentration at 5°S also differs by very little compared to TAG, with such differences making a greater impact on the oxidation rate compared to oxygen because this term is squared in the rate equation.

This oxidation rate can now be used to determine how much dissolved Fe should remain in the plume as it disperses away from the vent site. Two and a half kilometres down plume from the nearest vent site, at CTD 7, Fe concentrations in the non-buoyant plume still remain high. What is particularly notable about this station, however, is not that the

plume is rich in particulate material but that it retains very high concentrations (~20 nM) of dissolved Fe – approximately 30 times higher than typical deep-ocean values (Bergquist and Boyle, 2006). For a strong along-axis current of 10 cm s^{-1} (not uncommon in the deep Mid-Atlantic Ridge rift-valley - see, e.g. Thurnherr et al., 2002), a minimum advection time to this location can be calculated of ~7 h. This is long compared to the predicted dissolved Fe(II) oxidation rate for the local deep water-column (Millero, 1998; Millero et al., 1987) which has a calculated dissolved Fe(II) oxidation half-life of ~27 minutes.

For a typical dissolved Fe vent-fluid concentration of 1 mM, a 10^4-fold dilution can be predicted during buoyant plume mixing to ~100 nM at the top of the buoyant plume (McDuff, 1995) followed by a further reduction to the observed concentrations at CTD 7 of ~20 nM within just ~1 hour (2 half-lives). By contrast, the advection time to CTD 7 from the nearest vent-site at 10 cm s^{-1} would be equivalent to 15-16 dissolved Fe(II) half-lives. To travel the same distance within just one hour would require advection at quite unprecedented deep-ocean current velocities of ~70 cm s^{-1}.

A more plausible explanation for the higher-than-predicted dissolved Fe concentrations is that the operationally defined (<0.4 μm) dissolved Fe fraction includes both truly dissolved and colloidal Fe species. In the open oligotrophic Atlantic and Pacific Oceans it has been argued that a significant proportion of dissolved Fe is actually in colloidal form (Wu et al., 2001). There is also the possibility that a significant proportion of the dissolved Fe present within the 5°S hydrothermal plume may have been stabilised as soluble organic Fe complexes, similar to the stabilised dissolved Fe complexes present in the open-ocean, as well as stable dissolved Fe-sulfide clusters, formed immediately post-venting (Luther et al., 2001).

Organic interaction with hydrothermal Fe has been suggested in the previous chapter as well as from a study of dissolved Fe(II) oxidation rates in non-buoyant hydrothermal plumes overlying the Central Indian Ridge (Statham et al., 2005). More recently, measurements of a decreased fraction of reactive Fe in the vent fluids at the Logatchev vent-site (15°N, Mid-Atlantic Ridge) have been used to speculatively suggest increased complexation of Fe, for example with sulfur or organic compounds (Schmidt et al., 2007). Such complexes, if formed within buoyant hydrothermal plumes, would certainly

have the potential to sustain enhanced dissolved Fe concentrations at least as far as non-buoyant plume height.

5.4.4 Fe speciation in the plume

To investigate whether stabilising ligand complexes are, indeed, present in non-buoyant hydrothermal plumes, speciation studies have been carried out in the plumes at 5°S. As noted above, Fe concentrations in the centre of the plume were so high that they saturated any ligands present and therefore only in CTD 10, where a full vertical profile through a plume was selected for speciation studies, were any organic ligands detected. For samples immediately above and below the core of the plume analyses revealed ligand concentrations in the range 2.5- 4.2 nM (Table 5.3). These concentrations are 3.6 to 6.0 times higher than open-ocean dissolved Fe concentrations (0.7 nM;(Bergquist and Boyle, 2006)). The total ligand concentrations detected are not solely expected to be the result of organic complexation, as the presence of complex inorganic Fe-stabilising ligands, should also be expected to occur as part of this stabilised Fe fraction (Town and van Leeuwen, 2005).

The fraction of stabilised dissolved Fe determined in the buoyant plume appeared to be greater (56 – 79%) than that in the non-buoyant plume (32 – 48%). This is because as the plume disperses, the inorganic colloidal Fe species present in the dissolved Fe fraction will have aggregated and formed larger Fe species which will be separated into the particulate fraction rather than the dissolved fraction. As we can not prove that a fraction of the stabilised Fe will be organically complexed, only the organic ligands observed on the edge of the plume at CTD 10, will now be considered.

Between 2825 m and 2800 m, the ligand concentration increased from 3.4 nM to 4.2 nM toward the plume-core. This mimics the gradient seen for Mn *vs.* depth at CTD 10 (Figure 5.8), which increases from 3.3 to 4.7 nM over the same depth range, indicative of mixing between the plume's interior and the surrounding (both overlying and underlying) water column.

Of course, as demonstrated in the Atlantic Ocean, a fraction of this dissolved Fe is likely to be colloidal (Cullen et al., 2006; Wu et al., 2001). In a recent Fe enrichment

experiment in the Southern Ocean (Boye et al., 2005) it was reported that immediately after Fe addition, the concentration of ligands in the <200 kDa fraction (soluble) only represented 55% of the total ligand present in the <0.2 μm fraction (soluble and colloidal). However, whatever their size-distribution and chemical nature, the larger ligands were still stabilising Fe and preventing aggregation of large particles that would remove Fe to the seafloor (Boye et al., 2005). Further, what is at least as important to note is that even at their most dilute, the concentrations of ligand measured on the fringes of the non-buoyant plume in CTD 10 were significantly higher than typical deep-ocean values (0.7-1.4 nM;(Boye et al., 2001; Cullen et al., 2006)). While higher concentrations have been measured in near-shore waters, both in the NW Atlantic Ocean and in the Black Sea (Witter et al., 2000; Witter and Luther, 1998), Cullen et al. (2006) measured much lower ligand concentrations, down to 1.22 nM, in the deep South Atlantic Ocean (Cullen et al., 2006). It can be argued, therefore, that the simple entrainment of deep open-ocean waters into buoyant hydrothermal plumes at 5°S cannot account for the elevated levels of ligand at near-plume height reported here. Rather, some additional source must exist. Further, because ligand concentrations increased toward the core of the non-buoyant plume, the ligand source must be present during the process of plume emplacement and cannot be attributed, for example, to zooplankton that graze on the fringes of non-buoyant plumes (Burd et al., 1992; Cowen et al., 2001; Vereshchaka and Vinogradov, 1999) - any ligands sourced from outside the plume-core would be expected to exhibit a decreasing concentration inward.

Equally, it does not seem plausible that end-member vent-fluids should be the source of the high organic ligand concentrations measured, as mentioned in Chapter 4. The most likely source of dissolved organic matter will be that entrained into the plume from areas of diffuse flow adjacent to the high-temperature vent-sites or from microbial activity within the plume, referred to in Chapter 4. In support of diffuse flow entrainment, organic copper-binding ligand concentrations have recently been reported for diffuse-flow fluids from above a mussel field south of Lilliput (9°33.01'S, 13°12.38'W;(Koschinsky et al., 2006a)) that reach concentrations of up to 0.6 μM (Sander et al., 2007). These ligand concentrations represent an 8-fold excess over the total Cu present, indicating an abundance of free ligand sites that could potentially be available for Fe complexation if such fluids were, indeed, entrained into an adjacent, buoyant hydrothermal plume.

Such early entrainment of organic matter, into the base of buoyant hydrothermal plumes, would be important because the organic complexation of Fe(III) must be predicted to take place immediately after the oxidation of dissolved Fe(II) but before Fe can precipitate in the form of hydrolysis products. Because Fe(II) oxidation kinetics slow progressively along the thermohaline conveyor (Field and Sherrell, 2000; Statham et al., 2005) this implies that the time period for such complexation to occur should increase along the same trajectory from the Atlantic to Indian and Pacific Oceans, as long as there is an excess of ligand available. At 5°S complete Fe(II) oxidation would be predicted to occur in the first few hours after venting. Therefore, all complexation with organic ligands should either occur within the buoyant hydrothermal plume or within the youngest portions of the non-buoyant plume, immediately overlying the vent-site (Field and Sherrell, 2000; Rudnicki and Elderfield, 1993). This would be perfectly feasible if the principal source of ligand were, indeed, from entrainment of diffuse flow waters at the base of the buoyant plume followed by mixing and commencement of Fe-complexation during plume-rise.

There is also the potential for organically complexed Fe(II) species to be present in the stabilised dissolved Fe fraction (Hopkinson and Barbeau, 2007). Complexation of the Fe(II) would be dominant during buoyant plume rise because of the high abundance of Fe(II) species leaving the high-temperature hydrothermal vents and diffuse flow areas. The presence of such complexes would reduce the rate of Fe(II) oxidation enabling the dissolved Fe to be exported to the non-buoyant plume. Fe(II)-ligand complexes have already been hypothesised to be present in the vent environments in order for Fe oxidising bacteria to control Fe(II) oxidation during Fe sulfide dissolution (Edwards et al., 2004). But unfortunately at present no methods exist for the measurement of dissolved Fe(II)-ligand complexes.

5.4.5 Ligand-stabilised hydrothermal Fe and the global mass balance

The most recent estimation of the global volume flux for seawater passing through high-temperature hydrothermal venting is 7.2×10^{12} kg y^{-1}, calculated using chemical and isotopic mass balances of the element thallium (Nielsen et al., 2006). Allowing for ~10^4-fold dilution in buoyant hydrothermal plumes (McDuff, 1995), this equates to a 7.2×10^{16} kg y^{-1} flux of combined vent-fluid and oceanic deep-water entering non-buoyant hydrothermal plumes, worldwide. By taking the new measurements of stabilising Fe

ligands (4.2 nM) at CTD 10 as representative of young non-buoyant plumes in general, with the assumption that in the core of the plume these ligand concentrations may be even higher (because of less dilution), this would imply that the flux of such stabilising ligands through hydrothermal plumes would be at least 3.0 x 10^8 mol y^{-1}. Assuming 1:1 complexation, this would be accompanied by a global flux of hydrothermal Fe, stabilised by entrained ligands, which would also be estimated as >3.0 x 10^8 mol y^{-1}. This compares to a gross hydrothermal Fe flux of 7.2 x 10^9 mol y^{-1} assuming a nominal vent-fluid dissolved Fe concentration of 1 mM (Range = 5.4-47 x 10^9 mol y^{-1} for end-member Fe concentrations of 0.75 – 6.5 mM (Elderfield and Schultz, 1996)) – i.e our predicted flux of ligand-stabilised Fe passing through hydrothermal plumes would only represent ~4% of the global total (Range: 0.6-5.6%). Even so, this small proportion of the gross hydrothermal Fe flux, could still have a significant impact on global deep-ocean dissolved Fe budgets. The remaining 96% will precipitate and is likely to be lost to the seafloor.

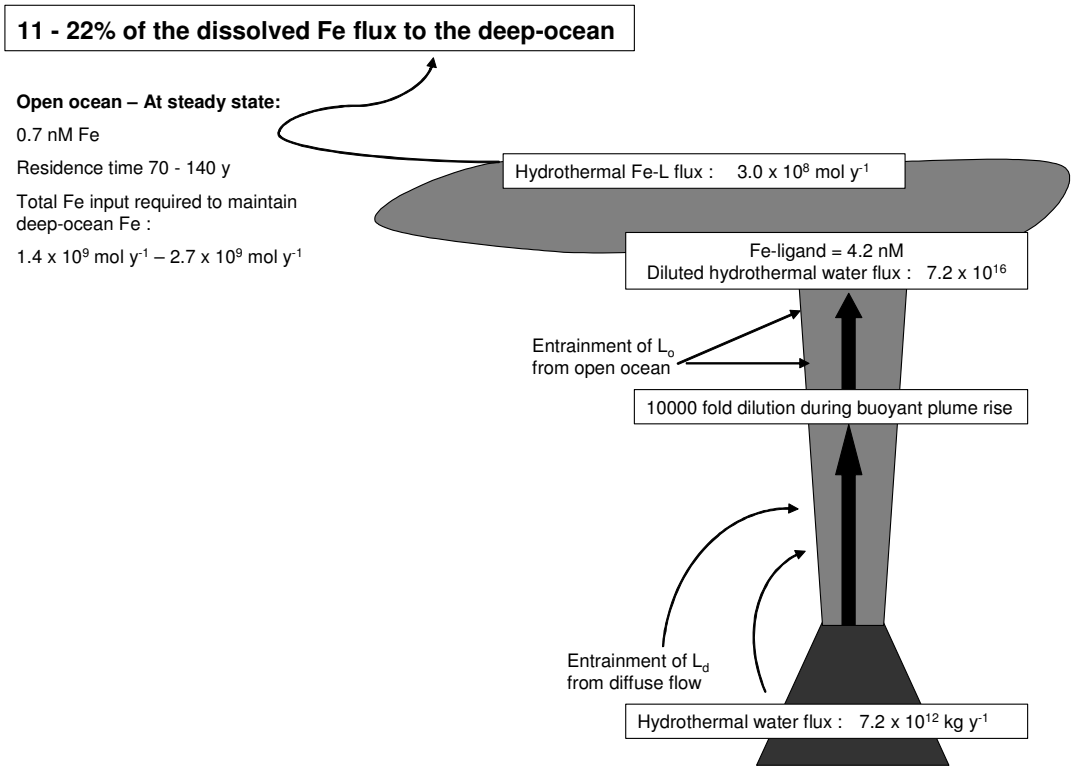

Figure 5.13 - Flux diagram for hydrothermal inputs of Fe to the deep-ocean. L_o is the ligand entrained from the open ocean and L_d is the ligand entrained from the diffuse flow areas.

The volume of the global deep-ocean is estimated as 2.6 x 10^{20} L (Libes, 1992). Assuming a uniform deep-ocean dissolved Fe concentration of 0.7 nM (Bergquist and Boyle, 2006), an instantaneous standing stock of deep-ocean dissolved Fe of 1.9 x 10^{11} mol can be calculated, of which 30–70% is potentially present in colloidal form (cf this study)(Wu et al., 2001). To maintain steady state, with dissolved Fe residence times of 70-140 y (Bruland et al., 1994), the required input flux of Fe to the oceans is 1.4-2.7 x 10^{9} mol y^{-1}. Combining the above, it can be concluded that the predicted ligand-stabilised flux of Fe from hydrothermal systems, which likely represents no more than ~4% of the global hydrothermal discharge, is nevertheless sufficient to supply some 11-22% of the dissolved Fe present throughout the global deep-ocean. This mass balance is summarised in Figure 5.13.

If hydrothermally-sourced Fe is prevalent throughout the deep-ocean then the possibility exists that seafloor hydrothermal venting, which interacts with the entire volume of the deep-ocean over timescales of a few thousand years (Elderfield and Schultz, 1996) might be more closely coupled than has previously been recognised with upper ocean processes - where Fe can act as a limiting micronutrient in HNLC regions (Morel et al., 2004). Key to this argument is the recent demonstration that mantle sourced dissolved ^{3}He from non-buoyant hydrothermal plumes overlying the southern East Pacific Rise (where hydrothermal plumes are at their most abundant (Baker and German, 2004) is, indeed, upwelled to the surface waters of the Southern Ocean, as a simple result of flow along isopycnal surfaces (Jenkins et al., 2007; Winckler et al., 2007). Helium is the most recognised tracer of hydrothermal circulation because of its inert characteristics in seawater. Therefore any ^{3}He found in the ocean can be assumed to be sourced from the mantle. Mn has also been considered to be a useful tracer of hydrothermal activity, even though it is not inert in the ocean (Boyle et al., 2005). This is because its lifetime in its reduced form is much longer compared to Fe as a result of its longer oxidation half-life, varying from weeks (Kadko et al., 1990) to years (Lavelle et al., 1992). Another non-conservative tracer of hydrothermal activity is methane, removed from the plume by microbial activity.

Of immediate future interest, therefore, is whether this same transport mechanism, from hydrothermal plume depths to surface ocean interactions might also be important for other dissolved hydrothermal tracers. For example, will this hydrothermally sourced

stabilised dissolved Fe remain in solution during its circulation throughout the ocean? Or will this Fe be consumed by biological processes before reaching the surface waters? These will be important questions to answer in future work.

5.5 Summary

Non-buoyant plumes collected from two different sites on the Southern Mid-Atlantic Ridge have been investigated for their Fe/Mn ratios. The Fe/Mn ratio has been observed to be constant in the plume at the non-transform discontinuity site (4°S) but to vary in plumes in the middle of the 5°S ridge segment. This is because there are a number of potential sources of the 5°S plumes, which will have different Fe/Mn end-member ratios. Also Fe lost from the plumes during dispersal as Fe sulfide particles results in none of the plumes having the same Fe/Mn ratio as their source.

The fate of Fe in the non-buoyant hydrothermal plumes dispersing away from vents near 5°S, Mid-Atlantic Ridge has also been investigated and it has been found that the dissolved Fe concentrations at plume-height are higher than would be predicted from dissolved Fe(II) oxidation-rates alone. Detailed speciation studies have revealed that a fraction of the dissolved Fe present is stabilised by Fe-complexing ligands and measurements of those ligand concentrations lead to the calculation that ~4% of the total Fe released from the 5°S vents may be stabilised in this way. If the results reported here were representative of all hydrothermal systems, it would imply that high-temperature venting may provide the source for 11-22% of the global deep-ocean dissolved Fe budget and, hence, that submarine venting may provide an important, previously-overlooked, source of dissolved Fe in global-ocean biogeochemical cycles.

Chapter 6. Geochemistry of Fe and some trace elements in a cross section through a buoyant plume

6.1 Introduction

Previous studies of hydrothermal plumes have focused on non-buoyant plumes and, in particular, elemental distributions as a plume disperses away from a vent site (e.g. Edmonds and German, 2004; Feely et al., 1998; German et al., 1991; James and Elderfield, 1996b). At increasing distance from a vent site the element to Fe ratios have been observed to change depending on whether there has been any particulate Fe loss or aging of the plume. The element to Fe ratios are dependent on the forms of the particulate Fe present (sulfides and oxyhydroxides) and their varying surface charge. Therefore, there is the potential to predict the particulate Fe composition based on the trace element concentrations. This is especially the case close to any given vent site where the abundance of sulfide minerals, relative to oxyhydroxides, is often seen to be greater.

In this chapter, a unique set of samples will be considered that were collected during an angled upward CTD section through a buoyant hydrothermal plume. Using data from multi element analyses carried out on the particulate phase, the relationship between Fe and other trace elements in the plume particles will be considered. In particular, the REE patterns within these plume particles will be examined, which are a useful tool for tracing sources and geochemical processes occurring in the ocean (Elderfield, 1988; Elderfield and Greaves, 1982). The conclusions drawn from these data will then be used to interpret the Fe isotope fractionation observed within the same buoyant plume samples (Chapter 7), to investigate whether Fe isotopes are a viable geochemical tracer of hydrothermal Fe sources to the ocean.

During the preliminary cruise to the vent sites at 5°S (CD169), buoyant plume waters, distinguished by marked positive temperature anomalies, were sampled with a CTD rosette, 30 to 60 m north of the Red Lion vent site. These samples were filtered in a clean laboratory aboard the ship through 0.4 μm membrane filters to separate the particulate and dissolved phase.

6.2 Results and discussion

6.2.1 Buoyant plume sampling

Changes in key parameters with time during the upcast of a CTD deployment (CTD 16, 4°47.80, 12°22.61) are shown in Figure 6.1**.** This CTD cast intercepted anomalously warm, particle rich seawater between 30 and 60 m north of the Red Lion vent field. The presence of both positive temperature anomalies and strong transmissometer signals, less than 50 m above the seafloor, indicated that a buoyant hydrothermal plume had been sampled at around 3000 m depth. Buoyant plumes have previously been detected away from their source because of changing tides and currents (Rudnicki et al., 1994). Even though the CTD cast was not occupied directly above the vent-site, its buoyant plume can still be intercepted.

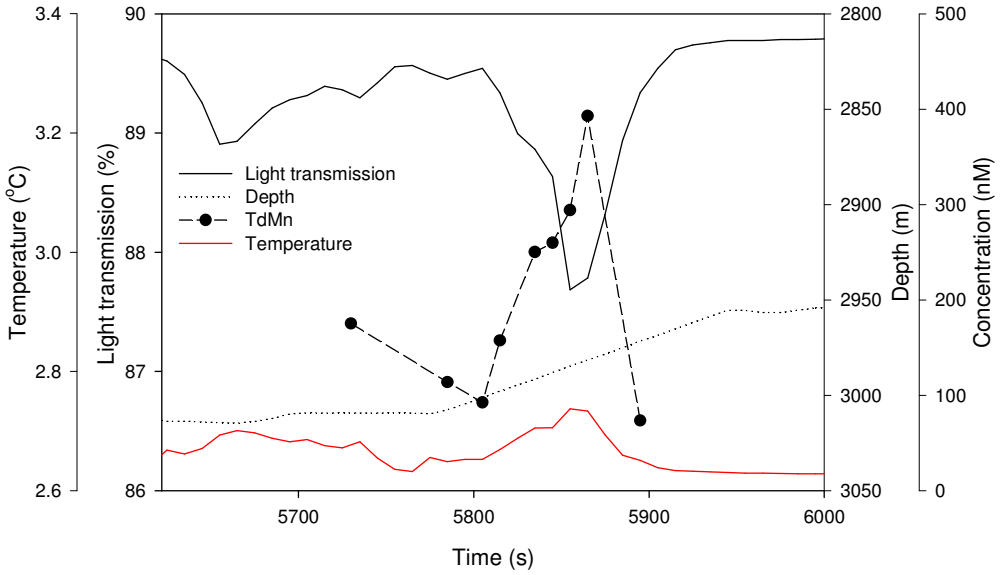

Figure 6.1 – Changes in key parameters with time for the CTD cast that intercepted particle rich water. Temperature, total dissolvable Mn (TdMn) concentration, depth and light transmission are shown.

The CTD drifted over time through different zones of warm particle rich water, at a relatively constant depth. As the CTD was pulled out of the plume at the end of the CTD cast, Niskin bottles were fired repeatedly, collecting samples throughout a lens of buoyant hydrothermal water. For all the samples collected positive temperature anomalies were recorded, along with varying particle and Mn concentrations. The most

Mn rich lens of plume water occurred over a small 'depth range' of approximately 30 m, which reflected passage through a lens of buoyant plume water. Therefore rather than collecting a suite of samples vertically through the rising buoyant plume, the CTD drift resulted in an oblique cross section of the buoyant plume being sampled. The inferred trajectory that the CTD took through the buoyant plume is shown schematically in Figure 6.2. The highest temperature and particle anomalies coincide with the core of the plume.

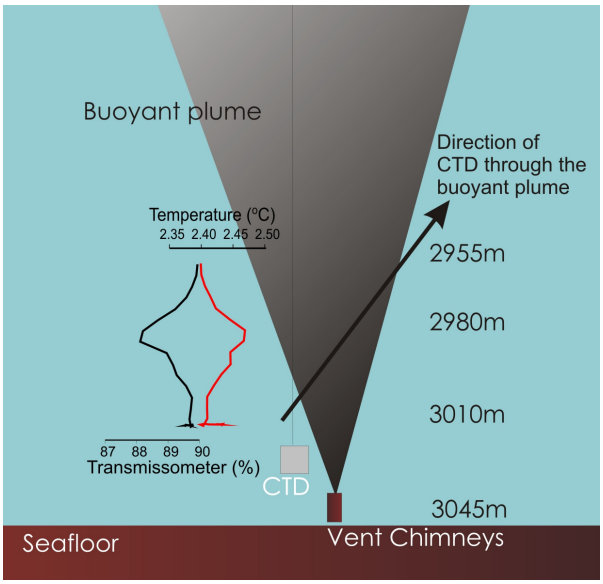

Figure 6.2 - Schematic of the potential upcast path the CTD took through the buoyant plume. The temperature (red) and transmissometer (black) plot is to scale with the height shown on the schematic.

For this study, the best way to visualise the horizontal movement of the CTD through the buoyant plume (and changes in chemical composition) is as a function of time rather than depth. This is because the change in height of the CTD as it bisected the buoyant plume was only small, whereas the movement of the CTD and the buoyant plume through tidal forces and water movement, can be represented more easily with time.

These samples are unique compared to the previously discussed non-buoyant plume samples (Chapter 5) because they have experienced much less dilution with the ambient seawater and represent a much earlier stage in the plume cycle. This provides the potential to study both Fe bearing sulfide and Fe oxide phases in greater detail because in

non-buoyant plumes, by contrast, a large proportion of polymetallic sulfide phases have already been removed via settling and/or oxidation.

The seafloor close to a hydrothermal vent is a dynamic and turbulent environment, therefore a first priority is to demonstrate that the particle samples collected are truly hydrothermal and not entrained resuspended particles from the surrounding sediments. A method developed by Bostrom et al. (1969) using particulate Al, Fe and Mn concentrations has previously been employed (German et al., 1991). Al, Mn and Fe have high solid phase concentrations within the sediments, whereas in the end-member fluids, Al is present as a trace element and Mn is present as a dissolved reduced species that is only slowly removed during mixing with the surrounding seawater (Trocine and Trefry, 1988). Fe on the other hand, initially present as a dissolved reduced species, precipitates rapidly forming solid phase Fe sulfides and Fe oxyhydroxides as soon as the vent fluids first mix with seawater. Therefore, a high ratio value of the Fe/(Fe+Mn+Al) can be used to indicate that samples have little detrital input, with particulate Mn and Al concentrations both low.

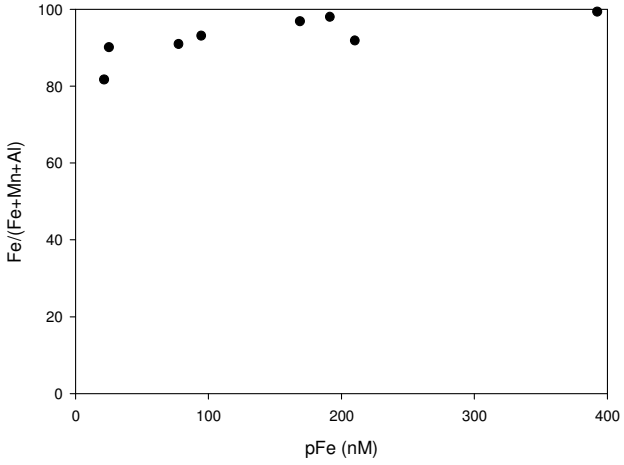

Figure 6.3 - The detrital influence on the plume samples relative to Fe concentration.

In this study, all the samples collected during the CTD upcast had Fe/(Fe+Mn+Al) values greater than 80% (Figure 6.3) indicating a high proportion of hydrothermal material with little influence from any re-suspended sediments. This is not unexpected as the basalts surrounding the vent sites at 5°S were volcanically fresh with minimal sediment cover.

6.2.2 Hydrothermal plume source

During the CTD cast the ship was located directly north of the Red Lion vent site, where four high-temperature chimneys were actively emitting hydrothermal fluids. Therefore all four chimneys represent potential sources of the warm particle rich seawater sampled in this study. The other vent sites, Turtle Pits and Comfortless Cove, are located too far (1.5 and 0.9 km, respectively) from the ship to be possible candidate sources.

The composition of the vent fluids at three of the high-temperature chimneys at Red Lion have been analysed by K. Schmidt, Jacobs University, Bremen and their chemistries have been observed to be very similar. The end-member concentration of the major elements at the Tannenbaum chimney are shown in Table 6.1.

Table 6.1 - End-member concentrations at the Tannenbaum chimney at Red Lion (Data from K. Schmidt, Jacobs University, Bremen)

	End-member (µM)	Elemental ratios
Fe	710	Fe/Mn 1.2
Mn	604	
Cu	7.8	Cu/Fe 0.01
Zn	117	Zn/Fe 0.16

6.2.3 Fe concentrations within the buoyant plume

Particulate Fe, dFe and total Fe (TFe=pFe+dFe) are shown with transmissometer readings as a function of time in Figure 6.4. During sample collection, total Fe concentrations varied from 71 nM to 413 nM. As the CTD rosette crossed the lens of the buoyant plume TFe concentrations increased, with maximum Fe concentrations observed at 2981 m, 65 m shallower than the Red Lion vents. At this depth, if it is assumed that there was no lateral movement of the plume (unlikely in an ocean with currents), any plume rising with a ~15° half-angle (Turner, 1962) would have spread to approximately 35 m in diameter. Therefore the CTD must, apparently, have been within ~20 m of the buoyant plume axis at this time.

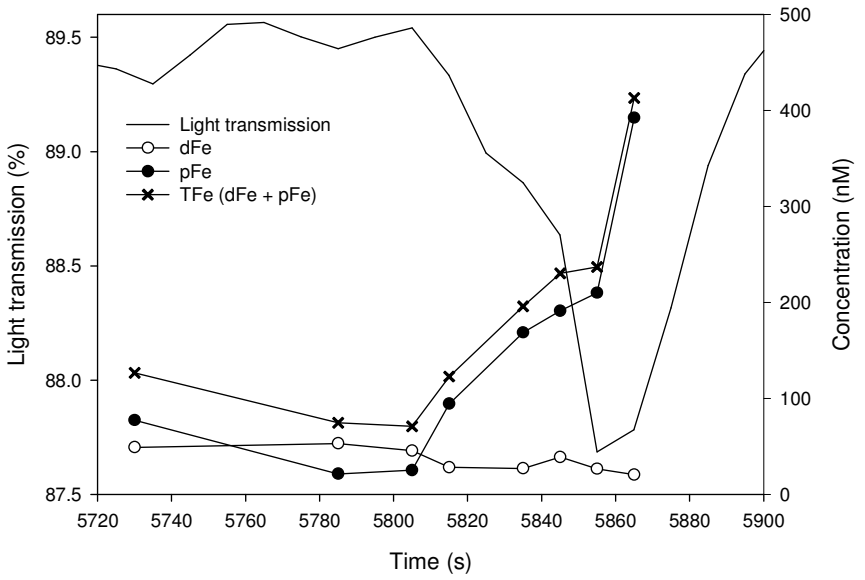

Figure 6.4 - Light transmission and measured particulate Fe (pFe), dissolved Fe (dFe) and Total Fe (dFe+pFe) as a function of time.

The pFe concentrations follow the same trend as TFe (Figure 6.4), ranging from 25 nM to 392 nM. Conversely, dFe concentrations decreased slightly as the CTD was brought up through the water column, ranging from 53 nM at depth to 21 nM measured in samples from the core of the major plume lens. These low dFe concentrations are almost certainly an artefact due to the delay between tripping the bottles at depth and filtration of particulate Fe from dissolved Fe aboard the ship. Because of the rapid Fe-oxidation kinetics involved, the Fe content (dissolved and particulate) measured within the samples does not correspond to the composition of the plume at the time of sampling. During sample recovery, the dissolved Fe will have been continually oxidising and precipitating to Fe oxyhydroxides. This would have resulted in a greater concentration of particulate Fe in the samples relative to the particulate Fe that was initially present in the plume at the instant of sampling.

The time between collecting the samples in the Niskin bottles and filtering them on board the ship was not measured exactly. However, the percentage of dFe which would have been present in-situ can still be predicted by using the oxidation rate calculated in Chapter 5 for the 5°S vent sites. The half-life for Fe oxidation was 27 minutes but it must be noted that this is a theoretical calculation of the oxidation half-life. In practice, in the Indian Ocean the oxidation half-life in hydrothermal plumes has been observed to

be slower than theoretical predictions (Statham et al., 2005) and Fe oxidation rates appear to deviate away from first order kinetics. This has previously been suggested by Statham et al. 2005, to be due to the presence of organically bound Fe, just as has been shown to be present in the plumes at 5°S (Chapter 5), and is likely to be the case for hydrothermal plumes throughout the oceans. Therefore at this site, the oxidation half-life will be considered to be a *minimum* of 27 minutes. This oxidation half-life can be applied to the samples at 5°S by knowing the age of the buoyant plume.

The time for the buoyant plume to reach neutral buoyancy is predicted to be approximately an hour after venting with a 10^4-fold dilution with ambient seawater (McDuff, 1995). Within the core of the plume the Mn concentration (392 nM) suggests that the vent fluid (~600 µM, K. Schmidt, pers. comms.) has been diluted 1500-fold with the surrounding water, i.e. 15 % of the total dilution to be expected during the ~1 hour of buoyant plume rise (Lupton, 1995). However plume dilution is not uniform; initially as a plume leaves a vent it dilutes rapidly but as it approaches neutral buoyancy, dilution progressively slows. It has been demonstrated in Chapter 4, for example, that only a few meters above a vent, a buoyant plume on the EPR had already experienced a 0.2 to 1% end-member fluid dilution with the surrounding seawater, equivalent to at least a ~100-fold dilution (Chapter 4, Table 4.2). As a conservative estimate, therefore, the buoyant plume samples at 5°S must be no more than 15% of one hour, i.e. less than 9 minutes old. The percentage of Fe that will have oxidised by 9 minutes can be calculated using the rate equation for a first order reaction:

$$N = N_0 e^{-\lambda t} \qquad (6.1)$$

Where N_0 is the initial Fe(II) concentration, N is the Fe(II) concentration not oxidised, λ is the Fe oxidation rate constant and t is time. This equation is useful here as it enables the ratio of Fe oxidised to be determined, even when the original Fe(II) concentration in the samples is not known. Therefore by rearranging this equation the percentage of Fe remaining as Fe(II) after t minutes can be calculated:

$$\%Fe(II) = e^{-\lambda t} \times 100 \qquad (6.2)$$

The Fe oxidation rate at 5°S has already been calculated in Chapter 5 as 0.0256 and therefore after 9 minutes, 79% of the Fe will remain as Fe(II) and 21% of the Fe will have oxidised. This demonstrates that the in-situ dissolved Fe concentrations at 5°S would have been much greater than that measured in the samples collected. Additionally, if the samples had been filtered in-situ, a proportion of the Fe(III) would have been present in the 'dissolved' Fe fraction because our operationally defined (<0.4 μm) dissolved Fe fraction includes both truly dissolved Fe(II) and colloidal Fe(III) species. Fe oxyhydroxides begin as small colloidal species which then aggregate to form particulate Fe. Therefore most of the Fe(III) present in-situ would have been present in the 'dissolved' phase because the plume was still very young and very little aggregation would have occurred.

In comparison, after sampling and recovery of the CTD, most of the dFe species would have been present as colloidal Fe(III) species as well as a small percentage of Fe that may have been stabilised by organic complexation. This is because between four and nine hours elapsed between sampling the plume and processing samples in the clean laboratory aboard the ship. During this time, because of the plentiful supply of oxygen in seawater, between 8 and 16 Fe(II) oxidation half-lives will have occurred, resulting in effectively quantitative oxidation of any Fe(II).

The elemental results in the particulate phase therefore represent a more oxide rich system than that present in-situ. The oxyanion and chalcophile to pFe ratios will now enable a deeper understanding of the forms of Fe in the particulate phase and processes occurring, which will be useful for interpretation of the REE and Fe isotope results.

6.2.4 Oxyanions and Chalcophile elements

The particulate phosphorus, vanadium, copper and zinc concentrations relative to pFe are shown in Figure 6.5. The oxyanions, phosphorus and vanadium, are positively correlated with pFe with an r^2 of 0.995 and 0.999 respectively and a negative y intercept. Phosphorus ranged from 0.8 to 34 nM and vanadium ranged from 0.02 to 1.11 nM.

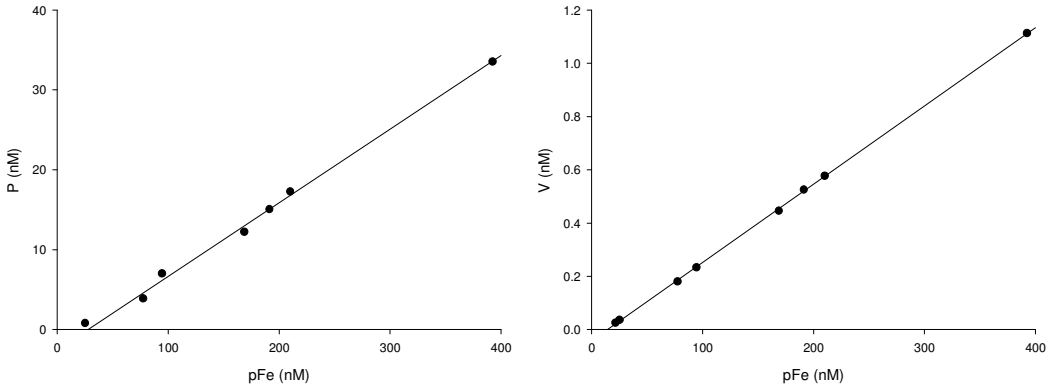

Figure 6.5 - Relationships between particulate P, V relative to particulate Fe

The chalcophiles, copper and zinc, are also positively correlated, with r^2 values equal to 0.976 and 0.981, respectively and with positive y intercepts. Copper concentrations ranged from 1.4 nM to 7.1 nM and zinc concentrations ranged from 4.2 nM to 35 nM.

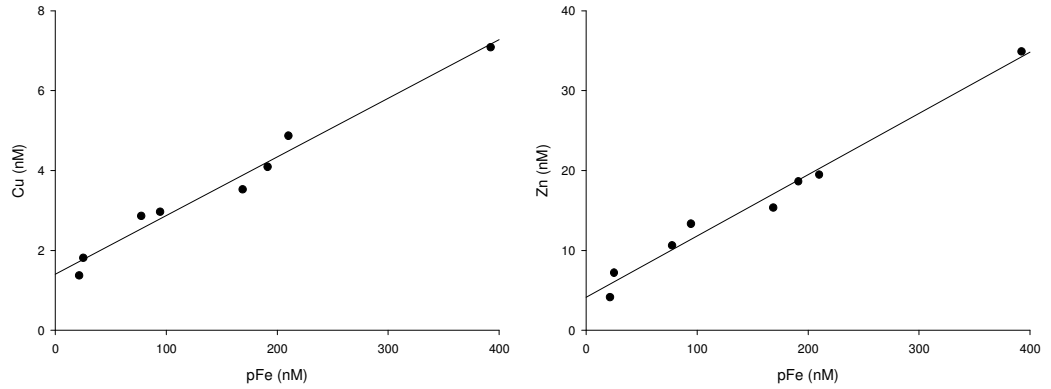

Figure 6.6 – Relationships between particulate Cu, Zn relative to particulate Fe

As discussed earlier, Fe(II) will no longer be present in these plume samples because of the fast oxidation rates in the South Atlantic and the time delay between sample collection and processing. The $Fe(III)_{aq}$ formed is unstable in its soluble form, and will be quickly converted to Fe oxyhydroxide precipitates (Millero et al., 1995). As well as oxidation, in the first few seconds of venting the Fe(II) forms particulate Fe(II) sulfides. Therefore the particulate samples will be made up of Fe oxides and Fe sulfides.

However, as the buoyant plume rises, heavy Fe sulfides are predicted to rapidly fall out of the plume due to gravitational settling (Mottl and McConachy, 1990) and therefore the fraction of Fe sulfides in these plume samples may vary. The Fe oxyhydroxides on the other hand are initially present as colloids and are expected to be swept up into the non-buoyant plume (Field and Sherrell, 2000).

During oxyhydroxide formation, oxyanions (i.e. HPO_4^{2-} and VO_4H^{2-}) are co-precipitated and scavenged (Feely et al., 1991; Trefry and Metz, 1989) with constant molar ratios of P/Fe, and V/Fe dependent on the open-ocean dissolved phosphate concentration (Feely et al., 1998). In the buoyant plume at 5°S, both P and V were observed to be linearly correlated to pFe (Figure 6.5), similar to vent systems at Rainbow and TAG (Edmonds and German, 2004; German et al., 1991).

Both the P to Fe and V to Fe relationships have negative y intercepts. This is unusual because at <1 nM Fe, background seawater, the particulate phosphorus concentration should be <5 nM (http://hahana.soest.hawaii.edu/hot/hot-dogs/interface.html). But at low phosphorus concentrations, the pFe concentrations are relatively high suggesting the presence of a particulate Fe species that does not associate with the oxyanions. In this hydrothermal system, the most likely phase is Fe bearing sulfides.

During Fe sulfide formation, rather than co-precipitating with oxyanions, it is the chalcophile elements, such as Cu and Zn, that are incorporated and therefore Cu/Fe and Zn/Fe relationships are observed depending on the amount of Fe sulfide in the particulate Fe fraction and the amount of Cu and Zn in the end-member fluid. In the buoyant plume at 5°S the Cu/Fe ratios were between 0.02 to 0.08, similar to the ratios measured at TAG and Rainbow (0.006 – 0.080 and 0.003 – 0.015, respectively (Edmonds and German, 2004; German et al., 1991)). The Cu to Fe relationship in the end-member fluids is less (0.01) and this is because not all the Cu emitted from the vent will associate with all the pFe species. The Zn/Fe ratios on the other hand ranged between 0.09 to 0.3, much greater than the ratios observed at TAG and Rainbow (0.001 – 0.008 and 0.001 – 0.066). However the most likely reason for these high ratios is the abnormally high Zn concentration in the end-member fluids at Red Lion, which have a Zn/Fe ratio of 0.16 (Table 6.1).

Previously, in other hydrothermal systems, the Cu and/or Zn relationship to Fe has been used to demonstrate a preferential loss of Fe sulfides from the plume through gravitational sinking and/or the removal of Fe sulfides via oxidative dissolution. This has been inferred from the relationship between Cu or Zn relative to Fe having a negative departure from linearity (German et al., 1991; Trocine and Trefry, 1988). In the *buoyant* plume at 5°S the relationship between Cu or Zn with Fe is linear and shows no negative departure (Figure 6.6). This indicates that there has been no loss of Fe in the more dilute samples. In fact the opposite is seen, and the y intercepts of both graphs are positive. This indicates that at low Fe concentrations particulate Cu and Zn concentrations are proportionally higher than in the high pFe samples. During the first few seconds of venting, quenching will result in the formation of polymetallic sulfides, which will incorporate Cu, Zn and Fe into them. This is followed by oxidation, precipitating Fe oxyhydroxides. The overall pFe fraction will therefore increase but the particulate Cu or Zn concentrations will remain the same. Therefore the Cu and/or Zn relationship to Fe will be controlled by the amount of sulfides and Fe oxides within the particulate fraction.

If the relative amount of Fe sulfide was higher in the low Fe samples, then the relative amount of Fe oxyhydroxides would have to be lower. Therefore an increasing Cu to pFe ratio would have to couple with a decreasing P to pFe ratio. This is demonstrated in Figure 6.7 with high chalcophile/Fe ratios and low oxyanion/Fe ratios observed at low Fe concentrations. The Cu/Fe and Zn/Fe ratios decrease exponentially towards the higher Fe concentrations and the reverse is seen for the P/Fe and V/Fe ratios.

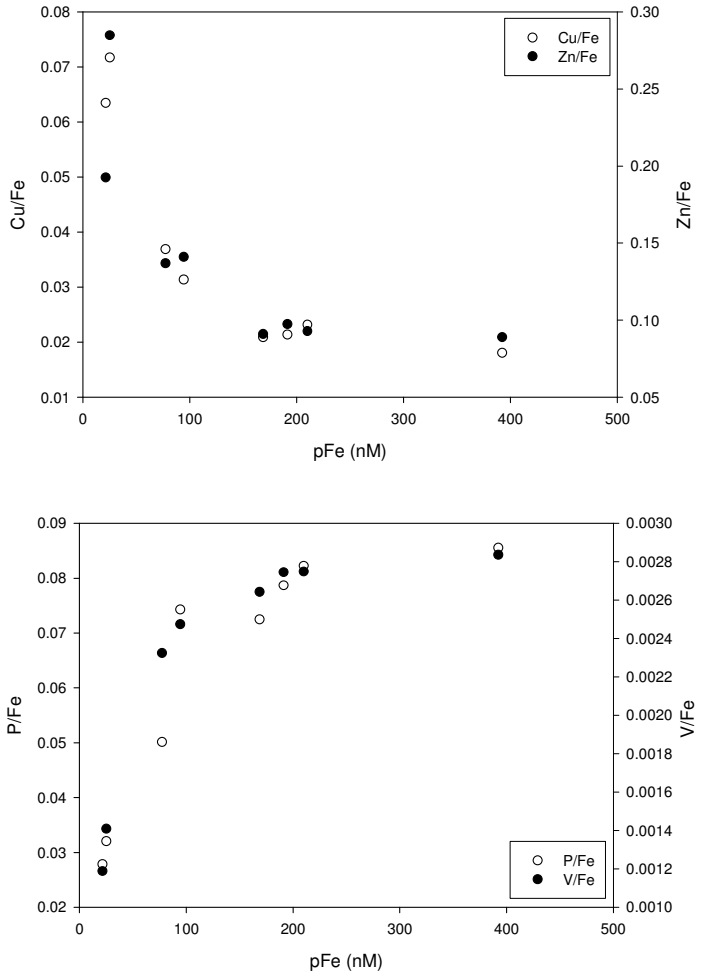

Figure 6.7 –Chalcophile/Fe and oxyanion/Fe relationships with pFe for the buoyant plume samples

Previously, Rudnicki and Elderfield (1993) predicted that ~50% of the Fe precipitated as Fe sulfides in the first few seconds of venting. However, in the vent system at 5°S, it appears that a varying amount of Fe has precipitated as Fe sulfide. This seems unusual as the samples collected were from the early stages of the buoyant plume and therefore very little of the Fe will have been lost from the plume due to gravitational settling before the Niskin bottles were fired. To investigate this further, the amounts of Fe oxyhydroxides and Fe sulfides in each of these buoyant plume samples needs to be calculated.

The proportion of Fe present as oxide can be calculated readily using the relationship observed between the amount of phosphorus scavenged and co-precipitated by Fe oxyhydroxides and the dissolved phosphate concentration in the background seawater (Feely et al., 1991).

The dissolved phosphate concentration at a background station at 5°S was 1.6 μmol L^{-1} (unpublished data), slightly greater than that at TAG. Using the linear relationship in Feely et al. (1998), the predicted P/Fe ratio for 5°S MAR can be read off the graph as 0.11. A similar correlation is reported for vanadium and at 1.6 μmol L^{-1} of phosphate, the V/Fe ratio is 0.004. Therefore the amount of FeOOH present in the plume particles can be calculated using Equation 6.3.

$$\text{FeOOH} = \text{P measured in the particulate sample} / 0.11 \qquad (6.3)$$

The results are shown in Table 6.2. The difference between the concentration of pFe and the calculated concentration of FeOOH will give the predicted concentration of Fe present in sulfides in the samples. Finally the fraction of Fe present in sulfides relative to the total Fe can also be calculated.

Table 6.2 - Calculated concentrations of FeOOH and FeS in the buoyant plume using P and V concentrations

Measured		Calculated		In particulate fraction		Relative to TFe
TFe (nM)	**P (nM)**	**FeOOH (nM)**	**Fe in sulfides (nM)**	**%Fe in sulfides**	**%FeOOH**	**%Fe in sulfides**
127	3.88	35	42	54	46	33
74.7	0.60	5	16	75	25	22
70.9	0.81	7	18	71	29	25
123	7.02	64	31	32	68	25
196	12.2	111	58	34	66	29
230	15.1	137	54	28	72	24
237	17.3	157	53	25	75	22
413	33.6	305	87	22	78	21
						Average : 25 ± 4
TFe	**V**	**FeOOH**	**Fe in sulfides**	**%Fe in sulfides**	**%FeOOH**	**%Fe in sulfides**
127	0.18	45	32	42	58	26
74.7	0.03	6	15	70	30	20
70.9	0.04	9	16	65	35	23
123	0.23	58	36	38	62	29
196	0.45	111	57	34	66	29
230	0.53	131	60	31	69	26
237	0.58	144	66	31	69	28
413	1.11	278	114	29	71	28
						Average : 26 ± 3

Both relationships with P and V result in similar Fe oxyhydroxide concentrations. In the particulate fraction the percent of Fe in sulfides decreases with increasing particulate Fe, as observed in Figure 6.7. However, relative to the total Fe (dissolved and particulate), the percent of Fe in sulfides is relatively constant, making up ~25% of the total Fe in all of the buoyant plume samples. This, therefore, explains the change in the fraction of Fe sulfide in the particulate fraction.

As mentioned in Chapter 5, the separation of particulate and dissolved species is an operationally defined process. 'Dissolved' Fe species are those that pass through a 0.4 µm membrane filter and include both truly soluble and colloidal Fe. As the Fe oxyhydroxides aggregate, less of the Fe will pass into the dissolved fraction. Therefore in the low pFe samples, there must be a larger percent of Fe still present in the 'dissolved' fraction as colloidal Fe(III) oxides, making it appear that these low pFe samples have a greater fraction of Fe sulfides relative to pFe. In fact, the actual Fe sulfide concentration relative to the total Fe *is* uniformly distributed across the plume, as previously predicted (Rudnicki and Elderfield, 1993) albeit at a lower percentage of the total: 25% *vs.* 50%.

The change in the relative amount of 'dissolved' Fe with increasing total Fe is shown in Figure 6.8 and demonstrates a similar exponential decrease to that seen for the Cu/Fe ratio relative to pFe (Figure 6.7). This demonstrates a decreasing percent of colloidal Fe species with increasing total Fe, presumably as a result of particle aggregation within the buoyant plume.

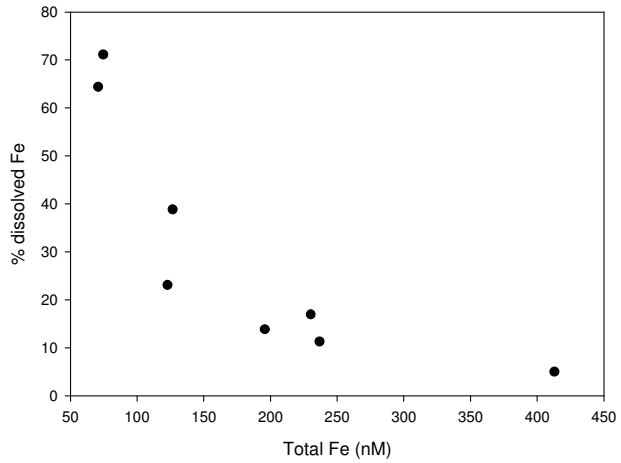

Figure 6.8 – Percent dissolved Fe relative to the total Fe concentration in the samples

It is particularly interesting that the *amount* of Fe in the dissolved fraction in each of the samples is relatively constant, supporting the presence of some Fe stabilisation that, hence, avoids aggregation. Fe stabilisation has already been observed in the non-buoyant plume at 5°S (Chapter 5) and the dFe concentrations in the buoyant plume samples in

this chapter (20 – 50 nM) are ~10 times greater than the stabilised ligand fraction measured in the non-buoyant plume (4.2 nM). By the time this buoyant plume would have reached neutral buoyancy it would have been diluted with seawater another 6-fold (see section 6.2.3) and have a dissolved Fe concentration between 3 and 8 nM. Potentially the dissolved Fe fraction in these buoyant plume samples contained similar stabilised dissolved Fe species to those detected in the non-buoyant plume.

6.2.5 Fe/Mn ratio within the buoyant plume

Mn can be used as a quasi-conservative tracer in any hydrothermal plume with a decrease in Mn indicative of plume dilution with ambient seawater. The TdMn concentration in the collected buoyant plume samples decreases towards the edge of the plume demonstrating dilution of the plume with the surrounding seawater. In comparison, Fe does not behave conservatively and therefore the Fe/Mn ratio in the plume samples can indicate whether there has been any loss or gain of Fe to the plume. The TFe/Mn ratio in the buoyant plume samples at 5°S remains relatively constant with a slight decrease in ratio in the more dilute samples (Figure 6.9). The highest Fe/Mn ratio measured (1.16) is almost identical to the Fe/Mn ratio in the end-member fluid at Red Lion (1.2). This suggests that no Fe has been lost from this sample and the concentration change is due to dilution of the vent fluid.

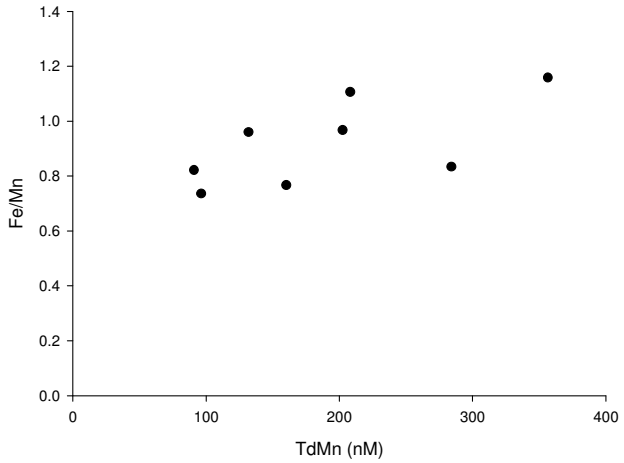

Figure 6.9 – Fe/Mn ratio in the buoyant plume samples relative to Mn

Fractionation of the Fe/Mn ratio to lower values can be caused by loss of Fe to the seafloor or entrainment of seawater with an Fe/Mn ratio less than the vent fluid. At the time of sampling, ~50 m above the vent site, the reaction of Fe(II) with H_2S to form polymetallic sulfides will already have occurred and any Fe loss is likely to be as particulate Fe sulfides (Mottl and McConachy, 1990; Rudnicki and Elderfield, 1993). However, the core plume sample has the same Fe/Mn ratio as the vent fluid with almost all the Fe in the particulate phase. Therefore the calculated percent of Fe sulfide in this sample is representative for the Red Lion buoyant plume prior to Fe loss. The calculated percent of Fe sulfide in the other plume samples are all similar in value to that in the core of the plume suggesting that no significant Fe has been lost as Fe sulfide. The Fe sulfide fraction would have been seen to decrease towards the plume edge if Fe sulfides had been lost.

Entrainment of Mn or seawater with an Fe/Mn ratio less than the vent fluid could also decrease the Fe/Mn ratio in the more dilute samples towards the edges of the buoyant plume. Fluids sourced from diffuse flow areas are a mixture of high-temperature fluids and entrained seawater and can have Fe concentrations significantly less than high-temperature end-member fluids because of sub-surface sulfide precipitation (e.g.James and Elderfield, 1996a). Therefore Fe/Mn ratios can be much less than their source high-temperature vent fluid. Aluminium has been used to trace the entrainment of diffuse flow into high-temperature plumes and therefore Mn would be expected to behave in a similar conservative way (Lavelle and Wetzler, 1999; Lunel et al., 1990).

However the Fe/Mn ratio in the buoyant plume samples does not change by very much, therefore it is a reasonable assumption that most of the Fe is made up of high-temperature fluids sourced from the Red Lion vents.

The relationships between pFe and other trace elements in the plume particles have enabled the forms of Fe within this buoyant plume to be determined. With this information the REEs will now be examined and compared to previous studies.

6.3 Rare earth elements in buoyant plume particles

6.3.1 Results

The particulate REE (pREE) concentrations are shown in Table 6.3. Also shown in this table are the background pREE concentrations in seawater from the TAG hydrothermal field (German et al., 1990). The lowest measured pREE concentrations in the buoyant plume are similar to or slightly lower than the pREE concentrations in seawater at TAG and therefore these samples will be used to blank correct the plume samples.

Table 6.3 – The particulate REE composition of the buoyant plume samples and background seawater (pSW) from the TAG hydrothermal vent site (German et al., 1990). Fe concentrations are in nM and REE concentrations are in pM.

Fe	La	Ce	Pr	Nd	Sm	Eu	Gd	Tb	Dy	Ho	Er	Tm	Yb	Lu
78	1.46	0.85	0.39	1.64	0.36	0.08	0.32	0.06	0.38	0.08	0.22	0.03	0.18	0.03
22	0.76	0.81	0.20	0.84	0.18	0.04	0.16	0.03	0.18	0.04	0.10	0.01	0.08	0.01
25*	0.57	0.69	0.15	0.60	0.13	0.03	0.11	0.02	0.13	0.02	0.07	0.01	0.06	0.01
95	2.02	0.94	0.56	2.34	0.51	0.11	0.44	0.08	0.55	0.11	0.32	0.04	0.26	0.04
169	3.63	1.40	0.95	4.02	0.86	0.20	0.77	0.14	0.97	0.20	0.55	0.08	0.46	0.07
191	4.26	1.47	1.11	4.73	1.02	0.24	0.91	0.17	1.14	0.23	0.67	0.09	0.55	0.09
210	4.12	1.27	1.09	4.64	0.99	0.24	0.89	0.17	1.15	0.24	0.69	0.10	0.58	0.09
392	6.84	1.98	1.74	7.33	1.54	0.39	1.43	0.27	1.86	0.39	1.14	0.16	0.96	0.16
pSW	0.65	1.46	0.15	0.59	0.12	0.03	0.11	0.02		0.02	0.05			

*Lowest concentration of REEs used to represent the background particulate REE composition

Light pREE (Nd) and heavy pREE (Er) relationships with pFe are shown in Figure 6.10. The REE concentrations increase linearly with increasing pFe with no deviation from the line. Positive deviation has been observed previously in non-buoyant plumes at TAG and Rainbow (Edmonds and German, 2004; German et al., 1991; German et al., 1990) and has been used to demonstrate continued scavenging of dREEs onto Fe oxyhydroxides as the plume disperses away from its source and the Fe concentrations decrease. But in this study, a cross section of a buoyant plume has been sampled rather than a dispersing non-buoyant plume, the samples are all around the same age, and there has not been time (<10 minutes) for additional scavenging to have occurred.

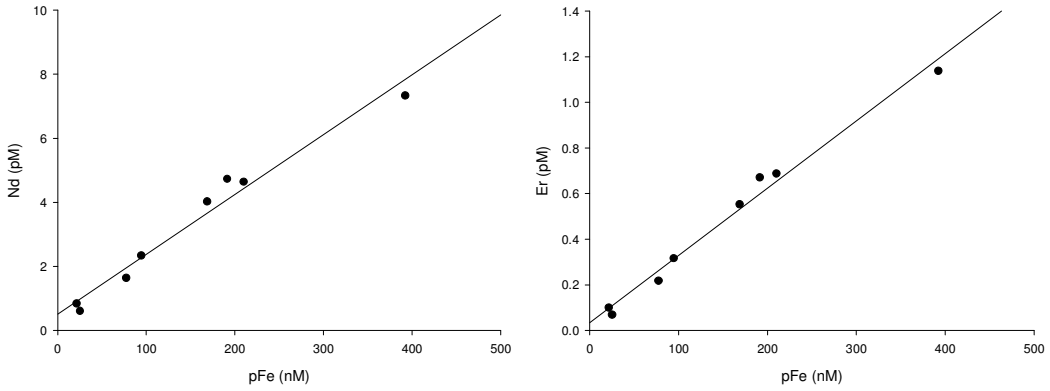

Figure 6.10 - Particulate REE concentrations relative to pFe in the buoyant plume samples at Red Lion.

Figure 6.11 shows the shale normalised REE patterns for the plume samples, after blank correction using the lowest concentrated REEs measured in the samples to represent the seawater pREE composition. Normalisation to shale (PAAS – post Archaen Australian Shale) has been used previously for hydrothermal plume studies to determine the impact of hydrothermal activity on oceanic cycles (German et al., 1990). Therefore shale normalisation has been used in this study to compare our samples with previous studies, even though black smoker end-member data are often normalised to chondrite (Douville et al., 1999; Mills and Elderfield, 1995; Mitra et al., 1994).

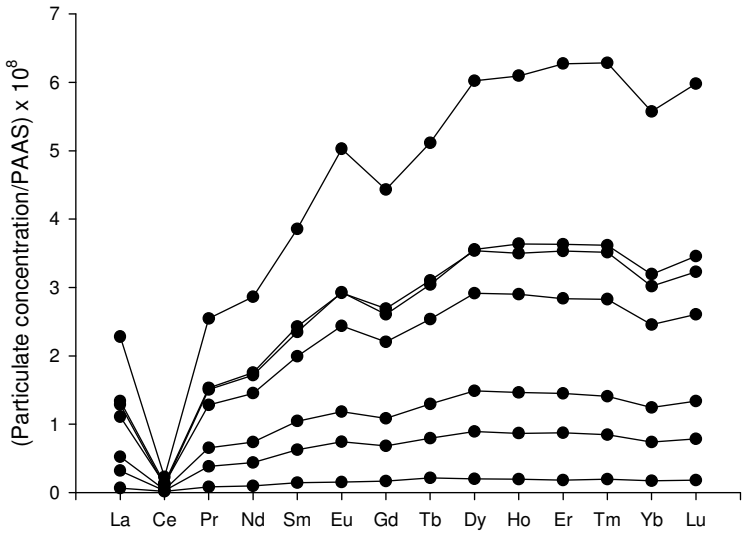

Figure 6.11 - Shale normalised REE pattern of the particulate buoyant plume samples. REE concentrations increase with increasing Fe concentration.

The results are remarkable in that they more closely resemble seawater rather than vent fluid patterns, even at this 'young' stage within the buoyant hydrothermal plume. For example, the plume particles show negative Ce anomalies, pronounced heavy REE enrichments and only slight positive Eu anomalies, all of which have been observed in previous non-buoyant plume studies (Edmonds and German, 2004; German et al., 1990; Sands, 2006). Eu and Ce are the only REEs that have multiple oxidation states and therefore do not display the same characteristic patterns as the other trivalent REEs. For example, the speciation of seawater dissolved REEs is dominated by carbonate ion complexes with increased complexation from light to heavy REEs, resulting in a preferential adsorption of light REEs onto particulate surfaces. The oxidation of soluble Ce(III) to insoluble Ce(IV) results in a positive Ce anomaly in the particulate phase and a negative anomaly in the dissolved phase (de Baar et al., 1988; German et al., 1995; Goldberg et al., 1963; Sholkovitz et al., 1994). Therefore it is the Ce depleted dissolved seawater REEs scavenged by the pFe, that results in the negative Ce anomaly observed in plume particles.

The positive Eu anomaly is also induced by oxidation state: the element is thought to be present in hydrothermal fluids as Eu^{2+} and enriched as a function of plagioclase alteration

(Klinkhammer et al., 1994). Therefore the Eu anomaly in the plume particles demonstrates the co-precipitation of REEs from vent fluid (German et al., 1990).

6.3.2 End-member vent fluids

The REE concentrations in the end-member vent fluids at the Red Lion vent site have been analysed by K. Schmidt, Jacobs University, Bremen. The shale nomalised REE profile of the vent fluid at Red Lion is shown in Figure 6.12 and compared with the vent fluid at TAG. Also shown in this figure is the dissolved seawater REE composition (Douville et al., 1999).

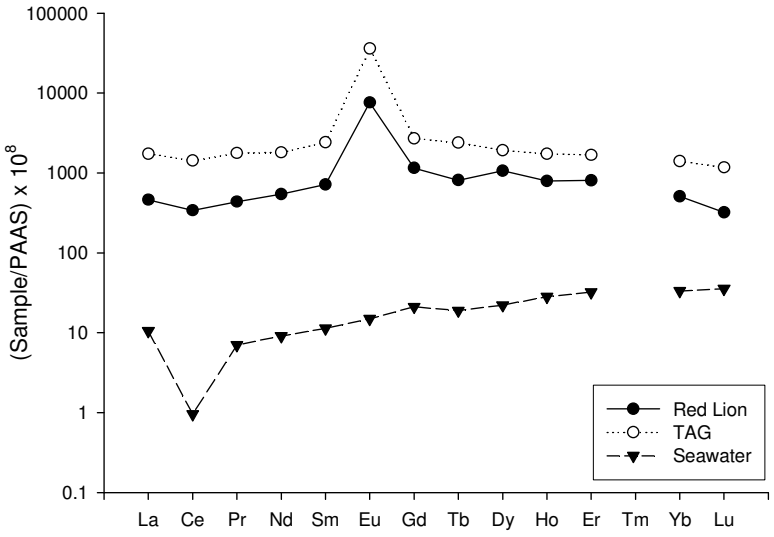

Figure 6.12 – Shale normalised REE pattern of the Red Lion (K. Schmidt) and TAG vent fluids and background seawater dissolved REE (Douville et al., 1999) (Logarithmic y axis)

The REE patterns of end-member fluids vary very little between different geological settings with enrichment in light REEs and a positive Eu anomaly (Klinkhammer et al., 1994; Michard et al., 1983). But they are strikingly different to seawater and basalt. The vents fluids at TAG are however more concentrated than the vent fluids at Red Lion. Both the vent fluid REEs and the seawater dissolved REEs will influence the composition of pREEs in the plume samples. In the first few meters above the vent site, Fe oxyhydroxides and Fe sulfides co-precipitate with the vent fluid REEs (German et al., 2002), which are 10 to 1000 times more enriched in REEs than seawater (Bau and

Dulski, 1999; Douville et al., 1999; Mitra et al., 1994). But then, as the plumes rise farther away from their source and dilute with the surrounding seawater, the REEs scavenged by the Fe oxyhydroxides become dominant and impose seawater-like patterns (German et al., 1990).

6.3.3 Discussion

Because the relative proportions of Fe oxyhydroxides and Fe sulfides have already been determined in the particulate fraction of these buoyant plume samples, the pREE composition can also be analysed relative to their Fe oxyhydroxide concentrations. Previous studies in hydrothermal plumes have demonstrated that REEs are co-precipitated and scavenged during the formation and transport of Fe oxyhydroxides rather than by Fe sulfides (Edmonds and German, 2004; German et al., 1990).

There have been two previous REE scavenging studies carried out in a buoyant plume and four studies carried out in non-buoyant plumes (Table 6.4). Four of the six studies were carried out in the Atlantic, one in the Pacific and one in the Indian Ocean. This provides only a hand full of data that can be compared to the buoyant plume study at 5°S – however, very similar samples have been collected from the buoyant plume at TAG, 40 to 100 m above the vent site (Mitra et al., 1994). In that work, the samples were collected using Niskin bottles carried in the basket on the front of DSV *Alvin*. Therefore those samples also experienced a time delay between sample collection and filtration on board the ship, as in this study. Delayed filtration is significant in both the TAG and 5°S studies because both vent systems were from the Atlantic, where oxidation rates are fast. Therefore on recovery of the samples to the ship, whether from a Niskin attached to a CTD rosette (this study) or a Niskin placed in the basket of DSV *Alvin* (Mitra et al., 1994), all the reactive Fe(II) will have oxidised. For the Mitra samples, both the *dissolved* and particulate fractions were analysed for their REE composition. Those samples therefore provide a useful comparison to the Red Lion samples.

Table 6.4 - Previous REE scavenging studies carried out on plume particles

Study site	Reference	Sample type	Sampling method
TAG, MAR	(Mitra et al., 1994)	0.5 m above vent	Filtered on board,
Snakepit, MAR			Ti syringes, 0.4 µm
TAG, MAR	(Mitra et al., 1994)	40 – 100 m	Filtered on board,
Snakepit, MAR		Buoyant plume	Niskin bottles, 0.4 µm
5°S, MAR	This study	35 – 65 m	Filtered on board,
		Buoyant plume	Niskin bottles, 0.4 µm
TAG, MAR	(German et al., 1990)	Non-buoyant plume	Filtered in-situ (SAPS), 1 µm
Rainbow, MAR	(Edmonds and German, 2004)	Buoyant plume	Filtered in-situ (SAPS), 1 µm
		Non-buoyant plume	
9°45'N, EPR	(Sherrell et al., 1999)	Non-buoyant plume	Filtered in-situ (RAPPID), 0.45 µm
Edmond and Kairei, [a]CIR	(Sands, 2006)	Non-buoyant plume	Filtered in-situ (SAPS), 1 µm

[a]CIR – Central Indian Ridge

The alternative sampling procedure used in some of the previous studies involves filtering the seawater in-situ, therefore eliminating the time delay experienced during the collection of samples using Niskins. All the non-buoyant plume studies and the two buoyant plume samples collected from Rainbow, were filtered in-situ using either Stand Alone Pumps (SAPS) or Rotating Automatic Pumps for particulate inorganics determination (RAPPID). Therefore they collected particulate material exactly as it would have been present in the plume. These in-situ filtration devices pump over 1000 L of water through the filter during their deployment and have been preferentially used in non-buoyant plumes where particle concentrations are low. However, they have the disadvantage that only a maximum of four independent samples can be collected on each deployment. In comparison, the collection of samples using a CTD rosette, enables 24 independent samples to be taken, but with much less material to analyse.

In the buoyant plume samples collected at 5°S, the pREE composition should be more concentrated than that present immediately prior to sampling because of a) greater co-

precipitation of REE during Fe oxyhydroxide precipitation and b) increased scavenging of REE onto the Fe oxyhydroxides from the seawater during recovery of the CTD to the ship, as long as an excess concentration of dissolved REEs is present. This suggests that these plume samples are likely to have REE compositions more similar to a non-buoyant plume than a buoyant plume. Comparison of this study with the buoyant and non-buoyant plume at TAG will be carried out, taking into account the sampling procedures used to collect the particulate material.

6.3.4 REE/Fe ratio in buoyant plume particles

Comparisons of the data from the present study with the buoyant and non-buoyant plume from TAG are shown in Table 6.5, with Nd/Fe used to represent the REE/Fe ratio.

Table 6.5 – Comparison of the Nd/Fe ratio in the buoyant plume at Red Lion and TAG as well as the non-buoyant plume at TAG

	Buoyant plume Red lion	**Buoyant plume TAG**	**Non-buoyant plume – TAG**
Fe	395 nM (FeOOH)	4.5 µM	212 nM
Mn	357 nM	800 nM	-
Nd/Fe	0.024	0.0053	0.020

The most concentrated sample from the Red Lion buoyant plume (pFe = 395 nM) was compared to the least concentrated buoyant plume sample from TAG (pFe = 4.5 µM) (Mitra et al., 1994), collected with a Niskin bottle between 40 and 100 m directly above the vent site. The end-member Fe concentration at TAG (5.2 mM) is at least six times greater than that at Red Lion and this is why at similar heights in the buoyant plume, the Fe concentrations are so different. The REE/Fe ratios are also very different but can easily be explained. In the TAG buoyant plume sample, the REEs in the dissolved fraction were close to zero. Therefore, after the Niskin bottles were fired, there would have been a finite concentration of dissolved REE that could be scavenged onto the Fe oxyhydroxides. Once the samples were filtered, the absence of dissolved REEs indicated that all the dissolved REEs must have been scavenged onto the Fe oxyhydroxides during samples recovery. Therefore the particulate REE/Fe ratios in these samples had reached

their maximum possible value and are unlikely to represent the in-situ composition, where further dilution would have provided more REEs for scavenging.

The Fe concentrations in the Red Lion buoyant plume were much lower and therefore if all the dissolved REEs in the Niskin bottle were scavenged during sample recovery, as was the case for Mitra et al. (1994), the REE/Fe ratio had the potential to be much higher. For example, the dissolved Nd concentration in seawater is 21.4 pM (3300 m at TAG, (Douville et al., 1999) and therefore when the Fe concentration is 4500 nM (in the TAG samples) and all the REE are scavenged, the Nd/Fe ratio will be 0.005, the same as reported by Mitra to be present in the particulate fraction. This compares to Red Lion, where the maximum total Fe concentration is 395 nM and therefore the maximum Nd/Fe ratio would be 0.05, ten times greater than the ratio in the buoyant plume at TAG. The actual measured value is lower suggesting that not all of the dissolved REE had been scavenged during recovery of the CTD.

The REE/Fe ratio in the buoyant plume at Red Lion is actually closer in value to the ratio in the non-buoyant plume at TAG (pFe = 212 nM)(German et al., 1990) rather than the buoyant plume and is a result of scavenging of dREEs from the seawater during recovery of the CTD rosette to the ship. The non-buoyant plume samples were filtered in-situ using SAPS and therefore represent the REE/Fe composition actually present within the plume.

For the rest of the buoyant plume samples at Red Lion the blank corrected REE/Fe ratio is relatively constant (Figure 6.13) with a similar REE/Fe ratio to some of the non-buoyant plume samples from TAG. However the TAG samples had varying REE/Fe ratios increasing with decreasing Fe. These samples were collected in-situ over a 2 km horizontal range and it was in this earlier study that continuous scavenging of REE was first suggested (German et al., 1990). It was shown that as Fe concentrations decreased with increasing distance from the vent, the REE/Fe ratio increased (e.g. Nd/Fe, Figure 6.13). Sherrell et al. (1999) argued against this theory using non-buoyant plume samples collected from the East Pacific Rise. They observed higher particulate Fe concentrations at increasing distance from the vent site because of slower oxidation rates and therefore slower formation of Fe oxyhydroxides. The Fe concentrations ranged between 10 and 25 nM, much less than those at TAG (17 – 212 nM). The REE/Fe ratio was again greater

at lower Fe concentrations, but this time these samples were younger and closer to the vent. Therefore they suggested that the increase in REEs with decreasing Fe was simply due to the mixing of Fe oxyhydroxides with background seawater, which contained older resuspended hydrothermal particles from the seafloor. This would require seawater entrained into the plume to have a particulate REE/Fe ratio much higher than the recently precipitated Fe oxyhydroxides (Sherrell et al., 1999).

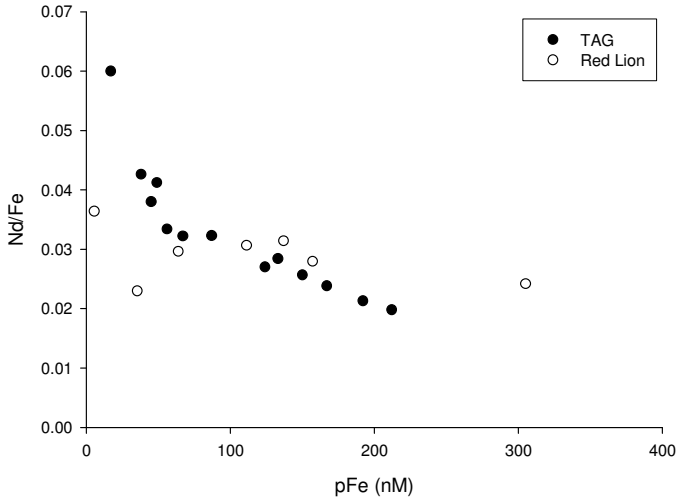

Figure 6.13 – Nd/Fe ratio in the buoyant plume samples at Red Lion relative to their FeOOH concentration and the Nd/Fe ratio in the non-buoyant plume samples from TAG (German et al., 1990)

Further insight into the mechanism controlling particulate REE concentrations in hydrothermal plumes was gained by Sands (2006). She suggested that if REEs were being entrained into the plume from background seawater, then deeper vent systems should have higher REE/Fe ratios for the same Fe concentration at a shallow vent system. This is because concentrations of REEs generally increase with depth in each particular ocean. However, by comparing the TAG hydrothermal vent field (3500 m) with the Rainbow vent field (2300 m), the REE/Fe ratio at TAG was found to be less than that at Rainbow. Therefore she concluded that continuous scavenging of REEs by the Fe oxyhydroxides is the dominant process occurring in hydrothermal plumes. In this study, continuous scavenging of REEs onto Fe oxyhydroxides is again supported.

6.3.5 Ce and Eu anomaly

The influence of vent fluid REEs and seawater REEs on the composition of the plume particles can be determined by considering the Eu and Ce anomaly. The Eu and Ce anomalies for the Red Lion buoyant plume can be calculated as below (Equation 6.4 and 6.5).

$$\text{Eu anomaly} = 2 \times (Eu/Eu_{shale})/(Sm/Sm_{shale} + Gd/Gd_{shale}) \quad (6.4)$$

$$\text{Ce anomaly} = 2 \times (Ce/Ce_{shale})/(La/La_{shale} + Pr/Pr_{shale}) \quad (6.5)$$

A positive anomaly has a value greater than one and a negative anomaly has a value less than one and the results are shown in Table 6.6.

The Ce and Eu anomaly for the Red Lion buoyant plume samples were constant with an average Ce anomaly of 0.88 ± 0.01 and an average Eu anomaly of 1.61 ± 0.08. This demonstrates that the samples have scavenged similar amounts of vent fluid REEs and seawater REEs relative to their Fe concentrations consistent with the near-identical (<10 minutes) age of these samples.

Table 6.6 – Calculated Ce and Eu anomalies in the particulate fraction of the buoyant plume samples at Red Lion and pFe concentration.

[pFe] (nM)	Ce anomaly	Eu anomaly
77.5	0.87	1.64
21.6	0.86	1.43
25.3	-	-
94.5	0.87	1.68
169	0.89	1.62
191	0.89	1.62
210	0.89	1.66
392	0.89	1.65

*Sample used to blank correct the REE composition in the plume samples

The presence of both Eu and Ce anomalies indicates the influence of both vent fluid and seawater dissolved REEs on the particulate composition of REEs in the buoyant plume samples and by using a simple model, the relative influences of the seawater and vent fluid REEs can be calculated. In Figure 6.14 the REE patterns for different proportions of vent fluid REEs from Red Lion relative to seawater dREEs are shown (10%, 1%, and 0.1% vent fluid to 90%, 99% and 99.9% seawater). Also shown is the vent fluid REE composition at Red Lion and the REE composition of the most concentrated buoyant plume sample.

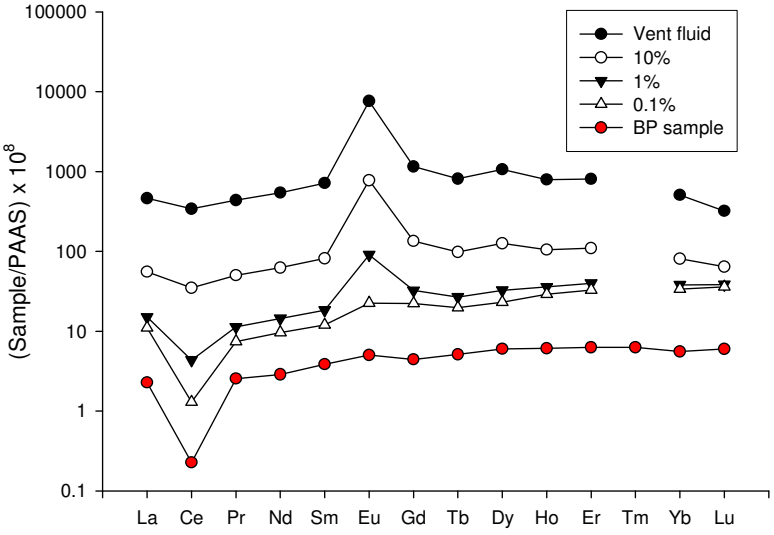

Figure 6.14 - Shale normalised REE pattern of modelled percentages of vent fluid and seawater compared to the Red Lion vent fluid and the most concentrated plume sample from Red Lion (BP sample, red circles) (Logarithmic scale).

The most representative composition for the buoyant plume sample is only generated through a 0.1% vent fluid and 99.9% seawater composition. On the logarithmic scale the Eu anomaly looks extremely small, especially compared to a similar model used for the TAG non-buoyant plume (German et al., 1990). This will be because of the lower REE concentrations in the end-member fluid at Red Lion compared to those at TAG. Therefore only a small percent of the REE composition is made up of vent fluid in these samples and the Eu anomaly is over-printed by efficient seawater REE scavenging during recovery of the Niskin bottles.

6.4 Summary

A cross section through a buoyant plume from a basalt hosted system on the Southern Mid-Atlantic Ridge has been quantified for various Fe species in the particulate phase. A time delay between collecting the samples in the Niskin bottle and filtering them on deck resulted in quantitative oxidation of any Fe(II) that would have been present in-situ. Therefore the Fe species present within the samples include colloidal and stabilized dissolved Fe(III), particulate Fe oxyhydroxides and particulate Fe sulfides.

Approximately 25% of the total Fe has been calculated to be present as particulate Fe bearing sulfides with no loss of Fe in sulfide form to the seafloor. The Fe oxyhydroxides are split between the dissolved and particulate fractions because smaller (colloidal) Fe(III) species are separated into the dissolved fraction. Consequently the percent of Fe sulfides as a proportion of *particulate* Fe varies.

The composition of the REEs in the buoyant plume samples have also been affected by the time delay between sampling and filtration, resulting in continued scavenging of the dREE from the seawater during sample recovery. Even so, these samples demonstrate that there is no extra entrainment of pREE from the seafloor during dilution of the samples with seawater, just as is seen for Fe:Al:Mn distributions.

This study has highlighted issues with sample collection in buoyant hydrothermal plumes and the impact this has on trying to understand the natural system. At present there has been no in-situ study of the rising buoyant plume and it would be particularly interesting to understand the processes that occur during co-precipitation of the REEs within the first 50 m of buoyant plume rise. It will be important to understand how much scavenging actually takes place within the buoyant plume or if this is a process that dominates only in the non-buoyant plume. In the next chapter, the conclusions drawn here will be used to interpret the Fe isotope fractionation also observed within these samples.

Chapter 7. Fe isotope fractionation in the buoyant plume

7.1 Introduction

The analysis of Fe isotopes in biogeochemistry is a relatively new technique that has the potential to act as a geochemical tracer of oceanic Fe sources and internal cycling (e.g. Anbar and Rouxel, 2007; Beard and Johnson, 2004; Dauphas and Rouxel, 2006). Within the modern ocean, the residence time of Fe is short (70 - 140 yr, Bruland et al., 1994) and therefore it is suggested that hydrogenous Fe-Mn crusts lining the ocean floor may record the Fe isotope composition of the ocean and be used to infer Fe sources through time (Beard et al., 2003b; Chu et al., 2006; Levasseur et al., 2004; Zhu et al., 2000). The actual isotopic composition of the ocean is still unknown due to low Fe concentrations and analytical constraints. Ferromanganese (Fe-Mn) crusts have been reported to have low δ^{56}Fe values down to -0.8‰ (δ^{56}Fe, relative to IRMM-014)(Beard et al., 2003b; Chu et al., 2006; Levasseur et al., 2004; Zhu et al., 2000) providing us with a first approximation of the isotope composition of the ocean. Even so, kinetic effects during crust formation, diagenetic remobilisation of Fe from sediments and isotopic fractionation of Fe during reactions in the water column mean that it is unlikely that the isotopic signature of any particular Fe source would be retained in the Fe-Mn crusts.

High-temperature hydrothermal fluid inputs have an Fe isotope composition ranging from -0.69‰ to -0.21‰ (δ^{56}Fe) (Beard et al., 2003a; Severmann et al., 2004; Sharma et al., 2001), within the isotopic range observed for Fe-Mn crusts (Figure 7.1). However, on entering the ocean, the Fe from hydrothermal vents forms polymetallic sulfide and oxide phases (Feely et al., 1987a), both of which may cause isotopic fractionation of Fe (Bullen et al., 2001; Butler et al., 2005). If Fe isotopes are to be used as a geochemical tracer of hydrothermal Fe in the oceans, it will be important to understand the fractionation processes that occur during plume formation and dispersal and any fractionation this imposes on the isotopic composition of the source vent fluid Fe. This would enable the isotope composition of the surrounding sediments to be predicted as well as the effect any Fe that is leaked out into the water column has on the isotopic composition of the open ocean. In this study, vent fluids from the 5°S vents and the buoyant plume samples discussed in Chapter 6 have been analysed for Fe isotopes, in order to study the evolution of the Fe isotopic signature.

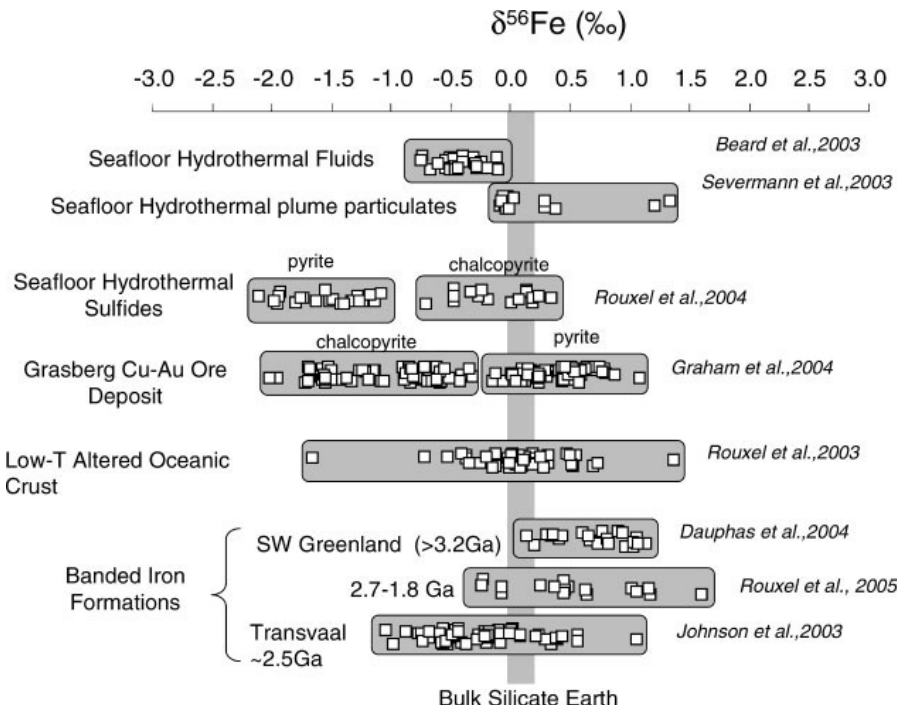

Figure 7.1 - Iron isotope variations in seafloor hydrothermal systems (Dauphas and Rouxel, 2005)

At present, data on the isotope fractionation of Fe in hydrothermal plumes is sparse. Only one study has been reported and this was from the Rainbow vent field in the North Atlantic (Severmann et al., 2004). From this study, Severmann et al. (2004) suggested that the Fe isotopic composition of hydrothermal end-member fluids were preserved in the non-buoyant plume and recorded in local hydrothermal sediments. However, the Rainbow vent field is unusual because of its ultramafic setting, which results in a high Fe/H_2S ratio in its end-member fluid. This causes $\leq 4\%$ of the Fe to be precipitated as Fe sulfides such that Fe isotope fractionation in the plume is dominated by Fe oxide formation (Severmann et al., 2004). This results in the transport of all the Fe in a single phase to the top of the buoyant plume and therefore the overall Fe isotope composition does not fractionate. In basalt hosted systems, where 25 to 50% of the Fe may be precipitated as Fe sulfides, Fe might be lost from the plume before reaching non-buoyant plume height. Therefore preservation of the original end-member Fe isotope composition in the buoyant and non-buoyant plume products may not occur and this chapter seeks to address the degree of fractionation this might cause.

The basalt hosted system at 5°S and the Fe rich buoyant plume samples collected here allows us to evaluate what effect the formation/precipitation of Fe sulfides might have on the isotopic composition of Fe emitted from the hydrothermal system. Vent fluids were collected from this area in 2006 (M68/1) from Two Boats (Turtle Pits), Sisters Peak (Comfortless Cove) and Mephisto and Tannenbaum (Red Lion) (Figure 3.5 and 3.6). Chapter 6 has already quantified the various Fe forms in the buoyant plume samples with the use of well characterized scavenging/co-precipitation reactions of trace elements onto/with Fe. This enables the isotope fractionation processes that occur within the buoyant plume to be distinguished and to determine if the Fe isotope composition of the end-member fluids is modified upon mixing with seawater. Finally, the implications of these fractionation processes for the isotopic signature of hydrothermal Fe exported to the deep-ocean and sediments will be discussed.

7.2 Background to Fe isotopes

Iron isotope measurements are calculated relative to the Fe isotopic composition of a reference material (IRMM-014). This gives a δ value quantified in permil (‰) as:

$$\delta^{i}_{j}\,Fe = [(^{i}Fe/^{j}Fe)_{sample} / (^{i}Fe/^{j}Fe)_{standard} - 1] \times 10^{3} \qquad (7.1)$$

where i and j are the relative molecular mass of each isotope.

Table 7.1 – The natural abundances of Fe isotopes

^{54}Fe	^{56}Fe	^{57}Fe	^{58}Fe
5.8%	91.8%	2.1%	0.3%

Table 7.1 shows the four stable isotopes of Fe and their natural abundances. Twelve different δ values can be calculated from these four isotopes (Dauphas and Rouxel, 2006) but for this chapter only the δ^{56}Fe (^{56}Fe/^{54}Fe) values have been calculated for comparison with other studies. During sample processing through the anion exchange column (See Chapter 2), complete recovery of the Fe was achieved, therefore eliminating any potential isotope fractionation caused during sample processing (Roe et al., 2003). The external precision for the isotope measurement is 0.09‰.

7.3 Results

7.3.1 Iron isotope composition of end-member fluids at 5°S

The Fe isotope composition of the non-filtered vent fluids sampled at 5°S MAR ranged from -0.21 to -0.50‰ for δ^{56}Fe (Table 7.2). Two different chimneys sampled at the Red Lion vent field, exhibited a 0.2‰ difference in their Fe isotope composition. At Mephisto the Fe isotope composition was -0.49‰ whereas the fluid at Tannenbaum was higher with an isotope composition of -0.29‰. At Turtle Pits, three different samples from the same chimney averaged -0.26‰ with only a 0.04 standard deviation and two samples from Comfortless Cove averaged -0.48‰. The isotope composition was also measured in vent fluids that had been filtered immediately after collection and their composition ranged from -0.46 to +0.16‰, i.e. different from the isotope compositions measured in non-filtered samples of the same fluids.

Table 7.2 - Fe concentrations in filtered and non-filtered end-member vent fluids and their associated isotope composition for δ^{56}Fe and δ^{57}Fe (external precision of 0.09‰ (2sd)). The difference between the δ^{56}Fe for the non-filtered and filtered samples is shown. See text for discussion on the samples in italics.

Site	Not filtered			Filtered			Difference
	Fe (µM)	δ^{56}Fe	δ^{57}Fe	Fe (µM)	δ^{56}Fe	δ^{57}Fe	δ^{56}Fe
Red Lion – Mephisto	179	-0.49	-0.74				
Red Lion – Tannenbaum	*91*	*-0.29*	*-0.44*	*40*	*+0.16*	*0.15*	*+0.45*
Turtle Pits	576	-0.26	-0.38	129	-0.28	-0.50	-0.02
	3161	-0.21	-0.36	2965	-0.40	-0.58	-0.19
	3357	-0.29	-0.40	3156	-0.39	-0.56	-0.10
Comfortless Cove	*827*	*-0.50*	*-0.70*	*454*	*-0.24*	*-0.32*	*+0.26*
- Sisters Peak	2798	-0.45	-0.70	2565	-0.46	-0.70	-0.01

The change in the isotope composition of the Fe between filtered and non-filtered samples has been calculated and is also shown in Table 7.2. This difference is due to the precipitation of vent fluid Fe in the sample bottles or to sulfide chimney particles

entrained along with the fluids. Approximately 50% of the Fe was lost during filtration, as was the case for the samples from Tannenbaum and Comfortless Cove (Table 7.2, italics), and the δ^{56}Fe value of the fluid increased by 0.45‰. This observation is consistent with significant Fe-isotope fractionation occurring with Fe sulfide particles acquiring lower values than the source fluids during kinetic sulfide precipitation (Butler et al., 2005; Rouxel et al., 2008). However, the changes in isotope composition between filtered and non-filtered samples is not consistent. For the Turtle Pits samples, the isotope composition of the filtered fluids are lower than the unfiltered samples rather than higher. Because this artefact cannot be readily explained, only the non-filtered samples are considered throughout the remainder of this chapter.

7.3.2 Iron isotope composition of the particulate Fe in the buoyant plume

The Fe isotope composition of the particulate Fe in the buoyant plume samples collected from above the Red Lion vent site varied from -0.31‰ to -0.70‰ for δ^{56}Fe and generally, higher with increasing pFe (Figure 7.2). All Fe isotope compositions were measured at the same time as the elemental analyses discussed in Chapter 6. As discussed in that chapter any Fe(II) initially present in those samples would all already have been oxidised by the time of elemental and isotopic analysis.

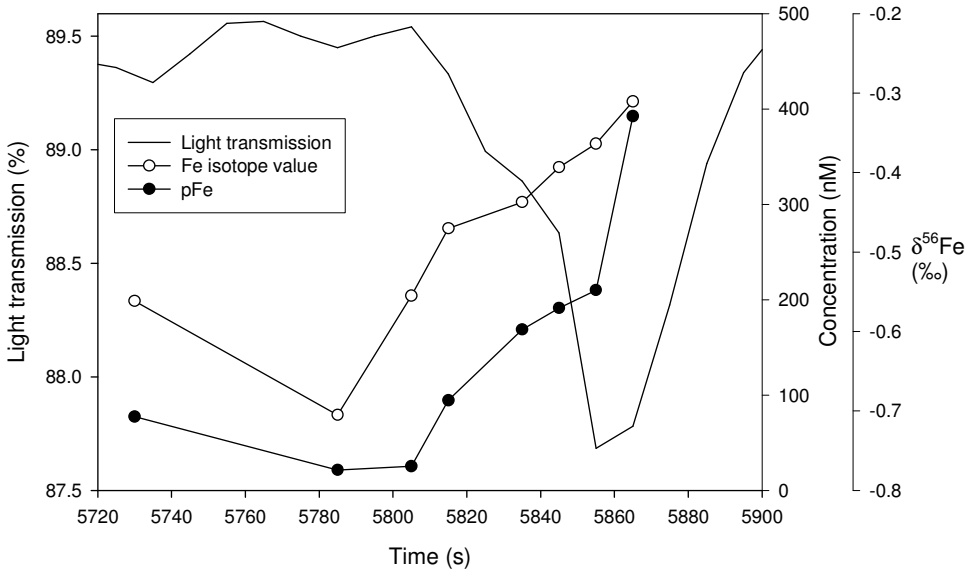

Figure 7.2 – Light transmission, particulate Fe (pFe) and the Fe isotope composition of the particulate Fe as a function of time.

7.4 Discussion

7.4.1 Isotope fractionation in the vent fluids

The isotope composition of vent fluids and the fractionation that occurs sub-surface has received much attention since the measurement of Fe isotopes became more widespread. So far it has been suggested that neither phase separation nor geological setting (i.e. basaltic or ultramafic rocks) can produce significant isotope variability (Beard et al., 2003b; Severmann et al., 2004; Sharma et al., 2001). For example, in the Brandon vents along the EPR, the isotope composition of both the vapour and brine phase were measured and were observed to have identical compositions (Beard et al., 2003a). The vent fluid Fe isotope compositions measured between sites in the current study vary by 0.3‰ but still lie within the same range as previously reported for Atlantic and Pacific vent fluids. There are a number of potential fractionation processes that could have caused the isotopic differences observed.

At each of the sites at 5°S, there would have been a different reaction zone through which the cold seawater would have percolated into, heated up, reacted with the surrounding rock and generally undergone phase separation, determining the chemical composition of the end-member vent fluids (Haase et al., 2007; Von Damm, 1995). These processes would also affect the isotope composition of the Fe in the end-member fluids. Rouxel et al. (2003) observed the results of low-temperature hydrothermal crust alteration on the Fe isotope composition of basaltic crust at the ODP site 801. In particular, highly altered basalts that were depleted by up to 80% from their original Fe concentration displayed an increase in δ^{56}Fe values relative to fresh rocks (up to 1.3 ‰), which suggested preferential leaching of low Fe isotope values (between –0.5‰ and –1.3‰) during alteration. Similar processes may also occur during high-temperature alteration of basalt, for example, through the formation of secondary minerals (e.g. Mg-Fe amphibole) in the high-temperature reaction zone.

However, at the Red Lion vent field, the Fe isotope composition of the Mephisto and Tannenbaum vent fluids varied by 0.2‰, even though their reaction zones were the same (Haase et al., 2007). A greater fraction of sub-surface precipitation of Fe sulfides could have made the fluid at Tannenbaum (-0.29‰) isotopically heavier than the fluid at Mephisto (-0.49‰)(Butler et al., 2005), but the result of such processes remain unclear

and may depend on sulfide precipitation pathways (Rouxel et al., 2008). Polyakov et al. (2007) have reported sulfide minerals that are isotopically enriched in heavy Fe relative to the source fluid. That would have resulted in source fluids becoming isotopically lighter, rather than heavier.

Finally, sub-surface mixing of seawater, as indicated potentially by non-zero Mg in the end-member fluids, is another potential fractionation process occurring at Red Lion. This would lead to partial oxidation of Fe(II) sub-surface, fractionating out heavy Fe(III) oxides and leaving behind an isotopically lighter fluid (Rouxel et al., 2003; Rouxel et al., 2008). This process might explain the difference between the fluids at Mephisto and Tannenbaum: the fluids at Mephisto may have experienced subsurface mixing with seawater yielding fluids that have an Fe isotope composition lower (-0.49‰) than those at Tannenbaum (-0.29‰).

However, there is not enough information on the fluids at 5°S to determine the exact fractionation processes occurring sub-surface, which does not matter as the main reason for analysing these samples, was to determine the isotope composition of the Fe being delivered to the buoyant plume.

7.4.2 Particulate Fe isotope fractionation in the plume

In nature, Fe isotope variations are controlled by both biotic and abiotic redox processes along with further significant kinetic and/or equilibrium fractionation from non-redox processes. Laboratory experiments have demonstrated some of the fractionation processes associated with Fe sulfide formation, oxidation and ferrihydrite (Fe oxyhydroxide) formation, making it possible to predict the fractionation processes occurring in this predominantly abiotic hydrothermal system (Bullen et al., 2001; Butler et al., 2005; Croal et al., 2004).

The predicted isotope fractionation of the particulate Fe occurring at various points in the plume evolution is shown in Figure 7.3, relative to the original vent fluid composition. Three main fractionation processes are to be expected in the buoyant plume. Initially, isotopic fractionation of Fe during Fe sulfide precipitation may preferentially enrich the particulate Fe sulfide in the light isotope (Butler et al., 2005; Rouxel et al., 2008). Next,

oxidation of Fe(II) to $Fe(III)_{aq}$ may enrich the particulate ferric Fe in the heavy isotope via an equilibrium fractionation process (Balci et al., 2006; Bullen et al., 2001; Croal et al., 2004). Finally, precipitation of $Fe(III)_{aq}$ as ferrihydrite has the potential to kinetically fractionate the light isotope into ferrihydrite, although the extent of fractionation will be dependent on the rate of precipitation (Bullen et al., 2001; Skulan et al., 2002). Oxidation and ferrihydrite precipitation will occur concurrently because of the instability of $Fe(III)_{aq}$ species in an oxygen rich environment, and the overall result produces enrichment of the particulate Fe in the heavy isotope (Bullen et al., 2001; Croal et al., 2004).

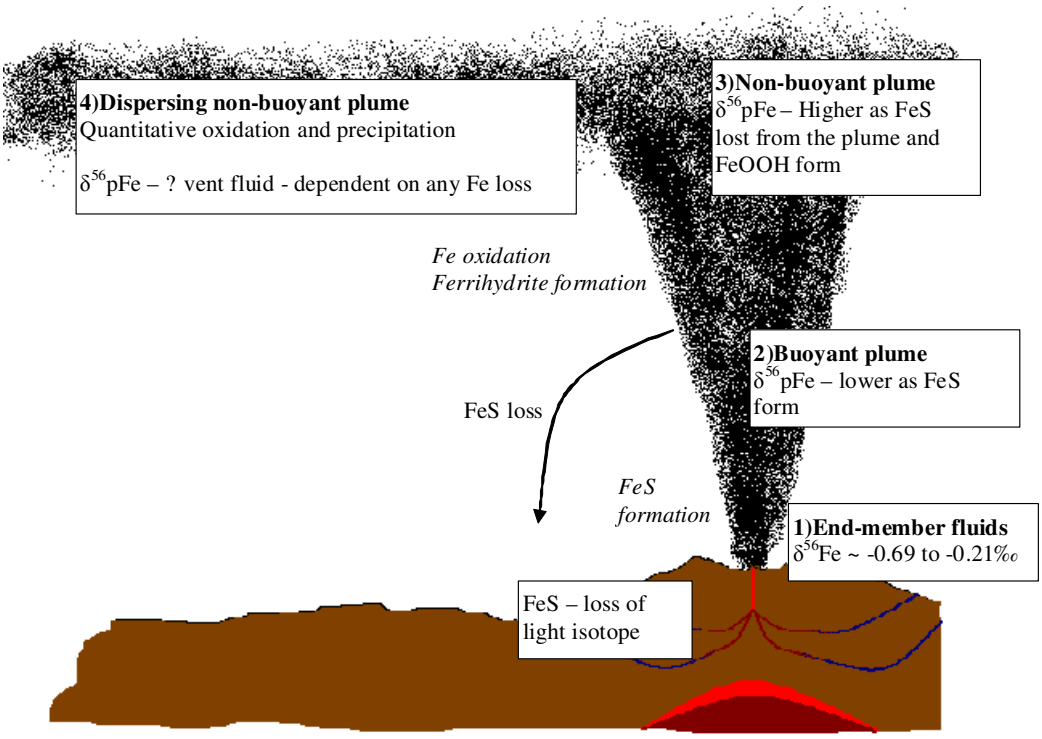

Figure 7.3 – Isotope fractionation processes occurring in the plume during dispersal. Changes in δ^{56}Fe for the particulate fraction are described relative to the original vent fluid isotope composition.

In addition to the three main processes described above, there may also be oxidative dissolution of FeS particles to Fe(II) or the formation of dissolved Fe ligand complexes, which likely produce an enrichment in the light isotopes in the dissolved phase (Brantley et al. 2004). While the extent of isotope fractionation associated with these latter

processes in hydrothermal plumes are unknown, all of the above processes are expected to result in fractionation of the original isotopic composition of the vent fluid.

For the samples collected at 5°S, MAR, Fe sulfide precipitation would have occurred in the first few seconds of venting and by the time these samples were filtered on deck, complete oxidation of all the dissolved Fe(II) present would also have occurred (See Chapter 6). Additionally, the majority of the Fe in the dissolved Fe fraction will be expected to be present as colloidal Fe oxyhydroxides rather than dissolved $Fe(III)_{aq}$ species, because of the instability of the dissolved $Fe(III)_{aq}$ species in an oxygen rich environment. There is also the potential for a fraction of the dissolved Fe species to be present as organic complexes but these will only make up a small fraction of the total Fe. Therefore if this was a closed system and all the Fe was separated into the particulate phase, the isotope composition should be the same as the original vent fluid. However, a range of Fe isotope values were measured for the buoyant plume samples and therefore there must be an alternative explanation for the isotope fractionation, other than chemical processes.

The only way to fractionate the Fe isotope composition of the Fe in the plume relative to the original vent fluid would be to either remove Fe from the plume (e.g. as rapidly sinking, dense Fe sulfide species) or to add Fe to the plume from an external source. Both these situations have been discussed in Chapter 6 and are unlikely for these samples. Additionally if Fe sulfide was being lost from the plume, the isotope composition of the particulate Fe samples would be expected to get higher with decreasing Fe/Mn ratio, as Fe sulfide precipitation removes Fe with a light isotope composition. No such trend is seen (Figure 7.4). The entrainment of Fe into the plume from the surrounding seawater has also been disregarded because this would change the proportion of Fe sulfide within the plume, which has been found to be relatively constant for the buoyant plume samples. Furthermore, very little correlation is observed between the Fe/Mn ratio and the isotope composition (Figure 7.4).

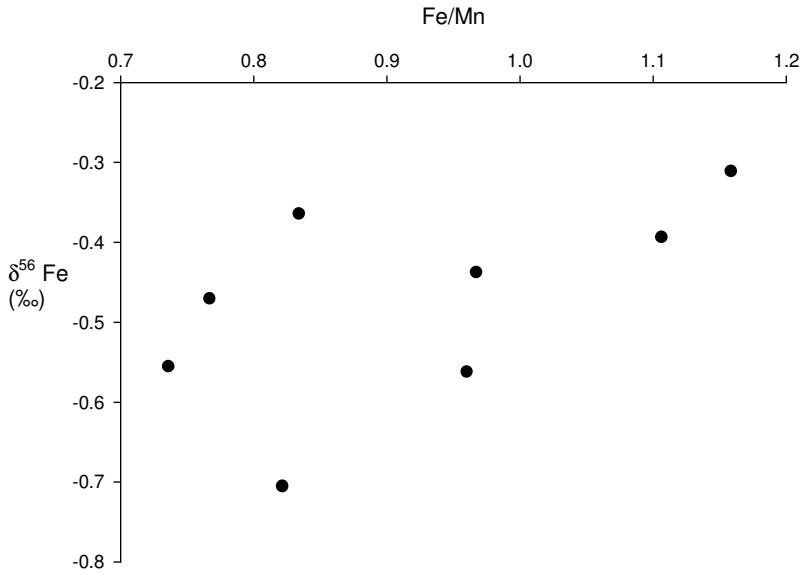

Figure 7.4 – The relationship between the Fe/Mn ratio and the isotope composition in the particulate Fe.

However, what are reported here are only the isotope compositions for the *particulate* fractions of these buoyant plume samples rather than the total Fe. Further the percent of dissolved Fe decreases with increasing total Fe (Chapter 6, Figure 6.8). Thus there appears to be a decreasing fraction of particulate Fe sulfides relative to particulate Fe oxyhydroxides as the particulate Fe concentrations increase. In Figure 7.5, the calculated percent of Fe sulfide present is plotted *vs.* the isotope composition of the whole particulate Fe material. A striking linear correlation is observed, consistent with simple two-component mixing. As the percent of Fe sulfide decreases in the particulate fraction, the isotope composition becomes heavier.

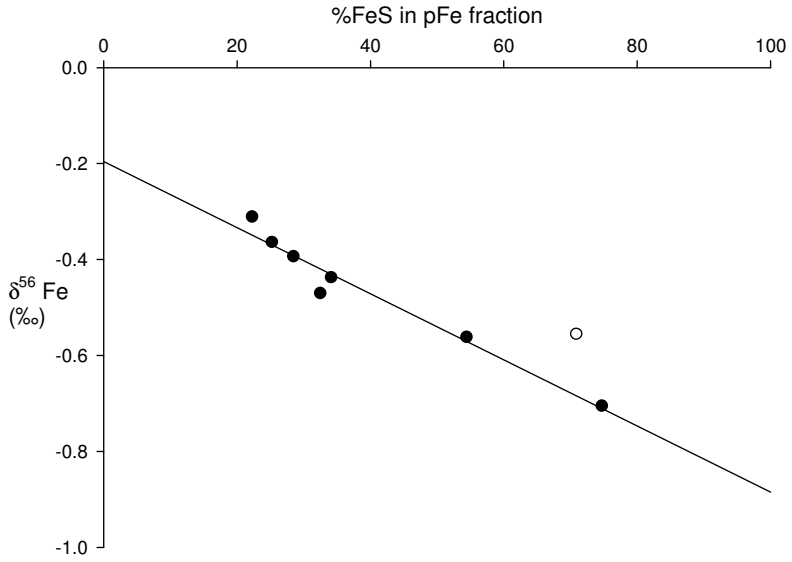

Figure 7.5 – The relationship between the percent of Fe sulfide in the particulate fraction and the isotope composition of the particulate Fe; open circle point excluded from regression.

All the samples, apart from one outlier, linearly correlate with an r^2 of 0.96. Therefore the isotope composition in the particulate fraction can be assumed to be controlled by the percent of Fe sulfide present. It has been shown in Chapter 6 that the Fe sulfide fraction is constant relative to the total Fe in the samples (~25%) and that there has been no loss of Fe sulfide from the plume, which would result in changing the isotope composition of the total Fe. Therefore it can be assumed that the isotope composition of the particulate Fe plus the dissolved Fe equals the isotope composition of the original vent fluid. This relationship in Figure 7.5 can therefore be used to quantify the isotope composition of both particulate and dissolved Fe species in the plume.

The isotope composition read off the graph at zero percent particulate Fe sulfide (-0.20‰) should represent the average isotope composition of any Fe oxyhydroxides in the particulate fraction. Conversely, at 100% particulate Fe sulfide, the isotope composition (-0.89‰) must represent the isotope composition of the 25% of Fe sulfide that has precipitated in all the samples.

If the remaining dissolved Fe is assumed to be composed of colloidal Fe oxyhydroxides, because of the rapid oxidation rates at 5°S MAR, then the isotope composition of the

dissolved Fe should be the same as that measured for the coarser particulate Fe oxyhydroxides (-0.2‰) (i.e. those retained on the filter). This would enable the isotope composition of the initial vent fluid to be calculated, such as:

$$((25\% \times -0.89‰) + (75\% \times -0.2‰)) / 100 = -0.37‰ \quad (7.2)$$

This is because at 100% precipitation and with no loss of pFe to the seafloor, the isotopic composition of the total Fe should mirror that of the vent fluid source. This predicts that the Fe-isotope composition of the source vent fluid was -0.37‰, which is consistent with Fe-isotope composition measured in the end-member fluids at Red Lion (Table 7.2). However, this model assumes that the dissolved Fe fraction is composed solely of Fe oxyhydroxides, which is unlikely as stabilised dissolved Fe complexes have also been detected in non-buoyant plumes at 5°S (Chapter 5). Therefore there is the potential that the Fe-isotope composition of the dissolved Fe fraction could have been different to the Fe-isotope composition of the Fe oxyhydroxides in the particulate fraction.

In Chapter 5, it was concluded that ~4% of the hydrothermal Fe input was stabilised as dissolved Fe species in the plumes at 5°S MAR. Therefore by assuming that 25% of the Fe will precipitate as Fe sulfide, 71% will precipitate as Fe oxyhydroxides and 4% will be stabilised as dissolved Fe, we can predict the potential isotope composition of this stabilised dissolved Fe fraction. This will be done by using the original isotope compositions measured in the vent fluids at Tannenbaum and Mephisto, such as:

$$(4 \times \delta^{56}Fe_{dissolved}) = (100 \times \delta^{56}Fe_{vent\ fluid}) - ((25 \times -0.89) + (71 \times -0.2)) \quad (7.3)$$

The two end-member fluids at Red Lion are both potential sources of Fe in the buoyant plume sampled in this study, occurring directly south of where the ship was positioned for the CTD cast. Therefore if the buoyant plume had been sourced from Tannenbaum (-0.49‰), the isotope composition of the dissolved fraction would have been -3.1‰ and if it had been sourced from Mephisto, the isotope composition of the dissolved fraction would have been +1.9‰. There were also two other high-temperature chimneys at the Red Lion vent site which would also have been potential sources of the buoyant plume, but vent fluids were not available from these sites for isotopic analysis.

The presence of organically complexed Fe ligand complexes have been investigated previously in the terrestrial system and it was reported that the formation of Fe-ligand complexes tend to fractionate the lighter Fe isotopes in the Fe-ligand fraction (Brantley et al., 2001; Brantley et al., 2004). This fits in with the buoyant plume being sourced from Tannenbaum. However, preferential stabilisation of isotopically heavy Fe has previously been observed by Brantley et al. (2001) during the assimilation of Fe by bacteria and by Matthews et al. (2001) during the formation of $[Fe(II)(bipy)_3]^{2+}$ complexes. Organic complexation of Fe(II) in hydrothermal plumes has been suggested by Toner et al. (2007), and would fit in with the fluids being sourced from Mephisto. But because of the uncertainty in the source of the buoyant plume it is difficult to predict the isotope fractionation caused during the formation of stabilised dissolved Fe species.

However, further evidence for the isotope composition of the stabilised dissolved Fe fraction can be gained by plotting the particulate Fe isotope compositions against %pFe. This gives rise to an excellent second order trend, with an r^2 of 0.975, suggesting an end-member vent fluid composition of -0.27‰ (at 100% particulate Fe precipitation), within error of the fluid measured at Tannenbaum (Figure 7.6). By using nonlinear regression analysis, the error of the intercept at 100% pFe was calculated to be ±0.0277‰ ($\delta^{56}Fe_{vent\ fluid}$ = -0.25 to -0.30‰).

Using this end-member vent fluid composition at its upper and lower limit and the isotope composition measured when 95% of the Fe has precipitated, the isotope composition of the dissolved Fe can be solved with mass balance.

$$\delta^{56}dFe = ((100\% \times \delta^{56}Fe_{vent\ fluid}) - (\%pFe \times \delta^{56}pFe)) / (100 - \%pFe) \qquad (7.4)$$

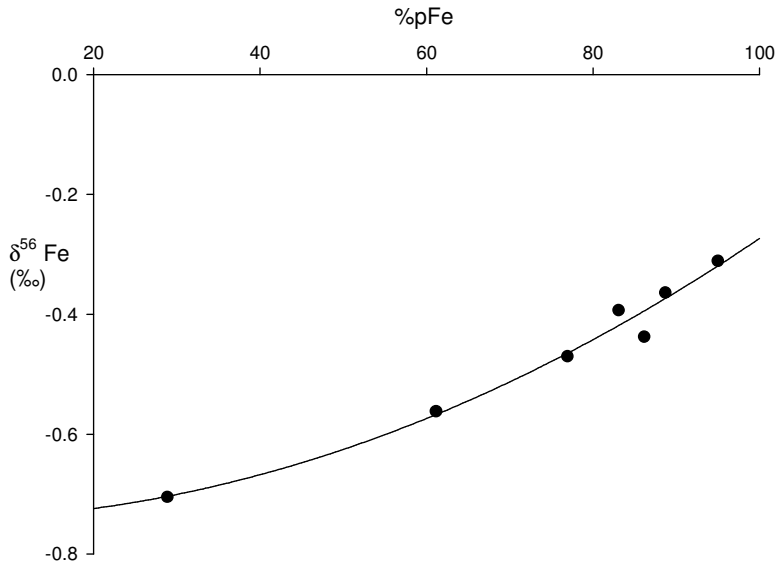

Figure 7.6 – The isotope composition measured in the particulate samples relative to the percent pFe

At 95% pFe, the isotope composition of the dissolved Fe fraction is predicted to lie within -0.13 to +0.98‰. This supports the fractionation of isotopically heavy Fe during the formation of stabilised dissolved Fe species.

There are of course potential errors associated with this calculation and unfortunately the isotope composition of the dissolved fraction was never measured. However this does give a first estimate of a diagnostic signature for a stabilised dissolved Fe fraction escaping from hydrothermal plumes into the deep-ocean with an isotope composition *heavier* than the original vent fluid.

7.4.3 Calculation of the Fe sulfide fractionation factor and modelling of in-situ Fe isotope fractionation in the buoyant hydrothermal plume

The fractionation factor for the Fe sulfide fractionation in the hydrothermal system can be calculated by using the isotope value at 100% Fe sulfide to represent the isotope composition when 25% Fe sulfide has precipitated from the vent fluid (Figure 7.5). This can be done by using a Rayleigh distillation model. This is an exponential model previously used to model partitioning of the light isotope during evaporation. The general form of a Rayleigh distillation equation (7.5) states that the isotope ratio (R_A) in a diminishing reservoir of the reactant is a function of its initial isotopic ratio (R_o), the

remaining fraction of that reservoir (*f*) and the equilibrium fractionation factor for the reaction (α) (Faure, 1986).

$$R_A = R_o f^{(\alpha-1)} \quad (7.5)$$

Where $\alpha = R_{solution} / R_{solid}$

R is the isotope ratio. Since $\alpha \approx 1$, this can be rewritten as (Beard and Johnson, 2004):

$$(\alpha - 1) \times 1000 \approx \delta_{solution} - \delta_{solid} \approx \Delta_{solution\text{-}solid} \quad (7.6)$$

The fractionation factor is dependent on the reaction mechanism and the environmental conditions.

The ratio in the other reservoir, i.e. the particulate fraction measured in the buoyant plume system in this study, can be obtained by mass balance and the equation rearranges to (Dauphas and Rouxel, 2006):

$$R_B = R_o \times (1-f^{\alpha} / 1-f) \quad (7.7)$$

When using the δ notation the equation must be modified as below:

$$(\delta^{56}{}_{\%pFe}+1000) = (\delta^{56}{}_{fluid} + 1000) \times (1-\%pFe^{\alpha})/(1-\%pFe) \quad (7.8)$$

Therefore the fractionation factor for Fe sulfide precipitation calculated for the hydrothermal plume at Red Lion with an end-member vent fluid Fe isotope composition of -0.24‰ (Figure 7.6) is 1.0007 with a $\Delta_{Fe(II)\text{-}FeS} = +0.75‰$. This is within the range determined in the laboratory by Butler et al. (2005), where they observed a kinetic isotope fractionation process with zero age Fe sulfides having an isotope fractionation of $\Delta_{Fe(II)\text{-}FeS} = +0.85‰ \pm 0.30‰$ over a temperature range between 2 and 40°C. During aging, the degree of fractionation decreased between the precipitates and the fluid down to 0.3‰. In the buoyant plume samples the precipitation of ferrihydrite will be rapid, upon mixing of the hydrothermal fluid with seawater and therefore it is not unexpected that a significant kinetic Fe isotope effect is observed.

This kinetic fractionation factor can be used to model the fractionation processes that would have been occurring in-situ in the buoyant plume. Initially ~25% of the Fe will have precipitated as Fe sulfides, followed by partial oxidation, Fe ligand formation and ferrihydrite formation of the remaining dissolved Fe.

The fractionation during the oxidation and precipitation of Fe(II) has been measured by Bullen et al. (2001), in a stream fed by a Fe rich ground water spring, with an overall fractionation of the heavy isotope ($\Delta_{Fe(II)-Ferri}$ = -1.0‰). This was supported in a study by Croal et al. (2004) that investigated the oxidative fractionation process that occurred under anaerobic conditions by photoautotrophic bacteria. They also observed fractionation towards the heavy isotope in ferric Fe relative to the $Fe(II)_{aq}$ ($\Delta_{Fe(II)-Ferri}$ = -1.5‰). They interpreted this as a two step process where a -2.9‰ fractionation occurred between $Fe(II)_{aq}$ and $Fe(III)_{aq}$ during oxidation, followed by a +1.4‰ fractionation between $Fe(III)_{aq}$ and ferrihydrite precipitation. The overall fractionation at low Fe(III)/Fe(II) ratios was -1.5‰. However, in the experiment by Croal et al. (2004), it was suggested that when the Fe(III)/Fe(II) ratio was low, ferrihydrite precipitation was fast, whereas when the ratio was high, ferrihydrite precipitation was much slower and therefore resulted in little kinetic fractionation (Johnson et al., 2004). When Fe(III) concentrations increased, the kinetic fractionation caused by ferrihydrite precipitation appeared to decrease ($\Delta_{Fe(III)-Ferri}$ = ~0 ‰). The fractionation was then dominated by the oxidation of Fe(II) to Fe(III) ($\Delta_{Fe(II)-Fe(III)}$ = -2.9‰).

The isotope composition of the particulate Fe during the evolution of the hydrothermal plume at Red Lion can be modelled with either a $\Delta_{Fe(II)-Ferri}$ = -1.0‰ or -2.9‰ fractionation during oxidation and ferrihydrite formation after a $\Delta_{Fe(II)-FeS}$ = +0.75‰ fractionation during the initial Fe sulfide formation (Figure 7.7). Only 95% of the particulate Fe has been modelled as the rest of the Fe is expected to remain stabilised in the dissolved fraction. The final isotopic composition of the particulate Fe will therefore be -0.38‰, that predicted when 25% of the Fe has precipitated with an isotope composition of -0.89‰ and when 70% of the Fe has precipitated with an isotope composition of -0.2‰. This model demonstrates the initial fractionation of light particulate Fe during the formation of Fe sulfides (25%) in the first few seconds of venting. This is followed by fractionation of the heavy isotope during the formation of Fe oxyhydroxides. There is a mass balance between the light Fe sulfides and the heavy

Fe oxyhydroxides, resulting in a positive curvature in the isotope composition as the particulate Fe increases. As the Fe isotope fractionation occurring during Fe oxyhydroxide formation is uncertain, the two extremes are modelled and therefore the composition of the particulate Fe may lie anywhere between these two lines.

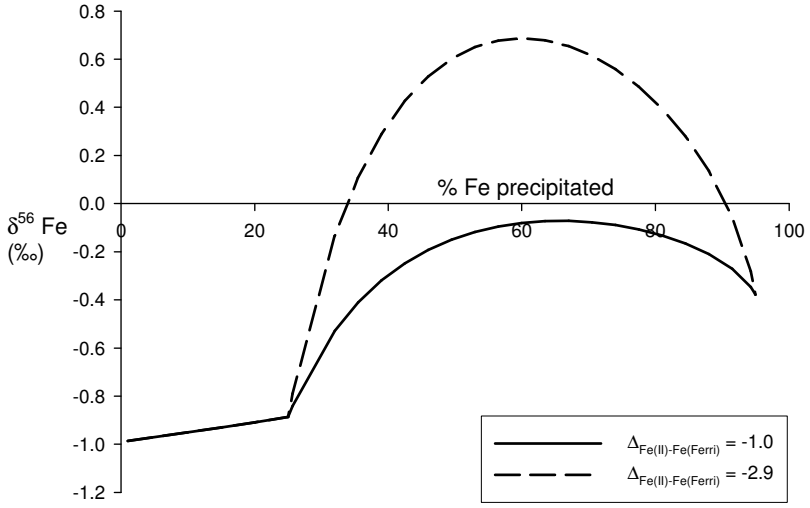

Figure 7.7 – A model of the in-situ Fe isotope composition of the pFe at the Red Lion vent as Fe precipitates during Fe sulfide and Fe oxyhydroxides formation.

However, this is still not a complete representation of the processes occurring in the plume because high up in the buoyant plume rise, dense Fe sulfides will fall out of the plume, causing the remaining Fe to become isotopically heavier. This was not the case at 5°S because the samples collected were from the early stages of the buoyant plume rise. Once all the Fe has oxidised, the maximum increase in the isotope composition of the dispersing plume particles at 5°S can be predicted by assuming that 25% of the Fe will have been removed from the plume by non-buoyant plume height as sulfides with an isotope composition of -0.89‰. Therefore the isotope composition of the remaining Fe oxyhydroxides in the non-buoyant plume will have a maximum Fe isotope composition of -0.20‰, only 0.04‰ less than the original vent fluid composition, assuming the vent fluid has an isotopic composition of -0.24‰. This is because the loss of Fe sulfides is compensated for by the presence of isotopically heavy dissolved Fe species. Fe oxyhydroxides associated with these sinking Fe sulfides may also decrease the extent of fractionation further. In Chapter 5, the Fe/Mn in the non-buoyant plume demonstrated a

loss of particulate Fe greater than 50% of the total Fe suggesting loss of both Fe sulfides and Fe oxyhydroxides. Therefore even after the loss of Fe from the plume the isotope composition of the particulate Fe in the non-buoyant plume will still have an isotope composition similar to the original vent fluid.

7.4.4 Comparison with the isotope study carried out in the plume at the Rainbow vent site

At present there is only one other study that has investigated Fe isotope fractionation in hydrothermal plumes and that was carried out at the Rainbow vent site (Severmann et al., 2004). Severmann et al. (2004) observed a narrow range of isotope values from in-situ particulate samples taken from the non-buoyant plume (-0.18‰) and from underlying sediments (-0.18‰), both of which, corresponded to the isotope composition of the end-member fluid (-0.23‰). Distinct variations were only observed in two samples collected from the buoyant plume, where they observed heavy δ^{56}Fe values of +0.15‰ and +1.20‰, which they explained to be due to partial oxidation.

These particulate samples were collected in-situ using stand-alone pumps (SAPS) and therefore did not have the same sampling artefacts which occurred in this study, due to the delay between sampling the hydrothermal plume and filtering. However, the very heavy δ^{56}Fe values observed at Rainbow are unique to that site because of the low Fe sulfide concentrations. The ultramafic setting of the Rainbow vent site provides end-member fluids with high chlorinity, low pH, high methane and extremely high Fe concentrations because of serpentinization of the host rock. Isotope fractionation is therefore dominated by oxidation rather than sulfide formation, preferentially precipitating the heavier isotope (Balci et al., 2006; Bullen et al., 2001; Croal et al., 2004). These Fe oxyhydroxides are then quantitatively transported to the non-buoyant plume, resulting in the original vent fluid isotope composition being conserved in the non-buoyant plume.

Mass balance predicts that no more than 4.2% of the total Fe at Rainbow can be precipitated as Fe sulfides and cause initial kinetic fractionation (Severmann et al., 2004). This will be followed by fractionation via partial oxidation and ferrihydrite formation. The potential fractionation paths if all the Fe is precipitated is shown in Figure 7.8.

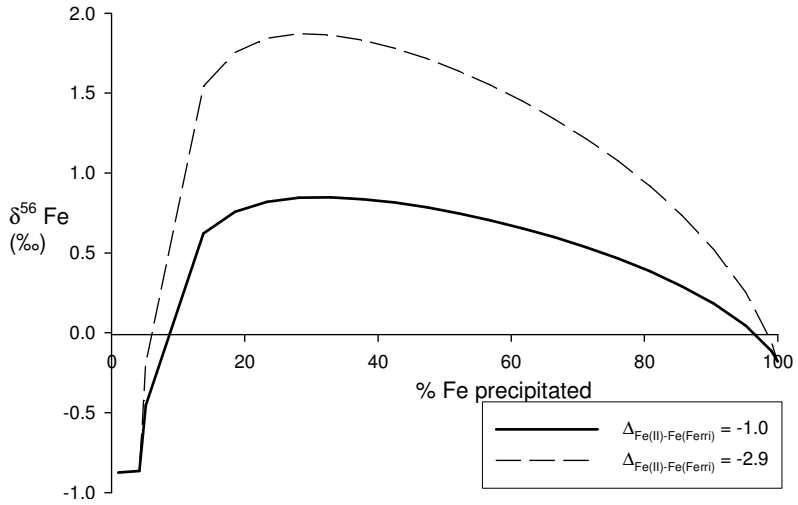

Figure 7.8 – A model of the Fe isotope composition of the Fe at the Rainbow vent as it is precipitated during 4% Fe sulfide formation, followed by Fe oxyhydroxide formation.

Severmann et al. (2004) measured a δ^{56}Fe value of +1.2‰ in one of the buoyant plume samples, which could not have resulted if the fractionation of Fe(II) to ferrihydrite was -1.0‰. Therefore the Fe(III) concentrations must have been high causing little kinetic fractionation during ferrihydrite precipitation and resulting in a fractionation of -2.9‰. The percent of Fe that would have precipitated if the ferrihydrite fractionation had been -2.9‰, would have been 10% or 70% for the sample with a δ^{56}Fe of +1.20‰ and 8% or 90% for the sample with a δ^{56}Fe for +0.15‰, as read off the graph in Figure 7.8. However, the lower values, 10% and 8% are unlikely as these samples were collected near the top of the buoyant plume and therefore over half the Fe will have oxidised and formed oxyhydroxide precipitates (half-life ~30 mins).

7.4.5 Implications for hydrothermal Fe sources to ocean

It was suggested from the first isotopic plume study carried out at the Rainbow vent site that the isotopic composition of hydrothermal end-member fluids was preserved in the non-buoyant plume and recorded in local hydrothermal sediments. However, the Rainbow vent field is not representative of the majority of hydrothermal venting because almost all the Fe emitted from the vent is quantitatively transported to the non-buoyant plume and oxidised during buoyant plume rise (German et al., 2008b). Therefore the

isotope composition of any particulate Fe in the non-buoyant plume will be the same as the original vent fluid composition as no Fe will have been lost during plume dispersal (Severmann et al., 2004).

However, the majority of hydrothermal venting occurs at basalt hosted systems and the Fe is expected to be fractionated by Fe sulfide precipitation. In the Atlantic, even though complete oxidation will have occurred by non-buoyant plume height, Fe sulfide precipitates will have been lost from the plume during buoyant plume rise. Therefore the particulate Fe transported to the top of the buoyant plume will have an isotope composition higher than the original vent fluid. In some systems, up to 50% of the particulate Fe has been predicted to be lost from the plume as Fe sulfide (Rudnicki and Elderfield, 1993). However, in this study it has been *shown* that the formation of stabilised dissolved Fe complexes fractionate the heavy isotope, and therefore the remaining Fe oxyhydroxides present in the non-buoyant plume are isotopically lighter than predicted after loss of the isotopically light Fe sulfide species. Therefore the loss of Fe sulfides combined with the formation of stabilised dissolved Fe counteract each other resulting in the isotope composition of any particulate Fe in the non-buoyant plume having a very similar composition to the original vent fluid.

Basalt hosted systems should dominate hydrothermal activity along the faster spreading ridges in the Indian and Pacific Oceans, where oxidation rates will be slower and dissolved Fe(II) species will still be present at non-buoyant plume height. However, it is difficult to predict the isotope composition of any precipitated Fe during the dispersal of the non-buoyant plume. This is because the amount of Fe oxyhydroxide that becomes associated with the dense Fe sulfide particles is unknown and additionally, stabilisation of colloidal Fe oxyhydroxides may get transported some distance away from the vent before they are deposited on the seafloor. This will need to be investigated further in future studies.

The stabilised dissolved Fe remaining in the plume and potentially adding to the deep-ocean dissolved Fe budget is suggested in this study to have an isotopic signature heavier than the original vent fluid. In the study by Chu et al. (2006) it was suggested that the negative isotope composition in the ferromanganese crusts in the central Pacific were influenced by hydrothermal inputs, but this study suggests than any Fe escaping from the

plume will have a *heavy* isotope composition. There is of course the potential that stabilised inorganic colloids from the hydrothermal plume could also be transported some distance from areas of hydrothermal venting. Such colloids would have an isotope composition similar to the original vent fluid and, hence, *could* influence more distal ferromanganese crusts in the manner suggested by Chu et al. (2006).

7.5 Summary

Fe isotope analysis has enabled the isotope composition of various Fe species within the hydrothermal plume to be determined. Within the buoyant plume, the isotope composition of the particulate Fe correlates to the percent of Fe sulfide in the particulate fraction. This has enabled a kinetic isotope fractionation, $\delta_{Fe(II)\text{-}FeS} = +0.75‰$, to be determined for Fe sulfides precipitated in the rising buoyant plume.

Comparison of the plume samples from Red Lion with those collected in-situ at the Rainbow vent site has enabled the three fractionation processes occurring in the buoyant plume during Fe precipitation to be modelled; Fe sulfide formation, partial oxidation and ferrihydrite formation. Additionally, a stabilised dissolved Fe fraction also appears to cause an isotopic fractionation in the plume, resulting in stabilisation of isotopically heavy dissolved Fe species, which will potentially add to the deep-ocean dissolved Fe budget.

This study provides new insights on the isotope fractionation processes occurring in hydrothermal plumes and helps support the presence of hydrothermal Fe in ferromanganese crusts lining the seafloor. It is important that these fractionation processes are understood if Fe isotopes are to be used as a geochemical tracer of oceanic Fe sources as this will be an extremely powerful tool for answering some of the in depth debates that have surrounded Fe biogeochemistry for the last 20 years.

Chapter 8. Conclusions

This thesis has examined the influence of hydrothermal activity on the biogeochemistry of Fe in the ocean. Three specific questions have been addressed:

1) Is dissolved organic carbon present within high-temperature hydrothermal plumes (either entrained or produced in-situ) with the potential to stabilise dissolved Fe?

2) If elevated concentrations of dissolved organic carbon are present in hydrothermal plumes, are stabilised dissolved Fe-ligand complexes formed that may be exported to the deep-ocean?

3) Is there a diagnostic hydrothermal δ^{56}Fe signal for any dissolved Fe that is exported from a vent field?

Until recently high-temperature hydrothermal systems have been assumed to be predominately inorganic and the role of organic compounds in hydrothermal plumes has been largely overlooked. On the East Pacific Rise, elevated DOC and POC concentrations have been found in hydrothermal plumes overlying high-temperature vents on the East Pacific Rise (9°50'N). It is unlikely that these high concentrations of organic carbon, relative to background, have end-member vents as their source. Therefore, the enrichments in organic carbon observed must either result from entrainment or in-situ production within the plumes.

At increasing height, hence dilution, DOC and POC concentrations within the EPR plumes decrease towards background seawater values, although elevated DOC concentrations have been observed in a couple of samples collected at non-buoyant plume height. The source of this organic carbon enrichment must ultimately come from microbial activity, whether in areas of diffuse flow or within the plumes themselves.

The presence of high dissolved organic carbon concentrations, together with high concentrations of Fe within these plumes have provided the first evidence that the building blocks for organically stabilised Fe to form are present within deep-sea

hydrothermal plumes. This study also revealed evidence for an interaction between Fe and organic compounds: Concentrations of TdFe and DOC exhibited a close linear correlation which would be consistent with, but does not prove that organic-Fe complexes were being formed.

In the Atlantic Ocean, quantitative oxidation and precipitation of any hydrothermally sourced dissolved Fe(II) should be expected to have occurred by the time a plume reaches non-buoyant height (~1 hr after emission of vent fluid from the seafloor). Therefore, measurement of any Fe still present in the dissolved fraction, at plume height, would infer the presence of stabilised dissolved Fe species. Dissolved Fe concentrations in dispersing non-buoyant plumes at 5°S on the Mid-Atlantic Ridge (MAR), did, indeed, exhibit elevated dFe concentrations relative to what would be predicted from theoretical Fe(II) oxidation rates.

To investigate this further, a CLE-CSV technique was applied to quantify organically complexed Fe in a suite of hydrothermal plume samples. This work has confirmed that stabilised Fe-ligand complexes were present in these hydrothermal plumes in concentrations that are sufficient for approximately 4% of the total Fe exiting the 5°S vents to be stabilised in solution at plume height. If these studies were representative of all hydrothermal systems, high-temperature seafloor venting could provide ~11 to 22% of the global deep-ocean dissolved Fe budget.

This potential source for dissolved Fe entering the deep-ocean was suggested previously by Chu et al. (2006), who reported ferro-manganese crusts with hydrothermal characteristics from the central Pacific distant from any hydrothermal sources. In that study the Fe isotope composition of the crust, in particular, demonstrated a constant, isotopically light signature interpreted to represent input from high-temperature hydrothermal vent fluids (Chu et al. 2006).

To investigate whether hydrothermally-sourced dissolved Fe really does carry a distinct isotopic signature, samples of the end-member vent fluids and the buoyant hydrothermal plume were collected by ROV and CTD rosette respectively. Because Fe isotope analysis is limited by Fe concentration, samples from the non-buoyant plumes contained insufficient Fe to allow for Fe isotope analysis. For the buoyant plume samples, a time

delay of some hours occurred, between collection and processing on deck. This meant that any dissolved Fe present in-situ at the time of sampling near the seafloor should have been quantitatively oxidised by the time the samples were filtered aboard the ship. This provided an unforeseen advantage because it allowed for isotopic fractionation associated with the formation of Fe sulfides, Fe oxyhydroxides and Fe ligands to be resolved, demonstrating a unique isotope composition for each chemical species. The diagnostic isotope signature of dissolved Fe present within the plume was calculated to be heavier than the original vent fluid, disapproving the assumptions of Chu et al. (2006), that the signal reported from Fe-Mn crusts represents the faithfully recorded pristine vent-fluid signature.

This does not mean that hydrothermal inputs can not be the source of dissolved Fe to the central Pacific, but that interpretation of Fe-Mn crusts should recognise that fractionation is likely to occur during the incorporation of Fe from seawater, into those crusts. This is also the case for Tl and Mo each of which demonstrate opposite fractionation processes to each other during incorporation into the crusts (Levasseur et al., 2004). The isotope composition calculated for the dissolved Fe fraction, heavier than the original vent fluid is the closest we have for a diagnostic signature of a hydrothermal dissolved Fe input to the deep-ocean, assuming that the 5°S MAR system is representative at the global scale.

8.1 Future work

This is the first investigation that has focused in such detail on the fate of dissolved Fe within deep-sea hydrothermal plumes. Previously, particulate analysis dominated because it had been assumed that all dissolved Fe from hydrothermal vents precipitated rapidly in buoyant and non-buoyant plumes. In this study, by contrast, it has been shown that ~4% of total Fe vent-output may be stabilised as dissolved Fe species, which are transported to the deep-ocean, even in the highly oxidising Atlantic ocean.

However, this work must be considered preliminary. There are, as yet, no complementary data sets for any of the DOC and POC distributions, Fe-ligand complex concentrations or calculated Fe isotope compositions of dissolved Fe in any other hydrothermal plumes. Thus, while the present study gives insights into the presence of

stabilised dissolved Fe species within hydrothermal plumes, a series of further compelling scientific questions arise. For example:

1) What is the source/sources of organic carbon (DOC and POC) to deep-sea hydrothermal plumes?

2) Where does organic complexation of dissolved Fe occur within a hydrothermal plume and over what timescales?

3) What are the compositions of the organic ligands responsible for this complexation?

4) Do similar Fe-ligand complexes exist in all hydrothermal systems and give rise to a similar proportion of the total Fe that is stabilised in solution, for export to the deep-ocean?

5) How does the Fe isotope signature of stabilised Fe-ligand complexes affect the overall isotope composition of the deep-ocean?

6) How do the processes controlling dissolved Fe complexation vary along the global thermohaline conveyor?

Future work should aim to address these questions.

A much more in depth study must be carried out on DOC and POC concentrations within the hydrothermal systems. This should include samples collected from diffuse flow areas, within buoyant and non-buoyant plumes and from the deep water column, locally, below non-buoyant plume height, representing any seawater that will be entrained into plumes from high-temperature vents. This work should be combined with complementary analyses of dissolved and particulate Fe in samples separated through the same size filter (even though different filter types are required). Additional useful measurements could include carbon isotope ratios of DOC and POC, which may be diagnostic of the carbon source (e.g. diffuse flow) and then traced into the plumes from the high-temperature vents. Further combining these measurements with microbial work

(e.g. ATP measurements, incubation experiments) could help determine the DOC source and provide insight into how microbes might be interacting with the dissolved Fe present.

To better constrain the role of organic complexation in the stabilisation of dissolved Fe from hydrothermal systems, further speciation studies using CLE-CSV could be carried out, focusing on the fringes of the hydrothermal plumes, diffuse flow areas and the local ambient water column. Analyses should be conducted both on-board ship and in shore based laboratories to maximise the number of samples that can be processed. Future investigations could involve varying the 'detection window' of the technique enabling determination of weaker and stronger ligands associated with the plume material. This could be done by varying the amount of competitive ligand added during the titration or by using a completely different competitive ligand.

In parallel with CLE-CSV studies, it would be informative to investigate this same speciation issue using a wider range of techniques. The concentration of the Fe ligand fraction measured within the hydrothermal plumes in this study are much higher than that measured in previous studies in the deep-ocean, enabling the use of less sensitive techniques for speciation analysis. Chromatography techniques, for examples, might be able to separate the organic fraction and then quantify any Fe associated with the organic species. If samples from buoyant plumes are analysed, high enough DOC concentrations might be obtained to enable a combined gas/HPLC chromatography - mass spectrometry analyses, enabling the composition of potential Fe complexing ligands to be determined.

In the particulate fraction, mineralogy techniques could also be used to investigate carbon and Fe speciation. Powerful tools such as scanning transmission X-ray microscopy (STXM) and near-edge X-ray absorption spectroscopy (NEXAFS) can provide spatial resolution better than 50 nm, enabling determination of oxidation states, mineralogical structure and organic interactions with Fe.

Finally the isotope signature of particulate Fe determined in this study needs to be confirmed by analysing both the dissolved and particulate fraction of similar samples to those collected in this study. To fully understand the impact of hydrothermal systems on the Fe isotope composition of the open ocean, it will be essential to measure the isotope

composition of open ocean dissolved Fe. A number of laboratories around the world are actively pursuing this problem.

The location for the studies described must consider the potential for variations in the chemistry occurring along the thermohaline circulation. For example, in the Pacific the oxidation rates will be slower and there will be the potential for a greater percentage of dissolved Fe to be stabilised. Also the biggest hydrothermal inputs have been determined to occur in the Pacific with hydrothermal ^{3}He inputs traced to the surface ocean. Therefore by carrying out the proposed studies in the Pacific, near to a GeoTraces transect (e.g. Southern EPR), would be a smart location for confirming whether stabilised, hydrothermally sourced, dissolved Fe exists in other areas of the oceans and whether any of this Fe can be detected in the surface ocean.

The history of oceanographic research has marched hand in hand with technology developments and continues to do so. In this study a number of concerns have been raised with current sampling techniques that can only be resolved with the development of relevant in-situ techniques. Much current attention is being paid to the development of in-situ sensors for Fe and Mn, with prototypes already in use. Miniaturisation of such technologies (e.g. Lab-on-a-chip) will help solve many key limitations of first generation oceanographic chemical sensors, minimising size, reagent consumption, power use and cost. Such systems will then be able to be deployed for long periods of time in harsh deep-ocean environments, either fixed in one place on ocean observatory installations or integrated into mobile vehicles (ROVs, AUVs and gliders) where they can be introduced into the flow and dispersal of hydrothermal plumes, enabling a much better understanding of the processes active within these chemically and physically dynamic environments. While it may not be realistic, especially in the short term, to render the more complicated techniques used in this study autonomous, a judicious combination of in-situ sensing and shipboard/land-based experiments, would serve well to better constrain those processes most sensitive (e.g. dissolved Fe(II) oxidation) to a time delay between sample collection at the seafloor and sample retrieval, processing and analysis aboard ship.

Relative to the more traditional sciences, oceanography is still young (e.g. Challenger Expedition in the late 1800s) and the study of hydrothermal systems is even younger.

Over the last thirty years since the first hydrothermal vents were discovered, studies have revolutionised our ideas with the recognition of a major new source of chemical input to the oceans. Despite significant active research in this field, there remain many new surprises. It has long been recognised that Fe is one of the most abundant elements released to the oceans by venting, in contrast to the rest of the ocean, where Fe is well established as a bio-limiting micronutrient. This study has determined that organic complexation may act to stabilise sufficient hydrothermally sourced dissolved Fe, to sustain up to 22% of the steady state flux to the deep-ocean and hence, play a major role in global-scale biogeochemical cycles.

Appendix 1 – DOC and POC data

	Depth (m)	Density (σ)	DOC (μM)	Error (μM)	POC (μM)
CTD 81	2487	1039.25	38.3	0.6	0.13
	2481	1039.23	38.6	0.6	0.22
	2472	1039.19	36.3	1.5	0.46
	2462	1039.14	37.4	1.2	0.07
	2453	1039.11	37.0	1.8	0.24
	2441	1039.05	38.5	0.9	0.10
	2433	1039.02	35.3	1.0	0.15
	2393	1038.83	38.8	1.1	0.09
	2338	1038.58	43.2	1.1	0.11
	2280	1038.31	38.3	1.6	0.18
CTD 91	2391	1039.28	38.6	1.2	0.15
	2335	1038.57	39.1	1.3	0.35
	2325	1038.52	40.6	0.8	0.38
	2310	1038.45	36.7	1.1	0.41
	2295	1038.38	36.4	1.2	0.34
	2285	1038.33	36.6	0.9	0.19
	2275	1038.28	38.5	1.2	0.08
	2215	1037.99	36.9	1.7	0.22
CTD 92	2448	1039.08	40.0	2.1	0.14
	2411	1038.91	36.3	1.3	0.13
	2354	1038.65	40.3	1.7	0.13
	2335	1038.56	36.6	1.6	0.17
	2324	1038.51	36.9	1.4	0.29
	2314	1038.47	64.8	2.2	0.16
	2310	1038.45	37.3	1.0	0.12
	2275	1038.29	38.7	2.0	0.18
CTD 48	2648	1036.04	41.7	1.8	
Background	2440	1035.55	36.1	1.5	0.38
	2353	1035.06	38.2	1.3	0.40

POC analysis had a 10% error

Appendix 2 – Fe and Mn data for non-buoyant plumes

			GFAAS	ICP-OES				
	Depth (m)	**TdFe (nM)**	**TdMn (nM)**	**dFe (nM)**	**pFe (nM)**	**pMn (nM)**	**TFe (nM)**	**Calc. dFe**
CTD 1	3746	17.9	2.7					
	3647	17.8	2.8					
	3550	19.4	2.9					
	3500	18.0	2.6					
	3477	18.1	3.7					
	3451	26.0	3.8					
	3428	39.6	8.1					
	3403	51.2	8.2					
	3354	51.4	8.3					
	3257	32.6	4.7					
	3158	15.2	2.4					
	2962	6.3	1.3					
	2717	4.5	0.8					
	2472	4.2	1.0					
	1980	5.7	0.8					
CTD 2	4140	22.0	3.7					
	4000	18.6	3.6					
	3800	21.5						
	3600	17.0	3.1					
	3500	63.6	11.4					
	3400	91.4	17.9					

		GFAAS		ICP-OES				
	Depth (m)	**TdFe (nM)**	**TdMn (nM)**	**dFe (nM)**	**pFe (nM)**	**pMn (nM)**	**TFe (nM)**	**Calc. dFe**
	3300	39.8	6.2					
	3200	15.1	3.0					
	3100	7.5	1.9					
	3000	4.3	1.1					
	2500	4.3	1.4					
	2000	2.1	0.5					
CTD 6	2880	3.6	1.4					
	2845	4.6	1.9					
	2804	5.1	1.2	2.5	2.5	0.2	5.0	
	2767	18.4	8.8	9.0	7.3	0.2	16.3	
	2758	21.0	12.8	10.2	10.1	0.3	20.3	
	2749	12.1	13.2	5.5	3.8	5.4	9.2	
	2729	8.6	6.5	3.9	3.8	0.2	7.8	
	2694	5.2	2.5	2.6	2.9	0.2	5.5	
	2652	4.8	1.7					
	2512	3.2	1.5					
	1999	2.1	0.5	1.7	1.5	0.1	3.3	
CTD 7	2995	8.2	5.9					
	2975	9.3	10.2	7.2	3.5	0.2	10.6	
	2924	12.5	13.2	8.3	5.1	0.2	13.4	
	2875	19.3	14.6	15.3	5.1	0.2	20.4	
	2825	13.6	13.4	7.4	6.5	0.3	13.9	
	2775	5.8	3.0					

		GFAAS		ICP-OES				
	Depth (m)	**TdFe (nM)**	**TdMn (nM)**	**dFe (nM)**	**pFe (nM)**	**pMn (nM)**	**TFe (nM)**	**Calc. dFe**
	2500	4.5	1.5					
	2000	2.9	0.6					
CTD 8	2825	6.9	7.0					
	2800	12.5	5.3	9.3				
	2775	7.6	7.1	7.1				
	2750	10.2	11.2	6.1	4.0	0.2	10.1	
	2725	10.7	16.0	6.6	4.4	0.2	11.1	
	2694	4.9	2.1					
CTD 9	2984	5.9	7.2					
	2951	8.7	10.5	5.3	3.7	0.2	9.1	
	2926	13.9	15.8	12.3	3.8	0.2	16.1	10.2
	2900	9.8	10.3	6.2	3.8	0.2	10.0	
	2875	7.6	5.5					
	2825	5.5	4.9					
CTD 10	2985	7.8	9.3	5.0	3.0	0.2	7.9	
	2960	11.3	13.8	11.7	2.4	0.1	14.1	8.9
	2940	13.8	13.6	12.7	3.4	0.3	16.2	10.3
	2900	8.7	7.8	4.4	3.9	0.2	8.3	
	2850	7.6	5.1	12.6	3.6	0.2	16.1	4.0
	2825	6.8	3.3	3.2	3.5	0.3	6.7	
	2800	6.6	4.7	4.1	3.4	0.2	7.5	
	2775	31.6	29.2	21.6	7.8	0.3	29.4	

		GFAAS		ICP-OES				
	Depth (m)	**TdFe (nM)**	**TdMn (nM)**	**dFe (nM)**	**pFe (nM)**	**pMn (nM)**	**TFe (nM)**	**Calc. dFe**
	2760	23.4	20.7	16.6	6.7	0.3	23.2	
	2740	4.1	2.5	2.3	2.2	3.8	4.5	
	2700	4.4	2.1	3.7	2.2	0.2	5.9	2.1
	2600	4.2	1.5	7.8	1.9	0.2	9.7	2.3
CTD 11	2938	6.7	15.5	7.1	2.7	0.2	9.9	4.0
	2925	7.4	18.5	6.8	3.1	0.2	9.9	4.3
	2901	12.9	21.2	7.4	3.2	0.1	10.6	
	2875	*52.9*	23.2	64.2	16.8	0.2	81.0	
	2850	*48.9*	24.9	62.5	15.1	0.2	77.5	
	2825	33.6	20.2	27.9	4.4	0.2	32.3	
	2800	12.0	7.1	8.7	3.4	0.2	12.1	
	2775	8.9	5.3	8.2	3.5	0.2	11.6	5.4
	2750	6.7	4.8	3.7	2.9	0.2	6.5	
	2500	4.3	1.5	2.6	2.8	0.2	5.4	
	1997	1.7	0.5					
CTD 16	3009	*55.6*	132.0	49.2	77.5	0.1	126.7	
(Buoyant	3006	*64.7*	91.0	53.2	21.6	0.1	74.7	
Plume)	3002	*68.6*	96.4	45.7	25.3	0.2	70.9	
	2996	*60.8*	160.3	28.4	94.5	0.1	122.9	
	2992	*60.2*	202.6	27.2	168.8	0.2	195.9	
	2989	*68.0*	208.2	39.0	191.3	0.1	230.4	
	2985	*74.8*	284.1	26.8	210.1	0.1	236.9	
	2981	*78.4*	356.6	20.7	392.3	0.2	413.0	

		GFAAS			ICP-OES		
Depth (m)	**TdFe (nM)**	**TdMn (nM)**	**dFe (nM)**	**pFe (nM)**	**pMn (nM)**	**TFe (nM)**	**Calc. dFe**
For [pFe] > 10 nM, the calculated total Fe concentration will be used to represent the total Fe rather than TdFe (Concentrations in italics)							

Appendix 3 – CLE-CSV

Total Fe (nM)	Fe added (nM)	Current (nA)	[Fe(TAC)] (nM)	[Fe'] (nM)	[FeL] (nM)	[Fe']/FeL]
CTD 10 6						
3.2	0	16.5	1.26	0.005	1.94	0.003
3.45	0.25	25.6	1.95	0.008	1.50	0.005
3.7	0.50	26.8	2.05	0.008	1.65	0.005
3.95	0.75	29.6	2.26	0.009	1.69	0.005
4.2	1.00	26.7	2.04	0.008	2.16	0.004
5.2	2	37.3	2.85	0.011	2.35	0.005
8.2	5	72.1	5.50	0.022	2.70	0.008
13.2	10	133.0	10.15	0.040	3.05	0.013
23.2	20	263.0	20.08	0.080	3.12	0.026
CTD 10 6						
3.2	0	25.3	1.93	0.008	1.27	0.006
3.45	0.25	25.6	1.95	0.008	1.50	0.005
3.7	0.50	29.6	2.26	0.009	1.44	0.006
3.95	0.75	32.2	2.46	0.010	1.49	0.007
4.2	1	34.2	2.61	0.010	1.59	0.007
5.2	2	41.2	3.15	0.013	2.05	0.006
8.2	5	74.5	5.69	0.023	2.51	0.009
13.2	10	141.0	10.76	0.043	2.44	0.018
23.2	20	264.0	20.15	0.080	3.05	0.026
CTD 10 7						
4.1	0	17.6	1.30	0.005	2.80	0.002
4.35	0.25	19.9	1.47	0.006	2.88	0.002
4.6	0.50	23.5	1.73	0.007	2.87	0.002
4.85	0.75	24.4	1.80	0.007	3.05	0.002
5.1	1	27.6	2.04	0.008	3.06	0.003
6.1	2	36.7	2.71	0.011	3.39	0.003
9.1	5	73.6	5.43	0.022	3.67	0.006
14.1	10	128	9.45	0.038	4.65	0.008
24.1	20	272.5	20.11	0.080	3.99	0.020
CTD 10 7						
4.1	0	21.3	1.55	0.006	2.55	0.002
4.35	0.25	20.9	1.52	0.006	2.83	0.002
4.6	0.50	25.5	1.85	0.007	2.75	0.003
4.85	0.75	28.3	2.06	0.008	2.79	0.003
5.1	1	28.3	2.06	0.008	3.04	0.003
6.1	2	39.3	2.86	0.011	3.24	0.004
9.1	5	73.4	5.34	0.021	3.76	0.006

Total Fe (nM)	Fe added (nM)	Current (nA)	[Fe(TAC)] (nM)	[Fe'] (nM)	[FeL] (nM)	[Fe']/FeL]
14.1	10	146.0	10.62	0.042	3.48	0.012
24.1	20	275.0	20.00	0.080	4.10	0.019
CTD 10 8						
21.6	0	70.7	12.9	0.051	8.75	0.006
21.85	0.25	73.7	13.4	0.053	8.45	0.006
22.1	0.50	74.9	13.6	0.054	8.48	0.006
22.35	0.75	77.6	14.1	0.056	8.24	0.007
22.6	1	79.1	14.4	0.067	8.22	0.007
23.6	2	85.4	15.5	0.062	8.08	0.008
26.6	5	107.5	19.6	0.078	7.05	0.011
31.6	10	131.0	23.8	0.095	7.78	0.012
41.6	20	189.5	34.5	0.137	7.15	0.019
CTD 10 9						
16.6	0	66.5	11.3	0.045	5.34	0.008
16.85	0.25	61.7	10.5	0.042	6.39	0.007
17.1	0.50	63.7	10.8	0.043	6.30	0.007
17.35	0.75	68.0	11.5	0.046	5.82	0.008
17.6	1	67.6	11.5	0.046	6.15	0.007
18.6	2	74.6	12.6	0.050	5.96	0.008
21.6	5	104.5	17.7	0.071	3.89	0.018
26.6	10	135.0	22.9	0.091	3.72	0.025
36.6	20	182.0	30.9	0.123	5.75	0.021
46.6	30	253.0	42.9	0.171	3.72	0.046
CTD 10 10						
2.3	0	16.3	1.30	0.005	1.00	0.005
2.55	0.25	19.1	1.53	0.006	1.02	0.006
2.8	0.50	21.5	1.72	0.007	1.08	0.006
3.05	0.75	25.1	2.01	0.008	1.04	0.008
4.3	2	37.1	2.97	0.012	1.33	0.009
7.3	5	69.6	5.57	0.022	1.73	0.013
12.3	10	126.0	10.08	0.040	2.22	0.018
22.3	20	251.0	20.08	0.080	2.22	0.036
CTD 10 10						
2.3	0	14.3	1.10	0.004	1.20	0.004
2.55	0.25	24.5	1.88	0.008	0.67	0.011
2.8	0.50	27.4	2.11	0.008	0.69	0.012
3.05	0.75	25.4	1.95	0.008	1.10	0.007
3.3	1	30.5	2.35	0.009	0.95	0.010
4.3	2	40.0	3.08	0.012	1.22	0.010

Total Fe (nM)	Fe added (nM)	Current (nA)	[Fe(TAC)] (nM)	[Fe'] (nM)	[FeL] (nM)	[Fe']/FeL]
7.3	5	74.2	5.71	0.023	1.59	0.014
12.3	10	131.0	10.08	0.040	2.22	0.018
CTD 7 4						
15.3	0	33.4	5.39	0.021	9.91	0.002
16.05	0.75	42.0	6.77	0.027	9.28	0.003
16.3	1	57.1	9.21	0.037	7.09	0.005
17.3	2	59.9	9.66	0.038	7.64	0.005
20.3	5	64.0	10.3	0.041	9.99	0.004
25.3	10	110.0	17.7	0.071	7.56	0.009
35.3	20	184.0	29.7	0.118	5.62	0.021
45.3	30	234.0	37.7	0.150	7.56	0.020
CTD 11 6						
28.15	0.25	85.6	13.8	0.055	14.4	0.004
28.4	0.50	90.1	14.5	0.058	13.9	0.004
28.65	0.75	91.3	14.7	0.059	13.9	0.004
28.9	1	94.9	15.3	0.061	13.6	0.004
29.9	2	104.0	16.8	0.067	13.1	0.005
32.9	5	121.5	19.6	0.078	13.3	0.006
37.9	10	152.5	24.6	0.098	13.3	0.007
47.9	20	206.5	33.3	0.133	14.6	0.009
57.9	30	277.0	44.7	0.178	13.2	0.013
CTD 16 16						
26.8	0	52.7	7.75	0.031	19.1	0.002
27.06	0.25	51.2	7.53	0.030	19.5	0.002
27.3	0.50	46.8	6.88	0.027	20.4	0.001
27.56	0.75	48.3	7.10	0.028	20.6	0.001
27.8	1	51.9	7.63	0.030	20.2	0.002
28.8	2	57.8	8.49	0.034	20.3	0.002
31.8	5	75.8	11.1	0.044	20.7	0.002
46.8	20	175.0	25.7	0.103	21.1	0.005
56.8	30	245.0	36.0	0.144	20.8	0.007
CTD 16 17						
20.7	0	73.6	5.94	0.024	14.7	0.002
20.95	0.25	74.9	6.04	0.024	14.9	0.002
21.2	0.50	90.0	7.26	0.029	13.9	0.002
21.45	0.75	88.3	7.12	0.028	14.3	0.002
21.7	1	91.0	7.34	0.029	14.3	0.002
22.7	2	100.0	8.06	0.032	14.6	0.002
25.7	5	152.0	12.3	0.049	13.4	0.004

Total Fe (nM)	Fe added (nM)	Current (nA)	[Fe(TAC)] (nM)	[Fe'] (nM)	[FeL] (nM)	[Fe']/FeL]
30.7	10	228.0	18.4	0.073	12.3	0.006
40.7	20	342.0	27.6	0.110	13.1	0.008
CTD 16 18						
33.15	0.25	82.8	12.6	0.050	20.6	0.002
33.4	0.50	87.3	13.2	0.053	20.1	0.003
33.65	0.75	89.2	13.5	0.054	20.1	0.003
33.9	1	90.8	13.8	0.055	20.1	0.003
34.9	2	93.4	14.2	0.056	20.7	0.003
37.9	5	117.0	17.7	0.071	20.1	0.004
42.9	10	162.0	24.6	0.098	18.3	0.005
52.9	20	224.0	33.9	0.135	18.9	0.007
62.9	30	294.0	44.6	0.177	18.3	0.010

Appendix 4 – CLE-CSV experiment

Speciation considerations

Method

Open ocean seawater was collected from the Canary Basin (dissolved Fe conc 0.26 nM) and stored in the dark at 4°C in a 1000 L cubic container back at NOCS. Eight litres of this water was filtered through a 0.4 μm acid clean membrane filter and then, after various permutations to aliquots of this water as listed below, the samples were analysed for organic ligands using the CLE-CSV procedure.

1) The sample was initially analysed in order to determine the Fe ligand concentration of the seawater

2) In order to destroy the organic ligands present, a fresh aliquot of sample was put in acid cleaned (10% HCl) quartz tubes and UV irradiated using a 400 watt medium-pressure Hg-vapor UV lamp (photochemical reactors). Some of this sample was analysed to confirm ligand degradation.

3) An hour after UV irradiation, the sample was poured into an acid cleaned Teflon bottle and placed in the fridge at 4°C. After cooling, a 300 ml fraction of the irradiated seawater was spiked with ~10 nM of Fe (II) solution as ferrous ammonium sulfate and allowed to equilibrate in a fridge for 1 hour and 24 hours. After each time period, 150 ml of the sample was filtered (0.4 μm acid cleaned syringe filter) and analysed by CLE-CSV.

Results

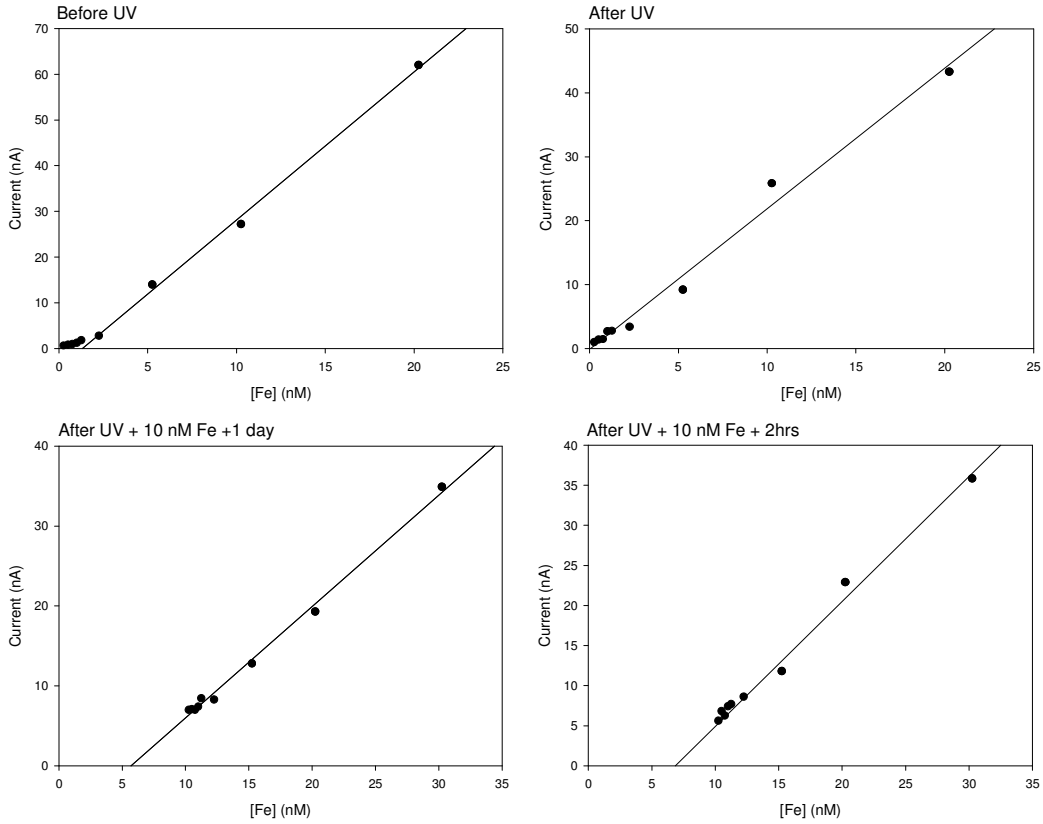

Conclusions

Repeated CLE-CSV analyses of a UV irradiated seawater sample at increasing times after first Fe addition have confirmed an absence of any organic ligands. This provides strong evidence that any ligands observed within natural hydrothermal plume samples will, indeed, partially be due to an organic effect (Van den Berg, 2006).

Appendix 5 – Major and trace elements

Depth	Mg (nM)	%RSD	Al (nM)	%RSD	P (nM)	%RSD	S (nM)	%RSD	Ca (nM)	%RSD	V (nM)	%RSD	Cr (nM)	%RSD
3009	613	1.7	10.1	3.3	3.9	5.7	269	2.1	155	3.1	0.18	7.5	0.08	16.9
3006	515	1.8	7.2	2.2	-1.5	bdl	223	2.8	79.1	2.2	0.03	11.3	-0.01	25.9
3002	485	1.5	9.6	3.3	0.8	bdl	202	3.2	166	2.6	0.04	12.4	0.05	14.4
2996	894	1.4	9.4	3.0	7.0	4.3	394	1.5	260	1.6	0.23	6.0	0.09	14.5
2992	488	2.0	7.8	2.0	12.2	3.4	239	2.3	86.6	2.5	0.45	5.3	0.26	18.3
2989	460	2.1	6.3	2.0	15.1	4.4	239	2.5	86.0	2.4	0.53	4.8	0.19	12.2
2985	647	1.7	21.1	1.8	17.3	2.8	316	1.7	123	2.8	0.58	3.7	0.26	9.5
2981	586	2.2	4.9	3.0	33.6	3.3	347	1.9	143	2.6	1.11	3.3	0.51	13.7

Depth	Mn (nM)	%RSD	Fe (nM)	%RSD	Cu (nM)	%RSD	Zn (nM)	%RSD	[1]Fe/(Fe+Mn+Al)
3009	0.1	5.5	77.5	1.8	2.9	2.6	10.6	2.6	91
3006	0.1	5.5	21.6	1.8	1.4	4.6	4.2	2.8	82
3002	0.2	5.9	25.3	1.8	1.8	3.3	7.2	2.2	90
2996	0.1	5.6	94.5	1.9	3.0	3.0	13.3	2.4	93
2992	0.2	4.1	169	1.8	3.5	2.8	15.3	2.2	97
2989	0.1	6.1	191	2.1	4.1	3.3	18.6	2.4	98
2985	0.1	5.5	210	1.6	4.9	2.7	19.5	2.4	92
2981	0.2	5.4	392	1.9	7.1	2.7	34.9	2.4	99

[1]Background corrected (Al = 2.4 nM, Mn = 0.11 nM)

Appendix 6 – REE

Depth	Y (pM)	%RSD	La (pM)	%RSD	Ce (pM)	%RSD	Pr (pM)	%RSD	Nd (pM)	%RSD	Sm (pM)	%RSD	Eu (pM)	%RSD	Gd (pM)	%RSD
3009	3.83	1	1.46	2.4	0.85	1.5	0.39	1.8	1.64	1.7	0.36	2.3	0.08	2.0	0.32	2.4
3006	1.79	2	0.76	2.0	0.81	1.7	0.20	1.8	0.84	1.4	0.18	2.7	0.04	1.9	0.16	2.4
3002	1.23	3	0.57	2.3	0.69	1.6	0.15	1.5	0.60	1.7	0.13	1.9	0.03	1.7	0.11	1.4
2996	5.35	2	2.02	2.1	0.94	1.5	0.56	1.9	2.34	1.7	0.51	2.2	0.11	1.9	0.44	2.0
2992	9.72	2	3.63	1.3	1.40	1.0	0.95	1.3	4.02	1.6	0.86	1.4	0.20	1.0	0.77	1.5
2989	11.6	2	4.26	1.6	1.47	1.4	1.11	1.3	4.73	1.3	1.02	0.9	0.24	1.5	0.91	2.0
2985	11.8	3	4.12	1.7	1.27	2.7	1.09	2.2	4.64	1.3	0.99	1.7	0.24	1.1	0.89	1.0
2981	20.0	2	6.84	1.9	1.98	2.6	1.74	2.6	7.33	1.7	1.54	1.2	0.39	1.8	1.43	2.3

Depth	Tb (pM)	%RSD	Dy (pM)	%RSD	Ho (pM)	%RSD	Er (pM)	%RSD	Tm (pM)	%RSD	Yb (pM)	%RSD	Lu (pM)	%RSD
3009	0.06	2.3	0.38	1.9	0.08	1.8	0.22	2.4	0.03	4.3	0.18	1.6	0.03	2.2
3006	0.03	1.5	0.18	2.2	0.04	2.7	0.10	1.8	0.01	2.9	0.08	2.8	0.01	2.8
3002	0.02	2.0	0.13	1.7	0.02	2.7	0.07	3.5	0.01	3.7	0.06	1.9	0.01	3.4
2996	0.08	1.8	0.55	1.9	0.11	2.4	0.32	3.0	0.04	3.7	0.26	3.5	0.04	1.6
2992	0.14	1.5	0.97	1.6	0.20	2.3	0.55	2.0	0.08	1.8	0.46	2.0	0.07	1.6
2989	0.17	2.0	1.14	1.4	0.23	2.0	0.67	2.6	0.09	2.9	0.55	2.2	0.09	1.3
2985	0.17	1.6	1.15	1.3	0.24	1.2	0.69	1.8	0.10	2.7	0.58	2.5	0.09	1.6
2981	0.27	1.5	1.86	1.5	0.39	2.1	1.14	1.0	0.16	1.7	0.96	1.9	0.16	1.0

Appendix 7 – Fe isotopes

Depth (m)	No. duplicates	δ^{56}Fe (‰)	1σ	δ^{57}Fe (‰)	1σ
3009	3	-0.56	0.05	-0.79	0.13
3006	3	-0.70	0.07	-0.96	0.07
3002	2	-0.56	0.03	-0.95	0.05
2996	4	-0.47	0.05	-0.65	0.04
2992	2	-0.44	0.00	-0.65	0.00
2989	4	-0.39	0.07	-0.66	0.03
2985	4	-0.36	0.03	-0.61	0.02
2981	4	-0.31	0.03	-0.58	0.05

References

Achterberg, E.P. and Braungardt, C., 1999. Stripping voltammetry for the determination of trace metal speciation and in-situ measurements of trace metal distributions in marine waters. Analytica Chimica Acta, 400: 381-397.

Anbar, A.D. and Rouxel, O., 2007. Metal stable isotopes in Paleoceanography. Annual Review of Earth and Planetary Sciences, 35: 717-746.

Atkins, P.W., 1999. Physical Chemistry. Oxford University Press, Oxford.

Baker, A.R. and Jickells, T.D., 2006. Mineral particle size as a control on aerosol iron solubility. Geophysical Research Letters, 33(17): L17608 SEP 12 2006

Baker, E.T., Chen, Y.J. and Phipps Morgan, J., 1996. The relationship between near-axis hydrothermal cooling and the spreading rate of mid-ocean ridges. Earth and Planetary Science Letters, 142(1-2): 137-145.

Baker, E.T. and German, C.R., 2004. On the global distribution of hydrothermal vent fields. In: C.R. German, J. Lin and L.M. Parson (Editors), Mid-Ocean Ridges: Hydrothermal Interactions between the Lithosphere and Oceans. Geophysical Monograph Series. American Geophysical Union, Washington, D.C., pp. 245-266.

Balci, N., Bullen, T.D., Witte-Lien, K., Shanks, W.C., Motelica, M. and Mandernack, K.W., 2006. Iron isotope fractionation during microbially stimulated Fe(II) oxidation and Fe(III) precipitation. Geochimica Et Cosmochimica Acta, 70(3): 622-639.

Ballard, R.D. and Grassle, J.F., 1979. Return to Oases of the Deep. National Geographic, 156(5): 684-703.

Bau, M. and Dulski, P., 1999. Comparing yttrium and rare earths in hydrothermal fluids from the Mid-Atlantic Ridge: implications for Y and REE behaviour during near-vent mixing and for the Y/Ho ratio of Proterozoic seawater. Chemical Geology, 155(1-2): 77-90.

Beard, B.L. and Johnson, C.M., 2004. Fe Isotope Variations in the Modern and Ancient Earth and Other Planetary Bodies. Reviews in Mineralogy and Geochemistry, 55: 319-357.

Beard, B.L., Johnson, C.M., Skulan, J.L., Nealson, K.H., Cox, L. and Sun, H., 2003a. Application of Fe isotopes to tracing the geochemical and biological cycling of Fe. Chemical Geology, 195(1-4): 87-117.

Beard, B.L., Johnson, C.M., Von Damm, K.L. and Poulson, R.L., 2003b. Iron isotope constraints on Fe cycling and mass balance in oxygenated Earth oceans. Geology, 31(7): 629-632.

Bender, M., Broecker, W., Biscaye, P., Sun, S., Gornitz, V., Middel, U. and Kay, R., 1971. Geochemistry of Three Cores from East Pacific Rise. Earth and Planetary Science Letters, 12(4): 425-433.

Bergquist, B.A. and Boyle, E.A., 2006. Dissolved iron in the tropical and subtropical Atlantic Ocean. Global Biogeochemical Cycles, 20(1): GB1015 MAR 18 2006.

Bostrom, K., Peterson, M.N.A., Joensuu, O. and Fisher, D.E., 1969. Aluminium-poor ferromanganoan sediments on active oceanic ridges. Journal of Geophysical Research, 74(12): 3261-3270.

Boyd, P.W., Watson, A.J., Law, C.S., Abraham, E.R., Trull, T., Murdoch, R., Bakker, D.C.E., Bowie, A.R., Buesseler, K.O., Chang, H., Charette, M., Croot, P., Downing, K., Frew, R., Gall, M., Hadfield, M., Hall, J., Harvey, M., Jameson, G., LaRoche, J., Liddicoat, M., Ling, R., Maldonado, M.T., McKay, R.M., Nodder, S., Pickmere, S., Pridmore, R., Rintoul, S., Safi, K., Sutton, P., Strzepek, R., Tanneberger, K., Turner, S., Waite, A. and Zeldis, J., 2000. A mesoscale phytoplankton bloom in the polar Southern Ocean stimulated by iron fertilization. Nature, 407(6805): 695-702.

Boye, M., Aldrich, A.P., Van den Berg, C.M.G., De Jong, J.T.M., Veldhuis, M.J.W. and De Baar, H.J.W., 2003. Horizontal gradient of the chemical speciation of iron in surface waters of the northeast Atlantic Ocean. Marine Chemistry, 80(2-3): 129-143.

Boye, M., Nishioka, J., Croot, P.L., Laan, P., Timmermans, K.R. and de Baar, H.J.W., 2005. Major deviations of iron complexation during 22 days of a mesoscale iron enrichment in the open Southern Ocean. Marine Chemistry, 96(3-4): 257-271.

Boye, M., Van den Berg, C.M.G., de Jong, J.T.M., Leach, H., Croot, P. and de Baar, H.J.W., 2001. Organic complexation of iron in the Southern Ocean. Deep-Sea Research Part I-Oceanographic Research Papers, 48(6): 1477-1497.

Boyle, E.A., Bergquist, B.A., Kayser, R.A. and Mahowald, N., 2005. Iron, manganese, and lead at Hawaii Ocean Time-series station ALOHA: Temporal variability and an intermediate water hydrothermal plume. Geochimica Et Cosmochimica Acta, 69(21): 5165-5166.

Boyle, E.A., Edmond, J.M. and Sholkovitz, E.R., 1977. Mechanism of Iron Removal in Estuaries. Geochimica Et Cosmochimica Acta, 41(9): 1313-1324.

Brantley, S.L., Liermann, L. and Bullen, T.D., 2001. Fractionation of Fe isotopes by soil microbes and organic acids. Geology, 29(6): 535-538.

Brantley, S.L., Liermann, L.J., Guynn, R.L., Anbar, A., Icopini, G.A. and Barling, J., 2004. Fe isotopic fractionation during mineral dissolution with and without bacteria. Geochimica Et Cosmochimica Acta, 68(15): 3189-3204.

Bruland, K.W., Franks, R.P., Knauer, G.A. and Martin, J.H., 1979. Sampling and Analytical Methods for the Determination of Copper, Cadmium, Zinc, and Nickel at the Nanogram Per Liter Level in Sea-Water. Analytica Chimica Acta, 105(1): 233-245.

Bruland, K.W. and Lohan, M.C., 2003. Controls of trace metals in seawater. In: H. Elderfield (Editor), The oceans and marine geochemistry. Treatise on Geochemistry. Elsevier, Oxford, pp. 23 - 47.

Bruland, K.W., Orians, K.J. and Cowen, J.P., 1994. Reactive Trace-Metals in the Stratified Central North Pacific. Geochimica Et Cosmochimica Acta, 58(15): 3171-3182.

Buck, C.S., Landing, W.M., Resing, J.A. and Lebon, G.T., 2006. Aerosol iron and aluminum solubility in the northwest Pacific Ocean: Results from the 2002 IOC cruise. Geochemistry Geophysics Geosystems, 7: Q04M07 APR 13 2006.

Bullen, T.D., White, A.F., Childs, C.W., Vivit, D.V. and Schulz, M.S., 2001. Demonstration of significant abiotic iron isotope fractionation in nature. Geology, 29(8): 699-702.

Burd, B.J., Thomson, R.E. and Jamieson, G.S., 1992. Composition of a Deep Scattering Layer Overlying a Mid-ocean Ridge Hydrothermal Plume. Marine Biology, 113(3): 517-526.

Butler, I.B., Archer, C., Vance, D., Oldroyd, A. and Rickard, D., 2005. Fe isotope fractionation on FeS formation in ambient aqueous solution. Earth and Planetary Science Letters, 236(1-2): 430-442.

Carlson, C.A. and Ducklow, H.W., 1995. Dissolved Organic-Carbon in the Upper Ocean of the Central Equatorial Pacific-Ocean, 1992 - Daily and Finescale Vertical Variations. Deep-Sea Research Part II-Topical Studies in Oceanography, 42(2-3): 639-656.

Cave, R.R., German, C.R., Thomson, J. and Nesbitt, R.W., 2002. Fluxes to sediments underlying the Rainbow hydrothermal plume at 36 degrees 14 ' N on the Mid-Atlantic Ridge. Geochimica Et Cosmochimica Acta, 66(11): 1905-1923.

Charlou, J.L., Fouquet, Y., Bougault, H., Donval, J.P., Etoubleau, J., Jean-Baptiste, P., Dapoigny, A., Appriou, P. and Rona, P.A., 1998. Intense CH4 plumes generated by serpentinization of ultramafic rocks at the intersection of the 15 degrees 20 ' N fracture zone and the Mid-Atlantic Ridge. Geochimica Et Cosmochimica Acta, 62(13): 2323-2333.

Chin, C.S., Coale, K.H., Elrod, V.A., Johnson, K.S., Massoth, G.J. and Baker, E.T., 1994. In-Situ Observations of Dissolved Iron and Manganese in Hydrothermal Vent Plumes, Juan-De-Fuca Ridge. Journal of Geophysical Research-Solid Earth, 99(B3): 4969-4984.

Chu, N.C., Johnson, C.M., Beard, B.L., German, C.R., Nesbitt, R.W., Frank, M., Bohn, M., Kubik, P.W., Usui, A. and Graham, I., 2006. Evidence for hydrothermal venting in Fe isotope compositions of the deep Pacific Ocean through time. Earth and Planetary Science Letters, 245(1-2): 202-217.

Clarke, W.B., Beg, M.A. and Craig, H., 1970. Excess He-3 in East Pacific. Journal of Geophysical Research, 75: 7676 - 7678.

Coale, K.H., Chin, C.S., Massoth, G.J., Johnson, K.S. and Baker, E.T., 1991. In-situ Chemical Mapping of Dissolved Iron and Manganese in Hydrothermal Plumes. Nature, 352(6333): 325-328.

Coale, K.H., Johnson, K.S., Chavez, F.P., Buesseler, K.O., Barber, R.T., Brzezinski, M.A., Cochlan, W.P., Millero, F.J., Falkowski, P.G., Bauer, J.E., Wanninkhof, R.H., Kudela, R.M., Altabet, M.A., Hales, B.E., Takahashi, T., Landry, M.R., Bidigare, R.R., Wang, X.J., Chase, Z., Strutton, P.G., Friederich, G.E., Gorbunov, M.Y., Lance, V.P., Hilting, A.K., Hiscock, M.R., Demarest, M., Hiscock, W.T., Sullivan, K.F., Tanner, S.J., Gordon, R.M., Hunter, C.N., Elrod, V.A., Fitzwater, S.E., Jones, J.L., Tozzi, S., Koblizek, M., Roberts, A.E., Herndon, J., Brewster, J., Ladizinsky, N., Smith, G., Cooper, D., Timothy, D., Brown, S.L., Selph, K.E., Sheridan, C.C., Twining, B.S. and Johnson, Z.I., 2004. Southern ocean iron enrichment experiment: Carbon cycling in high- and low-Si waters. Science, 304(5669): 408-414.

Comita, P.B., Gagosian, R.B. and Williams, P.M., 1984. Suspended Particulate Organic Material from Hydrothermal Vent Waters at 21-Degrees-N. Nature, 307(5950): 450-453.

Corliss, J.B., Dymond, J., Gordon, L.I., Edmond, J.M., Herzen, R.P.V., Ballard, R.D., Green, K., Williams, D., Bainbridge, A., Crane, K. and Vanandel, T.H., 1979. Submarine Thermal Springs on the Galapagos Rift. Science, 203(4385): 1073-1083.

Cowen, J.P., Bertram, M.A., Baker, E.T., Feely, R.A., Massoth, G.J. and Summit, M., 1998. Geomicrobial transformation of manganese in Gorda Ridge event plumes. Deep-Sea Research Part II-Topical Studies in Oceanography, 45(12): 2713-2737.

Cowen, J.P., Bertram, M.A., Wakeham, S.G., Thomson, R.E., Lavelle, J.W., Baker, E.T. and Feely, R.A., 2001. Ascending and descending particle flux from hydrothermal plumes at Endeavour Segment, Juan de Fuca Ridge. Deep-Sea Research Part I-Oceanographic Research Papers, 48(4): 1093-1120.

Cowen, J.P. and Bruland, K.W., 1985. Metal Deposits Associated with Bacteria - Implications for Fe and Mn Marine Biogeochemistry. Deep-Sea Research Part A-Oceanographic Research Papers, 32(3): 253-272.

Cowen, J.P., Fornari, D.J., Shank, T.M., Love, B., Glazer, B., Treusch, A., Holmes, R.C., Soule, S.A., Baker, E.T., Tolstoy, M. and Pomranin, K.R., 2007. Volcanic Eruptions at East Pacific Rise Near 9 degrees 50'N. EOS, Transactions, American Geophysical Union, 8(07): 81, 83.

Cowen, J.P. and German, C.R., 2003. Biogeochemical cycling in hydrothermal plumes. In: P.E. Halbach, Tunnicliffe, V., Hein, J.R. (Editor), Energy and Mass Transfer in Marine Hydrothermal Systems. Dahlem University Press, Berlin.

Cowen, J.P. and Li, Y.H., 1991. The Influence of a Changing Bacterial Community on Trace-Metal Scavenging in a Deep-Sea Particle Plume. Journal of Marine Research, 49(3): 517-542.

Cowen, J.P., Massoth, G.J. and Baker, E.T., 1986. Bacterial Scavenging of Mn and Fe in a Mid-Field to Far-Field Hydrothermal Particle Plume. Nature, 322(6075): 169-171.

Cowen, J.P. and Silver, M.W., 1984. The Association of Iron and Manganese with Bacteria on Marine Macroparticulate Material. Science, 224(4655): 1340-1342.

Croal, L.R., Johnson, C.M., Beard, B.L. and Newman, D.K., 2004. Iron isotope fractionation by Fe(II)-oxidizing photoautotrophic bacteria. Geochimica Et Cosmochimica Acta, 68(6): 1227-1242.

Croot, P.L. and Johansson, M., 2000. Determination of iron speciation by cathodic stripping voltammetry in seawater using the competing ligand 2-(2- thiazolylazo)-p-cresol (TAC). Electroanalysis, 12(8): 565-576.

Cruse, A.M. and Seewald, J.S., 2006. Geochemistry of low-molecular weight hydrocarbons in hydrothermal fluids from Middle Valley, northern Juan de Fuca Ridge. Geochimica Et Cosmochimica Acta, 70(8): 2073-2092.

Cullen, J.T., Bergquist, B.A. and Moffett, J.W., 2006. Thermodynamic characterization of the partitioning of iron between soluble and colloidal species in the Atlantic Ocean. Marine Chemistry, 98(2-4): 295-303.

Dauphas, N. and Rouxel, O., 2006. Mass spectrometry and natural variations of iron isotopes. Mass Spectrometry Reviews, 25(5): 831-832.

de Baar, H.J.W. and de Jong, J.T.M., 2001. Distributions, Sources and Sinks of Iron in Seawater. In: D.R. Turner and K.A. Hunter (Editors), The Biogeochemistry of Iron in Seawater. John Wiley & Sons Ltd, Chichester, pp. 123 - 253.

de Baar, H.J.W., German, C.R., Elderfield, H. and Vangaans, P., 1988. Rare-Earth Element Distributions in Anoxic Waters of the Cariaco Trench. Geochimica Et Cosmochimica Acta, 52(5): 1203-1219.

Decho, A.W., 1990. Microbial Exopolymer Secretions in Ocean Environments - Their Role(s) in Food Webs and Marine Processes. Oceanography and Marine Biology, 28: 73-153.

Degens, E.T. and Ross, D.A., 1969. Hot Brines and Heavy Metal Deposits in the Red Sea, A Geochemical and Geophysical Account. Springer, New York.

DeMets, C., Gordon, R.G., Argus, D.F. and Stein, S., 1990. Current Plate Motions. Geophysical Journal International, 101(2): 425-478.

Devey, C., 2006. Mantle to ocean on the southern Mid-Atlantic Ridge (5 - 10 degrees S) - Cruise report, IFM-GEOMAR.

Dick, G.J., Lee, Y.E. and Tebo, B.M., 2006. Manganese(II)-oxidizing bacillus spores in Guaymas Basin hydrothermal sediments and plumes. Applied and Environmental Microbiology, 72(5): 3184-3190.

Donat, J.R. and Bruland, K.W., 1988. Direct Determination of Dissolved Cobalt and Nickel in Seawater by Differential Pulse Cathodic Stripping Voltammetry Preceded by Adsorptive Collection of Cyclohexane-1,2-Dione Dioxime Complexes. Analytical Chemistry, 60(3): 240-244.

Douville, E., Bienvenu, P., Charlou, J.L., Donval, J.P., Fouquet, Y., Appriou, P. and Gamo, T., 1999. Yttrium and rare earth elements in fluids from various deep-sea hydrothermal systems. Geochimica Et Cosmochimica Acta, 63(5): 627-643.

Duce, R.A. and Tindale, N.W., 1991. Atmospheric Transport of Iron and Its Deposition in the Ocean. Limnology and Oceanography, 36(8): 1715-1726.

Edmond, J.M., Measures, C., McDuff, R.E., Chan, L.H., Collier, R., Grant, B., Gordon, L.I. and Corliss, J.B., 1979. Ridge crest hydrothermal activity and the balances of the major and minor elements in the ocean: the Galapagos data. Earth and Planetary Science Letters, 46(1): 1-18.

Edmonds, H.N. and German, C.R., 2004. Particle geochemistry in the Rainbow hydrothermal plume, Mid-Atlantic Ridge. Geochimica Et Cosmochimica Acta, 68(4): 759-772.

Edmonds, H.N., Michael, P.J., Baker, E.T., Connelly, D.P., Snow, J.E., Langmuir, C.H., Dick, H.J.B., Muhe, R., German, C.R. and Graham, D.W., 2003. Discovery of abundant hydrothermal venting on the ultraslow-spreading Gakkel ridge in the Arctic. Nature, 421(6920): 252-256.

Edwards, K.J., Rogers, D.R., Wirsen, C.O. and McCollom, T.M., 2003. Isolation and characterization of novel psychrophilic, neutrophilic, Fe-oxidizing, chemolithoautotrophic alpha- and, gamma-Proteobacteria from the deep-sea. Applied and Environmental Microbiology, 69(5): 2906-2913.

Elderfield, H., 1988. The Oceanic Chemistry of the Rare-Earth Elements. Philosophical Transactions of the Royal Society of London Series a-Mathematical Physical and Engineering Sciences, 325(1583): 105-126.

Elderfield, H. and Greaves, M.J., 1982. The Rare-Earth Elements in Sea-Water. Nature, 296(5854): 214-219.

Elderfield, H. and Schultz, A., 1996. Mid-ocean ridge hydrothermal fluxes and the chemical composition of the ocean. Annual Review of Earth and Planetary Sciences, 24: 191-224.

Elrod, V.A., Berelson, W.M., Coale, K.H. and Johnson, K.S., 2004. The flux of iron from continental shelf sediments: A missing source for global budgets. Geophysical Research Letters, 31(12): L12307.

Faure, G., 1986. Principles of isotope geology. John Wiley & Sons, Inc., New York.

Feely, R.A., Gammon, R.H., Taft, B.A., Pullen, P.E., Waterman, L.S., Conway, T.J., Gendron, J.F. and Wisegarver, D.P., 1987a. Distribution of Chemical Tracers in the

Eastern Equatorial Pacific During and after the 1982-1983 El Nino Southern Oscillation Event. Journal of Geophysical Research-Oceans, 92(C6): 6545-6558.

Feely, R.A., Lewison, M., Massoth, G.J., Robertbaldo, G., Lavelle, J.W., Byrne, R.H., Von Damm, K.L. and Curl, H.C., 1987b. Composition and Dissolution of Black Smoker Particulates from Active Vents on the Juan-De-Fuca Ridge. Journal of Geophysical Research-Solid Earth and Planets, 92(B11): 11347-11363.

Feely, R.A., Trefry, J.H., Lebon, G.T. and German, C.R., 1998. The relationship between P/Fe and V/Fe ratios in hydrothermal precipitates and dissolved phosphate in seawater. Geophysical Research Letters, 25(13): 2253-2256.

Feely, R.A., Trefry, J.H., Massoth, G.J. and Metz, S., 1991. A comparison of the scavenging of phosphorus and arsenic from seawater by hydrothermal iron oxyhydroxides in the Atlantic and Pacific Oceans. Deep-Sea Research Part A-Oceanographic Research Papers, 38(6A): 617-623.

Field, M.P. and Sherrell, R.M., 2000. Dissolved and particulate Fe in a hydrothermal plume at 9 degrees 45 ' N, East Pacific Rise: Slow Fe (II) oxidation kinetics in Pacific plumes. Geochimica Et Cosmochimica Acta, 64(4): 619-628.

Fornari, D.J., Tivey, M.K., Schouten, H., Perfit, M.R., Yoerger, D.R., Bradley, A.M., Edwards, M.H., Haymon, R., Scheirer, D., Von Damm, K.L., Shank, T.M. and Soule, S.A., 2004. A Submarine Lava Flow emplacement at the East Pacific Rise 9 degrees 50' N: Implications for Uppermost Ocean Crust Stratigraphy and Hydrothermal Fluid Circulation. In: C.R. German, J. Lin and L.M. Parson (Editors), Mid-Ocean Ridges: Hydrothermal Interactions between the Lithosphere and Ocean. AGU Monograph. Am. Geophys. Union, Washington DC.

Foustoukos, D.I. and Seyfried, W.E., 2004. Hydrocarbons in hydrothermal vent fluids: The role of chromium-bearing catalysts. Science, 304(5673): 1002-1005.

Froelich, P.N., Klinkhammer, G.P., Bender, M.L., Luedtke, N.A., Heath, G.R., Cullen, D., Dauphin, P., Hammond, D., Hartman, B. and Maynard, V., 1979. Early Oxidation of Organic-Matter in Pelagic Sediments of the Eastern Equatorial Atlantic - Suboxic Diagenesis. Geochimica Et Cosmochimica Acta, 43(7): 1075-1090.

German, C.R., Baker, E.T., Mevel, C. and Tamaki, K., 1998. Hydrothermal activity along the southwest Indian ridge. Nature, 395(6701): 490-493.

German, C.R., Bennett, S.A., Connelly, D.P., Evans, A.J., Murton, B.J., Parson, L.M., Prien, R.D., Ramirez-Llodra, E.Z., Jakuba, M., Shank, T.M., Yoerger, D.R., Walker, S.L., Baker, E.T. and Nakamura, K., 2008a. Hydrothermal activity on the southern Mid-Atlantic Ridge: Tectonically and volcanically controlled venting at 4-5 degrees S. Earth and Planetary Science Letters, In Press.

German, C.R., Campbell, A.C. and Edmond, J.M., 1991. Hydrothermal scavenging at the Mid-Atlantic Ridge: Modification of trace element dissolved fluxes. Earth and Planetary Science Letters, 107(1): 101-114.

German, C.R., Colley, S., Palmer, M.R., Khripounoff, A. and Klinkhammer, G.P., 2002. Hydrothermal plume-particle fluxes at 13 degrees N on the East Pacific Rise. Deep-Sea Research Part I-Oceanographic Research Papers, 49(11): 1921-1940.

German, C.R., Klinkhammer, G.P., Edmond, J.M., Mitra, A. and Elderfield, H., 1990. Hydrothermal Scavenging of Rare-Earth Elements in the Ocean. Nature, 345(6275): 516-518.

German, C.R., Klinkhammer, G.P. and Rudnicki, M.D., 1996. The Rainbow hydrothermal plume, 36 degrees 15'N, MAR. Geophysical Research Letters, 23(21): 2979-2982.

German, C.R., Masuzawa, T., Greaves, M.J., Elderfield, H. and Edmond, J.M., 1995. Dissolved Rare-Earth Elements in the Southern-Ocean - Cerium Oxidation and the Influence of Hydrography. Geochimica Et Cosmochimica Acta, 59(8): 1551-1558.

German, C.R., Parson, L.M., Murton, B.J., Bennett, S.A., Connelly, D.P., Evans, A.J., Prien, R.D., Ramirez-Llodra, E.Z., Shank, T.M., Yoerger, D.R., Jakuba, M., Bradley, A.M., Baker, E.T. and Nakamura, K., 2005. Hydrothermal Activity on the Southern Mid-Atlantic Ridge: Tectonically- and Volcanically-Hosted High Temperature Venting at 2-7 Degrees S. EOS, Transactions, American Geophysical Union, 86(52): Fall Meet, Suppl., Abstract OS34A-05.

German, C.R., Thurnherr, A.M., Radford-Knoery, J., Charlou, J.L., Jean-Baptiste, P. and Edmonds, H.N., 2008b. Export heat and chemical fluxes from submarine venting to the oceans: the Rainbow hydrothermal field Mid-Atlantic Ridge. Nature Geoscience, In Review.

German, C.R. and Von Damm, K.L., 2004. Hydrothermal Processes. In: H. Elderfield (Editor), The oceans and marine geochemistry. Treatise on Geochemistry. Elsevier-Pergamon, Oxford.

German, C.R., Yoerger, D.R., Jakuba, M., Shank, T.M., Langmuir, C.H. and Nakamura, K., 2008c. Hydrothermal exploration with the Autonomous Benthic Explorer. Deep-Sea Research Part I-Oceanographic Research Papers, 55(2): 203-219.

Gerringa, L.J.A., Herman, P.M.J. and Poortvliet, T.C.W., 1995. Comparison of the linear Van den Berg/Ruzic transformation and a non-linear fit of the Langmuir isotherm applied to Cu speciation data in the estuarine environment. Marine Chemistry, 48(2): 131-142.

Gledhill, M. and Van den Berg, C.M.G., 1994. Determination of Complexation of Iron(III) with Natural Organic Complexing Ligands in Seawater Using Cathodic Stripping Voltammetry. Marine Chemistry, 47(1): 41-54.

Gledhill, M. and Van den Berg, C.M.G., 1995. Measurement of the redox speciation of iron in seawater by catalytic cathodic stripping voltammetry. Marine Chemistry, 50(1-4): 51-61.

Goldberg, E.D., Koide, M., Schmidt, R.A. and Smith, R.H., 1963. Rare earth distributions in the marine enivironment. Journal of Geophysical Research, 68: 4209 - 4217.

Gordon, R.M., Johnson, K.S. and Coale, K.H., 1998. The behaviour of iron and other trace elements during the IronEx-I and PlumEx experiments in the Equatorial Pacific. Deep Sea Research Part II: Topical Studies in Oceanography, 45(6): 995-1041.

Gordon, R.M., Martin, J.H. and Knauer, G.A., 1982. Iron in Northeast Pacific Waters. Nature, 299(5884): 611-612.

Govindaraju, K., 1994. Compilation of working values and sample description for 383 geostandards. Geostandards Newsletter, 18(Special issue): 1-158.

Haase, K.M., Petersen, S., Koschinsky, A., Seifert, R., Devey, C.W., Keir, R., Lackschewitz, K.S., Melchert, B., Perner, M., Schmale, O., Suling, J., Dubilier, N., Zielinski, F., Fretzdorff, S., Garbe-Schonberg, D., Westernstroer, U., German, C.R., Shank, T.M., Yoerger, D., Giere, O., Kuever, J., Marbler, H., Mawick, J., Mertens, C., Stober, U., Ostertag-Henning, C., Paulick, H., Peters, M., Strauss, H., Sander, S., Stecher, J., Warmuth, M. and Weber, S., 2007. Young volcanism and related hydrothermal activity at 5 degrees S on the slow-spreading southern Mid-Atlantic Ridge. Geochemistry Geophysics Geosystems, 8: Q11002 NOV 13 2007.

Haymon, R.M., Fornari, D.J., Edwards, M.H., Carbotte, S., Wright, D. and Macdonald, K.C., 1991. Hydrothermal Vent Distribution Along the East Pacific Rise Crest (9-Degrees-09'-54'N) and Its Relationship to Magmatic and Tectonic Processes on Fast-Spreading Mid-ocean Ridges. Earth and Planetary Science Letters, 104(2-4): 513-534.

Haymon, R.M., Fornari, D.J., Vondamm, K.L., Lilley, M.D., Perfit, M.R., Edmond, J.M., Shanks, W.C., Lutz, R.A., Grebmeier, J.M., Carbotte, S., Wright, D., McLaughlin, E., Smith, M., Beedle, N. and Olson, E., 1993. Volcanic-Eruption of the Mid-ocean Ridge Along the East Pacific Rise Crest at 9-Degrees-45-52'N - Direct Submersible Observations of Sea-Floor Phenomena Associated with an Eruption Event in April, 1991. Earth and Planetary Science Letters, 119(1-2): 85-101.

Hersman, L., Maurice, P. and Sposito, G., 1996. Iron acquisition from hydrous Fe(III)-oxides by an aerobic Pseudomonas sp. Chemical Geology, 132(1-4): 25-31.

Hilton, J., Lishman, J.P., Mackness, S. and Heaney, S.I., 1986. An Automated-Method for the Analysis of Particulate Carbon and Nitrogen in Natural-Waters. Hydrobiologia, 141(3): 269-271.

Holm, N.G. and Charlou, J.L., 2001. Initial indications of abiotic formation of hydrocarbons in the Rainbow ultramafic hydrothermal system, Mid-Atlantic Ridge. Earth and Planetary Science Letters, 191(1-2): 1-8.

Hopkinson, B.M. and Barbeau, K.A., 2007. Organic and redox speciation of iron in the eastern tropical North Pacific suboxic zone. Marine Chemistry, 106(1-2): 2-17.

Hudson, R.J.M., Covault, D.T. and Morel, F.M.M., 1992. Investigations of Iron Coordination and Redox Reactions in Seawater Using Fe-59 Radiometry and Ion-Pair Solvent-Extraction of Amphiphilic Iron Complexes. Marine Chemistry, 38(3-4): 209-235.

Hunter, K.A., 2005. Comment on 'Measuring Marine Iron(III) Complexes by CLE-AdSV'. Environmental Chemistry, 2(2): 85-87.

James, R.H. and Elderfield, H., 1996a. Chemistry of ore-forming fluids and mineral formation rates in an active hydrothermal sulfide deposit on the Mid-Atlantic Ridge. Geology, 24(12): 1147-1150.

James, R.H. and Elderfield, H., 1996b. Dissolved and particulate trace metals in hydrothermal plumes at the Mid-Atlantic Ridge. Geophysical Research Letters, 23(23): 3499-3502.

Jenkins, W.J., Edmond, J.M. and Corliss, J.B., 1978. Excess He-3 and He-4 in Galapagos Submarine Hydrothermal Waters. Nature, 272(5649): 156-158.

Jenkins, W.J., Rona, P.A. and Edmond, J.M., 1980. Excess He-3 in the Deep-Water over the Mid-Atlantic Ridge at 26-Degrees-N - Evidence of Hydrothermal Activity. Earth and Planetary Science Letters, 49(1): 39-44.

Jickells, T.D., 1999. The inputs of dust derived elements to the Sargasso Sea; a synthesis. Marine Chemistry, 68(1-2): 5-14.

Jickells, T.D., An, Z.S., Andersen, K.K., Baker, A.R., Bergametti, G., Brooks, N., Cao, J.J., Boyd, P.W., Duce, R.A., Hunter, K.A., Kawahata, H., Kubilay, N., LaRoche, J., Liss, P.S., Mahowald, N., Prospero, J.M., Ridgwell, A.J., Tegen, I. and Torres, R., 2005. Global Iron Connections Between Desert Dust, Ocean Biogeochemistry, and Climate. Science, 308(5718): 67-71.

Jickells, T.D. and Spokes, L.J., 2001. Atmospheric Iron Inputs to the Oceans. In: D.R. Turner and K.A. Hunter (Editors), The Biogeochemistry of Iron in Seawater. John Willey & Sons Ltd, Chichester, pp. 85 - 121.

Kadko, D.C., Rosenberg, N.D., Lupton, J.E., Collier, R.W. and Lilley, M.D., 1990. Chemical-Reaction Rates and Entrainment within the Endeavor Ridge Hydrothermal Plume. Earth and Planetary Science Letters, 99(4): 315-335.

Karl, D.M., Taylor, G.T., Novitsky, J.A., Jannasch, H.W., Wirsen, C.O., Pace, N.R., Lane, D.J., Olsen, G.J. and Giovannoni, S.J., 1988. A Microbiological Study of Guaymas Basin High-Temperature Hydrothermal Vents. Deep-Sea Research Part A-Oceanographic Research Papers, 35(5): 777-791.

King, D.W., Aldrich, R.A. and Charnecki, S.E., 1993. Photochemical Redox Cycling of Iron in NaCl Solutions. Marine Chemistry, 44(2-4): 105-120.

Klinkhammer, G.P., Elderfield, H., Edmond, J.M. and Mitra, A., 1994. Geochemical Implications of Rare-Earth Element Patterns in Hydrothermal Fluids from Mid-ocean Ridges. Geochimica Et Cosmochimica Acta, 58(23): 5105-5113.

Koschinsky, A., Billings, A., Devey, C., Dubilier, N., Duester, A., Edge, D., Garbe-Schönberg, D., German, C.R., Giere, O., Keir, R., Lackschewitz, K., Mai, H., Marbler, H., Mawick, J., Melchert, B., Mertens, C., Peters, M., Sander, S., Schmale, O., Schmidt, W., Seifert, R., Seiter, C., Stöber, U., Suck, I., Walter, M., Weber, S., Yoerger, D.R., Zarrouk, M. and Zielinski, F., 2006a. Discovery of new hydrothermal vents on the Southern Mid-Atlantic Ridge (4°S-10°S) during cruise M68/1. InterRidge News, 15: 9-15.

Koschinsky, A., Devey, C., Garbe-Schonberg, D., German, C.R., Yoerger, D.R. and Shank, T.M., 2006b. Hydrothermal Exploration of the Mid-Atlantic Ridge, 5-10°S, using the AUV ABE and the ROV Quest – a brief overview of RV Meteor Cruise M68/1. EOS, Transactions, American Geophysical Union, 87(52): Fall Meet, Suppl., Abstract OS34A-05.

Lalou, C., Thompson, G., Arnold, M., Brichet, E., Druffel, E. and Rona, P.A., 1990. Geochronology of TAG and Snakepit Hydrothermal Fields, Mid-Atlantic Ridge - Witness to a Long and Complex Hydrothermal History. Earth and Planetary Science Letters, 97(1-2): 113-128.

Lam, P.J. and Bishop, J.K.B., 2008. The continental margin is a key source of iron to the HNLC North Pacific Ocean. Geophysical Research Letters, 35(7): L07608 APR 2008.

Landing, W.M. and Bruland, K.W., 1987. The Contrasting Biogeochemistry of Iron and Manganese in the Pacific-Ocean. Geochimica Et Cosmochimica Acta, 51(1): 29-43.

Lang, S.Q., Butterfield, D.A., Lilley, M.D., Johnson, H.P. and Hedges, J.I., 2006. Dissolved organic carbon in ridge-axis and ridge-flank hydrothermal systems. Geochimica Et Cosmochimica Acta, 70(15): 3830-3842.

Lavelle, J.W., Cowen, J.P. and Massoth, G.J., 1992. A model for the deposition of hydrothermal manganese near ridge crests. J. Geophys. Res, 97(C5): 7413-7427.

Lavelle, J.W. and Wetzler, M.A., 1999. Diffuse venting and background contributions to chemical anomalies in a neutrally buoyant ocean hydrothermal plume. Journal of Geophysical Research-Oceans, 104(C2): 3201-3209.

Levasseur, S., Frank, M., Hein, J.R. and Halliday, A., 2004. The global variation in the iron isotope composition of marine hydrogenetic ferromanganese deposits:

implications for seawater chemistry? Earth and Planetary Science Letters, 224(1-2): 91-105.

Libes, S.M., 1992. An Introduction to Marine Biogeochemistry. John Wiley & Sons, Inc.

Little, C.T.S., Glynn, S.E.J. and Mills, R.A., 2004. Four-hundred-and-ninety-million-year record of bacteriogenic iron oxide precipitation at sea-floor hydrothermal vents. Geomicrobiology Journal, 21(6): 415-429.

Liu, X. and Millero, F.J., 1999. The solubility of iron hydroxide in sodium chloride solutions. Geochimica et Cosmochimica Acta, 63(19-20): 3487-3497.

Liu, X. and Millero, F.J., 2002. The solubility of iron in seawater. Marine Chemistry, 77(1): 43-54.

Lunel, T., Rudnicki, M., Elderfield, H. and Hydes, D., 1990. Aluminum as a Depth-Sensitive Tracer of Entrainment in Submarine Hydrothermal Plumes. Nature, 344(6262): 137-139.

Lupton, J.E., 1995. Hydrothermal plumes: Near and far field. In: S.E. Humphris, R.A. Zierenberg, L.S. Mullineaux and R.E. Thomson (Editors), In Seafloor Hydrothermal Systems: Physical, Chemical, Biological, and Geological Interactions. Geophysical Monograph 91. American Geophysical Union, Washington, D.C., pp. 317-346.

Lupton, J.E., Baker, E.T., Massoth, G.J., Thomson, R.E., Burd, B.J., Butterfield, D.A., Embley, R.W. and Cannon, G.A., 1995. Variations in Water-Column He-3/Heat Ratios Associated with the 1993 Coaxial Event, Juan-De-Fuca Ridge. Geophysical Research Letters, 22(2): 155-158.

Lupton, J.E. and Craig, H., 1981. A Major He-3 Source at 15-Degrees-S on the East Pacific Rise. Science, 214(4516): 13-18.

Lupton, J.E., Delaney, J.R., Johnson, H.P. and Tivey, M.K., 1985. Entrainment and Vertical Transport of Deep-Ocean Water by Buoyant Hydrothermal Plumes. Nature, 316(6029): 621-623.

Lupton, J.E., Pyle, D.G., Jenkins, W.J., Greene, R. and Evans, L., 2004. Evidence for an extensive hydrothermal plume in the Tonga-Fiji region of the South Pacific. Geochemistry Geophysics Geosystems, 5: Q01003 JAN 2004.

Malinovsky, D., Stenberg, A., Rodushkin, I., Andren, H., Ingri, J., Ohlander, B. and Baxter, D.C., 2003. Performance of high resolution MC-ICP-MS for Fe isotope ratio measurements in sedimentary geological materials. Journal of Analytical Atomic Spectrometry, 18(7): 687-695.

Martin, J.H., Coale, K.H., Johnson, K.S., Fitzwater, S.E., Gordon, R.M., Tanner, S.J., Hunter, C.N., Elrod, V.A., Nowicki, J.L., Coley, T.L., Barber, R.T., Lindley, S., Watson, A.J., Vanscoy, K., Law, C.S., Liddicoat, M.I., Ling, R., Stanton, T., Stockel, J., Collins, C., Anderson, A., Bidigare, R., Ondrusek, M., Latasa, M., Millero, F.J., Lee, K., Yao, W., Zhang, J.Z., Friederich, G., Sakamoto, C., Chavez, F., Buck, K., Kolber, Z., Greene, R., Falkowski, P., Chisholm, S.W., Hoge, F., Swift, R., Yungel, J., Turner, S., Nightingale, P., Hatton, A., Liss, P. and Tindale, N.W., 1994. Testing the Iron Hypothesis in Ecosystems of the Equatorial Pacific-Ocean. Nature, 371(6493): 123-129.

Martin, J.H. and Gordon, M.R., 1988. Northeast Pacific iron distributions in relation to phytoplankton productivity. Deep Sea Research Part A. Oceanographic Research Papers, 35(2): 177-196.

Martin, J.H., Gordon, R.M. and Fitzwater, S.E., 1990. Iron in Antarctic Waters. Nature, 345(6271): 156-158.

Martin, J.H. and Windom, H.L., 1991. Present and Future Roles of Ocean Margins in Regulating Marine Biogeochemical Cycles of Trace Elements. In: R.F.C. Mantoura, J.H. Martin and R. Wollast (Editors), Ocean Margin Processes in Global Change. John Wiley & Sons Ltd, New York, pp. 45-67.

Massoth, G.J., Baker, E.T., Lupton, J.E., Feely, R.A., Butterfield, D.A., Vondamm, K.L., Roe, K.K. and Lebon, G.T., 1994. Temporal and Spatial Variability of Hydrothermal Manganese and Iron at Cleft Segment, Juan-De-Fuca Ridge. Journal of Geophysical Research-Solid Earth, 99(B3): 4905-4923.

Matthews, A., Zhu, X.-K. and O'Nions, K., 2001. Kinetic iron stable isotope fractionation between iron (-II) and (-III) complexes in solution. Earth and Planetary Science Letters, 192(1): 81-92.

McCollom, T.M. and Seewald, J.S., 2007. Abiotic synthesis of organic compounds in deep-sea hydrothermal environments. Chemical Reviews, 107(2): 382-401.

McCollom, T.M. and Shock, E.L., 1997. Geochemical constraints on chemolithoautotrophic metabolism by microorganisms in seafloor hydrothermal systems. Geochimica et Cosmochimica Acta, 61(20): 4375-4391.

McDuff, R.E., 1995. Physical dynamics of deep sea hydrothermal plumes. In: S.E. Humphris, R.A. Zierenberg, L.S. Mullineaux and R.E. Thomson (Editors), In Seafloor Hydrothermal Systems: Physical, Chemical, Biological, and Geological Interactions. Geophysical Monograph 91. American Geophysical Union, Washington, D.C., pp. 357-368.

Metz, S., Trefry, J.H. and Nelsen, T.A., 1988. History and Geochemistry of a Metalliferous Sediment Core from the Mid-Atlantic Ridge at 26-Degrees-N. Geochimica Et Cosmochimica Acta, 52(10): 2369-2378.

Michard, A., Albarede, F., Michard, G., Minster, J.F. and Charlou, J.L., 1983. Rare-Earth Elements and Uranium in High-Temperature Solutions from East Pacific Rise Hydrothermal Vent Field (13-Degrees-N). Nature, 303(5920): 795-797.

Millero, F.J., 1998. Solubility of Fe(III) in seawater. Earth and Planetary Science Letters, 154(1-4): 323-329.

Millero, F.J., 2006. Chemical Oceanography. CRC Press, Boca Raton.

Millero, F.J., Sotolongo, S. and Izaguirre, M., 1987. The Oxidation-Kinetics of Fe(II) in Seawater. Geochimica Et Cosmochimica Acta, 51(4): 793-801.

Millero, F.J., Yao, W. and Aicher, J., 1995. The speciation of Fe(II) and Fe(III) in natural waters. Marine Chemistry, 50(1-4): 21-39.

Mills, R.A. and Elderfield, H., 1995. Rare-Earth Element Geochemistry of Hydrothermal Deposits from the Active TAG Mound, 26-Degrees-N Mid-Atlantic Ridge. Geochimica Et Cosmochimica Acta, 59(17): 3511-3524.

Mitra, A., Elderfield, H. and Greaves, M.J., 1994. Rare-Earth Elements in Submarine Hydrothermal Fluids and Plumes from the Mid-Atlantic Ridge. Marine Chemistry, 46(3): 217-235.

Moore, R.M., Burton, J.D., Williams, P.J.L. and Young, M.L., 1979. The behaviour of dissolved organic material, iron and manganese in estuarine mixing. Geochimica et Cosmochimica Acta, 43(6): 919-926.

Moran, S.B., Charette, M.A., Pike, S.M. and Wicklund, C.A., 1999. Differences in seawater particulate organic carbon concentration in samples collected using small- and large-volume methods: the importance of DOC adsorption to the filter blank. Marine Chemistry, 67(1-2): 33-42.

Morel, F.M.M., Milligan, A.J. and Saito, M.A., 2004. Marine bioinorganic chemistry: The role of trace metals in the oceanic cycles of major nutrients. In: H. Elderfield (Editor), The oceans and marine geochemistry. Treatise on Geochemistry. Elsevier, Oxford, pp. 113-143.

Mottl, M.J., 2003. In: P.E. Halbach, Tunnicliffe, V., Hein, J.R. (Editor), Dahlem Workshop Report 89, Energy and Mass Transfer in Marine Hydrothermal Systems. Dahlem University Press, Berlin, pp. 365.

Mottl, M.J. and McConachy, T.F., 1990. Chemical Processes in Buoyant Hydrothermal Plumes on the East Pacific Rise near 21-Degrees-N. Geochimica Et Cosmochimica Acta, 54(7): 1911-1927.

Nagai, T., Imai, A., Matsushige, K., Yokoi, K. and Fukushima, T., 2004. Voltammetric determination of dissolved iron and its speciation in freshwater. Limnology, 5(2): 87-94.

Nature, 2006. Robot delves deep to find the hottest water. Nature, 441.

Nielsen, S.G., Rehkamper, M., Teagle, D.A.H., Butterfield, D.A., Alt, J.C. and Halliday, A.N., 2006. Hydrothermal fluid fluxes calculated from the isotopic mass balance of thallium in the ocean crust. Earth and Planetary Science Letters, 251(1-2): 120-133.

Nishioka, J., Takeda, S., Wong, C.S. and Johnson, W.K., 2001. Size-fractionated iron concentrations in the northeast Pacific Ocean: distribution of soluble and small colloidal iron. Marine Chemistry, 74(2-3): 157-179.

Obata, H. and Van den Berg, C.M.G., 2001. Determination of picomolar levels of iron in seawater using catalytic cathodic stripping voltammetry. Analytical Chemistry, 73(11): 2522-2528.

Ortmann, A.C. and Suttle, C.A., 2005. High abundances of viruses in a deep-sea hydrothermal vent system indicates viral mediated microbial mortality. Deep-Sea Research Part I-Oceanographic Research Papers, 52(8): 1515-1527.

Pan, X., Sanders, R., Tappin, A.D., Worsfold, P.J. and Achterberg, E.P., 2005. Simultaneous determination of dissolved organic carbon and total dissolved nitrogen on a coupled high-temperature combustion total organic carbon-nitrogen chemiluminescence detection (HTC TOC-NCD) system. Journal of Automated Methods & Management in Chemistry(4): 240-246.

Pearson, A., Seewald, J.S. and Eglinton, T.I., 2005. Bacterial incorporation of relict carbon in the hydrothermal environment of Guaymas Basin. Geochimica Et Cosmochimica Acta, 69(23): 5477-5486.

Pollard, R.T., Sanders, R., Lucas, M.I. and Statham, P., 2007. The Crozet Natural Iron Bloom and EXport Experiment (CROZEX). Deep Sea Research Part II: Topical Studies in Oceanography, 54(18-20): 1905-1914.

Polyakov, V.B., Clayton, R.N., Horita, J. and Mineev, S.D., 2007. Equilibrium iron isotope fractionation factors of minerals: Re-evaluation from the data of nuclear inelastic resonant X-ray scattering and Mossbauer spectroscopy. Geochimica Et Cosmochimica Acta, 71(15): 3833-3846.

Prieto, L. and Cowen, J.P., 2007. Transparent exopolymer particles in a deep-sea hydrothermal system: Guaymas Basin, Gulf of California. Marine Biology, 150(6): 1093-1101.

Reid, R.T., Live, D.H., Faulkner, D.J. and Butler, A., 1993. A Siderophore from a Marine Bacterium with an Exceptional Ferric Ion Affinity Constant. Nature, 366(6454): 455-458.

Roe, J.E., Anbar, A.D. and Barling, J., 2003. Nonbiological fractionation of Fe isotopes: evidence of an equilibrium isotope effect. Chemical Geology, 195(1-4): 69-85.

Rouxel, O., Dobbek, N., Ludden, J. and Fouquet, Y., 2003. Iron isotope fractionation during oceanic crust alteration. Chemical Geology, 202(1-2): 155-182.

Rouxel, O., Shanks, W.C., Bach, W. and Edwards, K.J., 2008. Integrated Fe and S isotope study of seafloor hydrothermal vents at East Pacific Rise 9-10 degrees N. Chemical Geology, In press.

Rouxel, O.J., Bekker, A. and Edwards, K.J., 2005. Iron isotope constraints on the Archean and Paleoproterozoic ocean redox state. Science, 307(5712): 1088-1091.

Rudnicki, M.D. and Elderfield, H., 1993. A Chemical-Model of the Buoyant and Neutrally Buoyant Plume above the Tag Vent Field, 26 Degrees-N, Mid-Atlantic Ridge. Geochimica Et Cosmochimica Acta, 57(13): 2939-2957.

Rudnicki, M.D., James, R.H. and Elderfield, H., 1994. Near-Field Variability of the TAG Non-buoyant Plume, 26-Degrees-N, Mid-Atlantic Ridge. Earth and Planetary Science Letters, 127(1-4): 1-10.

Rue, E.L. and Bruland, K.W., 1995. Complexation of iron(III) by natural organic ligands in the Central North Pacific as determined by a new competitive ligand equilibration/adsorptive cathodic stripping voltammetric method. Marine Chemistry, 50(1-4): 117-138.

Rue, E.L. and Bruland, K.W., 1997. The role of organic complexation on ambient iron chemistry in the equatorial Pacific Ocean and the response of a mesoscale iron addition experiment. Limnology and Oceanography, 42(5): 901-910.

Ruzic, I., 1982. Theoretical Aspects of the Direct Titration of Natural-Waters and Its Information Yield for Trace-Metal Speciation. Analytica Chimica Acta, 140(1): 99-113.

Sander, S.G., Koschinsky, A., Massoth, G., Stott, M. and Hunter, K.A., 2007. Organic complexation of copper in deep-sea hydrothermal vent systems. Environmental Chemistry, 4(2): 81-89.

Sands, C.M., 2006. Hydrothermal plumes and processes in the Indian Ocean, University of Southampton Thesis, Southampton, 191 pp.

Sarradin, P.M., Caprais, J.C., Riso, R., Kerouel, R. and Aminot, A., 1999. Chemical environment of the hydrothermal mussel communities in the Lucky Strike and Menez Gwen vent fields, Mid-Atlantic ridge. Cahiers De Biologie Marine, 40(1): 93-104.

Sarradin, P.M., Le Bris, N., Le Gall, C. and Rodier, P., 2005. Fe analysis by the ferrozine method: Adaptation to FIA towards in-situ analysis in hydrothermal environment. Talanta, 66(5): 1131-1138.

Schoenberg, R. and von Blanckenburg, F., 2005. An assessment of the accuracy of stable Fe isotope ratio measurements on samples with organic and inorganic matrices by

high-resolution multicollector ICP-MS. International Journal of Mass Spectrometry, 242(2-3): 257-272.

Severmann, S., Johnson, C.M., Beard, B.L., German, C.R., Edmonds, H.N., Chiba, H. and Green, D.R.H., 2004. The effect of plume processes on the Fe isotope composition of hydrothermally derived Fe in the deep ocean as inferred from the Rainbow vent site, Mid-Atlantic Ridge, 36°14'N. Earth and Planetary Science Letters, 225: 63 - 76.

Severmann, S., Johnson, C.M., Beard, B.L. and McManus, J., 2006. The effect of early diagenesis on the Fe isotope compositions of porewaters and authigenic minerals in continental margin sediments. Geochimica Et Cosmochimica Acta, 70(8): 2006-2022.

Shackelford, R. and Cowen, J.P., 2006. Transparent exopolymer particles (TEP) as a component of hydrothermal plume particle dynamics. Deep-Sea Research Part I-Oceanographic Research Papers, 53(10): 1677-1694.

Sharma, M., Polizzotto, M. and Anbar, A.D., 2001. Iron isotopes in hot springs along the Juan de Fuca Ridge. Earth and Planetary Science Letters, 194(1-2): 39-51.

Sherrell, R.M., Field, M.P. and Ravizza, G., 1999. Uptake and fractionation of rare earth elements on hydrothermal plume particles at 9 degrees 45 ' N, East Pacific Rise. Geochimica Et Cosmochimica Acta, 63(11-12): 1709-1722.

Sholkovitz, E.R. and Copland, D., 1981. The Coagulation, Solubility and Adsorption Properties of Fe, Mn, Cu, Ni, Cd, Co and Humic Acids in a River Water. Geochimica Et Cosmochimica Acta, 45(2): 181-189.

Sholkovitz, E.R., Landing, W.M. and Lewis, B.L., 1994. Ocean Particle Chemistry - the Fractionation of Rare-Earth Elements between Suspended Particles and Seawater. Geochimica Et Cosmochimica Acta, 58(6): 1567-1579.

Simoneit, B.R.T., Brault, M. and Saliot, A., 1990. Hydrocarbons Associated with Hydrothermal Minerals, Vent Waters and Talus on the East Pacific Rise and Mid-Atlantic Ridge. Applied Geochemistry, 5(1-2): 115-124.

Skulan, J.L., Beard, B.L. and Johnson, C.M., 2002. Kinetic and equilibrium Fe isotope fractionation between aqueous Fe(III) and hematite. Geochimica Et Cosmochimica Acta, 66(17): 2995-3015.

Spencer, D.W. and Brewer, P.G., 1971. Vertical Advection Diffusion and Redox Potentials as Controls on Distribution of Manganese and Other Trace Metals Dissolved in Waters of Black Sea. Journal of Geophysical Research, 76(24): 5877-5892.

Spiess, F.N., Macdonald, K.C., Atwater, T., Ballard, R., Carranza, A., Cordoba, D., Cox, C., Diazgarcia, V.M., Francheteau, J., Guerrero, J., Hawkins, J., Haymon, R., Hessler, R., Juteau, T., Kastner, M., Larson, R., Luyendyk, B., Macdougall, J.D., Miller, S., Normark, W., Orcutt, J. and Rangin, C., 1980. East Pacific Rise - Hot Springs and Geophysical Experiments. Science, 207(4438): 1421-1433.

Statham, P.J., 1985. The Determination of Dissolved Manganese and Cadmium in Sea-Water at Low nmol/L Concentrations by Chelation and Extraction Followed by Electrothermal Atomic-Absorption Spectrometry. Analytica Chimica Acta, 169: 149-159.

Statham, P.J., German, C.R. and Connelly, D.P., 2005. Iron(II) distribution and oxidation kinetics in hydrothermal plumes at the Kairei and Edmond vent sites, Indian Ocean. Earth and Planetary Science Letters, 236(3-4): 588-596.

Taylor, P.D.P., Maeck, R. and Debievre, P., 1992. Determination of the Absolute Isotopic Composition and Atomic-Weight of a Reference Sample of Natural Iron. International Journal of Mass Spectrometry and Ion Processes, 121(1-2): 111-125.

Thurnherr, A.M., Richards, K.J., German, C.R., Lane-Serff, G.F. and Speer, K.G., 2002. Flow and mixing in the rift valley of the Mid-Atlantic Ridge. Journal of Physical Oceanography, 32(6): 1763-1778.

Tolstoy, M., Cowen, J.P., Baker, E.T., Fornari, D.J., Rubin, K.H., Shank, T.M., Waldhauser, F., Bohnenstiehl, D.R., Forsyth, D.W., Holmes, R.C., Love, B., Perfit, M.R., Weekly, R.T., Soule, S.A. and Glazer, B., 2006. A sea-floor spreading event captured by seismometers. Science, 314(5807): 1920-1922.

Toner, B.M., Fakra, S.C., Manganini, S.J., Moffett, J.W., German, C.R. and Edwards, K.J., 2007. Particulate organic carbon and iron speciation within deep-sea hydrothermal plumes. EOS, Transactions, American Geophysical Union, 88(52): Fall Meet. Suppl., Abstract B23G-08.

Town, R.M. and van Leeuwen, H.P., 2005a. Measuring Marine Iron(III) Complexes by CLE-AdSV. Environmental Chemistry, 2(2): 80-84.

Town, R.M. and van Leeuwen, H.P., 2005b. Reply to Comments on "Measuring Marine Iron(III) Complexes by CLE-AdSV". Environmental Chemistry, 2(2): 90-93.

Trefry, J.H. and Metz, S., 1989. Role of Hydrothermal Precipitates in the Geochemical Cycling of Vanadium. Nature, 342(6249): 531-533.

Trocine, R.P. and Trefry, J.H., 1988. Distribution and Chemistry of Suspended Particles from an Active Hydrothermal Vent Site on the Mid-Atlantic Ridge at 26- Degrees-N. Earth and Planetary Science Letters, 88(1-2): 1-15.

Tsuda, A., Takeda, S., Saito, H., Nishioka, J., Kudo, I., Nojiri, Y., Suzuki, K., Uematsu, M., Wells, M.L., Tsumune, D., Yoshimura, T., Aono, T., Aramaki, T., Cochlan, W.P., Hayakawa, M., Imai, K., Isada, T., Iwamoto, Y., Johnson, W.K., Kameyama, S., Kato, S., Kiyosawa, H., Kondo, Y., Levasseur, M., Machida, R.J., Nagao, I., Nakagawa, F., Nakanish, T., Nakatsuka, S., Narita, A., Noiri, Y., Obata, H., Ogawa, H., Oguma, K., Ono, T., Sakuragi, T., Sasakawa, M., Sato, M., Shimamoto, A., Takata, H., Trick, C.G., Watanabe, Y.W., Wong, C.S. and Yoshie, N., 2007. Evidence for the grazing hypothesis: Grazing reduces phytoplankton responses of the HNLC ecosystem to iron enrichment in the western subarctic pacific (SEEDS II). Journal of Oceanography, 63(6): 983-994.

Turner, J.S., 1962. The 'starting plume' in neutral surroundings. Journal of Fluid Mechanics, 13(3): 356 - 368.

Ussher, S.J., Achterberg, E.P. and Worsfold, P.J., 2004. Marine Biogeochemistry of Iron. Environmental Chemistry, 1: 67-80.

Van den Berg, C.M.G., 1982. Determination of Copper Complexation with Natural Organic-Ligands in Sea-Water by Equilibration with MnO2 .1. Theory. Marine Chemistry, 11(4): 307-322.

Van den Berg, C.M.G., 1995. Evidence for organic complexation of iron in seawater. Marine Chemistry, 50(1-4): 139-157.

Van den Berg, C.M.G., 2005. Organic Iron Complexation Is Real, The Theory Is Used Incorrectly. Comment on 'Measuring Marine Iron(III) Complexes by CLE-AdSV'. Environmental Chemistry, 2(2): 88-89.

Van den Berg, C.M.G., 2006. Chemical speciation of iron in seawater by cathodic stripping voltammetry with dihydroxynaphthalene. Analytical Chemistry, 78(1): 156-163.

Van den Berg, C.M.G., Nimmo, M., Daly, P. and Turner, D.R., 1990. Effects of the Detection Window on the Determination of Organic Copper Speciation in Estuarine Waters. Analytica Chimica Acta, 232(1): 149-159.

van Leeuwen, H.P. and Town, R.M., 2005. Kinetic limitations in measuring stabilities of metal complexes by Competitive Ligand Exchange-Adsorptive Stripping Voltammetry (CLE-AdSV). Environmental Science & Technology, 39(18): 7217-7225.

Veirs, S.R., McDuff, R.E. and Stahr, F.R., 2006. Magnitude and variance of near-bottom horizontal heat flux at the Main Endeavour hydrothermal vent field. Geochemistry Geophysics Geosystems, 7: Q02004.

Verardo, D.J., Froelich, P.N. and McIntyre, A., 1990. Determination of Organic-Carbon and Nitrogen in Marine-Sediments Using the Carlo-Erba-Na-1500 Analyzer. Deep-Sea Research Part a-Oceanographic Research Papers, 37(1): 157-165.

Vereshchaka, A.L. and Vinogradov, G.M., 1999. Visual observations of the vertical distribution of plankton throughout the water column above Broken Spur vent field, Mid-Atlantic Ridge. Deep-Sea Research Part I-Oceanographic Research Papers, 46(9): 1615-1632.

Von Damm, K.L., 1995. Controls on the Chemistry and Temporal Variability of Seafloor Hydrothermal Fluids. In: S.E. Humphris, R.A. Zierenberg, L.S. Mullineaux and R.E. Thomson (Editors), Seafloor Hydrothermal Systems: physical, chemical, biological and geological interactions. AGU Monograph Am. Geophys. Union, Washington DC, pp. 222 - 247.

Von Damm, K.L., 2004. Evolution of the Hydrothermal System at East Pacific Rise 9 degrees 50'N: Geochemical Evidence for Changes in the Upper Oceanic Crust. In: C.R. German, J. Lin and L.M. Parson (Editors), Mid-Ocean Ridges: Hydrothermal Interactions between the Lithosphere and Ocean. AGU Monograph. Am. Geophys. Union, Washington DC.

Von Damm, K.L. and Lilley, M.D., 2004. Diffuse Flow Hydrothermal Fluids from 9 degrees 50' N East Pacific Rise: Origin, Evolution and Biogeochemical controls. In: W.S.D. Wilcock, E.F. Delong, D.S. Kelley, J.A. Baross and S. Craig Cary (Editors), The Subsurface Biosphere at Mid-Ocean Ridges: Issues and Challenges, in the Subseafloor Biosphere at Mid-Ocean Ridges. AGU Monograph. Am. Geophys. Union, Washington DC.

Von Damm, K.L., Lilley, M.D., Shanks, W.C., Brockington, M., Bray, A.M., O'Grady, K.M., Olson, E., Graham, A. and Proskurowski, G., 2003. Extraordinary phase separation and segregation in vent fluids from the southern East Pacific Rise. Earth and Planetary Science Letters, 206(3-4): 365-378.

Von Damm, K.L., Oosting, S.E., Kozlowski, R., Buttermore, L.G., Colodner, D.C., Edmonds, H.N., Edmond, J.M. and Grebmeier, J.M., 1995. Evolution of East Pacific Rise Hydrothermal Vent Fluids Following a Volcanic-Eruption. Nature, 375(6526): 47-50.

Winn, C.D., Karl, D.M. and Massoth, G.J., 1986. Microorganisms in Deep-Sea Hydrothermal Plumes. Nature, 320(6064): 744-746.

Witter, A.E., Hutchins, D.A., Butler, A. and Luther, G.W., 2000. Determination of conditional stability constants and kinetic constants for strong model Fe-binding ligands in seawater. Marine Chemistry, 69(1-2): 1-17.

Witter, A.E. and Luther, G.W., 1998. Variation in Fe-organic complexation with depth in the Northwestern Atlantic Ocean as determined using a kinetic approach. Marine Chemistry, 62(3-4): 241-258.

Wong, C.S., Johnson, W.K., Sutherland, N., Nishioka, J., Timothy, D.A., Robert, M. and Takeda, S., 2006. Iron speciation and dynamics during SERIES, a mesoscale iron enrichment experiment in the NE Pacific. Deep-Sea Research Part II-Topical Studies in Oceanography, 53(20-22): 2075-2094.

Wu, J. and Luther III, G.W., 1995. Complexation of Fe(III) by natural organic ligands in the Northwest Atlantic Ocean by a competitive ligand equilibration method and a kinetic approach. Marine Chemistry, 50(1-4): 159-177.

Wu, J.F., Boyle, E., Sunda, W. and Wen, L.S., 2001. Soluble and colloidal iron in the oligotrophic North Atlantic and North Pacific. Science, 293(5531): 847-849.

Zbinden, M., Le Bris, N., Gaill, F. and Compere, P., 2004. Distribution of bacteria and associated minerals in the gill chamber of the vent shrimp Rimicaris exoculata and related biogeochemical processes. Marine Ecology-Progress Series, 284: 237-251.

Zhu, X.K., O'Nions, R.K., Guo, Y.L. and Reynolds, B.C., 2000. Secular variation of iron isotopes in North Atlantic Deep Water. Science, 287(5460): 2000-2002.